A Study of Environmental Exposure on Structural Adhesively Bonded Austenitic Stainless Steel

Scott M^{C}Cann

A thesis submitted in partial fulfilment of the requirements of Sheffield Hallam University for the degree of Doctor of Philosophy

May 2003

Collaborating Organisation: AvestaPolarit Ltd

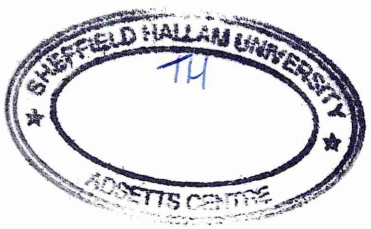
SHEFFIELD HALLAM UNIVERSITY
ADSETTS CENTRE

Loose ends, things unrelated, shifts,
nightmare journeys, cities arrived at and left,
meetings, desertions, betrayals,
all manner of unions, adulteries,
triumphs, defeats....these are the facts.

Alexander Trocchi, Cain's Book (1960)

A Study of Environmental Exposure on Structural Adhesively Bonded Austenitic Stainless Steel

Abstract

Structural adhesive bonding is becoming a popular alternative to the more traditional joining methods, such as spot and laser welding, for joining metallic substrates intended for structural applications. Structural adhesive bonding offers many advantages, for example enhancing fatigue resistance, the ability to join dissimilar materials and providing cost effective joining solutions. The work presented in this thesis studies the effectiveness of bonding austenitic stainless steel using a two-part structural epoxy adhesive.

A comprehensive review of literature has been carried out covering the mechanisms of adhesion, the importance of surface pre-treatments and surface analytical techniques used to evaluate the chemical and physical attributes of substrates prior to bonding and the failure analysis of fracture surfaces. In addition techniques used to study the environmental durability and fatigue performance of adhesive joints has being appraised. The first experimental phase evaluated the effect of commercially available stainless steel finishes on adhesive joint durability using the standard overlap specimen. Environmental exposure included natural outdoor weathering and a high humidity environment coupled with the application of an applied load. It was noted that to further appraise more durable pre-treatments used prior to bonding different testing configurations was required. Perforated single overlap joints and wedge test specimens were used to assess eleven different pre-treatments, ranging from relatively simply to more complex electro-chemical techniques. All pre-treatments included in the research were physically and chemically characterised using scanning electron microscopy (SEM), surface profilometry and X-Ray Photoelectron Spectroscopy (XPS). The complementary data from the perforated lap shear and wedge crack extension testing ranked the pre-treatment used in a similar fashion. The two most durable treatment were the Accomet C proprietary coating and the sulphuric acid sodium dichromate anodisation process. A pattern emerged revealing the more durable pre-treatments produced higher Cr:Fe ratios on the surface. Post failure analysis of fractured specimens was carried out using SEM and XPS. It was shown that after the environmental exposure of specimens to a high humidity hydro-thermal stress regime the most durable pre-treatments initially failed cohesively within the adhesive and then interfacially between the adhesive and associated oxide layer.

The second stage of the experimental work evaluated the fatigue performance of single overlap joints. The fatigue performance of joints was increased using cost-effective surface conditioning techniques. It was also shown the fatigue response of the adhesive joints is dependant upon test frequency, the effect of which being more prominent at low frequencies. The effect of mean load has also been evaluated, and revealed a reduction in load amplitude seriously diminishes the fatigue lifetime of specimens. The effects of aqueous ageing in distilled water at ambient temperatures was assessed. It was shown that continuous immersion for up to 72 weeks caused total delamination of the adhesive from the substrate. It was postulated that moisture ingression into the interfacial region fills air voids and caused the adhesive to displace from the adherend.

An elastic model based on beam theory has being developed to determine the elastic rotation of the overlap region of single lap joints under the application of a tensile load. The model was validated by experimental results, and evaluated the effects of adherend thickness and overlap length. The model has the potential to aid engineers when designing structures using adhesive bonding, especially concerning thin gauge applications where plastic deformation can occur under comparatively small loads.

Advanced Studies

The following taught lectures, short courses and conferences were attended as part of the research programme;

Taught Lectures:

Crystallography
Dr. J. Cawley
Materials Research Institute, Sheffield Hallam University, 1997

Polymers and Liquid Crystals
Dr. S. Spells
Materials Research Institute, Sheffield Hallam University, 1997

Electron Microscopy and X-Ray Techniques
Prof. J. Titchmarsh
Materials Research Institute, Sheffield Hallam University, 1998

X-Ray Diffraction
Dr. B. Lewis
Materials Research Institute, Sheffield Hallam University, 1998

Analytical Scanning Electron Microscopy
Dr. J. Cawley
Materials Research Institute, Sheffield Hallam University, 1999

Infra Red Spectroscopy
Prof. J. Yarwood
Materials Research Institute, Sheffield Hallam University, 1999

Short Courses:

The Science and Technology of Adhesive Bonding
Loughborough University, 1998

IGDS Module - Surface Analysis and Testing
Prof. D. Munz
Materials Research Institute, Sheffield Hallam University, 1999

Conferences:

Adhesion and Adhesives
35th Annual Conference, Oxford Brookes University, Oxford, UK. 9th April 1997

Adhesives in Transport
Institute of Materials, London, UK. 2nd December 1997

Structural Adhesives in Engineering V
5th International Conference. Bristol, UK. 1st – 3rd April 1998

Structural Adhesives in Engineering VI
6th International Conference, Loughborough University, UK. April 1999

Miscellaneous:

AvestaSheffield Research Foundation – Annual Review of Research
Stockholm, Sweden, 1997

AvestaSheffield Research Foundation – Annual Review of Research
Stockholm, Sweden, 1998

AvestaSheffield Research Foundation – Annual Review of Research
Stockholm, Sweden, 1999

Research Studies – Linköping University of Technology, Linköping, Sweden. May – July 1999

AvestaSheffield Research Foundation – Annual Review of Research
Stockholm, Sweden, 2000

Acknowledgements

I would like to thank the people who have helped, contributed and listened during the time it has taken to finally complete this thesis.

I would like to sincerely thank my Director of Studies Prof. Hans Nordberg for all the time, effort and patience he has given during my period of study. See I told you it would be finished before you retire.

My true thanks to my supervisor Dr. Jess Cawley for all his assistance, chats and again above all else patience.

A huge cheers to Bob Boyes for the help, laughs and confidence he gave me.

Thanks to the AvestaPolarit Research Foundation.

A big thank you to all the School of Engineering Technicians for their help, laughs and honesty – they are Brian, Roger, Dick, Dick W, Joe, Tony, Ray, Brian P, Mac, and John.

Cheers to the Avesta Office lads and lassies for the good company and banter.

Thanks to all the staff at the MRI, especially Mike Simmonds for his kind assistance.

Thanks to Ruth and Lesley at the MRI, so I didn't get bogged down in all the paperwork.

A thank you to all the Swedes, Roger, Johan, Anders and Margareta for all the good times and laughs in Sweden.

I would like to thank my Mother, Father and Brother for all their love, support and encouragement. I love you all very much. Nin you will be forever in our thoughts.

And finally, a huge heart filled thanks to my soul mate, best friend and wife Claire. You have gone through all the good times and bad times with me, and without your support and love this thesis would never have got finished. I love you.

Contents Page

List of Tables

List of Figures

List of Plates

1.0 Introduction

Although the application of adhesives is a recently established technology, there is evidence that the ancient Greeks and Egyptians used glues for veneering precious items for their leaders and spiritual gods. In all centuries up to and including the nineteenth century, glues originated from the manipulation of animal and plant products, but with the advent of the twentieth century and the innovation of synthetic chemicals the more renowned name of adhesives was introduced.

Structural adhesive bonding began during World War II, when the De Haviland aircraft's plywood construction was adhesively bonded. Since then the aerospace industry has employed and developed structural adhesive bonding to join primarily the respective alloys of aluminium and titanium. However, there has been a considerable increase in the utilisation of adhesive bonding in the construction and engineering industries, where attention and funding has been put into research and development. In contrast the development and drive for the structural bonding of stainless and carbon steels has been governed largely by economic factors.

The sponsor of the present research programme was AvestaPolarit, a company formed from the merger between Avesta Sheffield and Outokumpo Polarit. AvestaPolarit is the second largest stainless steel manufacturer, with potential production to exceed 2.7 million tonnes per year. The company has a commitment to research and development, where one particular area of interest is joining methods for stainless steel for structural applications. The majority of stainless steel sales are thin gauge cold rolled coil products. The ability of adhesive bonding to efficiently join thin sheet has been the principal driving force for the current research.

Stainless steels have been the popular choice of architects, designers and engineers for a wide range of consumer goods and industrial applications. No other material exhibits the durability, versatility and formability stainless steels offer. In addition the aesthetic properties, ease of fabrication, hygienic qualities and corrosion resistance offer specifiers the realisation to use stainless steels in ever more demanding applications and environments.

Structural adhesive bonding can offer substantial economic, design and performance advantages compared with the more conventional methods of joining. However as with any relatively new technology, adhesive bonding is subjected to limitations. The advantages and limitations are listed below;

Advantages

- Ability to join thin sheet efficiently
- Ability to join dissimilar materials
- Weight savings over mechanical fasteners
- Adhesive joints can be hermetic

- Capital and/or labour costs are often reduced
- Corrosion between dissimilar metals maybe reduced or eliminated
- More uniform stress distribution across the bonded area
- No requirements for high energy inputs during the joining operation

Limitations

- Elevated in-service temperatures can be limited
- Non Destructive Testing techniques are limited compared with welding
- Surface pre-treatments are usually a prerequisite
- Poor creep performance of bonded assemblies at elevated temperatures
- Equipment and jigging costs may be high
- Some adhesives are toxic and flammable
- Long curing times may be incurred
- Long term durability data relatively limited

Project Objectives

The main aims of the present research include the effects of surface pre-treatments, dynamic performance of adhesive joints and the properties of single lap joints. The main project objectives are listed below;

- To assess the environmental durability of surface pre-treatments applicable to austenitic stainless steel
- To use surface analytical techniques to characterise austenitic stainless steel surfaces, both physically and chemically
- To appraise the fatigue performance of austenitic stainless steel joints bonded with a structural epoxy resin
- To develop an analytical model to predict the elastic rotation of single overlap joints

Outline of Thesis

Chapter 2 reviews the relevant literature on the theories of adhesion, surface preparation and pre-treatments, durability testing, fatigue testing of adhesive joints and aspects of surface analytical techniques applicable to adhesion studies. Chapter 3 details the adhesive and substrate systems used, methods used for surface pre-bonding, preparation of specimens, testing equipment and analytical techniques incorporated into the study. Chapter 4 presents the influence of surface finish and pre-bonding treatments on the environmental durability of adhesive joints on exposure to various environments. Scanning electron microscopy (SEM), X-ray photoelectron spectroscopy (XPS), and surface profilometry has been used to characterise the physical and chemical attributes of pre-bonded substrates. The locus of failure has been verified using SEM and XPS. Chapter 5 evaluates the effects of; surface pre-treatment, test frequency, load ratio and ageing in an aqueous environment on the fatigue behaviour of single

overlap joints. Chapter 6 concentrates on a model used to elucidate the elastic component of rotation experienced by single overlap joints in tension. Finally Chapter 7 discusses the main conclusions and proposes areas for future work.

Chapter 2

Review of Literature

2.1 Introduction

The aim of this chapter was to review the relevant literature applicable to the present research. The theories and mechanisms of adhesion, environmental durability of adhesively bonded structures, the dynamic performance of adhesive joints and surface characterisation techniques will be discussed.

2.2 Interfacial Contact

2.2.1 Introduction

To enable strong durable adhesive bonds it is necessary to establish intimate molecular contact. To achieve this the adhesive must be able to spread over the solid surface, and in doing so displace air and surface contamination. Essentially the adhesive must do two things:

(i) Wet the surface in such a manner that the resulting contact angle approaches zero.

(ii) The adhesive must then harden to form a cohesively strong solid, usually performed by a chemical reaction or loss of solvent or water.

The most common form of physical attractive forces are van der Waals forces which attribute to two effects, namely[1]

(a) Dispersion forces, which are created from internal electron motions.

(b) Polar forces, which arise from the orientation of permanent electric dipoles and the induction effect of permanent dipoles on polarizable molecules.

2.2.2 Wetting Equilibria

Surface tension is a direct measurement of intermolecular forces. Within the bulk of a liquid the attractive forces exerted on molecules by their neighbour's balance in all directions. At the surface however this balance does not exist, hence surface layers are attracted to the bulk. If new molecules are to be brought to the surface work has to be done on them, thus giving surface molecules higher energy than bulk molecules. This increase in energy is the surface free energy, and relates to the energy required to create a unit area of new surface.

When a liquid comes into contact with a solid surface, the liquid adopts a characteristic drop shape. This is shown in Figure 2.1.

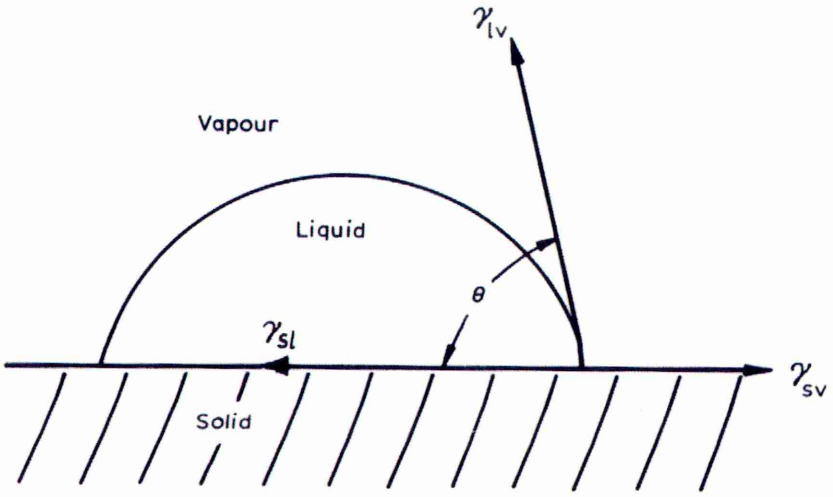

Figure 2.1 *- A liquid drop resting at equilibrium on a solid surface*[1]

Surface energy and surface tension are comparable both dimensionally and numerically, and are defined by γ. Figure 2.1 shows the surface tensions acting at a three phase contact point of solid, vapour and liquid. The Young equation[2] relates these tensions to θ, by:

$$\gamma_{SV} = \gamma_{SL} + \gamma_{LV}\cos\theta \qquad (2.1)$$

Where γ_{SV} responds to the surface free energy of the solid substrate resulting from the adsorption of vapour from the liquid. This will be lower than the surface free energy of the clean surface under a vacuum, γ_S, by an amount known as the equilibrium spreading pressure, π_S. As a consequence equation 2.1 can be rewritten as:

$$\gamma_{SV} = \gamma_{SL} + \gamma_{LV}\cos\theta + \pi_S \qquad (2.2)$$

When $\theta > 0^0$ the liquid adhesive does not spread. However when $\theta = 0^0$ the liquid spreads spontaneously over the surface, at a rate dependant upon the viscosity of the adhesive and the roughness of the surface. For wetting to occur:

$$\gamma_{SV} \geq \gamma_{SL} + \gamma_{LV} \qquad (2.3)$$

or

$$\gamma_{SV} \geq \gamma_{SL} + \gamma_{LV} \quad + \pi_S \qquad (2.4)$$

Dupré[3] considered the work needed to separate a layer of liquid from a solid surface. The work was defined as, energy of new surface created minus the energy of the interface destroyed. This is the work of adhesion, W_A, and is represented by the Dupré equation:

$$W_A = \gamma_S + \gamma_{LV} - \gamma_{SL} \quad (2.5)$$

Combining equations (2.1) and (2.5) gives the Young - Dupré equation[4] :

$$W_A = \gamma_{LV} + \gamma_{LV}\cos\theta = \gamma_{LV}(1 + \cos\theta) \quad (2.6)$$

Therefore the work of adhesion is directly related to the surface tension of the liquid and the contact angle that the liquid makes with the solid. Equation (2.1) states that the maximum work of adhesion occurs when $\theta = 0$, but equation (2.6) shows that the work of adhesion can never be zero as all liquids have a surface tension under normal conditions.

2.2.3 Surface and Interfacial Free Energies

Contact angles between solids and liquids of known surface tension produces an indirect measurement of solid surface free energy. As liquids have a surface tension or surface energy, solid surfaces similarly have these surface energies. Zisman et al[5-9] introduced an empirical approach to discriminating between low and high energy surfaces. Most liquids and organic materials such as polymers have surface free energies below $100mJ.m^{-2}$, whilst organic adhesives have low surface free energies in the order of $50mJ.m^{-2}$, and are described as low energy surfaces. Metals, metal oxides and ceramics are termed high energy surfaces where their surface free energies are in excess of $500mJ.m^{-2}$. A high energy surface allows a wetting liquid to spread readily upon it, therefore an organic adhesive should wet a metallic oxide surface, as the relationship $\gamma_{SV} > \gamma_{LV}$ occurs. Complications arise when a high energy surface in a pre-bonded state attracts atmospheric contamination, in the form of water vapour and hydrocarbons. This lowers the surface free energy of the substrate and in turn can hinder the wetting of the adhesive and therefore the degree of interfacial contact made. Gledhill et al[10] examined the wettability of mild steel adherends with a variety of surface roughness. They found that at low humidities the increased joint strengths were related to enhanced wetting of the steel. This emphasised the point that when a clean hydrophilic metal oxide was exposed to a humid environment the surface energy was diminished. The results are shown in Figure 2.2.

Therefore when adhesively bonding high energy substrates are used the joining process must be conducted in conditions free from apparent contamination and environments of high humidity. If contamination is not kept to a minimum, the adhesive will not readily displace these contaminants and they will then act as a weak boundary.

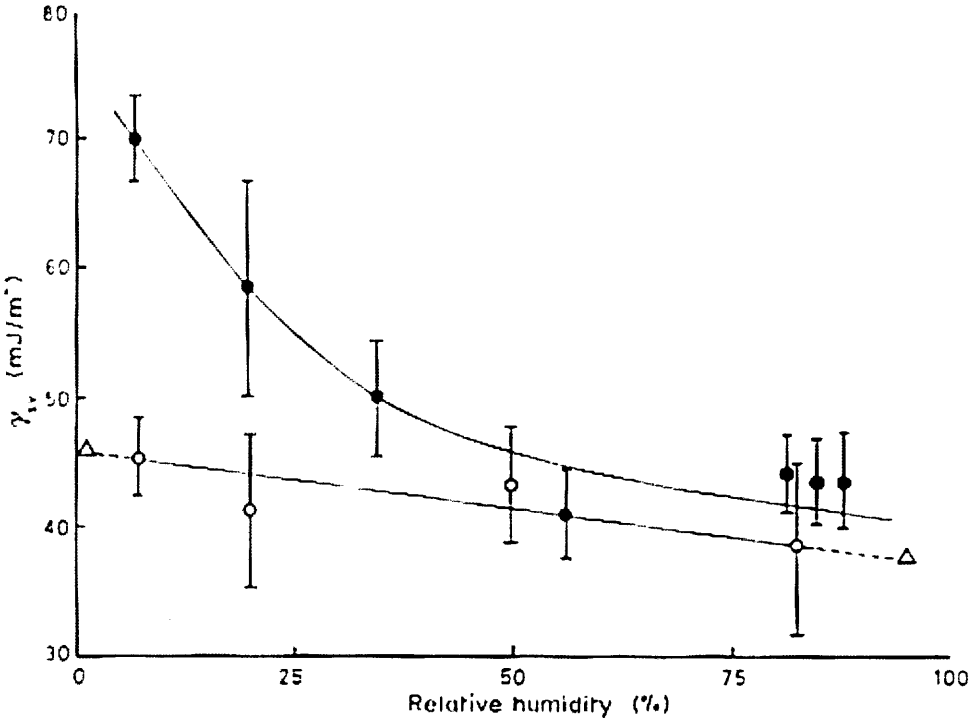

***Figure 2.2** - The effect of humidity on the surface energy of mild steel[10]. • = grit blasted ○ = polished smooth*

2.3 Mechanisms of Adhesion

2.3.1 Introduction

When sufficient interfacial contact has been made between the adhesive and the substrate, the adhesive cures to form a structure capable of transmitting stresses. Many theories of adhesion exist in the literature, with each forming a different hypothesis or an exclusive explanation of the mechanism of adhesion, whilst disregarding other postulations. An important point to consider when discussing theories of adhesion is that assumptions are made both on a practical and theoretical basis. Where practical adhesion is often described as being the strength of an adhesive bond and the theoretical aspects are usually concerned with the forces occurring on a microscopic scale between interfaces. As intimated by Kinloch[11], much of the confusion undoubtedly arises because of the common test methods employed to measure the strengths of adhesive joints are not well suited to theoretical considerations. Geometrical factors and loading factors are introduced which are difficult to analyse, and the measured joint strength includes indeterminate contributions from rheological energy losses in the adhesive and substrate. Therefore although the intrinsic adhesion forces acting across the adhesive/substrate interface may affect joint strength they are usually completely obscured by other contributions. Hence information concerning the magnitude of such forces may only be indirectly obtained. This inability to measure the interfacial interactions has been the main obstacle to the development of a comprehensive theory of adhesion.

There are four main proposed theories on the mechanisms of adhesion, namely:

(1) Mechanical interlocking

(2) Diffusion theory

(3) Electronic theory

(4) Adsorption theory

2.3.2 Mechanical Interlocking

This concept suggests that the adhesive mechanically interlocks with irregularities or pores on the adherend surface, and forms the oldest theory of adhesion probably due to its simplicity, which led to the roughening of substrates to enhance adhesion. Commonly encountered examples of mechanical interlocking are; iron on patches for clothing where the patch contains a hot melt adhesive which when molten impregnates the textile and mercury amalgam fillings, which are inserted into 'ink bottle' pits to secure in place. Borroff and Wake's[12] early work concerning the adhesion of rubber to textiles agreed well with the idea of mechanical interlocking. The early tyre cords were spun from staple of natural origin, mainly cotton. Their work confirmed that the bond strength was dependent upon the penetration of the fibre ends from the spun yarn into the rubber. Although adhesion between fibre and rubber arises intrinsically from primary and secondary forces, this is as an indirect consequence and it simply determines the length of fibre required before the interfacial shear strength exceeds the tensile strength of the fibre.

Venables[13] studied the surfaces of both aluminium and titanium alloys after they had been treated with aerospace standard pre-treatments, using high resolution scanning electron microscopy. After both alloys had been treated with a Forest Products Laboratory etch (FLP) and phosphoric acid anodising (PAA), the resultant oxides exhibited porous whisker like formations on a micro-roughness scale. The improvement in durability was concluded as a result of the mechanical keying action of the adhesive into the newly formed oxide.

Jennings[14] carried out experiments to investigate the effect of surface roughness on the adhesive bonding of stainless steel and aluminium alloy substrates. Comparisons were made between smooth polished surfaces to that of rough surfaces from abrasion or machining. It was found that joint strength increased when rougher adherends were bonded together. Jennings concluded the better wetting and surface area increase, yielded by the roughened substrates contributed to higher joint strengths. The joint strengths are shown below in Table 2.1.

***Table 2.1** - Joint strength as a function of surface roughness*[14]

Surface Condition	Butt Joint Strength (MPa)	Coefficient of variation (%)
Aluminium Alloy (6061)		
Polished 1μm diamond paste	28.8	24.4
Abrades 600 SiC paper	30.9	24.9
Abrades 280 SiC paper	39.0	17.5
Abrades 180 SiC paper	36.7	20.4
Sandblasted 40 to 50 mesh SiO_2 grit	48.5	11.4
Stainless Steel (AISI 304)		
Polished 1μm diamond paste	27.8	20.8
Regular machined grooves	35.2	20.0
Sandblasted 40 to 50 mesh SiO_2 grit	53.4	10.8

However, sandblasting and abrading treatments provide macroscopically rough surfaces in a completely random fashion and are not indicative of a surface that would favour mechanical interlocking. Kinloch[15] found that roughening the substrate may lead to increased joint strengths but that such improvements do not generally arise from just a simple mechanical interlocking. They may arise from the effective cleaning action of the abrasion process, the increase in available surface area for bonding and the improved kinetics of wetting. Moreover, an increase in roughness may increase localised energy dissipation in the adhesive near to the interface and prevent cracks at or near to the interface from aligning and therefore propagating.

The mechanical interlocking theory was further questioned by the work of Tabor et al[16,17] and Johnson[18], who confirmed adhesion can be accomplished between smooth surfaces when they bonded smooth mica and rubber surfaces respectively.

It has been shown that mechanical interlocking in certain situations can promote intrinsic adhesion mechanisms, for fibrous materials on a macro scale while for metal oxides this is on a micro scale. However, the substrate must be treated in such a way as to provide a surface that is representative of producing a keying action, which is not commonly found within industry. Increasing the roughness of an adherend may well increase joint strength, but in reality it is as a consequence of effectively removing weak boundary layers, increasing the bonding area and improving the interfacial contact.

2.3.3 Diffusion Theory

This theory was first proposed by Voyutskii[19], and is mainly concerned with the adhesion of polymers to polymers, namely autohesion. Essentially it states that if two polymers are in close contact at temperatures above their glass transition temperatures, then the long chain molecules will interdiffuse. This requires that the macromolecules of the polymers to be joined must be

mutually soluble and for diffusion to occur have adequate mobility. For processes such as solvent bonding, where compatible polymers are joined, the diffusion theory is applicable. However when dissimilar materials are concerned, and solubility parameters are not alike then interdiffusion is an unlikely mechanism of adhesion. Although it has been suggested[20] that when an adhesive penetrates into the fine structure of a metal oxide, the mechanism involved is one of diffusion of the polymer into the interstices of the oxide.

2.3.4 Electronic Theory

Derjaguin et al[21] proposed the electronic theory, where essentially adhesion is due to the balance of electrostatic forces from the transfer of electrons between the adhesive and substrate. The transfer results in the formation of a double layer of electrical charge at the interface. The two layers, i.e. adhesive and substrate, are treated as a capacitor which is charged due to the contact of two different materials. When the layers are detached a separation of charge results which leads to a potential difference which increases until a discharge occurs. The dominant criticism of this approach is rupture and is assumed to take place at the adhesive/substrate interface and not cohesively within the adhesive. However, support of this theory includes evidence that fractured parts of adhesive joints do charge, but this can be caused during fracture. Kinloch[22] remarked that for typical adhesive/substrate interfaces, any electrical double layer which is generated does not contribute significantly to the intrinsic adhesion.

2.3.5 Adsorption Theory

This theory has been discussed in depth by various workers[23,24], and is a generally accepted mechanism of adhesion. The theory postulates that the adhesive macromolecules are physically adsorbed onto the substrate surface, and are held there by the forces of attraction from the two surfaces. The forces of attraction include van-der-Waals forces of several types, as they are universally present in all materials, and in some cases hydrogen bonding, both of which are termed secondary bonds, (depending on the chemistry of the materials primary bonds i.e. ionic or covalent, the term chemisorption is used).

Secondary force interactions are responsible for adhesion across an interface between two different materials. They are only effective over very short distances, in the order of a few Angstroms, so intimate contact is required therefore the adhesive will readily wet the adherend. Huntsberger[24] showed that for dispersion forces at a separation distance of one nanometre, the attractive force would yield a tensile joint strength of 100MPa. The difference between theoretical and experimental joint strengths was a consequence of defects such as surface cracks and voids, or geometrical factors that act as stress concentrators. This indicated that high joint strengths could be attained in theory from the intrinsic adhesion resulting from only dispersion forces acting across the interface.

Within the literature there is evidence that the mechanism of adhesion in a variety of adhesive joints is solely via interfacial secondary forces[25,26].

To attain primary bonding across the interface, specialised techniques such as; the incorporation of particular side groups along the polymer chain of the adhesive or by the use of certain phenolic and organometallic primers[22]. Apart from increasing joint strength, primary bonding is a prerequisite to obtaining environmentally stable interfaces. The work of Gettings and Kinloch[27] provided evidence of chemical bonding between various silane primers and mild steel substrates. Using Static Secondary Ion Mass Spectrometry (SSIMS) and X-ray Photoelectron Spectroscopy (XPS), they analysed the first one or two monolayers of the surface. It was concluded that the presence of SiO_2H^-, $SiOH^+$ and SiO_2^- were a result of the silane primer polymerising to give a polysiloxane structure on the metal substrate, providing strong evidence of chemical bonding between the primer and metal. Further work[28] was carried out on the adsorption of a silane primer (γ-glycidoxypropyltrimethoxy silane) to AISI 301 Stainless Steel substrates. Using SSIMS fragments of Fe-O-Si and Cr-O-Si these were detected at the interface, suggesting the primer/substrate interactions were strong. An enhancement in durability of adhesive joints was found where primary interfacial bonding was detected between the primer and the adherend.

2.4 Surface Pretreatments

2.4.1 Introduction

To attain sufficient strength and subsequent durability from structural adhesive joints, some form of pre-treatment of the adherends is required. This section will outline the different types of surface pre-treatments currently in use. As this research programme was concerned with the structural bonding of stainless steel, this review will only cover surface pre-treatments used for metallic, and wherever applicable stainless steel substrates.

Most common engineering metals will have contaminated surfaces as a result of their manufacturing paths, this contamination will be cohesively weak and if left may form a weak boundary layer between the adhesive and substrate interfaces. Examples of manufacturing contaminants include:

(a) lubricating oils and greases
(b) hydrocarbon contamination
(c) dust and particulate pickup

The primary requirement of any pre-treatment is to clean the surface and remove contaminants. More elaborate techniques change both the physical and chemical appearance of the substrate. Kinloch stated the particular purpose of a pre-treatment should be one or more of the following[15] ;

(a) To remove, or prevent the subsequent formation of any weak surface boundary layers on the substrate (For example, weak oxide scale on metallic substrates).

(b) To maximise the degree of intimate contact attained between the adhesive (or primer) and the substrate during the bonding operation.

(c) To ensure that the level of intrinsic adhesion forces established across the interface(s) are sufficient for obtaining both the initial joint and subsequent service life required.

(d) To generate a specific topography on the substrate.

(e) To protect the surface prior to the bonding operation. This is frequently necessary for high energy substrates. After pre-treatment the surface is highly active not only to the adhesive but to atmospheric contamination. Applying a primer that is compatible with the adhesive can combat this.

2.4.2 Types of Pretreatments

2.4.2.1 Degreasing

Some form of degreasing is required to remove soluble contaminants formed from processing paths. For low load bearing applications, degreasing with solvent wetted cloths may be all that is needed. However, weak boundary layers are removed more effectively in liquid or vapour degreasing baths, which commonly include ultrasonic agitation. Where ferrous metals are concerned alkaline solutions are incorporated into the degreasing baths, where the contamination is held in solution to avoid re-deposition onto the substrates. For more demanding applications the degreasing stage is followed by a mechanical and/or chemical treatment.

2.4.2.2 Mechanical Techniques

Mechanical roughening techniques involve the removal of inactive oxide layers by a deformation process, this constitutes an effective way of removing weakly adhering layers. The abrasion processes involve sand and emery papers, grit and shot blasting and wire brushing. Within industry the most reproducible results are given using shot or grit blasting techniques[15]. Grit blasting media typically consists of angular alumina abrasive of 180/220 mesh. The blasting parameters include blast pressure, blast angle, grit size and blast distance. Harris et al[29], conducted a detailed study of the effects of grit blasting with different alumina grits on the surface characteristics of mild steel and aluminium substrates. It was concluded that higher adhesive joint strengths, compared with as-rolled surfaces, were achieved with the grit blasted joints, and that the size of the grit and other blasting parameters did not affect strength. Bonded lap and butt joints were exposed in de-ionised water at 60°C for up to twelve weeks. The results indicated that the changes in joint properties could not be explained by the increased roughness characteristics, such as mechanical interlocking and increased effective bond area. The changes in physical and chemical properties of the surface, and joint behaviour arose from the grit blasting process.

2.4.2.3 Chemical Techniques

High energy metallic substrates are subjected to more complex chemical pre-treatments to enhance the durability of adhesive joints when exposed to demanding conditions such as high humidity and corrosive environments. Chemical pre-treatments are divided into two groups, namely; etching and electrochemical processes. Etching the substrate not only cleans but also produces a microscopically rough surface. Electrochemical techniques provide strong resilient porous oxides, on a micro-roughness scale. The major limitation of chemical pre-treatments is the continuous monitoring of bath compositions and temperature, toxicity of the materials and waste disposal problems. Also the level of joint durability achieved is dependent on alloy composition and the manufacturing paths of the treated substrates.

The increased use of structural adhesive bonding in the aerospace industry has been the main impetus for the development of chemical pre-treatments, to further enhance joint durability. The considerable time spent on the research and development of chemical pre-treatments has concentrated its efforts on aluminium and to a lesser extent titanium, of which there are numerous detailed evaluations[30-35]. Chromic acid etching (CAE) and phosphoric acid anodising (PAA), have become industry standards as the pre-treatments for aluminium, with the latter increasing bond durability. The etching process preferentially dissolves the original oxide layer, and is replaced with a new oxide layer. The anodising processes form specific features and topography, in the appearance of fibrils which allow the adhesive or primer to penetrate the oxide layer. Figures 2.3 depict a transmission electron micrograph of aluminium surfaces treated with CAE and PAA processes.

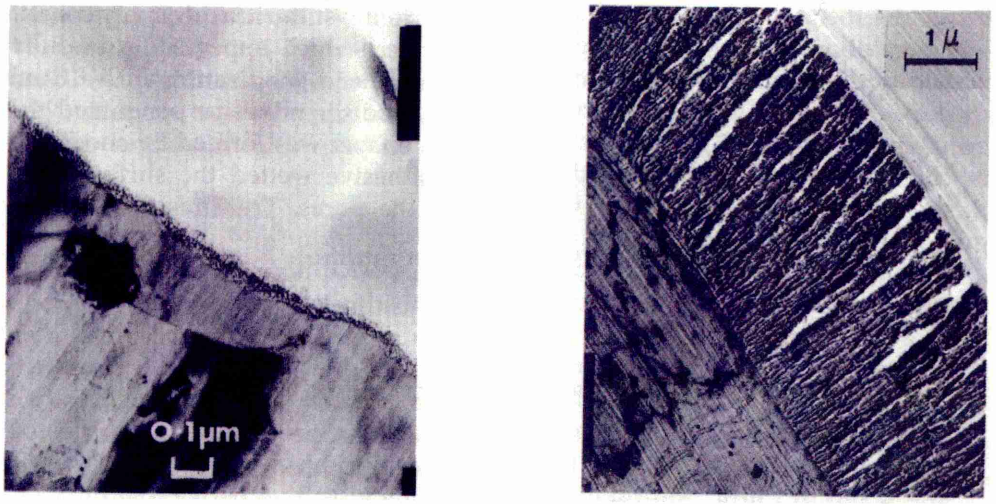

Figure 2.3 *- Transmission electron micrographs of treated aluminium surfaces*[34]

2.4.2.4 Primers

A primer is defined as a coating applied to a surface prior to the application of the adhesive to improve the performance of the bond. The coating can be a low viscosity fluid that is typically 10% solution of the adhesive in an organic solvent, which can wet out the adherend surface leaving a coating over which the adhesive can readily flow[33].

The application of a primer to an adherends surface prior to bonding serves one or more of the following functions:

(a) A primer applied immediately to a freshly prepared surface serves to protect it until the bonding operation is carried out[34]. Increased production and design flexibility can be achieved this way, because the primed surfaces can be stored without the need for instantaneous bonding.

(b) It wets the surface more easily than the adhesive. The primer will penetrate surface roughness and oxide microporosity, for example when aluminium has been treated with etchants or anodising techniques.

(c) When bonding difficult to bond adherends, the primer establishes interfacial bonds with the adhesive and substrate. If the service life of the joint involved has been exposed to wet/humid conditions, silane based primers can be used to form moisture resistant interfacial bonds, thus enhancing durability[15].

(d) Improved corrosion resistance is achieved when primers contain corrosion inhibitors, usually in the form of chromate compounds. As the primer is in close proximity with the surface, it is protected from corrosion and hydration.

(e) The adsorption of the primer to the substrate may be so strong that instead of being physically adsorbed, it has the nature of a chemical bond. This may not correspond to a chemical compound that can be isolated or who's chemistry is understood. This form of adsorption is referred to as chemisorption, to distinguish it from the reversible physical adsorption[34].

2.5 Pretreatments for Stainless Steel

2.5.1 Introduction

There is still limited data and publications on the surface preparation of stainless steel available, when compared to the numerous literature regarding aluminium and titanium alloys[35]. This is in stark contrast to the increased use of stainless steel adhesive joints in the aerospace, construction, automotive and transportation industries[36-38]. The current pre-treatments are discussed.

2.5.2 Pre-treatments

Stainless steel has proved inherently difficult to bond, because of the passive non-interacting oxide layer that is indicative of these alloys. The discussion so far has concentrated on the forms of

surface preparation required in the fabrication of structural adhesive joints, whereby it can be a simple degreasing operation or more complex treatments such as chemical treatment. This section will review the treatments that have been successfully implemented and will detail the effect pre-treatments have on joint durability.

Boyes[39] evaluated several degreasing methods, including, acetone and inhibisol wipe and a multi stage alkaline degrease with ultrasonic agitation. He found that the cleaning procedure did not have to be sophisticated to fabricate AISI 304 stainless steel – epoxy joints within acceptable limits of variation of strength. The mechanical abrading and roughening of ferrous materials in industry is commonly adopted for pre-bonding preparations, especially when mild steel is to be joined. Bottrell[40] mechanically abraded FV 520, a precipitation hardened stainless steel, using 180/220 alumina grit with a blast pressure of 90lb per inch and a distance of 152.4mm. It was suggested the roughened surface provided satisfactory keying for the adhesive, and the wetting ability was improved with contact angles of 13^0 being achieved. In view of earlier sections, the author was inclined to believe the improvement in wetting was attributed to the grit blasting effectively removing weak boundary layers and increasing the surface energy of the stainless steel.

When the in-service conditions become more demanding, the complexity of surface preparation increases to include chemical techniques. The chemical treatment of ferrous metals is particularly troublesome, because of the precipitation of free carbon (smut) to the surface, this creates the need for a de-smutting procedure. De-smutting includes wire brushing or chemical rinses to remove the carbon, which acts as a weak boundary layer. Chemical rinsing is more effective, because brushing pushes carbon into the valleys of the microrough surface, rendering it difficult to remove. The etchants for treating stainless steel commonly have to be in excess of 70^0C, where induction times can be up to one hour, which constitute major limitations.

Ciba Speciality Chemicals[41] recommend two surface pre-treatments for stainless steel. Firstly the adherends should be degreased, either by vapour degreasing with halocarbon solvents or alkaline degreasing preferably with ultrasonic agitation. This is followed by mechanically abrading the surface. Secondly the specimens are degreased and then etched in a solution of oxalic acid, concentrated sulphuric acid and water, at 55-65^0C for five to ten minutes. Adherends are washed in cold water, and the smut is removed by immersing for five to twenty minutes at 60-65^0C in a solution of sulphuric acid and sodium dichromate, accompanied by washing and drying. Brockmann[42] agreed that the only chemical treatment generally recommended for stainless steel involved etching in an aqueous solution containing 10% oxalic acid and 10% sulphuric acid at 80^0C for ten minutes, followed by rinsing in water and removing the smut layer by brushing. A further source[43] suggests immersing adherends in an aqueous solution of concentrated hydrochloric acid, a ratio of 4:1 acid to water, for 30-40 minutes at room temperature. The user is advised to use a solution of concentrated sulphuric acid and sodium dichromate to facilitate smut layer expulsion.

The surface preparation of a martensitic stainless steel, FV520B, was investigated by Allen *et al*[44]. The relation in bond strength to the surface pre-treatment was considered for three adhesives: epoxy-phenolic, epoxy and a polyamide adhesive. The adhesive joint properties were determined from torsional shear napkin ring specimens, with a bond area of 0.707cm^2. After observing that the FV520B became passive in all chromate solutions and was only very slowly affected by solution containing oxidising agents, the following treatments were evaluated:

(1) Sulphuric acid alone
(2) Sulphuric acid + oxalic acid
(3) Sulphuric acid + sodium sulphate
(4) Hydrochloric acid alone
(5) Hydrochloric acid + sodium chloride
(6) Hydrochloric acid + ferric chloride
(7) Hydrofluoric acid

The preferential attacking nature of the etchants, forms a smut layer on the test specimen surface. De-smutting by mechanical brushing was considered ineffective, so the de-smutting procedure was appraised using solutions of nitric acid, sodium dichromate, acidified potassium permanganate, hydrogen peroxide and sulphuric acid with chromium trioxide. From mechanical joint strengths, sulphuric and hydrofluoric acid etches were the preferred surface pre-treatments. The work concluded the most effective de-smutting procedure used either nitric or chromic acid.

The effect of surface pre-treatment on the initial lap shear strength of a martensitic and an austenitic stainless steels, was assessed using a polyvinyl-formal-phenolic adhesive, the results quoted by Sykes[45] are from work carried out at SIRA. The results are shown below in Table 2.2.

Considering the martensitic grade, there was a slight improvement in bond strength when high temperature etches are used in comparison with the grit blasting method. This maybe attributed to cleaning the surface more effectively or providing a microrough surface for the adhesive to key into. In contrast, the vapour blast and degrease offers the highest lap shear strength for the austenitic grade. However, the higher strength attained by the martensitic lap joints may not be dependent on surface treatment, but be imparted by the higher inherent stiffness compared with austenitic grades.

Already numerous surface preparations have been described, providing an introduction into the various pre-treatments that have been developed and realised both in academic and industrial applications. However it is critical to review the effect surface modifying techniques have on the level of durability retained from exposure to realistic and accelerated degenerating environments.

***Table 2.2** - The effect of surface pre-treatment on the initial strength of lap joints*[45]

No.	Surface Pre-treatment	Martensitic	Austenitic
		Bond Strength (MPa)	
1	Grit blast with No. 40 chilled iron shot	35.4	28.4
2	Vapour blast with garnet grit → degrease with trichloroethylene	42.6	34.2
3	Vapour degrease → 15mins at 65^{0}C in 5pbw sodium metasilicate, 9pbw Empilan NP4, 236pbw water → rinse and dry	30.2	24.6
4	Cleaned in proprietary alkaline solution	35.6	22.2
5	Etch 15mins at 50^{0}C in 0.35pbw $Na_2Cr_2O_7$ 10pbw conc. H_2SO_4 → brush off carbon layer → rinse and dry	40.0	14.88
6	Vapour blast as No.2 then etch in No.5	42.8	
7	Etch 10mins at 65^{0}C in 100pbw conc. HCl, 20pbw formalin solution, 4pbw 30% hydrogen peroxide, 90pbw water → rinse → etch 10mins at 65^{0}C in 100pbw conc. H_2SO_4, 10pbw $Na_2Cr_2O_7$, 30pbw water → rinse and dry at 70^{0}C	50.5	25.6
8	Anodic etch 90 sec 6V in 500g.litre^{-1} H_2SO_4 → rinse and dry at 70^{0}C	45.4	24.8
9	As No.8 → Passivate in chromic acid	46.6	26.3
10	Etch 5mins at 50^{0}C in 10% HCl → rinse in 1% H_3PO_4 →dry at 70^{0}C	25.6	0.66
11	Etch 10mins at 70^{0}C in 10% HNO_3 2% HF → rinse and dry at 70^{0}C	45.5	22.2
12	As No. 11 → Passivate in chromic acid	46.4	23.8

2.6 Durability Test Methods

2.6.1 Introduction

Adhesive joints consist of a 'system', which include: adhesive, substrates, primers, surface pre-treatments, oxide layers and interfaces, therefore testing of adhesively bonded structures presents complex issues that are difficult to interpret. The end use of the adhesively bonded structures is dictated by the joint having the capability to withstand the demands of a particular application, therefore the structure must offer sufficient durability to resist deterioration from in-service conditions. In-service environments can change the properties of adhesive joints, the most commonly observed factor been a decrease in strength[46]. The most demanding environmental factor, and commonly encountered, is the absorption of water in humid environments. An environment may be defined as[46] the sum of all factors acting on the adhesive joint, this means the surrounding media, temperature, radiation and mechanical forces. Durability testing usually comprises of exposing bonded assemblies to environments of high humidity and temperature, and assessing the residual strength obtained over time. Testing may also include the simultaneous

application of a load or stress, to provide a hydro-thermal stress regime. Therefore durability testing involves several factors that will affect the performance of the adhesive bond with respect to time.

2.6.2 Single Over Lap Joints

The most commonly encountered adhesive bond configuration is the single over lap joint. It is widely used for durability studies due to its ease of fabrication and replicates structures found in industry. Not surprisingly various test methods are based on single over lap joints, whereby joints are exposed to controlled environments and tested to failure to determine the loss in strength over time. The results reveal the strength-time degradation characteristics for which different adhesive systems can be compared. To accelerate adhesive joint ageing, high humidities and temperatures are used to increase the rate of degradation, for example 60°C and 100% relative humidity. Single lap shear specimens subject the adhesive to cleavage as well as shear stress, this simulates the actual use of structural adhesive used in realistic applications. However, the ratio of normal to shear stress can be very different from those usually encountered in real situations.

It is generally acknowledged that the most discriminating means of testing adhesive joint durability is to impose both a stress and environmental exposure simultaneously. Many studies[47-50] have been carried out on stressing single lap joints with subsequent exposure to degrading conditions, however a majority of the work focuses on aluminium adherends. Lap joints are loaded to varying degrees of stress where the time to failure of specimens is recorded to produce stress-endurance data. If the environmental conditioning of specimens is kept benign, durable joints may avoid failure at low loads in excess of 1 year thus requiring undesirably long periods of environmental exposure. To combat this some researchers[51-53] have fabricated lap joints with smaller bond areas and perforations through the overlap area. The result is a reduction in the diffusion path for ingressing media and therefore the length of environmental exposure time required, an example of which is shown in Figure 2.4.

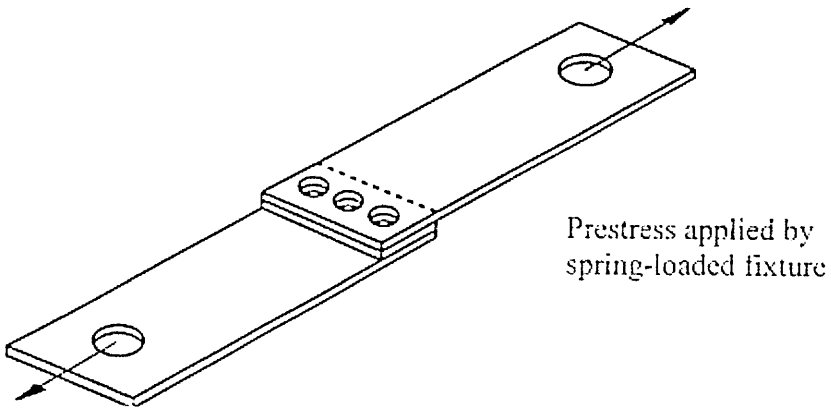

***Figure 2.4** - Perforated single overlap joint*

2.6.3 Wedge Test

The wedge test was first developed by Boeing, and has been standardised for aluminium adherends in ASTM D3762[9]. The fracture test utilises mode I opening of the specimen as shown in Figure 2.5. The test requires the insertion of a wedge into the non-bonded end to develop an initial crack in the adhesive layer, and then monitoring the crack propagation with time. Once wedges have been inserted the specimens is usually exposed to an aqueous environment. The resulting crack growth and mode of failure is monitored. The driving force for the propagation of the crack comes from the stiffness of the adherends separated by the wedge, this driving force reduces as the crack propagates. Upon the introduction of the wedge the crack propagates a length designated 'a'. The crack creates two new surfaces, each of area 'A', and also releases elastic energy stored in the adherends. If the elastic energy in the beams is denoted U_E and the energy to create the two new surfaces is given by U_S, then:

Release rate of elastic energy is given by, $G = \delta U_E / \delta A$

Energy needed to create a unit surface is, $W_S = \delta U_S / \delta A$

The crack will cease to advance when $G = W_S$. When G is higher then W_S the crack will propagate. The wedge test allows a quantitative measure of the strain energy release rate, G, by:

$$G = \frac{3Et^3h^2}{16a^4} \qquad (2.7)$$

Where: E = Young's modulus of the adherend

t = thickness of the beam

h = wedge thickness

a = crack length

The assumptions for using the above equation are that the adherends will not plastically deform, and the specimen compliance is primarily due to beam bending. One disadvantage of the wedge test is the removal of the specimen from the test environment to monitor crack lengths, and whether the viewed crack length is equal to the crack front in the middle of the joint.

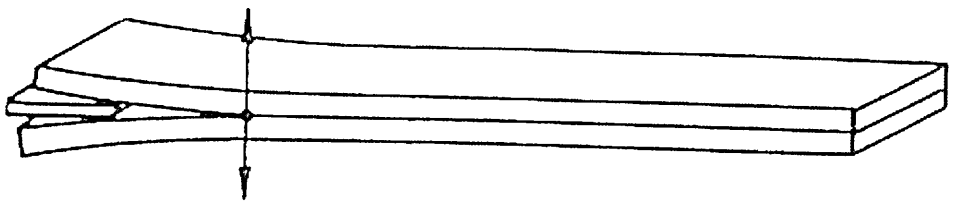

***Figure 2.5** - Wedge test specimen*

2.6.4 Review of Durability Studies

2.6.4.1 Single Lap Joints

Ramani *et al*[55] used lap shear joints manufactured from hot dipped galvanised steel bonded to fibre reinforced unsaturated polyester with moisture cured urethane adhesives. A variety of ageing environments were used, namely, cataplasma and cyclic moisture ageing, UVA ageing and oven ageing in natural convection oven at 60°C (an ageing condition commonly used in the aerospace industry). The most damaging environment was the cataplasma and moisture cycling which imposed the biggest reduction in lap shear strengths, approximately 28% from 5 weeks of exposure. Critchlow *et al*[56] evaluated the retained strength of single lap joints, made from 5251 aluminium alloy, after immersion in distilled water at 60°C. Good durability was attained from the joint incorporating a simple alkaline degrease, despite the high magnesium content on the surface region. Gosselin[57] studies the durability of steel-adhesive bonds using lap shear tests after exposure to high humidity environment. It was concluded that moisture ingression resulted in the greatest reduction in apparent shear strength.

The perforated lap shear specimen, incorporating aluminium adherends, was first appraised by Arrowsmith and Maddison[52], to evaluate the effectiveness of this new test configuration against standard lap shear joints for durability testing. Experimental work found that the perforated lap shear specimens were capable of highly sensitive discrimination between different adhesive combinations and surface pre-treatments. Fay *et al*[53], used stressed perforated steel overlap joints to evaluate several pre-treatments under salt spray and hydrothermal stress conditions. It was found that the durability of steel specimens bonded in the as-received condition performed poorly. The use of a silane primer and Accomet C coating enhanced durability in high humidity environments. The work highlighted that durable joints can withstand long periods of exposure without exhibiting any stress-related loss of strength. Wilson *et al*[58] used stressed aluminium perforated lap shear test specimens to investigate the influence of high humidity, salt spray and outdoor weathering on the durability of Alcan's AVT manufacturing system pre-treatment, that is applied direct to coil product. Their findings found the perforated lap shear configuration provided sufficient sensitivity to show differences in durability when exposed to different environments.

2.6.4.2 Wedge Tests

Rider *et al*[59] used wedge test specimens incorporating 2024 T3 aluminium alloy adherends and FM-73 structural epoxy adhesive, to study the durability of pre-treatments when exposed to 50°C and 95% relative humidity. The pre-treatments examined included, as received condition, methyl ethyl ketone (MEK), grit blasting with 50μm alumina powder and in combination with an organosilane-coupling agent. It was found that roughening the substrate surface increased durability, studies revealed that mechanically treating the specimens increased the fracture toughness of an aluminium-epoxy joint exposed to humid conditions by two orders of magnitude.

Scardino and Marceau[60] used the wedge test to evaluate the long term stressed durability performance of two aluminium alloys, one clad and one bare, used in the aerospace industry. Two types of primer and three surface preparation processes were used; chromic acid anodising, phosphoric acid anodising and forest products laboratory (FPL) etch. Specimens were exposed to a 5% salt spray environment at 45°C for 1 year. The wedge test procedure provided discrimination between the bonding systems to rank the factors that affected joint durability. The phosphoric acid anodising process produced the most durable adhesive joints. In addition the use of a corrosion inhibiting primer also offered increased durability. Armstrong[61] carried out a detailed investigation on the long-term durability of an aluminium alloy bonded with 9 different structural epoxy adhesives. Wedge test specimens were manufactured with 2024 T3 aluminium alloy, incorporating the following pre-treatments; chromic acid anodise, phosphoric acid etch and abrasion with 100 grit paper. The test specimens were immersed in water at room temperature. The significance of choosing the correct adhesive to attain sufficient long term durability was highlighted. Although surface preparation techniques are critical for providing excellent joint performance, durability is dependent on the adhesive's chemistry and it permeability with respect towards water. Elsewhere[62] marine grade 5351-H34 aluminium alloy was bonded with two commercially available epoxies to fabricate wedge test samples. The test allowed the authors to differentiate the effects of environment on the subsequent crack growth rate. Immersion in distilled water and exposure to 0.5% salt spray environment was deleterious on joint durability when compared to standard laboratory conditions. Further work[63] assessed the influence of surface pre-treatments on bond durability, using wedge tests made from L165 clad aluminium alloy bonded with Redux 321/5 epoxy adhesive. The treatments included the Boeing phosphoric acid anodising (PAA) and sulphuric acid anodising, in combination with a phosphoric acid dip and a sulphuric acid/ferric sulphate etch. It was shown that increased bond durability was linked to adhesive penetration into the porous oxide layers. The sulphuric acid anodising produced fine pores which did not allow the adhesive to penetrate, however the phosphoric acid dip in combination with the PAA process opened up the pores and improved durability. It was noted that penetration of the adhesive did not only depend on pore dimensions but also on the contact angle between the adhesive and the substrate, the adhesive viscosity and the viscosity time characteristics at the temperature of application. Similar findings were observed by Jones *et al*[64] when investigating the durability of titanium alloy joints. Five different titanium alloys were used in the study to assess the effects of alloy type and surface pre-treatment on durability using wedge test samples exposed to 50° and 96% relative humidity. The resistance to crack growth was dependent on both surface treatment and alloy type. Resistance was poor when only an alumina grit blast was used, however, good bond performance was attained using alumina grit blasting with sodium hydroxide anodise. A good correlation between joint durability and microporosity of the adherend surface was observed, good durability resulted when adherend surfaces exhibited extensive microporosity and poor durability was obtained from relatively smooth surfaces.

2.6.5 Effect of Stainless Steel Surface Pre-treatments on Durability

Haak and Smith[65] carried out a detailed evaluation of nineteen surface pre-treatments on AM355 stainless steel, bonded with Hysol EA9210 primer and Hysol EA9628H epoxy adhesive. The pre-treatments ranged from simple degreasing, etching and anodising in concentrated acidic solution through to flame and UV radiation treatments. Wedge test specimens were exposed to 50^{0}C and 100% relative humidity to evaluate durability in a hydro-thermal regime. Five surface treatments produced exceptional surfaces for forming strong durable bonds, they are itemised in Table 2.3.

***Table 2.3** – Durable pre-treatments assessed by Haak and Smith[65]*

Number	Description	Temp (^{0}C)	Duration (min)	Wedge test mm/24hrs	Comment
1	$H_2SO_4/Na_2Cr_2O_7$ Etch	75-80	60	1.5	
2	$H_2SO_4/Na_2Cr_2O_7$ Anodise	75	20	1.8	Pb cathode 2V applied
3	H_2SO_4 etch + HNO_3 passivation	75-80 75-80	5 60	2.5	
4	HNO_3/ $Na_2Cr_2O_7$ Etch	75-80	60	2.5	10% w/o HNO_3
5	HNO_3 Anodise	22	60	1.0	50% w/o HNO_3 Stainless cathode 0.9V

From the five methods numbers 1 and 5 were thought to be the most promising for industrial applications. Treatment 3 was deemed unattractive due to the multi stage operation, which would incur added expense without any significant increase in bond durability. All methods, except the HNO_3 anodising, require elevated temperatures, thus again comprising cost and health from the carcinogenic nature of dichromate's. The authors commented on the attractiveness of HNO_3 anodising, because the energy requirement for anodising (approximately 3mW/cm^2) is significantly less than the energy needed to heat large tanks of solution.

The above was taken a stage further[66] to study the mechanism of the adhesive bond, for the most durable treatments with comparisons made to the least resistant joints. Using a plethora of surface analysis techniques the chemical and physical properties of the adherend surfaces were resolved. Electron microscopy showed the least durable surface to be smooth with a bright appearance, whereby durable surfaces showed evidence of attack with an increase in macroscopic roughness. After applying contact potential difference (CPD) to the treated surfaces, the results suggest that not only does the morphology of the surface contribute to an increase in durability, but also the chemical nature of the stainless steel is equally important. If the treatment leaves the surface with sites covered with chemisorbed base OH^-, which bonds strongly to acid functional groups in the epoxy there is no thermodynamic driving force for further reaction with water. This renders the surface stable under hydro-thermal stress and hence durable. However if the surface is left with no

adsorbed OH^-, they are thermodynamically unstable and will react further with water and therefore form non-durable bonds. Interesting to note, it was hypothesised that the strongly oxidising surface treatments, (H_SSO_4-$Na_2Cr_2O_7$ etch), dissolved layers of the steel alloy and that a chromium, nickel, molybdenum intermetallic layer reprecipitates in the form of a chromium-oxide-coated dentritic capillary structure. This suggests enhanced durability of stainless steel epoxy joints may be dependant upon the chromium enrichment of the adherend surface.

Gaskin *et al*[67] studied the effect of various surface pre-treatments on three stainless steel, namely; two austenitic grades AISI 301 and AISI 347, and a precipitation hardened alloy 15-5PH. The surface treatments included;

(1) Wet hone abrasion
(2) Sulphuric acid pickle and sodium dichromate de-smutting
(3) Wet hone abrasion + sulphuric acid-Nacconol etch followed by a nitric-hydrofluoric acid de-smutting
(4) Ferric chloride acid etch followed by a sodium dichromate de-smutting
(5) Sulphuric acid pickle followed by a nitric-hydrochloric acid de-smutting

It was found that the treatment that yielded a stable surface for one particular stainless steel grade, did not perform well for another. Wedge crack extension tests were exposed to 60^0C and 100%RH, for 672 hours. They concluded that for AISI 301 the sulphuric acid pickle faired well. For AISI 347 the sulphuric acid Nacconol etch produced the most stable surfaces, and for the 15-5PH alloy the sulphuric acid pickle followed by sodium dichromate de-smutting should be considered. Unfortunately the chemical compositions and etchant temperatures were not given.

Pocius *et al*[68] noticed variability in the adhesive bonding characteristics of AISI 301 stainless steel, bonded with a compatible epoxy structural adhesive and silane primer. The surface preparation comprised etching in a sulphuric acid/sodium bisulphate bath at 59^0C for eight minutes, followed by de-smutting in a solution of sodium dichromate/sulphuric acid, held at 65^0C for three minutes. Peel specimens were constructed from various coils of nominally the same grade. Differences in peel strength were observed from coil to coil. It was found using high resolution scanning electron microscopy, that peel strength could be correlated to surface microroughness and adherend thickness. This variation corresponded to the electrochemical reactivity of the steel samples in the etch bath, determined by cathodic polarisation curves. The increased peel strength related to the amount of martensite produced in the austenitic grade by the cold working operation.

The resistance to water immersion of lap joints made with austenitic stainless steel was evaluated by Garnish[69]. Three pre-treatments, namely; alkaline degreased, grit blasting and etching were incorporated to assess their degree of aqueous degradation. Table 2.4 below details the results.

Table 2.4 *- Effect of surface pre-treatment on the strength and water resistance of stainless steel lap joints*[69]

		Initial Strength (MPa)		Strength after 30 days water immersion at 40°C (MPa)	
Material	**Treatment**	**23°C**	**80°C**	**23°C**	**80°C**
EN58B	Degrease	23.9	25.6	15.7	17.7
(AISI 321)	Grit Blast	25.6	32.0	14.1	16.7
	Etch	27.4	35.1	27.2	29.7
EN58J	Degrease	27.8	31.9	16.7	17.0
(AISI 316)	Grit Blast	27.3	34.0	29.0	25.0
	Etch	27.8	39.9	30.1	33.6

Although high initial strengths were obtained from all three treatments an enhancement in environmental resistance was afforded from etching in a solution of sulphuric and oxalic acid (~5:1 ratio), at 60°C for five minutes. This outlines the need to use adequate and appropriate pre-treatments when hot/wet conditions are encountered.

2.6.6 Concluding Remarks

The essential function of surface pre-treatments is to clean the adherend surface by removing surface contamination that would act as weak boundary layers. The influence of surface micro-roughness appeared to be an important feature in enhancing the level of adhesion between the adhesive and metallic oxide, possibly encouraging mechanical interlocking on a micro scale. The surface pre-treatment of stainless steel is an indispensable requirement, regardless of complexity, to fabricate bonded structures that will facilitate any applied load or environmental exposure. The previous examples have illustrated that there is no general agreement on which treatment performs best, where results have varied from one researcher/group to the next. One common finding however is the manufacturing path of the alloy is dependent on how good or bad the pre-treatment subsequently performs. Therefore it seems any treatment performing well is related to the precise metallurgy of the alloy concerned, rather than been applied as a guide to other stainless steel grades. The next section considers environmental attack and important factors that influence the susceptibility of adhesively bonded joints to environmental degradation.

2.7 Environmental Attack

2.7.1 Introduction

The increased use of adhesive bonded joints in engineering applications has prompted an improvement to be made in the reliability of these structures during their intended in-service life. Benefits such as weight reduction and excellent dynamic properties compared with traditional joining methods, has been a major driving force for adhesive joint applications in the aerospace and transportation industries. In-service conditions will involve extreme environments, for example adhesive bonds in aircraft are subjected to harsh surroundings. On the runway an aircraft can have

skin temperatures in excess of 50^{0}C at nearly 100% relative humidity; minutes later at altitude ambient temperatures may be –50^{0}C. The drop in temperature coexist with a drop in pressure, which can cause the rapid removal of moisture from the adhesive leading to blister and void formation. In addition the structures encounter stresses from shock loading and vibrations, and exposure to de-icing fluids, fuel and cleaning solvents.

Adhesive bonds in transportation undergo harsh environmental conditions. Apart from extremes in temperature and humidity, joints are exposed to salts and other de-icing agents that chemically react with the adhesive and corrode the metallic substrates. Cyclic stresses are imparted from the terrain, coupled with exposure to ozone, chemical pollutants and seawater from cities and coastal areas. The above has highlighted conditions that severely limit structural adhesive joints and how the joint strength can deteriorate when exposed to working environments. Table 2.5 below which indicates factors that affect both strength and durability, whereby select factors are discussed in more detail.

Table 2.5 *– Factors affecting adhesive joint strength and durability*

Factor	Effects
Water	Absorption causes adhesive to plasticise
Temperature	Elevated temperatures increase degradation process. Possibility of post curing the adhesive.
Adherend	Surface stability. Permeability.
Surface pre-treatments	Chemical and physical compatibility with adhesive and adherend.
Adhesive	Cure temperature. Rheological properties.
Internal stress	Cure shrinkage. Swelling from moisture content. Environmental conditions.
External stress	Strained areas susceptible to attack. Can cause increased rate of diffusing medium. Application and duration.

2.7.2 Effect of Water

The most hostile and indeed commonly encountered deleterious medium for structural adhesive joints is water. When water penetrates into an adhesive bond both reversible and irreversible effects are found. This ingression has two main detrimental effects on joint performance, namely, the adsorption of water by the adhesive and the adsorption of water at the interface. Comyn[70] reported that water may enter the joint by one or more of the following ;

(a) Diffusion through the adhesive.

(b) Transport along the interface, a process which is often referred to as wicking.

(c) Capillary action through cracks and crazes in the adhesive. This is more likely to occur in joints that have been aged rather then those that are freshly prepared.

(d) Diffusion through the adherend if it is permeable, i.e. composites.

Secondly, having entered a joint, water may cause weakening by one or a combination of the following:

(e) Alteration of the properties of the adhesive in a reversible manner, i.e. plasticisation or swelling.

(f) Alteration of the properties of the adhesive in an irreversible manner, i.e. hydrolysis, cracking or crazing.

(g) Attacking the adhesive/adherend interface either by displacing the adhesive or by hydrating the metal or metal oxide surface.

(h) Inducing swelling stresses in the adhesive joint.

2.7.2.1 Water and Solubility

Water is a highly polar molecule that is permeable to most polymers and thus adhesives preferentially adsorb water molecules. The high level of polarity in water molecules is due to oxygen atoms having a net negative charge and hydrogen atoms having a net positive charge. The net negative charge of oxygen provides a site for hydrogen bonding between water molecules. The water molecule's polarity and ability to form hydrogen bonds allow it to dissolve, soften or swell organic substances whose own molecules contain sufficient polar groups, for example strong localised interactions between water molecules and polar groups of epoxides can develop. The relatively small size of a water molecules also encourages it to pass through an organic material, as well as the compatibility with (i.e. effectively soluble in) the polymer. Therefore polar adhesives are hydrophilic in nature i.e. "water liking".

2.7.2.2 Diffusion of water

A film of adhesive exposed to a humid environment or immersed in water will adsorb moisture. In the case of metal-to-metal joints, for water to affect the joint it must enter by diffusion into the adhesive from exposed edges. The rate of water diffusion into a polymer is typically 'non-Fickian', such that the diffusion coefficient is not a constant, however by assuming Ficks law of diffusion it implies that the fractional uptake of water can be associated to the diffusion coefficient by[70];

$$M_t/M_\infty = 4/l \times (Dt/\pi)^{1/2} \qquad (2.8)$$

Where, M_t and M_∞ are the masses of uptake of water at time t and at equilibrium respectively, l is the film thickness and D is the diffusion coefficient. The solubility of water in the adhesive and the diffusion coefficient are calculated by following the mass uptake of water with respect to time.

Brewis *et al*[71] studied the effect of water concentration on the durability of aluminium lap joints bonded with an epoxy based on diglycidylether of bisphenol-A cured with 1, 3-diaminobenzene. Adhesive joints were exposed to 50^{0}C and a variety of humidities for up to 10080 hours. Thin films

of the adhesive were suspended in the various environments to calculate the water adsorption isotherm and diffusion coefficients. The work concluded that there is a clear critical relative humidity of 65%, which corresponds to a critical water concentration in the adhesive of 1.45%, as shown below in Table 2.6. Above 65% relative humidity the rate of joint degradation increases. The mechanism of environmental attack when the critical water concentration of 1.45% was exceeded, is associated with weakening of the interphase region of the joint. It was postulated that salt hydration is an interpretation for this mechanism of attack and for the existence of a critical relative humidity.

***Table 2.6** - Values of diffusion coefficient and equilibrium uptake for experiments from water vapour at 50^{0}C[71]*

Relative Humidity (%)	Diffusion coefficient, D ($10^{-13}m^2s^{-1}$)	Mass adsorbed at equilibrium, M_E(%)
23	7.2	0.54
42	7.4	0.84
66	8.1	1.5
72	8.5	1.6
83	9.7	2.0
86	11.0	2.0
95	12.0	2.1
100	14.0	2.1

Other work[72] investigated the uptake of water for a number of epoxy adhesives at various temperatures. The sorption plots revealed an initial linear region of water uptake up to M_t/M_∞ of 0.6, at which point a plateau occurs suggesting equilibrium has been reached. The linear uptake of water is associated with Fickian type diffusion, which is usually found in the diffusion of polymers above their glass transition temperature, T_g, and not in glassy polymers such as epoxides. Glassy polymers usually show non-Fickian diffusion, resulting in an S-shaped sorption curves where additional water uptake takes place after long exposure times.

De Nève *et al*[73] evaluated the ageing effects on a structural epoxy adhesive exposed to relatively high temperature and humidity. The adhesive was based on DGEBA with dicyandiamide as the cross linking agent. From gravimetric and viscoelasticimetric results, it was found the water uptake was significant at 70^{0}C and 100% relative humidity and that the adsorption was typically Fickian in nature. As water uptake proceeded the glass transition temperature, T_g, and the elastic modulus of the adhesive decreased, these effects were probably due to plasticisation of the polymer.

The behaviour of the diffusion of water between bulk specimens and adhesive joints was compared by Zanni-Deffarges *et al*[74]. Two structural epoxy adhesives were investigated, namely; a modified epoxy based on DGEBA and tetraglycidylmethylene dianiline (TGMDA) with dicyandiamide as the curing agent. The substrate material was a duplex stainless steel, 16% Cr and 4% Ni, which was solvent degreased followed by sandblasting and cleaning with compressed air. All bulk specimens and adhesive joints were aged at 70^{0}C and 100% relative humidity for different times. Using

standard gravimetric techniques the diffusion coefficient, D, was determined for the bulk adhesive samples at 70^{0}C and 100% relative humidity. As water diffused into the bulk adhesive a decrease in elastic modulus was observed. Torsional joint tests using the same adhesives found that the elastic modulus of the adhesive reduced more quickly compared with bulk samples. A composite model based on mechanical properties was developed to estimate the diffusion coefficient, D, for metal/polymer assemblies. After applying the model the value of D was considerably higher compared with bulk samples. It was therefore suggested that the diffusion of water into the adhesive joint is occurring by another route as well as by conventional diffusion into the polymer. The phenomenon of 'capillary diffusion' was proposed where water is entering the joint by seepage close to the interface or in the interface region. The increase in overall diffusion was split into two parts ;

(1) Water diffuses into the thickness of the bulk polymer causing classic ageing and a reduction in mechanical properties.

(2) Water seeps or spreads close to the interface at a faster rate and may then diffuse back towards the bulk of the glueline.

However, the increase in the diffusion coefficient for the adhesive joints may well be related to the effects of shrinkage stresses. These stresses at the interface region can lead to the effective dilation of the polymer producing a less dense structure, thereby assisting water ingress and developing a higher local diffusion coefficient.

2.7.3 Effect of Water on the Adhesive

As mentioned earlier, once water has entered it may cause weakening by one or more of the following: plasticisation, hydrolysis, cracking or crazing, attacking the interface or inducing swelling stresses. The influence of water on the adhesive is commonly reversible, whereby any deterioration in mechanical properties can be recovered by drying. However the extent of reversible or irreversible processes is largely dependant upon the adhesive composition.

2.7.3.1 Plasticisation and Swelling

Plasticisation and swelling are both reversible processes, whereby the mechanical properties and glass transition temperatures are adversely affected. Many workers[75-78] have researched the plasticising effect of water on epoxy resins. Turf and Vinson[77] studied the effect of moisture on two modified epoxy structural adhesives, FM73M and FM300M. For FM73M the T_g reduced from 99^{0}C in ambient conditions to 91^{0}C and 80^{0}C after ageing in 63% and 95% relative humidity respectively. This phenomenon was also observed for FM300M adhesive, where the T_g fell from 155^{0}C to 146^{0}C and 128^{0}C under the same ageing environment. Brewis *et al*[79] considered the effects of exposing aluminium adhesive joints to warm moist air. They found that adhesive joint strength fell as the humidity increased, compared with joints exposed to 20^{0}C and 50% humidity that were unaffected.

The results indicated a linear relationship between the loss in joint strength and the fractional water uptake of the joint, based on the assumption that water entered by diffusion. The work concluded that joint strength was impeded by plasticisation of the adhesive.

Water uptake by adhesives may further impair properties caused by swelling. The swelling of adhesives causes a volumetric change that introduces residual stresses into the joint thus weakening bond performance.

2.7.3.2 Hydrolysis

Hydrolysis requires the presence of water, and in addition the accompaniment of a strong acid or base. This degradation mechanism is activated by elevated temperatures and stress on the joint[70]. Hydrolytic attack can affect the adhesive or the adhesive/adherend interface, and its effects are irreversible. Specific chemical linkages are susceptible to hydrolytic attack, e.g. ester groups, and if present in the adhesive or interfacial region are inclined to react with water, i.e. that has either entered the joint or bulk of the adhesive. In the presence of water with a high pH, hydrolytic attack on the ester groups causes chain shortening or main chain scission in the adhesive. This can lead to a loss in the cohesive strength of the adhesive and in certain circumstances catastrophic failure. The work of Antoon *et al*[80,81] studied the hydrolysis of epoxides using Fourier transform infrared spectroscopy, FTIR. A structural epoxy adhesive based on DGEBA-MNA and dimethylbenzylamine resin was immersed in water at 80^0C for up to 90 days. In the first few weeks of exposure there was evidence of hydrolysis and the leaching out of un-reacted anhydride[80]. The irreversible affects of hydrolysis were more profound with the application of stress[81]. The relative ester content fell as the applied stress increased, unstressed specimens were unaffected as shown in Figure 2.6. Further studies on water induced ageing are described by Comyn[70].

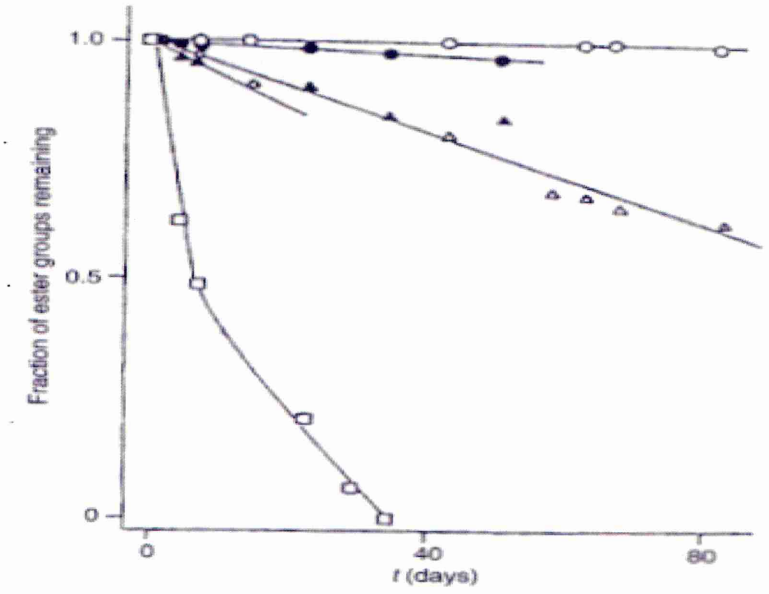

Figure 2.6 *- Relative ester content against time under varying applied loads*[81]

2.7.3.3 Cracking and Crazing

Cracking or crazing of the adhesive may occur after prolonged exposure to moisture. Cracking or crazing is probably more important than hydrolysis[70], especially when adhesives are exposed to varying climatic conditions. An example is the exposure of epoxide-fibre composites to thermal spikes to simulate flight conditions of military aircraft. A supersonic dash will cause aircraft skin temperatures to rise from below zero to 150^{0}C, and once at cruising speed the temperature will fall back to below zero. Adhesives within the aircraft will contain moisture from the atmosphere, but voids will be formed at temperatures above boiling point. Browning[82,83] exposed an epoxy resin to thermal spikes, and found equilibrium water uptake to increase with spiking. Samples were subjected to one or four spikes per day, and subsequent weight gains were proportional to the number of spikes. Evidence of micro-cracking was observed using scanning electron microscopy, it was concluded that the water entered the adhesive and was retained by the cracks. The T_g was not depressed, so the additional water adsorbed did not contributed to plasticisation. Cracks therefore may increase the rate of water ingress, and lead to a growth in the coefficient of diffusion. Also the crack may grow due to the effect of water, a possible mechanism for this is a change in joint strength at the crack tip thus causing a reduction in cohesive energy[70].

2.7.4 Effect of Water on the Interface

2.7.4.1 Displacement of the Adhesive

For any long-term durability to be attained by an adhesive joint, the most important factor is the stability of interfacial adhesion against moisture. As previously discussed the ingress of water into an adhesive can result in irreversible changes such as hydrolysis and cracking. However, the adsorption of water into an interface may cause displacement of the adhesive, hence leading to premature failure. There is considerable evidence to support the locus of failure (discussed in more detail in section 2.8.2.6) of adhesive joints changes from cohesive within the adhesive to failure within the interfacial zone after exposure to moisture. The intrinsic stability of this adhesive/adherend interfacial region in the presence of a liquid may be treated using a thermodynamic approach, as initially proposed by Gledhill *et al*[84]. The thermodynamic work of adhesion, W_A, as defined in section 2.2.2 is the energy required to separate a unit area of two phases forming an interface. If only secondary forces are acting, i.e. van der Waals forces, then the work of adhesion in a liquid environment is expressed as:

$$W_{AL} = \gamma_{AL} + \gamma_{SL} - \gamma_{AS} \qquad (2.9)$$

Where γ_{AL} and γ_{SL} are the interfacial free energies between the adhesive/liquid and substrate/liquid interfaces respectively. The values of W_A and W_{AL} can be determined from:

$$W_A = 2(\gamma_A^D \gamma_S^D)^{1/2} + 2(\gamma_A^P \gamma_S^P)^{1/2} \qquad (2.10)$$

And

$$W_{AL} = 2[(\gamma_L - (\gamma_A^D \gamma_L^D)^{½} - (\gamma_S^D \gamma_L^D)^{½} - (\gamma_A^P \gamma_L^P)^{½} - (\gamma_S^P \gamma_L^P)^{½} + (\gamma_A^D \gamma_S^D)^{½} + (\gamma_A^P \gamma_S^P)^{½}] \quad (2.11)$$

Where, D and P denote the dispersion and polar forces of the surface free energy, γ, and are determined from contact angle measurements. Typical values of γ_S^D and γ_S^P are shown in Table 2.7[1].

Table 2.7 *- Typical values of dispersion and polar force components*[1]

Material	Surface Free Energy (mJ/m^2)		
	γ^D	γ^P	γ^{Total}
Ferric Oxide	107	1250	1357
Aluminium Oxide	100	577	677
Silica	78	209	287
Water	22	50.2	72.2
Toughened Epoxy	37.2	8.3	45.5
Amine-Epoxy	41.2	5.0	46.2

A negative value of W_{AL} indicates that the surface is unstable and will dissociate, where as a positive value indicates the interface is thermodynamically stable. When there is a change from positive to negative for the work of adhesion there is a driving force for the displacement of the adhesive on the adherend surface by the liquid. Therefore if an adhesive joint was exposed to such an environment there will be progressive encroachment into the joint of debonded interface. It is further noted[85] that this will have the effect of progressively changing the locus of failure to interfacial between the adhesive and adherend. And that the thermodynamic approach also reveals that since both metal oxides and water are relatively polar, water will have a tendency to be preferentially adsorbed on to the oxide surface and create a weak boundary layer between the adhesive and the metallic oxide. Therefore high energy metallic adherends are the most difficult materials to adhesively bond when trying to ensure a long durable in-service life in the presence of moisture. Table 2.8 shows examples of values of W_A and W_{AL} for a variety of interfaces and environments.

Table 2.8 - *Values of W_A and W_{AL} for various interfaces and environments*[85]

Interface	W_A in inert medium	W_{AL}	Interfacial debonding
Epoxy adhesive/ferric oxide (mild steel)	291	22 (ethanol)	No
		-166 (formamide)	Yes
		-255 (water)	Yes
Epoxy adhesive / aluminium oxide	232	-137 (water)	Yes

Epoxy adhesive / silica	178	-57 (water)	Yes
Epoxy adhesive / CFRP	88-90	22-44 (water)	NO
Vinylidene chloride – methacrylate copolymer / polypropylene	88	37 (water)	No
		1.4 (Sodium n-octyl sulphate)	No
		-0.9 (Sodium n-dodecyl sulphate)	Yes
		-0.8 (Sodium n-hexadecyl sulphate)	Yes

The thermodynamic approach does not take into account the effect of interfacial adhesion forces arising from primary bonds or mechanical interlocking. Also this approach provides no information on the kinetics of the failure mechanism, therefore it cannot be used to predict the expected in-service life of adhesive joints. It is solely used to provide an indication of interface stability, however, when coupled with a continuum fracture mechanics approach as developed by Gledhill *et al*[86], service life predictions can be made. One disadvantage of the thermodynamic approach as commented by Comyn[70], is that it implies that joint strength will fall to zero, but in many cases it levels out at a moderate fraction of the initial dry strength. In addition, it does not allow for the recovery of strength upon drying, as once the adhesive is displaced it seems unlikely that there would be sufficient molecular mobility for the adhesive to re-establish contact with the substrate. Additional complications arise when the surface of the adhesive has been cured against a substrate, when compared to the same adhesive cured in air as a bulk specimen. The values of γ^D and γ^P for the bulk adhesive may not reflect the behaviour of the adhesive joint, as a consequence of orientation or preferential adsorption of one adhesive component at the interface, chemical bond formation across the interface or mechanical interlocking.

2.7.4.2 Primary Forces across the Interface

The rate of water penetration is dependent upon a number of factors, such as an increase in temperature, application of external stress, internal stresses and swelling stresses.

2.8 Surface Characterisation and Failure Analysis

2.8.1 Surface Characterisation Techniques

2.8.1.1 Introduction

There are a variety of surface analytical techniques available for measuring the composition of a solid surface. The analysis of the properties of surfaces is becoming more commonplace in adhesion related studies. The properties of a thin film or of a surface can be very different from those of the bulk material[87]. These differences may form where, for example; there are changes in atomic bonds between the surface and the bulk, segregation of alloying elements, adsorption of molecules from gases or liquids and oxide layers. The properties of a surface are governed by their interaction with its environment; therefore it is easy to understand why the properties of surfaces have such an immense effect on adhesion related phenomena. By the early 1970's major advances in several surface analytical techniques had been made, these include; X-ray photoelectron

spectroscopy (XPS), Auger electron spectroscopy (AES), secondary ion mass spectrometry (SIMS) and secondary neutral ion mass spectrometry (SNMS). Each technique has the ability to determine the composition of the outermost atomic layers the advantages and limitations of each technique are given in Table 2.9[87].

***Table 2.9** - Advantages and limitations of XPS, AES, SSIMS and SNMS[87]*

Technique	Advantage	Limitation
XPS	Is sensitive to 2-10 monolayers; metal< oxides<<polymers. Can detect about 10^{-3} at.% Is quantitative to ~10 to 20 % without standards. Is especially useful for chemical shifts from the same element in different compounds. Is the least destructive of all techniques. Has a sensitivity range within a factor of 10 for most atomic numbers. Has minimal sample charging.	Has relatively poor lateral resolution and poor imaging capability. Requires deconvolution techniques, for example surface monolayer. Has inadequate data acquisition rates for compositional depth profiles, inferior to other methods. Sample may suffer from carbon contamination.
AES	Is sensitive to 2-10 monolayers. Can detect about 10^{-3} at.% Is outstanding for compositional depth profiles. Is quantitative to ±10% with standards. Has superb lateral resolution (20-50nm). Is fastest of the four methods. Has superb imaging and lateral mapping capabilities. Is useful for the chemical shifts of some elements.	May alter surface composition from ESD. May have severe charging problems. Will form carbon from polymers (electron beam cracking). Has a slow rate of element mapping.
SIMS	Is sensitive down to 1-2 monolayers. Can detect 10ppm or less. Is superb for compositional depth profiles. Can detect isotopes. Can detect hydrogen and deuterium present. Can acquire data rapidly. Has lateral imaging capability. Molecular information.	Requires sample destruction. Is quantitative with difficulty at best. Has varying elemental sensitivity. Has complex spectra. May have chemical state changes from ion bombardment.
SNMS	Has first 6 advantages of SSIMS. Is quantitative with modest use of standards.	Requires sample destruction. May have chemical state changes from ion bombardment.

2.8.2 Techniques

2.8.2.1 *X-Ray Photoelectron Spectroscopy, XPS*

XPS is widely used in many areas of adhesion related studies, and has been reviewed in great depth[87-90]. In XPS, the specimen of interest is excited by some form of controllable energy (the excitation source) and its subsequent response to that excitation, in the form of an emission of some species, is observed[90]. In XPS the primary excitation is accomplished by irradiating the specimen by a source of monochromatic X-rays. The X-ray source causes photoionisation of atoms in the specimen and the response of the specimen (photoemission) is observed by measuring the energy spectrum of the emitted photoelectrons. The resultant photoelectrons have a kinetic energy, E_K, which is related to the X-ray energy, hv, by the Einstein relation:

$$E_K = hv - E_b \qquad (2.12)$$

Where E_b is the binding energy of the electron in the material, and is characteristic of the individual atom. The electron binding energy increases with increasing atomic number. Thus information of the binding energies of electrons within a sample allows a direct qualitative analysis. The energy levels occupied by electrons are quantified, the photoelectrons have a kinetic energy distribution consisting of a series of discrete bands that reflects the shell form of the electronic structure of the sample. This causes the electron binding energies within any one element not to be fixed, where small variations of up to 10eV can occur[89]. These variations in binding energy are known as 'chemical shifts'. XPS spectra are produced, by plotting the number of electrons detected per unit energy versus binding energy. The energies of the peaks allow elemental identification and provide chemical state information on the surface. The heights or areas of the peaks permit the quantification of the elements present.

2.8.2.2 *Auger Electron Spectroscopy, AES*

Davis[87,88] gives a comprehensive review of AES principles and topics related to adhesion. AES is commonly used to supplement XPS studies, however quantitative and chemical state analyses are not as good. AES in combination with inert ion sputtering can provide depth profiles. AES involves bombarding the surface of the specimen, under vacuum, with 2-10keV electrons which ionise some of the atoms, causing a vacancy in a core electron energy level. The energy of this ion is reduced when an electron drops down to fill the core vacancy. To conserve energy a second electron is emitted from the atom, hence it is doubly ionised. The kinetic energy, $E_K(WXY)$, of an Auger electron from transition WXY is given by;

$$E_K(WXY) = E_B(W) - E_B(X) - E_B(Y) \qquad (2.13)$$

Where; $E_B(W)$ is the binding energy of an electron in core level W, which had the initial core hole. And $E_B(X)$ and $E_B(Y)$ are the binding energies of electrons in levels X and Y in the presence of a hole in level W. This is illustrated schematically in Figure 2.7. With the exception of hydrogen, helium and gaseous lithium, elements are identified by a unique spectrum with one or more Auger peaks.

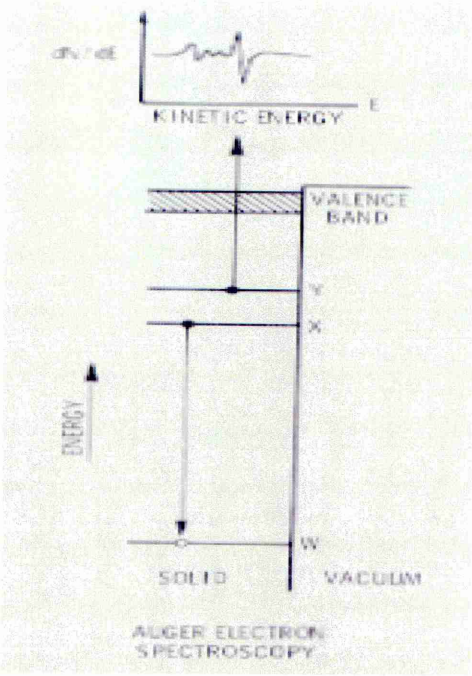

Figure 2.7 - *Schematic representation of a WXY Auger transition and typical spectrum*[88]

2.8.2.3 *Secondary Ion Mass Spectrometry, SIMS*

SIMS is the mass spectrometry of elemental and molecular ions which are emitted when a surface is bombarded by energetic primary particles, a process known as sputtering. Sputtering occurs when the primary particle loses energy and momentum when colliding with the surface. This sets up a collision cascade and can result in the ejection of material from the surface. Approximately 99% of sputtered material carries no charge, but the remaining 1% will be ionised. This ionised material can be attracted to the mass spectrometer, and a plot of mass/charge ratio versus intensity produces the SIMS mass spectrum. Extracting quantitative information from SIMS data requires an understanding of the relationship between ion yield and total sputtered yield (ions plus neutral species). This relationship depends on many variables such as chemical environment, for examples oxides give a greater ion yield than metals.

2.8.2.4 *Sputtered Neutral Mass Spectrometry (SNMS)*

As mentioned approximately 99% of species emitted under ion bombardment of a solid surface carry no charge. These neutral species are far more representative of a sample surface, than the secondary ions generated in SIMS. A mass analysis of these neutral atoms/molecules is termed the 'sputtered neutral mass spectrum'[91]. To acquire a SNMS mass spectrum, ions generated during the sputtering process must first be electrostatically rejected. The neutral species are then post ionised by electron bombardment and mass analysed. SNMS is far less sensitive than SIMS because the neutral species can not be attracted to the mass analyser and so it is only those with

the correct trajectory to take them to the post ionisation region that are analysed. However, because SNMS data does not suffer matrix effects[87] it is much more amenable to quantification through the application of appropriate sensitivity factors. The reduced sensitivity associated with SNMS is compensated by using a high energy incident beam. The technique is therefore erosive and the incident beam etches the surface as the experiment continues. By collecting a mass analysis as the etching process continues a SNMS compositional depth profile can be produced.

2.8.2.5 Applications

It is useful to assess chemical changes that have taken place after surfaces have been pre-treated prior to adhesive bonding. Bouquet *et al*[92] studied 15 different surface treatments used to bond AISI 304 stainless steel. The chemical composition of the surfaces was assessed using XPS and SIMS, combined with erosive techniques to determine the thickness of the oxide layers. It was noted the thickest layer was obtained using a sulphuric-chromic acid etching, where the oxide has a thickness of 250nm. It was observed that there was a correlation between bond strength, surface topography and the oxide film composition. Critchlow *et al*[93] used AES, in combination with SEM and atomic force microscopy, to determine the surface composition of plain carbon steel treated with several conversion coatings, silane primer and simple alkaline degrease. Pre-treated surfaces were characterised in terms of surface contamination, i.e. the concentration of carbon on the surface. Enhanced durability was observed for specimens containing relatively low levels of carbon contamination, the work demonstrated that low carbonaceous surface allow the adhesive to readily wet the adherend surface. Critchlow and Brewis[56] used AES to determine magnesium to aluminium ratios on coupons of 5251 aluminium alloy both before and after grit blasting with different sized alumina powder. The largest Mg:Al ratio was detected on the alkaline degreased surface, grit blasting irrespective of media size reduced the Mg:Al ratio. The alkaline degreased offered the most durable joints, despite the fact the result was in contrast to work by Kinloch *et al*[94] who found that for alkaline degreased only joints incorporating aluminium adherends, environmental durability was poor when high magnesium content substrates were used. Dillingham *et al*[95] incorporated XPS combined with several other surface analytical techniques to determine the near surface properties of titanium-6Al4V alloy, 2024-T3 aluminium alloys and interstitial free steel. XPS studies detected carbonaceous material on all surfaces, possibly as a carbonate or bicarbonate, it was noted that different behaviour was apparent when used as adherends during the long-term environmental exposure. Additional work by Brewis *et al*[96] review several applications where AES, Static Secondary Ion Mass Spectrometry (SSIMS) and XPS have been used to evaluate the chemistry of surfaces before and after pre-treatments.

2.8.2.6 Failure Analysis

Adhesively bonded metal joints can fail in a variety of ways. It is essential to determine the locus of failure within bonded structures, in order to understand the cause of failure and identify the weakest link. The adhesive 'system' consists of several components and interfaces as shown in Figure 2.8.

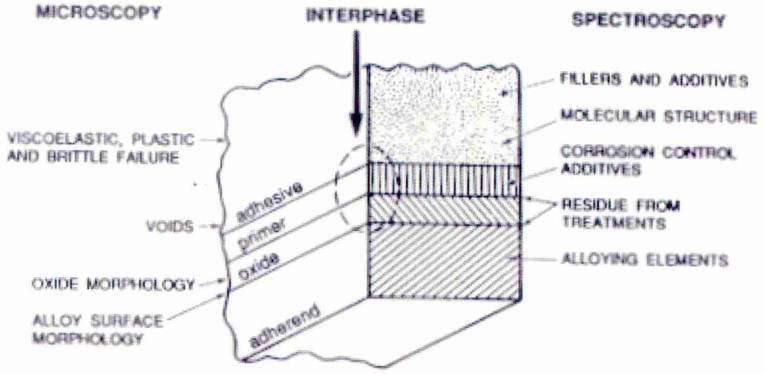

Figure 2.8 - Interfaces of an adhesively bonded metal joint[97]

Each interface is linked to it neighbour, the weakest link in the chain will determine the strength and durability of the joint. Bond failure either initially or after environmental exposure can occur in one of four modes; cohesive, interfacial, adhesive or mixed, these are illustrated in Figure 2.9. Cohesive failure can occurs within the adhesive, oxide layer or adherend. Interfacial failure takes place between the metal oxide and metallic substrate or between the adhesive and primer. Adhesive failure, generally implying a reduction in performance, occurs between the adhesive/oxide or adhesive/primer interface. The visual inspection of fractured surfaces is the first step of failure analysis. If cohesive failure within the adhesive has occurred then visual analysis will be adequate. The human eye is not able to detect thin layers of less than 100nm[98]. For this reason it is difficult to identify the true loci of failure because, for example, a failure may visually appear interfacial or adhesive, but the crack may have advanced within one of the bond components close to an interface. To fully elucidate the loci of failure both faces of the fracture are examined using surface analytical techniques such as XPS, AES and SIMS. Knowledge of the chemical composition and any possible surface contaminants is useful when interpreting failure analysis results. A solitary element or chemical state can be used as a fingerprint or identifier of the surface chemistry of the fractured specimens. For example the filler material in adhesives or the obvious elements of the associated metal oxide can be used as fingerprints.

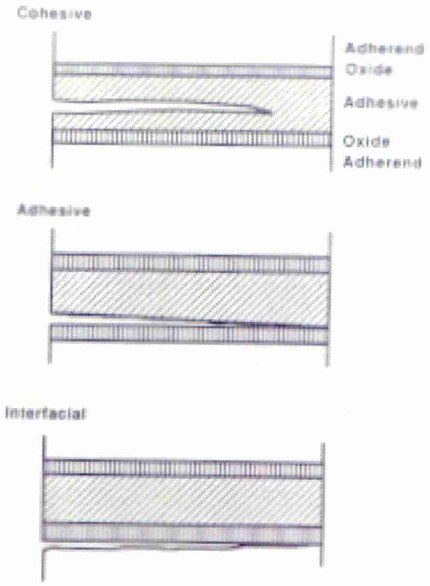

***Figure 2.9** - Possible loci of failure of an adhesively bonded joint*[98]

After adhesively bonded metal-to-metal joints have been exposed to wet conditions many researchers[11,42] confirm the mode of failure is usually at or near the surface. The use of the surface analytical techniques to attain the loci of failure in adhesively bonded structures will now be discussed. Guimon *et al*[99] fabricated single overlap joints comprising of an epoxy bonded to (i) hot dipped galvanised steel (G2F) and (ii) electroplated phosphated steel (EZ2). The specimens were aged in two ways; firstly specimens wrapped in cotton, soaked with distilled water sealed in a polyethylene bag and place in an oven at 70°C for 28 days, secondly specimens were immersed in water at 90°C for 8 days. XPS analysis was carried out on un-aged and aged samples to establish the locus of failure and determine the nature of the environmental attack. Failure analysis revealed that the ingress of water into the bond area was responsible for; (i) the dissolution of the phosphate layer starting from the edges of the bonded joints for EZ2 samples, and (ii) the dissolution of aluminium oxides on the metal interfacial side of G2F samples. For both specimen types the failure occurs in a layer of zinc corrosion products.

In addition to zinc coated steels, also denoted EZ2 and G2F, Bremont and Brockmann[100] investigated aluminium alloys (2024-T3 and 5225) all bonded with an epoxy/dicyandiamide adhesive to form lap shear and T-peel specimen. Samples were exposed to total immersion in water at 70°C or 90°C and a 5% salt spray environment at 35°C. The degradation mechanisms of the specimens after ageing were investigated using XPS, it was found for aluminium based joints the bonds failed in a layer of hydrated aluminium oxides.

Hong *et al*[101] showed the durability of steel joints prepared by curing epoxide adhesives against oil contaminated substrates using amidoamine curing agents depended on the amine number of the

curing agent. When joints were immersed in boiling water, epoxide adhesives cured with amidoamines having high amine numbers delaminated from oil contaminated steel substrates before those cured with amidoamines having low amine numbers. XPS showed that the adhesives prepared using curing agents having a high amine number were unable to displace the oil from the substrate. Failure of such samples during boiling water immersion was within a layer of oil between the adhesive and the substrate. Whilst for samples incorporating the curing agents with low amine numbers were able to displace the oil form the adherend. Little oil was detected on the fracture surfaces of these samples. In addition joints using silane primers based on, γ-glycidoxypropyltrimethoxysilane (γ-GPS) and N-(2-aminoethyl)-3-aminopropyltrimethoxysilane (AAMS), improved durability. Increased amounts of epoxy were detected on the fracture faces indicating the silanes had helped the epoxy displace the oil contamination.

Kinloch *et al*[102] used XPS and electron spectroscopy techniques to identify the mechanisms of environmental attack exhibited by tapered double cantilever beam specimens, comprising 2014A aluminium alloy adherends and hot curing toughened epoxy, when subjected to cyclic loading coupled with immersion in room temperature distilled water. It was shown the role of the interface was crucial in determining joint durability. Specimens pre-treated with alumina grit blasting performed worst; the locus of joint failure was along the adhesive/oxide interface. For phosphoric acid anodise pre-treated specimens, fatigue failure occurred from the weakening and failure of the oxide layer. Superb durability was achieved from specimens pre-treated with chromic acid anodising process. No failure was observed through the interface, and that the adhesive had penetrated into the microstructure of the oxide and formed a 'micro-composite'.

Gettings *et al*[103] using AES and XPS to study the locus of failure in mild steel epoxy bonded joints under dry and wet conditions. Failure analysis indicated that in dry joints fracture occurred near an epoxy/metal interface. For specimens exposed to wet conditions, fracture occurred between the iron and iron oxide hence the joint failed in an interfacial manner. They concluded that although they studied mild steel epoxy joints, they reasoned interfacial failure would occur for any epoxy to metal bonded systems after sufficient exposure to wet environments.

2.9 Fatigue

2.9.1 Introduction

The unexpected and detrimental failure of materials from the application of cyclic loading is known as *'fatigue failure'*. In engineering structures and components cyclic loads are often imposed, causing failure at stresses lower than those under monotonic loading. This form of failure phenomena accounts for a large percentage of engineering failures, thus highlighting the importance for the designer to take appropriate actions. The majority of fatigue testing and analysis has traditionally being based on metals. However, with the growth of adhesive bonds utilised in primary and secondary structures, the need for reliable fatigue data for adhesively bonded joints is greatly required.

The following section will review various aspects that affect the fatigue performance of adhesive joints, be they impart parameters associated with mechanical testing, joint configuration or factors imposed from environmental exposure.

2.9.2 Effect of Adhesive Formulation

The choice of adhesive is of paramount importance and must be compatible with the adherends to be bonded and conditions the structure is likely to encounter. Chernenkoff[104] investigated the fatigue performance of single lap joints, incorporating two low carbon steels (one pre-primed and one electrogalvanised). A total of four structural adhesives were considered, namely; toughened epoxy, vinyl-epoxy, expandable epoxy and epoxy-acrylic, each deemed suitable for automotive applications whilst offering sole advantages and limitations. Dynamic testing was performed with a constant amplitude, load controlled, tension-tension pattern. The results concluded the highest fatigue strength was obtained from the toughened epoxy and the epoxy-acrylic adhesives. Interestingly the fatigue performance was increased when the cyclic creep strains in the bonded area were kept to a minimum.

A comprehensive study by Mackie and Su[105,106] on the effects of ageing and environment on the static and fatigue strength of adhesive joints, also highlighted the significance of selecting the correct adhesive system. Double lap joint specimens bonded with a variety of modified epoxies and bright mild steel adherends, were aged for 8-9 years in 6 environments. Static and fatigue testing after environmental exposure was compared to that of control samples tested prior to ageing. Fatigue tests were load controlled with a sinusoidal tension - tension cycle at a frequency of 15Hz. Apart from indicating that adhesive joints can tolerate long periods of environmental ageing whilst retaining a sufficient level of fatigue strength, the work pointed out that the effects of long term ageing on the static strength may contradict that of fatigue resistance. The adhesive that achieved the superior fatigue life was the epoxy adhesive cured with polyamine hardener, which formed good initial joint strengths and has a high Young's modulus. Although a similar resin was used in all adhesives, the selection of the hardening compound was critical. However, it should be noted that

all adhesives were cold cured so any improvement in durability or strength offered from curing at elevated temperatures was eliminated. The fatigue performance of toughened epoxy adhesives was also evaluated by Luckyram *et al*[107]. Bulk adhesive compact tension specimens were manufactured from a single-part, hot cure type and a two-part cold cure system. The single-part, hot cure adhesive offered the superior performance. Upon inspection there was no evidence of crazing on the fracture surface of the single-part adhesive, however, the fracture surface of the two-part adhesive indicated crazing had occurred suggesting this was the main energy absorption mechanism. Other workers[108] have implied that enhanced fatigue performance in polymeric materials is characteristic of a high fracture toughness, conversely in the above work the single-part epoxy had the lower fracture toughness.

Further studies[109] assessed the fatigue strength of an epoxy-polyamide structural adhesive and it's modification with the addition of carboxy-terminated butadiene acrylonitrile (CTBN). Using butt-joint specimens manufactured from 0.15%C steel adherends with an adhesive thickness of 0.1mm, non-impact fatigue tests were conducted in air. Results are shown in Figure 2.10 on an S-N diagram.

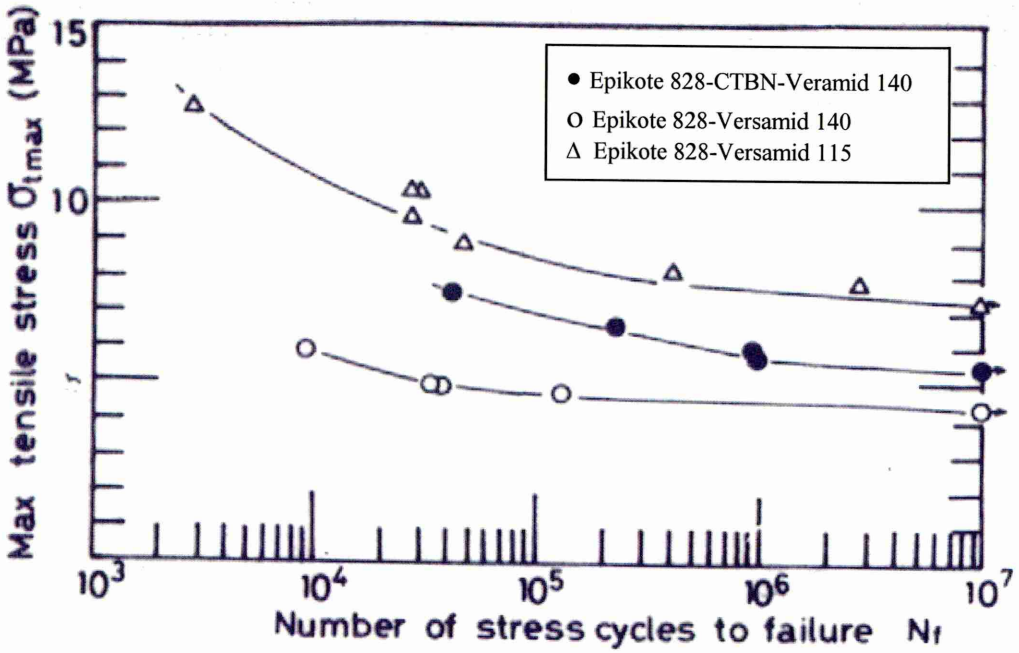

***Figure 2.10** - Effect of adhesive modification on fatigue strength*[109]

Comparing the black and white circular points on Figure 2.10, which corresponds to the CTBN modified adhesive and the standard type respectively, the fatigue strength increases with the addition of CTBN. The authors concluded that CTBN inclusion attributed to the dispersion of rubber particles that absorb impact energy and hinder the development and growth of voids. However, CTBN addition may reduce the residual stresses that evolve when the adhesive is curing, thus

minimising areas of crack initiation sites. Another observation indicates the increase of fatigue strength was directly related to the increase in the loss tangent of the adhesive with CTBN modification, implying that fatigue strength can be correlated with the internal friction loss. Furthermore the above authors[110] investigated the fatigue response of the aforementioned epoxy-polyamide adhesive, modified by adding 15 wt% of chrysotile asbestos filler agent, a practice commonly used to reduce manufacturing costs. The fatigue life and static strength of butt joint specimens was enhanced when filler additions were made. Thus proposing the filler ascribes some form of reinforcement in the adhesive layer, providing increased resistance to tensile loading.

The above discussion places emphasis on the need to select a suitable adhesive system where any form of cyclic loading is applied. Although epoxies account for most structural adhesive applications, it has been highlighted how crucial the other components in the formulation, i.e. hardener, toughening agent and fillers, are in offering increased dynamic performance.

2.9.3 Effect of Test Frequency

The effect of frequency as a test parameter has received a limited amount of investigations from the adhesion community. Chen *et al*[111] using plastic to plastic and metal to plastic single lap joints assessed, amongst other factors, the effect of fatigue frequency in the range 0.55 - 1.5Hz. They concluded that the fatigue performance of epoxy (unnamed) loaded joint was not dependent on test frequency. The frequency range may not of been capacious enough for any effect to be detected. Similar observations were reported by Kayaki *et al*[112], where cold rolled steel sheet (SPCC) was bonded with an epoxy adhesive (E6973: Sunstar Engineering) to form single overlap joints. Specimens were tested in tension-tension sinusoidal pattern with a stress ratio of 0.1. When loaded between a cyclic range of 10-30Hz, virtually no effect fatigue life was attributed to frequency effects, as shown in Figure 2.11. In addition Luckyram *et al*[107] reviewed numerous crack growth models and highlighted that none of them takes into account the frequency of the loading path. Nevertheless no frequency dependence was detected, with consistent behaviour between the range 0.5-5Hz. However, the authors highlighted the possibility a different result could be obtained at more extreme frequencies. For example at very low frequencies, creep influences adhesive response and at very high frequencies thermal effects can come into play.

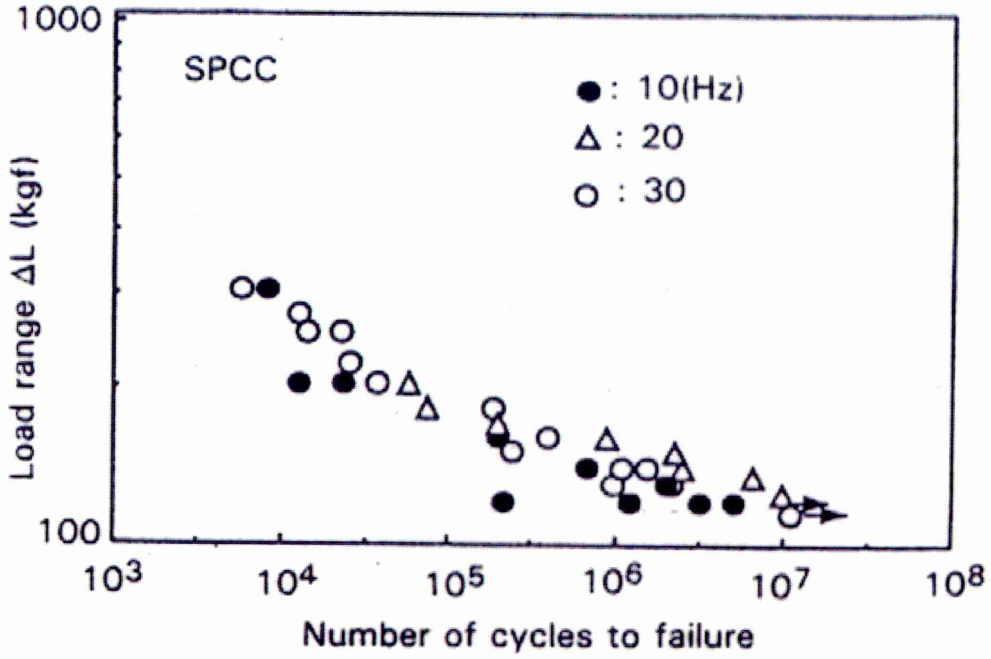

***Figure 2.11** - Effect of frequency on fatigue behaviour*[112]

Xu *et al*[113] conducted mode I fatigue crack growth tests, using steel to steel double cantilever beam (DCB) specimens. Two unnamed structural epoxy adhesives: Adhesive 'A' – filled, adhesive 'B' – filled and toughened, were used. The effect of cyclic frequency was appraised by applying as follows: Frequencies of 20 and 2Hz to adhesive 'A' and frequencies of 20, 2, 0.2 and 0.02Hz to adhesive 'B'. They found the fatigue crack rate (FCR) for adhesive 'A' was relatively independent of frequency. Whilst the FCR for adhesive 'B' increased with decreasing frequency. Using SEM fractography the authors found the fracture surfaces of both adhesives did not change as the frequency was altered. They postulated the fatigue mechanism, for both adhesives, involves microcracking ahead of the major crack and the subsequent linkage of these microcracks with the main crack. The study concluded the variance in behaviour of the two adhesives was ascribed to the variation of strength of the adhesives with strain rate, resulting in different plastic zones. The plastic zone ahead of the crack tip in adhesive 'B' was greater than that in adhesive 'A', and increased in size as the cyclic frequency was decreased. Therefore demonstrating that a rubber-toughened matrix does not guarantee improved fatigue performance. However, it should be noted the above testing was carried out in ambient laboratory conditions with no environmental exposure.

Similar studies by Joseph *et al*[114] used a room temperature curing epoxy composed of a standard DGEBA resin, Epon 828, blended with an aliphatic diglycidyl ether epoxy resin, Epon 871. The epoxy mixture was cured with a polyamide curing agent, V-40. DCB specimens were constructed from aluminium (6061T-6) adherends and cyclic loaded at frequencies of 1, 3 and 5Hz in ambient

conditions. The authors found fatigue crack growth to be relatively frequency independent in the 1-5Hz range.

2.9.4 Effect of Environment and Surface Pre-treatments

Recently Briskham[115] applied cyclic stress regimes to single overlap joints, in an attempt to assess the durability of several aluminium pre-treatments when immersed in water at 55±1°C and its effectiveness as an accelerated test procedure. To minimise the time required for the hostile environment to affect the bond, 5.5 mm diameter holes were drilled in aluminium (6063 T6) and Twintex™ (co-mingled polypropylene composite containing 60% glass fibre) adherends, so when joints were formed the hole was situated in the centre of the bond area. The apparatus allowed four specimens to be tested simultaneously with a cyclic stress set between 0.15 and 1.2Mpa at a frequency of 2Hz. The surface pre-treatments used for the aluminium are shown in Table 2.10, Twintex adherends were solvent wiped using IPA. Metal to metal joints were bonded using Terokal 5051-LV2 heat cured epoxide adhesive, whilst the hybrid joints were fusion bonded. For the hybrid specimens the Alodine 4840 and PAA treatments performed well with the latter been the superior, as shown in Figure 2.12. This was in good agreement for results obtained for unstressed specimens, shown in Figure 2.13. For the aluminium-aluminium joints the best performing pre-treatment was PAA, though EP2472, hydrated oxide and Bonder 787 performed relatively well. However, the results are not in good agreement with those for unstressed durability.

***Table 2.10** - Aluminium surface pre-treatments[115].*

Pre-treatment	Description
PAA	Phosphoric acid anodise, conducted to Boeing spec. BAC 5555
Alodine	Titanium/zirconium based conversion coating with polymeric constituent
EP2472	Zirconium based conversion coating with polymeric constituent
Bonder 787	Titanium/zirconium based conversion coating with an organic constituent
Hydrated oxide	De-oxidised aluminium hydrated in boiling distilled water
Amino silane primer	1% amino silane in an IPA solvent solution
Epoxide silane primer	1% epoxide silane in an IPA solvent solution
Abrade and degrease	IPA degrease and Scotchbrite™ abrade

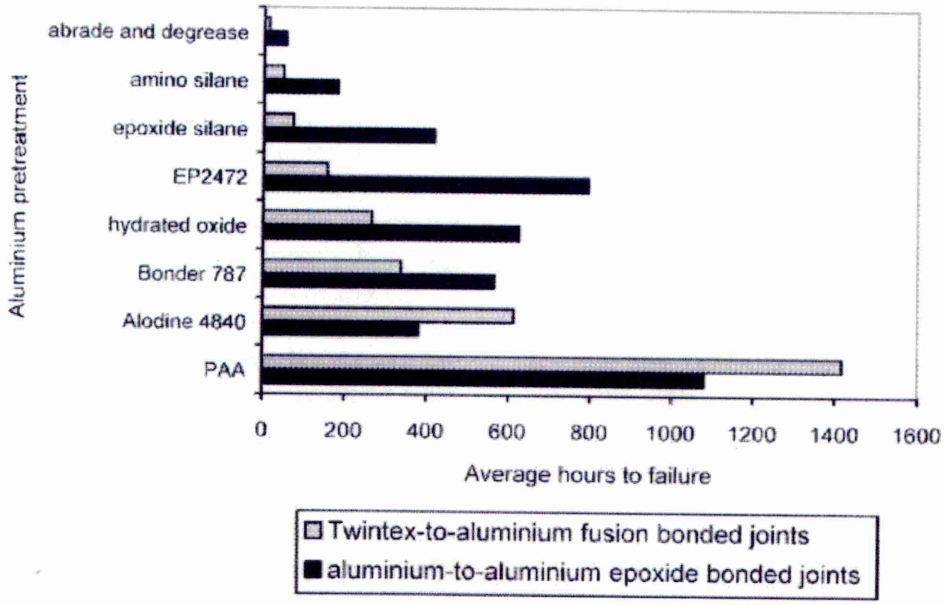

Figure 2.12 - *Hours to failure under a cyclic stress of 0.15 - 1.2MPa immersed in water at 55°C*[115]

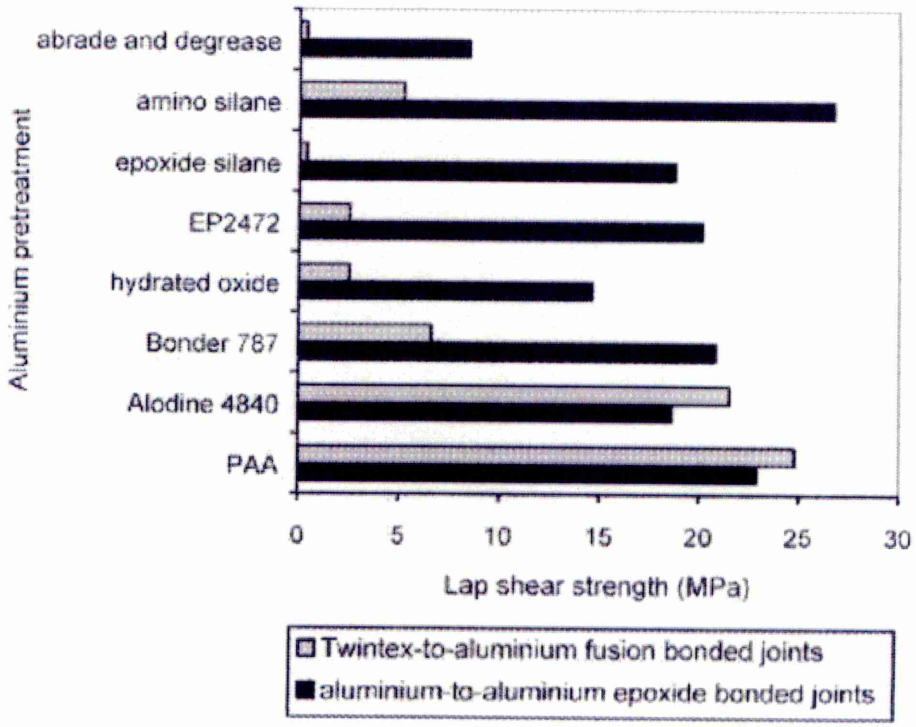

Figure 2.13 - *Remaining lap shear strengths after unstressed exposure to 100%RH at 42-48°C for 1500 h, followed by immersion in water at 55°C for 1500 h*[115]

The results indicate that the categorising of surface pre-treatments under cyclic stress cannot be directly assessed using unstressed specimens. But results suggest the discrimination of pre-treatments using cyclic stress durability testing has the potential for comparing the durability of different adhesive systems more quickly than static stress testing.

In a study by Hirko *et al*[116] five etchant solutions were appraised in an attempt to improve the existing surface pre-treatment of AM355 stainless steel, used for the blade component for AH-64A Apache Attack Helicopters. The pre-treatments used are shown in Table 2.11, pre-treatment 1 is the existing processing path.

***Table 2.11** - Surface Pre-treatments assessed*[116]

Pre-Treatment	Procedure
1. Citric acid/alkaline permanganate etch	Two step process. 19-20% by weight potassium permanganate with 4.5-5.5% by weight sodium hydroxide at 190°F. Immersion time 20 minutes.
2. Sulphuric acid/sodium dichromate etch	30% vol. H_2SO_4 with 40% by weight $Na_2Cr_2O_7$ at 75-80°C. Immersion time 60 minutes.
3. Sulphuric acid/sodium dichromate anodise	26% vol. H_2SO_4 with 40% by weight $Na_2Cr_2O_7$ at 75°C. Anodised using lead cathode and potential of 2V for 20 minutes.
4. Nitric acid anodise	50% vol. HNO_3 for 60 minutes at 3mA/cm^2.
5. Hydrochloric acid/ferric chloride solution	50% vol. HCl with 50% vol. $FeCl_3$. Immersed at ambient temperature for 20 minutes.

Adherends were 1mm thick and 25.4mm wide and constructed single overlap joints with an overlap length of 12.7mm incorporating Hysol EA 9210H primer and EA 9628H adhesive. S-N curves, Figure 2.14, were generated using tension-tension sinusoidal waveform with a load ratio of 0.05. Even though other stainless steel grades are susceptible to hydrogen embrittlement from treatment 5, it surprisingly performed very well, and with the behaviour similar to the existing process a direct substitution of process was made without additional testing.

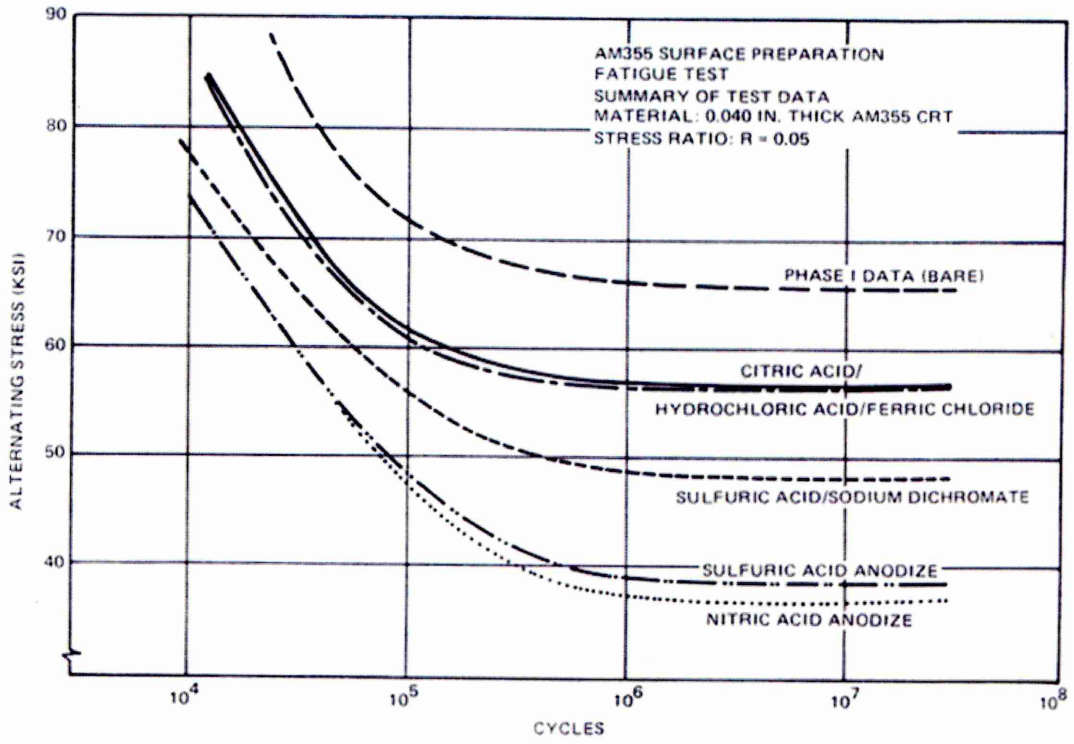

***Figure 2.14** - AM 55 Stainless steel surface preparation fatigue test*[116]

The effect of mechanical roughening on the fatigue performance of aluminium (7075-T6) was evaluated by Abdo[117]. He worked with single overlap joints made in accordance with ASTM D1002, one set was manufactured with mechanically roughened substrates using Scotchbrite™ followed by degreasing in 50/50 mixture of IPA and water. The other set was only degreased. An initial debond of 2mm was introduced to each free end of the overlap. The adhesive used was a scrim cloth structural adhesive prepeg (AF-163-2K, 3M) cured at 121°C under pressure. The debond area was calculated for each cycle, under tension-tension sinusoidal waveform at a frequency of 3Hz. The relationship between the debond area and the fatigue lifetime for both pre-treatments is shown in Figure 2.15. The surface preparation with the abrasive Scotchbrite™ had increased the joints lifetime significantly. Although no environmental exposure occurred, the work illustrated how simple economic processing will improve dynamic performance.

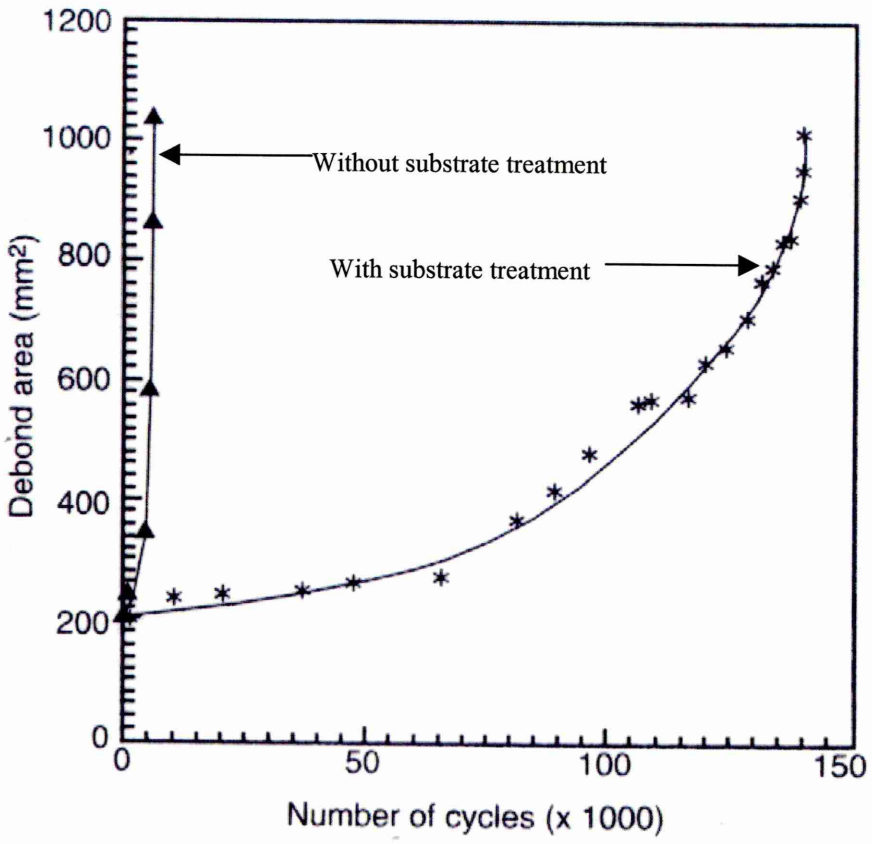

Figure 2.15 - *The relationship between the debond area and the number of cycles for adhesively bonded joints with and without substrate treatment*[117]

Ashcroft *et al*[118] studied the ageing effect on the fatigue performance of single lap and lap strap joints, fabricated from carbon fibre reinforced plastic composites bonded with an unspecified rubber toughened epoxy. Fatigue tests performed between temperatures of –50° to 90°C had little effect on the fatigue threshold. Also ageing the specimens in a hot/wet environment had little effect on fatigue threshold when tested at 22°C. However, a combination of moisture in the joint and testing at 90°C radically reduced the fatigue initiation load, the authors concluded this was attributed to the plasticising effect of moisture meaning at 90° the adhesive is close to its glass transition temperature. Further work[119] on carbon fibre reinforced plastic/epoxy lap strap joints was investigated, where specimens were fatigue tested, at 5Hz, in –50, 25 and 90°C at ambient humidity and ~97% relative humidity at 25 and 90°C. It was shown the fatigue performance of lap strap joints did not vary significantly until the glass transition temperature was approached, at which point a considerable reduction in fatigue threshold was observed. The mode of failure in the composite joints was dependent on environmental conditions. At low temperatures failure was in the composite substrate, whereas at 90°C the specimens failed along the adhesive layer/composite interface. Also observed, was that a high level of moisture within the joint only had any detrimental effect on fatigue performance at elevated temperatures.

Temperature effects on the fatigue performance of mild steel single lap joints bonded with polybutadiene and epoxy adhesives, were evaluated by Harris and Fay[120]. Fatigue tests were carried out at 30Hz in sinusoidal waveform, on specimens with nominal adhesive layers of 0.2, 0.9 and 2.0mm at test temperatures of –30, 20 and 90°C. Fatigue resistance diminished as the test temperatures were increased, it was reported at higher temperatures more creep strains accumulated causing failure. Thinner adhesive layers were found to be stronger and more fatigue resistant.

Fernando *et al*[121] used a fracture mechanics approach to examine the effects of moisture and surface pre-treatments on the cyclic fatigue behaviour of 5083 aluminium alloy substrates bonded with AF-163-2M hot curing toughened epoxy in supported film form. Three pre-treatments were used, namely; chromic acid etch (CAE), phosphoric acid anodising (PAA) and PAA with EC-3924B corrosion inhibiting primer. Fatigue crack growths were monitored for dry joints and specimens immersed in distilled water at 26±2°C. Wet testing had a dramatic effect on fatigue life for pre-treatments, where strain energy release rates were reduced and the associated crack growth increased, as shown in Figure 2.16. The PAA and PAA + primer treatments offered the best fatigue crack growth resistance, where visual analysis of the fracture surface indicated the crack propagated cohesively within the adhesive, suggesting the interface region has sustained no environmental attack. In contrast the CAE specimens has failed interfacially between the adhesive and aluminium alloy. Similarly Jethwa and Kinloch[122] found fatigue cracks propagated more rapidly in aqueous environments. Tapered double cantilever beam specimens of 5083 aluminium alloy, CAE treated, bonded with a rubber toughened epoxy were immersed at room temperature in distilled water. The effects of moisture had also forced the advancing crack through the adhesive/substrate region.

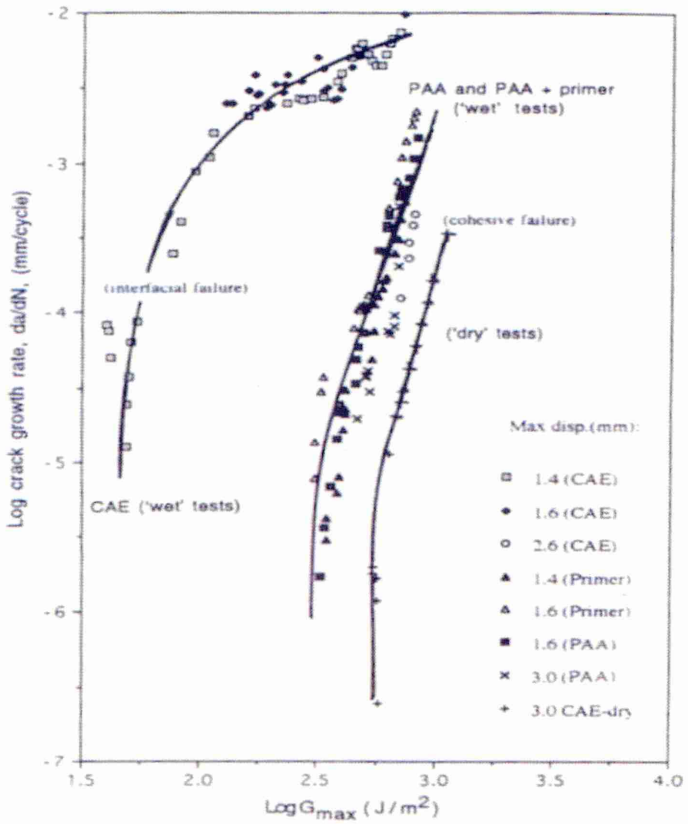

***Figure 2.16** - Crack growth rate per cycle versus G_{max} for joints tested in wet and dry conditions*[121]

2.9.5 Comparison of Fatigue Performance with other Joining Methods

The fatigue performance of welded structures in comparison to adhesive joints, is well documented[123-128]. However, research comparing the fatigue performance of adhesive bonding versus welding has been limited. Chernenkoff[104] reported an improvement of up to 440% over as-welded joints in the fatigue life region of 10^6cycles to failure, when comparing three adhesive formulations with spot welded specimens, as shown in Figure 2.17.

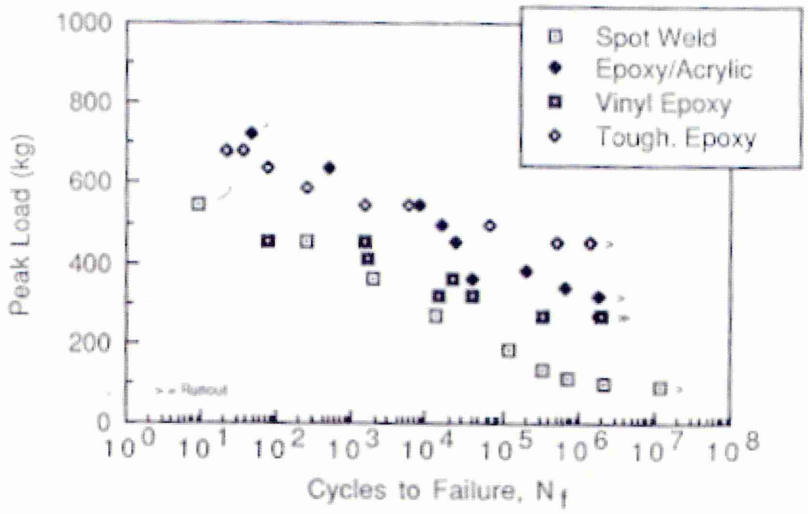

***Figure 2.17** - Fatigue life comparison of adhesively bonded joints versus spot welded joints*[104]

The fatigue response of adhesive and adhesive/rivet combined joints was evaluated by Imanaka *et al*[129]. Lap joints were manufactured from high strength steel bonded with DP490 structural epoxy and C-355 acrylic adhesives. It was observed the fatigue strength increased when combined adhesive/rivet joints were used. A detailed investigation by Mann and co-workers[130] studied reducing the effects of rivet holes on fatigue life by incorporating adhesive bonding on aircraft structures. Fatigue tests were structured to mimic in-service cyclic load conditions for a 100 flight sequence. The materials studied were 2014-T651 aluminium alloy adherends, where the rivets were bonded in position using Ciba Geigy K136 epoxy adhesive. The fatigue crack propagation rate was reduced by 50% when rivets were adhesively bonded, when compared to open hole specimens. Finite element analysis indicated the adhesive bonding significantly reduces both the local stress concentration at the hole and the stress intensities at the crack tips, thus retarding initiation and reducing crack growth rates.

Recently Chang *et al*[131] studied the fatigue behaviour of adhesively bonded, spot welded and weld-bonded single lap joints. The marked improvement in fatigue life of adhesive and weld-bonded specimens was attributed to the reduction in stresses at the periphery of the weld spots. Fatigue test results showed that adhesive-bonded samples gave the highest fatigue resistance, fatigue strength of weld-bonded joints being much greater than that of spot welded joints. It was concluded that the presence of adhesives in spot welded joints is favourable whilst the presence of weld spots in adhesively bonded joints has a negative effect. In similar fashion it was shown by Melander *et al*[132] that the fatigue strength of spot welded specimens was increased when a single-part structural epoxy was used in combination to form weld-bonded structures, when fatigue tested in a variety of harsh environments.

2.9.6 Effect of Joint Geometry on Fatigue Performance

The effects of overlap length and adhesive layer thickness on the fatigue response of single lap joints was evaluated by Imanaka and co-workers[133]. Mild steel, S45C, substrates (4mm thickness) and an epoxy adhesive (Epikote 828 resin with Versamid 115 resin) were used to fabricate single lap joints, with overlaps of 20 and 45mm and an adhesive thickness of 0.1 and 0.3mm. When cycles to failure were plotted against apparent shear stress range, it indicated that the fatigue strength at 10^7 stress cycles was reduced by half when the lap length was increased from 20 to 45mm, and the thicker the adhesive layer the higher the strength. They postulated that the increase in overlap corresponded to an increase in stress concentration, and the increase in adhesive thickness reduced the stress concentrations at the overlap edges. Further work[134] extended the testing to include 15 and 25mm overlaps, and 3mm thick substrates. In contrast[135] the fatigue strength of carbon steel (JIS.S55C) single and double lap joints was increased with an increase in a lap length from 20 to 40mm. Kinloch and Osiyemi[136] used a fracture mechanics approach to develop a model capable of predicting the fatigue life-time of single overlap joints. It was calculated both theoretically and experimentally that increasing the overlap length from 6.4mm in increments through to 25.4mm the fatigue resistance of the bonded joint was significantly improved. The effects of bondline thickness on debond growth rate under cyclic loading has been studied by Mall and Ramamurthy[137]. Double cantilever beam specimens consisted of two bonded composite adherends each having 14 unidirectional plies of graphite/epoxy, with adhesive layer thickness of 0.102, 0.254 and 0.508mm. In summary, the results revealed that specimens with 0.102 and 0.254mm bondline thicknesses were found to have almost the same critical strain energy release rate value, whilst for samples with 0.508mm bondlines the strain energy release rate increased by 50%. The fatigue resistance of the composite beams did not change when the bondline was increased from 0.102 to 0.254mm, however, it did improve when a 0.508mm bondline was used. Lee *et al*[138] found that the torsional fatigue strength of tubular single lap joints increased as the adhesive thickness was decreased. The optimal adhesive thickness was 0.15mm, a thinner bondline could not be achieved for practical reasons. Interestingly to note was the enhancement of fatigue strength by reduction of the bondline thickness which was contrary to specimens that were statically loaded.

2.10 Types of Structural Adhesives

2.10.1 Introduction

The numerous commercially available adhesives can be classified in terms of various criteria, such as chemical type, price, mode of application, physical form and compatibility with substrates. Each adhesive is formulated to satisfy the requirements of one or several specifications in a particular industrial sector. These requirements concern the constraints imposed by their implementation, such as the application and curing methods, and the time required for drying and cross-linking compared to production rates. More importantly they also include the performance levels expected

from the bonded assembly, in terms of bond strength and durability. The most widespread classification is that based on the chemical family, i.e. the chemical nature of the polymer which forms the basis of the adhesive. Other constituents, such as mineral additives, dilutants, catalysts, etc., can be incorporated with the polymer to change the composition and adjust the properties to meet specific requirements. Therefore within a given chemical family, the physical and mechanical properties can vary considerably depending on formulation. Another form of classification that distinguishes the adhesives is their mechanical properties. For example if the function of the adhesive is simply to ensure a hermetic joint between two components then it will usually be considered a sealant or adhesive cement. If the role of the adhesive both guarantees the leak tight nature of the joint and contributes to the strength and stiffness of the structure, then it is a semi-structural adhesive. The term 'structural adhesive bonding' should be reserved for the case where the joint is subjected to permanent or transitory loading, and where the bond ensures the integrity of the structure either alone or in combination with another joining technique.

The most commonly used structural adhesive types will be discussed in turn. Table 2.12 gives an overview of the principal properties of different adhesive families.

2.10.2 Epoxide Adhesives

Epoxides are the most widely used structural adhesives and also used extensively as matrix resins for fibre reinforced composites. There are only a few commercially available epoxide resins, but they can be mixed with a wide range of hardeners. The main advantage of epoxides is that there are no volatiles formed during curing and they have low shrinkage. The main limitation is they can cause skin irritation. The most commonly used epoxy resin is named the diglycidyl ether of bisphenol-A (DGEBA) and is produced by reacting the sodium salt of bisphenol-A with epichlorohydrin, as shown in Figure 2.18. Further reactions involving the opening of epoxide rings occurs as shown in Figure 2.19. The pure compound is a solid but the commercial product is a liquid. Hardeners are usually aromatic and aliphatic amines, where the stoichiometry is one epoxide ring will react with one hydrogen-amine atom during the condensation polymerisation reaction. Epoxy adhesives with aliphatic amine hardeners can be cured at room temperature or at elevated temperature, i.e. 2 hours at 80°C. Those with aromatic amine hardeners require elevated temperature for curing, typically 2 hours at ~150°C, the cured adhesive has a higher glass transition temperature and often exhibit improved durability. Other epoxy formulations include; one component adhesives where the hardener is insoluble in DGEBA at room temperature but dissolves when the adhesive is heated, film adhesives that contain a textile carrier to improve handling and rapid curing epoxides that contain polythiol hardeners which can cure in several minutes at room temperature.

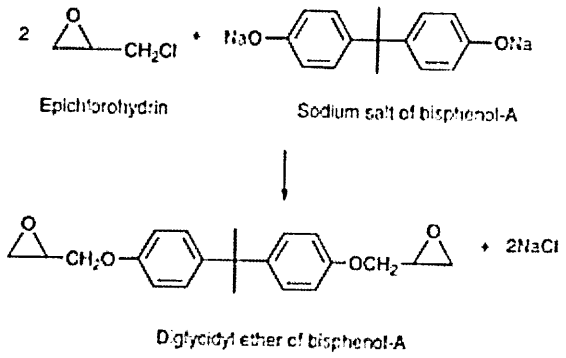

***Figure 2.18** - Structure of diglycidyl ether of bisphenol-A (DGEBA)*[139]

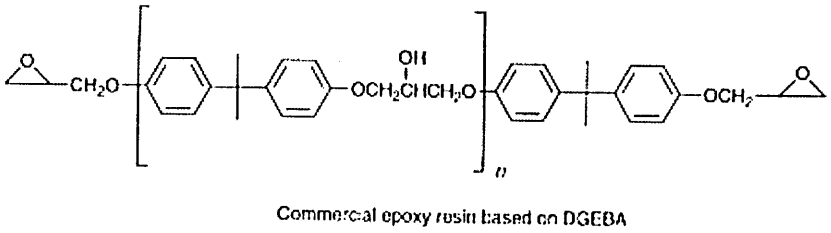

***Figure 2.19** - Commercial structure of an epoxy resin based on DGEBA*[139]

2.10.3 Polyurethane Adhesives

Polyurethane adhesives are produced by reacting a low molecular weight polymer containing at least two OH end groups with a diioscyanate. Usually the polymers include; polyethers, polybutadiene and aliphatic polyesters. Two-part polyurethanes are used by mixing the polymer with the isocyanate and then applying to adherends. One-part polyurethane adhesives consist of low molecular weight linear polymer molecules which have isocyanate end groups, water vapour from the atmosphere causes chemical reactions to take place that join the molecules together to form larger linear molecules.

2.10.4 Acrylic Adhesives

The most common monomer used in acrylic adhesives is methyl methacrylate (MMA) they cure by free-radical addition polymerisation at ambient temperatures. For two-part acrylics one component is applied to one adherend, and the other component to mating adherend, when the surfaces are brought together the curing process initiates.

2.10.5 Cyanoacrylates

Ethyl cyanoacrylate is a molecule that contains two strongly electron withdrawing groups, namely: CN and COO. The polymerisation process starts from the presence of water, which is adsorbed from the atmosphere, and is over within several seconds. The process is discouraged in the presence of oxygen, the hardening process does not take part until both surfaces of the joint are brought together and the oxygen supply cut off.

2.10.6 Anaerobic Adhesives

Anaerobic adhesives cure in the absence of oxygen. The most commonly used are based on dimethacrylates of polyethylene glycol, and contain a redox free-radical initiator. To ensure a sufficient shelf life they are packaged in containers that are partially full to maintain a supply of oxygen and safeguard against premature curing.

***Table 2.12** - Comparative properties of different families of structural adhesives*

Properties	1 and 2 part epoxies	1 and 2 part polyurethane's	2 component acrylics	Anaerobics	Cyanoacrylates
Shear Strength	Excellent	Good	Good to excellent	Excellent	Excellent
Peeling Resistance	Low to excellent	Good to excellent	Medium	Medium	Low
Temperature resistance (°C) **Max** **Min**	200-250 -60	100-120 -60	120 -40	90 -40	90 -40
Chemical inertia	Excellent	Good	Medium to good	Medium to good	Poor resistance to solvents
Toxicity	Possible dermatosis problem	Residual NCO level problem	Avoid skin contact	Avoid skin contact	Avoid skin contact
Sensitivity to contamination	Low	Low to medium	Good to medium	Medium	Medium
Adhesion without primer	Good to excellent	Medium to excellent	Medium to good	Medium	Medium
Means of rapid curing	IR or induction heating	IR or induction heating	UV		
Bondline thickness	0.1 to 2mm	0.1 to >5mm	0.1 to 1mm	<0.5mm	<0.5mm

2.11 Stainless Steel

In 1913 the corrosive resistance of stainless steels was initially discovered by a Sheffield steelmaker, Harry Brearley, who found that chromium additions to steel produced a corrosion resistant material. The corrosion rate of steel decreases dramatically with increasing amounts of chromium, and very low corrosion rates are observed when the chromium content is above 12%.

For over 75 years stainless steel has been the popular choice of designers, architects, engineers and other specifiers for a wide range of industrial applications and consumer goods. Its performance is well proven, and no other material can completely match stainless steel for its durability, versatility and formability. In addition, add its aesthetic qualities, ease of fabrication, resistance to corrosion and hygienic qualities, it is easy to understand why stainless steels play an increasingly important role in industry and out domestic environment. Stainless steel demand continues to grow by ~5% per annum, whilst the growth of steel has stagnated as shown in Figure 2.20.

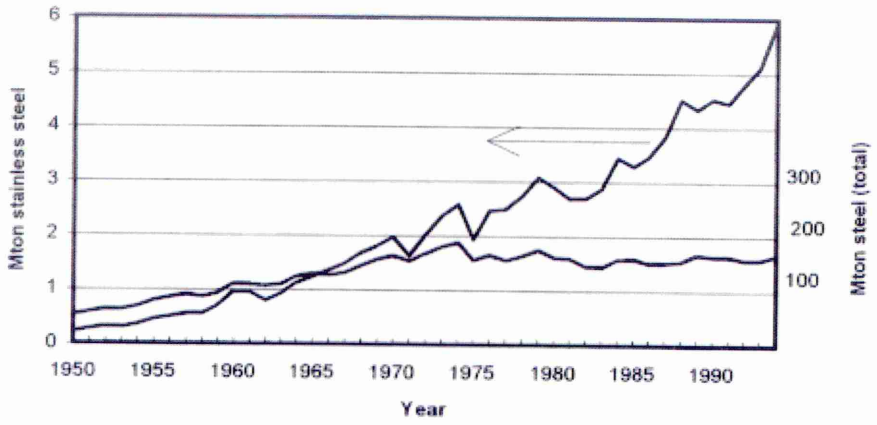

***Figure 2.20** - Steel production in the western Europe*[140]

The versatile nature of stainless steel, with its extensive range of properties and benefits, means that it has many applications within many market sectors. A few major areas dominate usage: consumer products, equipment for the oil and gas industry, the chemical process industry and the food and beverage industry. Table 2.13 details the usage of stainless in the industrialised world.

***Table 2.13** - Use of stainless steel in the industrialised world*[140]

Product Forms		Applications		
Cold rolled sheet	60%	***Consumer Products***		***26%***
Bar and wire	20%	Washing machines etc.	8%	
Hot rolled plate	10%	Pans, cutlery etc.	9%	
Tube	6%	Sinks and kitchen equipment	4%	
Castings and other	4%	Other	5%	
		Industrial Equipment		***74%***
		Food industry and breweries	25%	
		Chemical, oil and gas	20%	
		Transport	8%	
		Energy production	7%	
		Pulp, paper and textile industry	6%	
		Building and construction	5%	
		Other	5%	

Generally most stainless steels contain 18% chromium for increased corrosion protection. Most also contain nickel to improve corrosion properties and enhance fabrication characteristics. Other alloying elements, such as titanium, molybdenum, vanadium and niobium are added to develop specific properties. There are over 200 different types of stainless steels, covering a range of mechanical properties, corrosion resistance, heat resistance, impact and fatigue properties.

There are four main types of stainless steel, named after their room temperature microstructure: austenitic, ferritic, martensitic and duplex. Austenitic steels are the most common stainless steel types, where they dominate more than 50% of global production. Austenitics are characterised by very good corrosion resistance, good toughness and excellent weldability. The austenitic stainless steels are used in almost all types of applications and industries, typically in pipe exchangers and vessels for the food and drinks industry.

2.12 Concluding Remarks

This chapter has reviewed the relevant literature concerning the structural adhesive bonding of metal-to-metal structures, and wherever possible specific attention has been made to stainless steel adhesive joints.

The review has discussed the accepted theories of adhesion applicable to metal-to-metal adhesive bonds. It has been shown that no single theory exists that explains the phenomena of adhesion. Surface pre-treatments techniques for stainless steel and applications have been described. In addition, the influence of pre-bonding treatments on subsequent joint durability have been discussed, and the importance of adherend composition and morphology have been highlighted. An introduction to surface analytical techniques that are useful in characterising pre-treated substrates has been discussed, and how appropriate information can be used to establish the mode and mechanism of fracture that has caused failure of bonded assemblies. Finally the dynamic performance of adhesive joints has been reviewed with emphasis on the importance of implementing proficient pre-treatments and joint geometry's to hinder premature catastrophic failure of adhesively bonded structures.

2.13 References

[1] Kinloch A.J. Adhesion and Adhesives – Science and Technology, Chapman Hall 1987, London, ISBN 0-412-27440-X, Chapter 2 p18-51

[2] Young T. Transactions of the Royal Society 95, 65 (1905)

[3] Dupré A. Theorie Mechanique de la Chaleur, Gauthier-Villars, Paris (1869), p393

[4] Structural Adhesives: Chemistry and Technology, Ed Hartshorn SR, Plenum Press 1986, p49.

[5] Fox H.W. and Zisman W.A., Journal of Colloid Science. 5, 514 (1950).

[6] Fox H.W. and Zisman W.A., Journal of Colloid Science. 7, 109 (1952).

[7] Fox H.W. and Zisman W.A., Journal of Colloid Science. 7, 428 (1952).

[8] Shafrin E.G. and Zisman W.A., Journal of Physical Chemistry. 64, 519 (1960)

[9] Zisman W.A., Advances in Chemistry Series 3, Ed Gould R.F., American Chemical Society, Washington, p1, (1964).

[10] Gledhill R.A., Kinloch A.J., Shaw S., "Effect of relative humidity on the wettability of steel surfaces", Journal of Adhesion, vol. 19, (1977), pp81-85.

[11] Kinloch A.J., "Review: The Science of Adhesion", Journal of Materials Science 15, (1980), p2150.

[12] Boroff E.M., Wake W.C., "Adhesion of rubber and textiles part 3: Examination of test technique", Trans. Institute Rubber Industry 25, (1949), p199-209.

[13] Venables J.D., "Adhesion and durability of metal polymer bonds", Journal of Materials Science 19, (1984), p2431-2453.

[14] Jennings C.W., Journal of Adhesion, 4,(1972), p25.

[15] Kinloch A.J. Adhesion and Adhesives – Science and Technology, Chapman Hall 1987, London, ISBN 0-412-27440-X, Chapter 4 p143

[16] Tabor D., Winterton R.H.S., "The direct measurement of normal and retarded van der Waals forces", Proc. Roy. Society, A312, 1511, (1969), p435-450.

[17] Isrealachvili J.N., Tabor D., "The measurement of van der Waals dispersion forces in the range 1.5 to 130nm", Proc. Roy. Society, A331, 1584, (1972), p19-38.

[18] Johnson K.L., Kendall K., Roberts A.D., "Surface energy and the contact of elastic solids", Proc. Roy. Society, A324, (1971), P301-313

[19] Voyutskii S.S., Autohesion and Adhesion of High Polymers, Wiley Interscience, New York, 1963, p117-140.

[20] Allen K.W., "A review of contemporary views of theories of adhesion", Journal of Adhesion, vol, 21, 1987, p261-277.

[21] Deryaguin B.V., Smilga V.P., Adhesion, Fundamentals and Practice, M^{C}Laren and Son, London, 1969, p152.

[22] Kinloch A.J. Adhesion and Adhesives – Science and Technology, Chapman Hall 1987, London, ISBN 0-412-27440-X, Chapter 23, p70.

[23] Wake W.C., Adhesion and the Formulation of Adhesives, 2nd Edition, Applied Science Publishers, London and New York, 1982.

[24] Huntsberger J.R., Treatise on Adhesion and Adhesives, vol. 1, Ed Patrick R.L., Edward Arnold Ltd, London, 1966, Chapter 4.

[25] Bell J.P., MCCarrill W.T., Journal of Applied Polymer Science, 18, (1974), p2243.

[26] Yaniv A.E., Klein I.E., Sharon J., Dodiuk., Surface and Interface Analysis, 5, (1983), p93.

[27] Gettings M., Kinloch A.J., "Surface analysis of polysiloxane/metal oxide interfaces", Journal of Materials Science, 15, (1977), p2141-2166.

[28] Gettings M., Kinloch A.J., Surface characterisation and adhesive bonding of stainless steel-Part 2 The steel/adhesive interface", Surface and Interface Analysis, vol. 1, no. 6, 1979, p189-195.

[29] Harris A.F., Beevers A., "The effects of grit blasting on surface properties for adhesion", International Journal of Adhesion and Adhesives, 19, (1999), p445-452.

[30] Critchlow G.W., Brewis D.M., "Review of surface pre-treatments for aluminium alloys", International Journal of Adhesion and Adhesives, 16, (1996), p255-275.

[31] Brewis D.M., Durability of Structural Adhesives, Ed Kinloch A.J., Chapter 5, Applied Science Publications, ISBN 0-85334-214-8, 1983.

[32] Mahoon A., Durability of Structural Adhesives, Ed Kinloch A.J., Chapter 6, Applied Science Publications, ISBN 0-85334-214-8, 1983.

[33] ASM Engineered Materials Handbook, Adhesives and Sealants, vol. 3, 1990.

[34] Adams R.D., Comyn J., Wake W.C., Structural Adhesive Joints in Engineering, 2nd Edition, Chapman Hall, 1997, ISBN-0-412-70920-1.

[35] Critchlow G.W., Brewis D.M., "Review of surface pre-treatments for titanium alloys", International Journal of Adhesion and Adhesives, 15, (1995), p161.

[36] Nordberg H., "Stainless steel in structural applications", Proceedings of the NI-seminar "Stainless Steel in Transport Industry", February 4-5th 1998, Helsinki.

[37] Vilpas M., "Corrosion properties of stainless steels in bus structures", Proceedings of the NI-seminar "Stainless Steel in Transport Industry", February 4-5th 1998, Helsinki.

[38] Llewellyn D.T., Steels – Metallurgy and Applications, Butterworth Heinmann, ISBN 0-7506-2086-2, 1992

[39] Boyes, R., "Adhesive bonding of stainless steel: Strength and durability", PhD Thesis, Sheffield Hallam University, 1998.

[40] Botrell N.L., "Preparation of surfaces for adhesive bonding", ISME Proceedings, Royal Aeronautical Society, 1965, p667-672.

[41] Ciba Speciality Chemicals, Surface Preparation and Pre-treatments Handbook, 1998.

[42] Brockmann W., Durability of Structural Adhesives, Ed Kinloch A.J., Chapter 7, Applied Science Publications, ISBN 0-85334-214-8, 1983.

[43] Private communication, Centre for Adhesive Technology, TWI, Cambridge, UK.

[44] Allen K.W., Alsalim H.S., "Surface preparation of a stainless steel for adhesive bonding", Journal of Adhesion, 1977, vol. 8, p183-194.

[45] Sykes J.M., "Surface treatments for steel", Surface Analysis and Pre-treatments of Plastics and Metals, Ed Brewis D.M., Applied Science Publications, London, 1982.

[46] ASM Engineered Materials Handbook, Adhesives and Sealants, vol. 3, 1990, p656

[47] Bowditch M.R., "The durability of adhesive joints in the presence of water", International Journal of Adhesion and Adhesives, vol. 16, 1996, p73-79.

[48] Minford J. D., "Etching and anodising pre-treatments and aluminium joint durability", SAMPE Quarterly, July 1978, p18.

[49] Brewis D. M., Critchlow G.W., "The durability of aluminium-epoxide lap joints", Transactions of the Institute of Metal Finishing, 74 (6), 1996, p198-201, ISSN 0020-2967

[50] M^{C}Millan J. C., Bonded Joints and Preparation for Bonding, AGARD Lecture Number 102, 1979.

[51] Minford J. D., Treatise on Adhesion and Adhesives, Edited Patrick R. L., Applied Science Publications, London, 1983.

[52] Arrowsmith D.J., Maddison A., "The use of perforated lap shear specimens to test the durability of adhesive-bonded aluminium", International Journal of Adhesion and Adhesives, vol. 7, no. 1, January 1987, p15-24.

[53] Fay P.A., Maddison A., "Durability of adhesively bonded steel under salt spray and hydro-thermal stress conditions", International Journal of Adhesion and Adhesives, vol. 10, no. 3, July 1990, p179-186.

[54] ASTM Standards, ASTM D3762.

[55] Ramani K., Verhoff J., Kumar G, Blank N., Rosenberg S., "Environmental durability of moisture cured polyurethane joints", International Journal of Adhesion and Adhesives, vol. 20, 2000, p377-355.

[56] Critchlow G.W., Brewis D.M., "Influence of surface macroroughness on durability of epoxide-aluminium joints", International Journal of Adhesion and Adhesives, vol. 15, 1995, p173-176.

[57] Gosselin C.A., SAE Special Publications SP-612, Warrendale, Pennsylvania, 1984, p15-23.

[58] Wilson I., Sheasby P.G., Maddison, A., "The significance of environment for performance of structural adhesive bonding", Journal of Materials and Manufacturing, vol. 116, issue 5, 1997, p6-14.

[59] Rider A.N., Olsson-Jacques C.L., Arnott D.R., "Influence of adherend surface preparation on bond durability", Surface and Interface Analysis, 27, 1999, p1055-1063.

[60] Scardino W., Marceau M., "Comparative stressed durability of adhesive bonded aluminium alloy joint", Journal of Polymer Science, Applied Polymer Symposium, 32, 1977, p51-63.

[61] Armstrong K.B., "Long term durability in water of aluminium alloy adhesive joints bonded with epoxy adhesives", International Journal of Adhesion and Adhesives, vol. 17, no. 2, 1997, p89-105.

[62] Spinks G.M., Isles N.A., Egan B.J., Noakes A.,"Evaluation of adhesive joints performance in hostile environments", Materials Forum, (1992), vol. 16, p253-257.

[63] Digby R.P., Packham D.E., "Pretreatment of aluminium: topography, surface chemistry and adhesive bond durability", International Journal of Adhesion and Adhesives, vol. 15, no. 2, 1995, p61-71.

[64] Jones M.T., Pitcher P.D., Pole P., Stone M.H., "Effect of surface pretreatment and alloy type on the durability of adhesive bonded titanium alloy joints", Structural Adhesives in Engineering, ImechE Conf. Proc. 1986, p93-104.

[65] Haak R.P., Smith T., "Surface treatment of AM355 stainless steel for adhesive bonding", International Journal of Adhesion and Adhesives, January 1983, p15-23.

[66] Smith T., "Mechanisms of adhesive bond endurance: Steel-epoxy under hydrothermal stress", Journal of Adhesion, vol. 17, 1984, p1-20.

[67] Gaskin G.B., Pilla G.J., Brown S.R., "Preparation of stainless steel adherends for adhesive bonding", Journal of Testing and Evaluation, vol. 22, no. 3, May 1994, p222-225.

[68] Pocius A.V., Almer C.J., Waid R.D., Wilson T.H., "Investigation of variability in the adhesive bonding characteristics of stainless steel", SAMPE Journal, vol. 20, Dec/Jan 1984, p11-16.

[69] Garnish E.W., Adhesion 2, Ed Allen K.W., Applied Science Publications, London, 1978, p35.

[70] Comyn J., Durability of Structural Adhesives, Ed Kinloch A.J., Chapter 3, Applied Science Publications, ISBN 0-85334-214-8, 1983.

[71] Brewis D.M., Comyn J., Ravel A.K., Kinloch A.J., "The effect of humidity on the durability of aluminium-epoxide joints", International Journal of Adhesion and Adhesives, vol. 10, no. 4, October 1996, p247-253.

[72] Brewis D.M., Comyn J., Shalash R.J.A., Tegg T.L., "Interaction of water with some epoxide adhesives", Polymer, 1980, vol. 27, p357.

[73] De Néve B., Shanahan M.E.R., "Effects of humidity on an epoxy adhesive", International Journal of Adhesion an Adhesives, vol. 12, no. 3, July 1992, p191-196.

[74] Zanni-Deffarges M.P., Shanahan M.E.R., " Diffusion of water into an epoxy adhesive: comparison between bulk behaviour and adhesive joints" International Journal of Adhesion and Adhesives, vol. 15, no. 3, 1995, p137-142.

[75] Ellis T.S., Karaz F.E., "Interaction of epoxy resins with water: The depression of the glass transition temperature", Polymer, May 1984, vol. 25, p665.

[76] Moy P., Karaz F.E., "Epoxy-water interactions", Journal of Polymer Engineering and Science, Mid March 1980, vol. 20, no. 4, p315.

[77] Jurf R.A., Vinson J.R., "Effect of moisture on the static and viscoelastic shear properties of epoxy adhesives", Journal of Material Science, vol. 20, 1985, p2979.

[78] Butt R.I., Cotter J.L., "The effect of high humidity on the dynamic mechanical properties and thermal transition of epoxy-polyamide adhesives", Journal of Adhesion, vol. 8, 1976, p11.

[79] Brewis D.M., Comyn J., Tegg J.L., "The durability of some epoxide adhesive bonded joints on exposing to moist warm air", International Journal of Adhesion and Adhesives, vol. 1, 1980, p35.

[80] Antoon M.K., Koenig J.L., Serafini T.J., "Fourier transform infrared study of the reversible interaction of water with a cross linked epoxy matrix", Journal of Polymer Science, Physics Edition, vol. 19, 1981, p1567.

[81] Antoon M.K., Koenig J.L., "Irreversible effects of moisture on the epoxy matrix in glass reinforced composites", Journal of Polymer Science, vol. 19, 1981, p197.

[82] Browning C.E., Journal of Polymer Engineering and Science, vol. 18, 1978, p16.

[83] Browning C.E., Hudman G.E., Whitney J.M., ASTM Special Technical Publication. 617, (1977), p481.

[84] Gledhill R.A., Kinlock A.J., "Environmental failure of structural adhesive joints", Journal of Adhesion, vol. 6, 1974, p315-330.

[85] Kinloch A.J., Durability of Structural Adhesives, Ed Kinloch A.J., Chapter 1, Applied Science Publications, ISBN 0-85334-214-8, 1983.

[86] Gledhill R.A., Kinloch A.J., Shaw S., "A model for predicting joint durability", Journal of Adhesion, vol. 11, 1980, p3-15.

[87] Davis G.D., ASM Adhesives and Sealants Engineered Materials Handbook, vol. 3, 1990, p236.

[88] Davis G.D., Durability of Structural Adhesives, Ed Kinloch A.J., Chapter 2, Applied Science Publications, ISBN 0-85334-214-8, 1983.

[89] Davis G.D., Surface Analysis and Pretreatments of Plastics and Metals, Ed Brewis D.M., Chapter 2, p13-44, Applied Science Publications, London, 1982.

[90] Christie A.B., Methods of Surface Analysis – Techniques and Applications, Ed Walls J.M., Chapter 5, p127-168.

[91] Read S., Corus Research and Development Technical Notes.

[92] Bouquet F, Cuntz J.M., Coddet C., "Influence of surface treatment on the durability of stainless steel bonded with epoxy", Journal of Adhesion Science and Technology, vol. 2, 1992, p233-242.

[93] Critchlow G.W., Webb P.W., Tremlett C.J., Brown K., "Chemical conversion coating for structural adhesive bonding of plain carbon steel", International Journal of Adhesion and Adhesives, vol. 20, 2000, p113-122.

[94] Kinloch A.J., Bishop H.E., Smart N.R., Journal of Adhesives, vol. 14, 1982, p105.

[95] Dillingham R.G., Ondrus D.J., Boerio F.J., "Chemical and thermodynamic characterisation of metal surfaces for the adhesive bonding of metal", Journal of Adhesion, vol. 21, p95-114.

[96] Brewis D.M., Critchlow G.W., "Adhesion and surface analysis", Journalof Adhesion, vol. 54, 1995, p175-199,

[97] Baun W.L., "Applications of surface analytical techniques to the studies of adhesion", Applied Surface Science, vol. 4, 1980, p291-300.

[98] Davis G.D., Adhesive Bonding, Ed Lee L.H., ISBN 0-306-43471-7, 1991, Chapter 6, p139-173.

[99] Guimon M.F., Pfister-Guillouzo G., Brémont M., Brockmann W., Quet C., Chenard J.Y., "Application of XPS to study the degradation mechanisms of epoxy joints of zinc coated steel", Applied Surface Science, vol. 108, 1997, p149-157.

[100] Brémont M., Brockmann W., "Comparison of the degradation mechansims of zinc coated steel, colled rolled steel and aluminium/epoxy bonded joints", Journal of Adhesion, vol. 58, 1996, p69-99.

[101] Hong S.G., Boerio F.J., "Adhesive bonding of oil contaminated steel substrates", Journal of Adhesion, vol. 32, 1990, p67-88.

[102] Kinloch A.J., Little M.S.G., Watts J.F., "The role of the interface in the environmental failure of adhesive joints", Acta Materialia , vol. 48, 2000, p4543-4553.

[103] Gettings M., Baker F.S., Kinloch A.J., "Use of Auger and X-Ray photoelectron spectroscopy to study the locus of failure of structural adhesive joints", Journal of Applied Polymer Science, vol. 21, 1977, p2375-2392.

[104] Chernenkoff R.A., "Fatigue characteristics of overlap bonded joints", Conf. Proc. Fatigue 90, p2505-2510.

[105] Mackie R.I., Su N., "The effect of ageing and environment on the static and fatigue strength of adhesive joints", Journal of Adhesion, vol. 42, 1993, p191-207.

[106] Su N., Mackie R.I., Harvey W.J., "The effects of ageing and environment on the fatigue life of adhesive joints", International Journal of Adhesion and Adhesives, vol. 12, no. 2, April 1992.

[107] Luckyram J., Vardy A.E., "Fatigue performance of two structural adhesive", Journal of Adhesion, vol. 26, 1988, p273-291.

[108] Herzberg R.W., Manson J.H., Fatigue of Engineering Plastics, Academic Press, New York, 1980.

[109] Makoto I., Kistimoto W., Okita K., "Improvement of impact fatigue strength of adhesive joints by CTBN modification", Journal of Applied Polymer Science, vol. 29, 1984, p373-382.

[110] Makoto I., Kistimoto W., Okita K., "Improvement of fatigue strength of adhesive joints through filler addition", Journal of Composite Materials, vol. 18, Spetember 1984, p412-422.

[111] Chen N.N.S., Niem P.I.F., Lee R.C., "Fatigue behaviour of adhesive bonded joints", Journal of Adhesion, vol 21, 1987, p115-128.

[112] Kayaki H., Takagi J., Yamamoto H., Mukov R., "Studies on a technique for predicting the fatigue properties of steel/steel adhesive joints – fatigue results in hot and humid environments", JSAE Review, vol. 13, no. 4, October 1992, p58-63.

[113] Xu X.X., Crocombe A., Smith P.A., "Frequency effect on fatigue crack growth rate in joints bonded with either filled or unfilled toughened adhesive", Conf. Proc. EURADH 94, 12-15 September, Mulhouse, France, p232-236.

[114] Joseph R., Bell J.P., M^{C}Evily A.J., Liang J.L., "Fatigue crack growth in epoxy/aluminium and epxoy/steel joints", Journal of Adhesion, vol. 41, 1993, p169-187.

[115] Briskham P., Smith G., "Cyclic stress durability testing of lap shear joints exposed to hot-wet conditions", International Journal of Adhesion and Adhesives, vol. 20, 2000, p33-38.

[116] Hirko A.G., Schibler J.E., Taylor L.G., Improved surface preparation of AM355 for adhesive bonding", 29thNational SAMPE Symposium, April 3-5 1984, p282-291.

[117] Abdo Z., Aglan H., "Effect of surface treatment on the fatigue failure behaviour of structural adhesive joints", Journal of Material Science Letters, vol. 15, p469-472.

[118] Ashcroft I.A., Hughes D.J., Shaw S.J., "The effect of test environment on the fatigue life of mixed mode composite joints", Conf. Proc. Polymeric Materials Science and Engineering, Fall Meeting, August 22-26, 1999, New Orleans, Louisiana.

[119] Ashcroft I.A., Abdel wahab M.M., Crocombe A.D., Hughes D.J., Shaw S.J., "The effect of environment on the fatigue of bonded composite joints: Part 1 Testing and fractography", Composites Part A: Applied Science and Manufacturing, vol. 32, 2001, p45-58.

[120] Harris J.A., Fay P.A., "Fatigue life evaluation of structural adhesives for automotive applications", International Journal of Adhesion and Adhesives, vol. 12, no. 1, January 1992.

[121] Fernando M., Harjoprayitno W.W., Kinloch A.J., "A fracture mechanics study of the influence of moisture on the fatigue behaviour of adhesively bonded aluminium alloy joints", International Journal of Adhesion and Adhesives, vol. 16, no. 2, 1996, p113-119.

[122] Jethwa J.K., Kinloch A.J., "The fatigue performance of adhesively bonded metal joints", Conf. Proc. 17th Annual Meeting of the U.S. Adhesion Society, Florida, 1994, p231-234.

[123] Linder J., Larsson M., "Fatigue properties of spot welded sheet steels", Research Report, Swedish Institute for Metals Research, IM-2000-044.

[124] Lindgreen C., Sperle J., Jonsson M., "Fatigue strength of spot welded beams in high strength steels", Welding in the World, vol. 37, no. 1, 1996, p90-104.

[125] Davidson J.A., "A review of the fatigue properties of spot welded sheet steels", SAE Technical Paper Series, 83003, 1983.

[126] Wilson R.B., Fine T.E., "Fatigue behaviour of spot welded high strength steel joints", ", SAE Technical Paper Series, 810354, 1981.

[127] Pollard B., "Fatigue strength of spot welds in titanium bearing HSLA steels", ", SAE Technical Paper Series, 820284, 1982.

[128] Iwasaki T., Tanaka J., Kabasawa M., Nagae M., "Fatigue strength of base metal and spot welded joints in HSLA steels for automotive applications", Nippon Kokan technical Report. Overseas no. 34, 1982.

[129] Imanaka M., Haraga K., Nishikawa T., "Fatigue strength of adhesive/rivet combined joints", JSAE Technical Report, 1992.

[130] Mann J.Y., Pell R.A., Jones R., Heller M., "Reducing the effects of rivet holes on fatigue life by adhesive bonding", Theoretical and Applied Fracture Mechanics, vol. 3, 1985, p113-124.

[131] Chang B., Shi Y., Lu L., "Studies on the stress distribution and fatigue behaviour of weld-bonded lap shear joints", Journal of Materials Processing Technology, vol. 108, 2001, p37-313.

[132] Melander A, Larsson M., Stensiő H., Gustavsson A., Linder J., "Fatigue performance of weld-bonded high strength sheet steels tested in Artci, room temperature and tropical conditions", International Journal of Adhesion and Adhesives, vol. 20, 2000, p415-425.

[133] Imanaka M., Fukuchi Y., Kishimoto W., Okita K., "Fatigue life estimation of adhesively bonded lap joints", Transactions of the ASME, vol. 110, October 1988, p350-354.

[134] Imanaka M., Kishimoto W., Okita K., Nakayama H., "Fatigue life prediction of adhesive bonded joints", Conf. Proc. Fatigue 90, Hawaii, 15-20 July 1990, p2499-2504.

[135] Imanaka M., Ishii K., Nakayama H., "Evaluation of fatigue strength of adhesively bonded single and single step double joints based on stress singularity parameters", Engineering Fracture Mechanics, vol. 62, 1999, p409-424.

[136] Kinloch A.J., Osiyemi S., "Predicting the fatigue life of adhesively bonded joints", Journal of Adhesion, vol. 43, 1993, p79-90.

[137] Mall S., Ramamurthy G., "Effect of bond thickness on fracture and fatigue strength of adhesively bonded composite joints", International Journal of Adhesion and Adhesives, vol. 19, no. 1, January 1989.

[138] Lee D.G., Kim K.S., Im Y., "An experimental study of fatigue strength for adhesively bonded tubular single lap joints", Journal of Adhesion, vol. 35, 1991, p39-53.

[139] Comyn J., Adhesion Science, Royal Society of Chemistry, ISBN 0-85404-543-0, 1997.

[140] Leffler B., Stainless: Stainless steel and their properties, 2nd Edition, Avesta Sheffield Research Foundation, ISBN 91-9720-216-9.

Chapter 3 Experimental Procedure

3.1 Introduction

The aim of this chapter will firstly introduce the substrates and adhesives studied together with aspects of joint preparation and test methods used throughout the research programme. Secondly, the techniques used to physically and chemically characterise substrate surfaces are described.

3.2 Substrate Material

AvestaPolarit Plc supplied AISI 304L austenitic stainless steel, cold rolled, off the coil. Three distinct surface finishes were incorporated in the programme; bright annealed, semi-bright anneal and matt finish, which are designated BA, 2B and 2D respectively. The typical chemical composition and mechanical properties for AISI 304L are shown below in Tables 3.1 and 3.2.

***Table 3.1** - Chemical composition of AISI 304L stainless steel*

Element	C	Si	Mn	P	S	Cr	Mo	Ni	Al	Cu
Mass %	0.024	0.36	1.41	0.026	0.002	18.23	0.31	9.21	0.001	0.30

Element	Sn	B	Co	N	Ti	Nb	V	W	As
Mass %	0.010	0.0014	0.13	0.040	0.010	0.010	0.08	0.06	0.010

***Table 3.2** - Mechanical properties of AISI 304L stainless steel*

Position on coil	0.1% Proof N/mm^{-2}	0.2% Proof N/mm^{-2}	1.0% Proof N/mm^{-2}	UTS N/mm^{-2}	Elongation %	Hardness Hv
Front	278	295	335	603	55	152
Back	275	291	333	600	54	152

3.3 Adhesives

3.3.1 Introduction

An extensive screening program was carried out by Boyes[1], in order to evaluate the suitability of bonding stainless steel, using six commercially available structural adhesives supplied by 3M Plc. Table 3.3 details the screened adhesives.

Boyes concluded that if stainless steels are to be joined using adhesives, with the intention of employing the resulting fabrications in structural applications, toughened epoxy systems must be considered. The epoxy systems DP460 and DP490 were the preferred choice.

***Table 3.3** - Candidate adhesives for the screening programme*[1]

Adhesive	Curing Requirements
7823-S One component epoxy	40 minutes at 180^{0}C
9323B/A Two component epoxy	1 week at 23^{0}C
DP460 Two component epoxy	1 week at 23^{0}C
DP490 Two component epoxy	1 week at 23^{0}C
3532B/A Two component polyurethane	1 week at 23^{0}C
EP801 Two component acrylic	Within 30 minutes at 23^{0}C

3.3.2 Candidate Adhesive

DP490 toughened epoxy adhesive, supplied by 3M Plc, was incorporated into the research programme. The adhesive is supplied in 'Duo Pak' double tube cartridges, one resin and catalyst, and one hardener. To apply the adhesive a special gun applicator, 3M EPX applicator, is used which forces the two components through a mixing nozzle, whereby upon exiting the exact proportions are obtained.

The DP490 adhesive is toughened with a discrete acrylonitrile butadiene rubber phase, which constitutes between 10-15% of the adhesive composition. It is thixotrophic in nature with good gap filling properties, and designed for situations where toughness, high strength and excellent heat and environmental resistance are required.

3.4 Surface Pre-treatments

During the course of the research a variety of pre-treatments have been integrated into the research programme. Each treatment is described individually below.

3.4.1 Alkaline Degreasing

Stainless steel specimens were degreased, to remove processing oils, lubricants and atmospheric contamination using the cleaning line at Bodycote Ltd. The procedure is a fully automated multi stage operation used to obtain clean surfaces on drill bits and tooling before the deposition of hard coatings. The procedure is detailed below in Table 3.4. Once dried, specimens are wrapped in aluminium foiled prior to bonding.

***Table 3.4** - Alkaline degreasing procedure*

Stage	Medium	Temperature (^{0}C)	Duration (mins)	Ultrasonics
1	Decospray N©	65	2	Y
2	Galvex SU 93©	65	2	Y
3	Galvex 1730	35	0.5	N
4	Rodastel 10	65	1	Y
5	Galvex 1730	35	0.5	N
6	Galvex 1730	65	2	Y
7	Galvex 1730	35	0.5	N
8	Deionised water	35	0.5	Y
9	Deionised water	50	1	Y
10	Deionised water	50	2	Y
11	Vacuum Drier	200	5	N/A

3.4.2 Mechanical Abrasion

Specimens were degreased with Isopropanol Alcohol (IPA), to remove any residual processing contaminants. The abrasion technique was carried out in accordance with BS:2451:1963, using Guyson high purity alumina blast media, in a pressure assisted chamber. The blasting conditions were as detailed in Table 3.5.

Once specimens were roughened they were passed through the alkaline degreasing process as detailed in Table 3.4 to remove loosely adhered blast media and contamination.

***Table 3.5** - Mechanical abrasion parameters.*

Factor	Parameter
Blast Media	High Purity aluminium oxide (99.99%) BS 871
Blast Pressure	80 lbs/in^2
Blast Distance	200mm
Blast Angle	90^0
Grit Size	80/120 mesh
Blast Duration	30 seconds

3.4.3 Chemical Pre-treatments

3.4.3.1 Sulphuric Acid Sodium Dichromate Anodise

Prior to the electrochemical treatment all specimens were alkaline degreased. Specimens were held in the conditions specified in Table 3.6.

***Table 3.6** - Sulphuric acid – sodium dichromate anodising parameters*

Factor	Parameter
Solution composition	H_2SO_4 260ml/l, $Na_2Cr_2O_7$ 400g/l
Bath Temperature	80^0C
Anodic Voltage	2v
Duration	20 minutes
Cathode material	Lead

After the electrochemical treatment specimens are rinsed for ten minutes in deionised water, and then dried at 85^0C for thirty minutes. All samples are wrapped in aluminium foil prior to bonding.

3.4.3.2 Nitric Acid – Sodium Dichromate Anodise

Prior to the electrochemical treatment all specimens were alkaline degreased. Table 3.7 below shows the bath composition and pre-treatment parameters. All samples were rinsed for ten minutes in deionised water and dried for thirty minutes at 80^oC.

***Table 3.7** - Nitric acid – sodium dichromate anodising parameters.*

Factor	Parameter
Solution composition	HNO_3 156ml/l, $Na_2Cr_2O_7$ 30g/l
Bath Temperature	80^0C
Anodic Voltage	3v
Duration	3 minutes
Cathode material	Stainless Steel

3.4.3.3 Oxalic Acid Etch

Prior to etching all specimens were alkaline degreased. The bath composition is detailed below.

***Table 3.8** – Oxalic acid etch parameters*

Factor	Parameter
Bath Composition	$((COOH)_2.2H_2O)$ 143g/l, H_2SO_4 457ml/l
Bath Temperature	65^0C
Treatment Duration	10 minutes

.

The etching process leaves a deposit of carbon on the surface known as smut. As a result all samples need to be de-smutted to reduce the level of surface contamination. The de-smutting stage is summarised below.

***Table 3.9** - De-smutting procedure.*

Factor	Parameter
Bath composition	HNO_3 30%o/v
Bath Temperature	55^0C
Treatment Duration	1 minute

Specimens are subsequently rinsed in deionised water for ten minutes, and dried at 85^{0}C for thirty minutes.

3.4.3.4 Ferric Chloride Etch

Samples were alkaline degreased prior to etching. The etching process is presented below.

***Table 3.10** - Ferric chloride etching parameters.*

Factor	Parameter
Bath Composition	$FeCl_3$ 100g/l, HCl 10% o/v
Bath Temperature	50^{0}C
Treatment Duration	10 minutes

Samples were de-smutted as outlined in Table 3.9. All specimens were rinsed in deionised water, and dried at 85^{0}C for thirty minutes.

3.4.5 Primer

The primer chosen is silane based and supplied suspended in methanol. It is commercially available from 3M UK Plc, designated 3901. The primer was applied to alumina blasted surfaces using a brush, once applied the methanol evaporated within a few seconds. The treated samples were dried at 85^{0}C for five minutes, allowed to cool and stored in a desiccator prior to bonding.

3.4.6 Accomet C

Accomet C is a well established pre-treatment process for aluminium, steel and galvanised steel prior to the application of stoving paints and adhesives, and supplied by Albright and Wilson UK Ltd. Essentially it is a proprietary chromium compound, as detailed below :

***Table 3.11** - Constituents of Accomet C.*

Component	Concentration %
Chromium trioxide	0.1 – 0.8
Amorphous silica	5.0 – 20.0
Chromium III compounds	3.0 – 6.0

When Accomet C is used as a pre-treatment for adhesive bonding, its application must ensure the deposition of a thin uniform layer that will not form a weak boundary interface between the adhesive and the substrate. The thickness of the dried film is dependent on the wet film thickness and concentration of Accomet C. A dilution rate of 9:1, clean tap water to Accomet C respectively produced consistent uniform layers. The solution was applied to alumina blasted surfaces with a brush, excess solution at the edges was shaken off to avoid locally thick areas. The specimens were then dried at 100^{0}C for five minutes, allowed to cool and stored in a desiccator.

3.4.7 Albritect AZS

Albritect AZS is commercially available from Albright and Wilson. It's fundamental usage is to improve the adhesion of coatings to carbon steel substrates, and is a chrome free version of Accomet C. The product is supplied in solution form and using a brush was directly applied to the stainless steel substrates. Specimens were then dried at 100°C for five minutes, allowed to cool and stored in a dessicator prior to bonding

3.4.8 Albritect CP30

Albritect CP30 is a chrome free proprietary coating used to provide optimum adhesion and corrosion protection on hot dip galvanised steel and structural bonding applications. The solution is typically a carbon back bone attached to which are phosphoric acids and carbon silicates. The solution relies on acid-base reactions between itself and the substrate. The solution needs to be used at a very low coating weight, approaching a mono-molecular layer. Private communication[2] suggested applying using a brush technique with a solution concentration ideally around 0.1% w/w. After application specimens are dried at 50°C for five minutes, and stored in a dessicator prior to bonding.

3.5 Specimen Preparation

During the research three types of joint configuration have been employed, namely ; single overlap joint, perforated single overlap joint and the wedge test.

3.5.1 Single Overlap Joint

The notable advantages of the single overlap joint is the ease of manufacture, and its representation of the most common joint configuration found in industry. Stainless steel coupons, 100x25mm or 55x25mm with gauges of 1.5 and 3.0mm, were laser cut to size. A specially made jig allowed adherends to be inserted, allowing overlap lengths from 12.5 to 50mm to be fabricated. Adhesive was applied to both overlap areas, and spread across the bondable region to increase wetting and reduce the amount of air entrapment. Bondline control was achieved by inserting 2mm lengths of 0.25mm diameter (No. 10 guitar string) steel wire at convenient distances, parallel to the tensile axis on the overlap area of one adherend. Both adherends were brought together in the jig, where a 1Kg weight or mechanically sprung clips were carefully positioned around the overlap to provide a uniform nominal pressure during the curing cycle. If fillets were removed it was done so at this stage. Once curing was complete the joints were removed.

3.5.2 Perforated Single Overlap Joint

The perforated single overlap joint is a modification of the standard lap shear joint, however perforations are fabricated in the overlap region to reduce the bond area and hence reduce the length of the diffusion path of any ingressing medium. This alteration in configuration allows the lap joint to be easily stressed and then exposed to environmentally degrading surroundings. AISI 304L stainless steel coupons, 1.5mm gauge, were laser cut to the dimensions shown in Figure 3.1, and bonded to form the joint geometry shown in Figure 3.2.

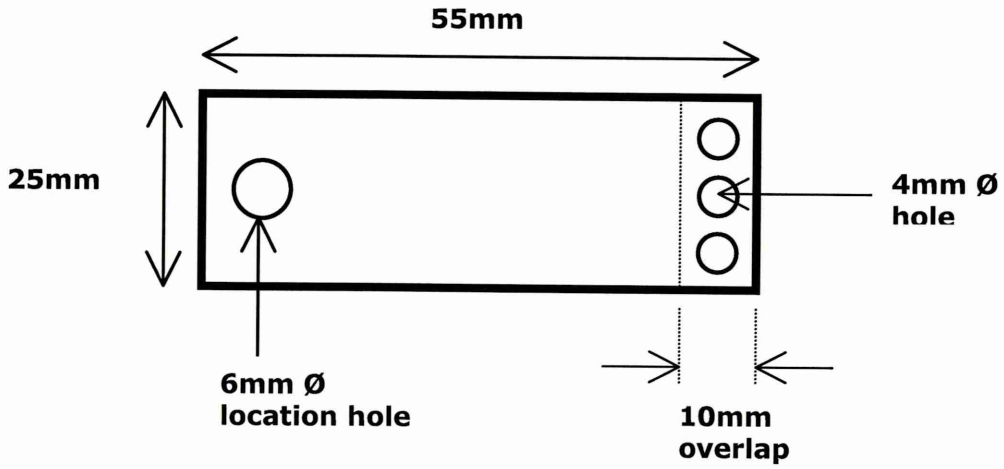

Figure 3.1 *- Perforated single overlap joint adherend dimensions*

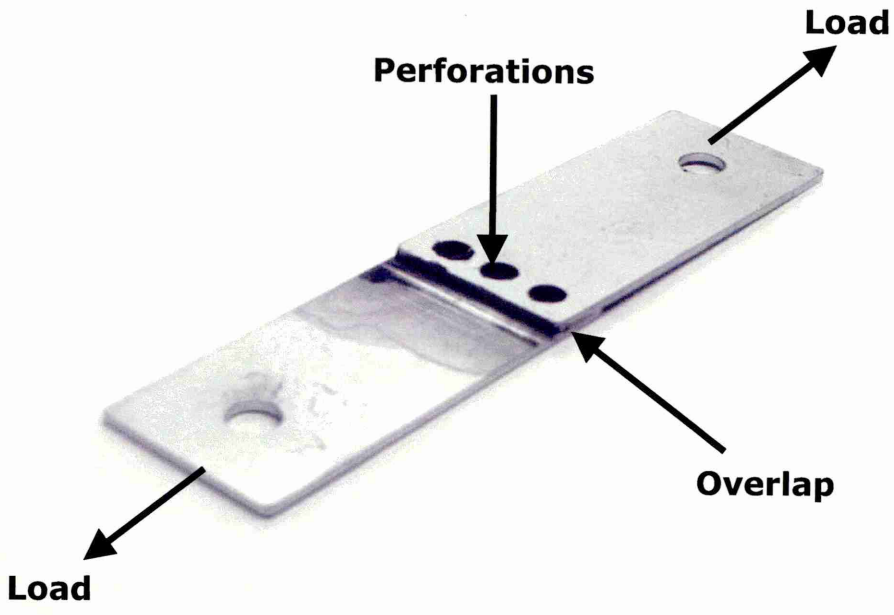

Figure 3.2 *- Perforated single overlap joint adherend dimensions*

A specially constructed jig permitted the fabrication of the perforated lap joints. Once suitable pre-treatments had been completed, adhesive was applied to both adherends constituting the joint and spread to wet the bondable area. The jig housed three locating pins that were machined to fit into the perforations. A substrate with adhesive is positioned onto the pins, and bondline control is enabled at this stage. The other substrate is then brought down through the pins and the two brought together, at which stage a mechanically sprung clip is attached to either side of the joint and all excess adhesive removed. The joint is removed from the locating pins and cured for 1 hour at 120°C.

3.5.3 Wedge Test Specimens

The Wedge test specimen was developed by Boeing to provide qualitative information on the environmental durability of surface pre-treatments. The configuration represents a double cantilever beam, allowing crack propagation to be measured, as shown in Figures 3.3 and 3.4.

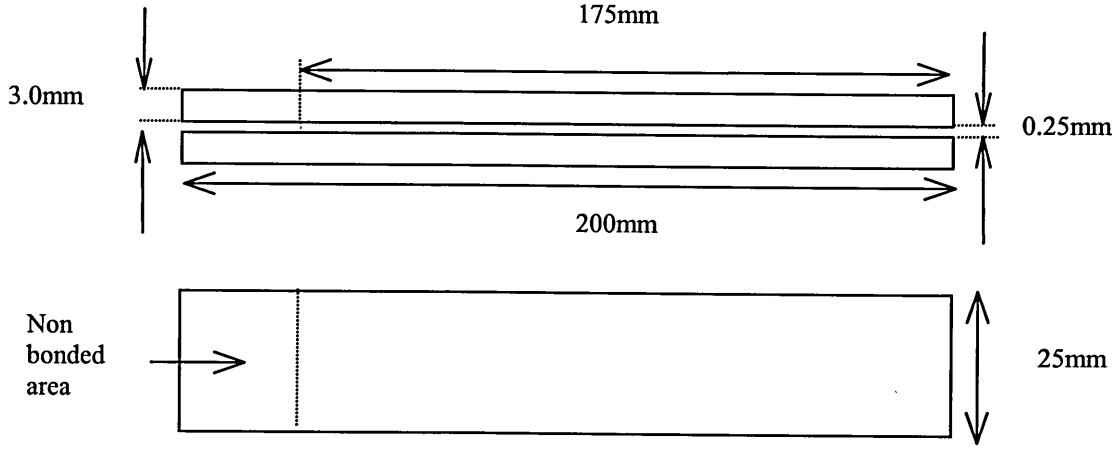

***Figure 3.3** - Wedge test specimen dimensions*

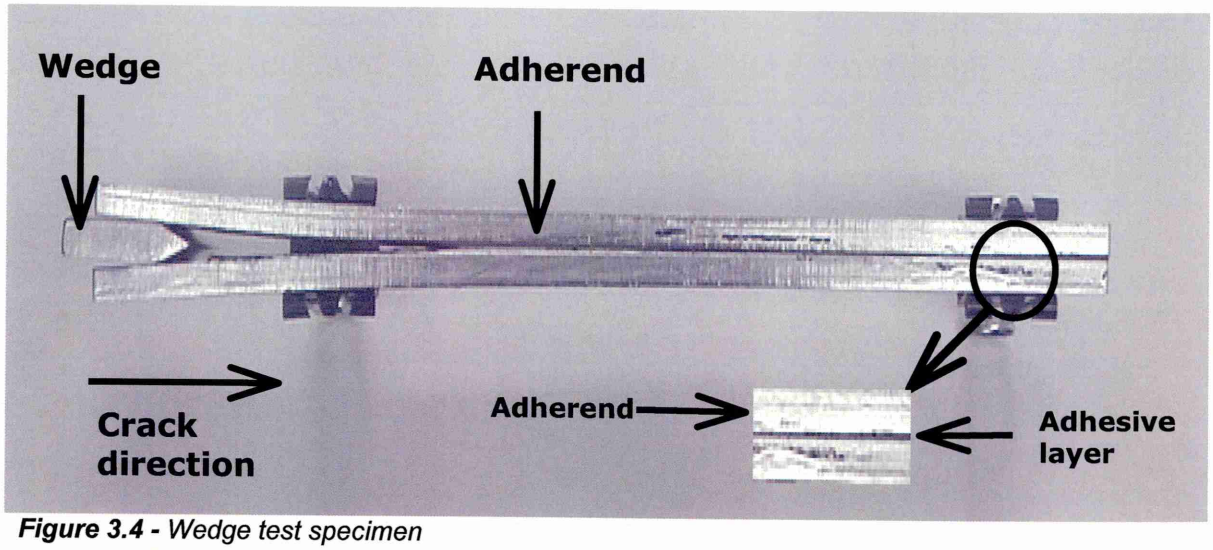

***Figure 3.4** - Wedge test specimen*

AISI 304L stainless steel coupons were fabricated using laser technology. After been pre-treated, adhesive was applied to the adherends and wire was inserted to achieve a bondline thickness of 0.25mm. A layer of PTFE 25mm in length was introduced at the end where the wedge is inserted. The substrates were then brought together and aligned, at which stage a series of mechanically sprung clips were attached along each side of the specimen. Once curing was complete, 1 hour at 120°C, the clips and adhesive fillets were removed. The edges were dry polished with diamond paste to ease observation of the propagating crack. A wedge is inserted into the non-bonded end and initial crack growth was recorded using a travelling microscope. The wedge test specimens were then exposed to appropriate environments and subsequent crack extension monitored at regular intervals using an optical travelling microscope.

3.6 Mechanical Testing

3.6.1 Apparent Lap Shear Strength

The apparent lap shear strength of single overlap joints was carried out in accordance with ASTM D 1002-94[3] using an Instron 4200 tensile testing machine, which has a response time short enough not to affect the accuracy of the load applied. The specification stipulates that the strain rate adopted must ensure fracture has occurred within 65±20 seconds. A constant displacement of the cross head was kept at $1.5mm^{-1}$. Standard laboratory conditions of $23\pm2^{0}C$ and a relative humidity of 50±5% were encountered whilst testing. The application of end tabs and suitable grips allowed the applied load to fall through the centre line of the assembly.

3.6.2 Sustained Load Testing

Room temperature sustained load tests were conducted in accordance with ASTM D 1780-94[4], using a Mayes creep rig. Single overlap joint specimens were loaded in tensile shear, with the time to fracture recorded at varying loads of the ultimate static fracture load.

3.6.3 Hydro-Thermal Stressing

Stress tubes where used to simultaneously apply loads to perforated lap shear specimens whilst been exposed to pre-determined environments. The stress tubes were manufactured to hold 6 perforated lap shear joints that have been bolted together in parallel. One end of the aluminium casing houses a locating pin, whilst the other houses the pre-calibrated spring and adjustment nut used to apply loads.

3.6.4 Fatigue Testing

Fatigue testing was carried out in accordance with ASTM D 3166-93[5], using a Mayes servo-hydraulic test machine. A suitable set of pinned grips was manufactured to hold the lap shear specimens in alignment when the load was applied. Specimens were tested in tension and subjected to a constant load amplitude and frequency in sinusoidal form. The cycles to failure was measured automatically, unless the specimen was removed prior to fracture.

3.7 Surface Characterisation

3.7.1 Physical Characterisation

3.7.1.1 Scanning Electron Microscopy

Scanning electron microscopy (SEM) was carried out using the Philips XL40. Specimen surfaces were cut to appropriate sizes and mounted onto SEM holders. SEM studies were used to characterise the modifications taken place due to surface pre-treatments prior to bonding, and the investigation of fracture surfaces. Where necessary samples were gold coated with a thickness of 100 to 200Å, using an Edwards 500 sputter coater. Surfaces were examined using secondary and back scattered electron images with an acceleration voltage of 20 kV.

3.7.1.2 Environmental Scanning Electron Microscopy

Environmental scanning electron microscopy (ESEM) was carried out using the Philips XL30, a microscope that includes a Field Emission Gun (FEG) and a gaseous secondary electron detector. The main advantage of the ESEM is the ability to view live specimens and samples at high temperature (~1000^{0}C), without the need for extensive sample preparation. The benefits of not coating samples allow artefacts to be detected that would usually be disguised. Samples were

examined using the gaseous secondary electron detector at a working distance of ~11mm, and an accelerating voltage of 20 kV.

3.7.1.3 Surface Profilometry

Surface roughness parameters of pre-bonded surfaces were attained using a Talysurf Profilometer, which incorporates a diamond tipped stylus that transverses across the samples to generate two and three dimensional profiles of the surface. Specimens were cut into 10 x 10mm pieces on which a 2 x 2mm-assessment zone was analysed.

3.7.1.4 Optical Microscopy

Olympus Vanox optical microscope coupled with Bruers image analysis package was used to optically observed fracture surfaces, and capture subsequent digital images.

3.7.2 Chemical Characterisation

3.7.2.1 X-ray Photoelectron Spectroscopy

X-ray Photoelectron Microscopy (XPS) was completed using a VG Microtech system with an Al(kα) source and a 15 kV incident beam. Data was collected via a triple channeltron detection (CLAM 2/4), from wide survey scans incorporating binding energies of 1100 – 0 eV. Samples surfaces of both pre-bonding and fractures surfaces were cut to 10 x 10mm pieces, to evaluate the surface chemistry introduced from surface pre-treatments and to attain the true loci of failure within fracture specimens. All the data produced was quantified.

3.8 Chapter References

[1] Boyes R. Adhesive Bonding of Stainless Steel: Strength and Durability, PhD Thesis, Sheffield Hallam University, 1998, ISBN 91 9720 217 7

[2] Private communication with Archer A, Albright and Wilson UK Limited, March 2000

[3] ASTM-D1002-94 'Apparent Shear Strength of Single Lap Joint Adhesively Bonded Metal Specimens by Tension Loading'

[4] ASTM-D1780-94 'Standard Practice for Conducting Creep Tests of Metal to Metal Adhesives'

[5] ASTM-D3166-93 'Standard Test Method for Fatigue Properties of Adhesive in Shear by Tension Loading (Metal/Metal)'

4.0 Environmental Durability

4.1 Introduction

Although initial joint strength is desirable, strength over a long period of time is an important parameter. Once an adhesive bond is fabricated and exposed to in-service environments, i.e. high humidity, cyclic loading and elevated temperatures, the mechanical properties of the bonded component may deteriorate rapidly. In certain circumstances the loss of a joints load bearing capacity has been so severe, components have failed at low levels of applied load with only a small fraction of its intended lifetime completed[1]. Before any in-service exposure commences it is of vital importance that the adhesive selected is capable of withstanding the expected loads and conditions the structure will encounter. The adherend is also eminently significant, since agents may depress or attack the interfacial zone between the adhesive and substrate, with may induce premature or catastrophic failure.

Single overlap shear joints were used to scrutinise between the degree of environmental durability acquired for various stainless steel adhesively bonded systems. The program incorporated DP490 toughed epoxy adhesive, due to its performance in the screening schedule devised by Boyes[2].

4.2 Effect of Surface Condition

The initial set of experiments were designed to assess the significance of the physical and chemical nature of the surface of three commercially available surface finishes, with respect to joint durability. Alumina blasted adherends were also incorporated as control specimens to aid comparison. Single overlap shear joints with an overlap length of 12.5mm, substrate thickness of 1.5mm and a width of 25mm were assembled, following details described in Chapter 3 section 3.4.1. Adherend material comprised of AISI 304L stainless steel, incorporating three surface finishes, namely bright annealed, semi-bright and dull matt, designated BA, 2B and 2D respectively. In addition single overlap joints with an alumina grit blasted and alumina grit blast + silane primer pre-treatments, as detailed in section 3.3.2 and 3.3.4, were produced with the 2B finish. Prior to bonding all adherends were alkaline degreased as outlined in section 3.3.1. All substrates were bonded with DP490 with a bondline thickness of 0.25mm, and left at room temperature to fully cure. Subsequent fillets were left intact to mimic real adhesive structures.

Sufficient single overlap shear joints were manufactured to make up three or four batches of thirty six joints to include each surface finish and pre-treatment. Each batch was then sub-divided into three sets of twelve. From each batch six joints were bolted together in series and subsequently loaded in a stress tube. Table 4.1 below details the loading and exposure conditions.

Table 4.1 - Loading and exposure conditions

Surface Finish	Surface Condition	Applied Load (kN)	Environment
BA	AD	1.6 2.5 3.0	60°C and 100% RH
2B	AD	1.6 2.5 3.0	60°C and 100% RH
2D	AD	1.6 2.5 3.0 4.0	60°C and 100% RH
2B	Alumina Grit Blast	1.6 2.5 3.0 3.5 4.0 5.0	60°C and 100% RH
2B	Alumina Grit Blast + Primer	1.6 4.0	60°C and 100% RH
2B	AD	1.6 2.5 3.0	Outdoor weathering*
2D	AD	1.6 2.5 3.0	Outdoor weathering*

***Stress tubes and non-stressed specimens were located on top of the departmental building.**
AD = Alkaline degreased

For each batch six joints were tested to failure to enable initial strength values to be obtained. The three remaining joints were conditioned as non-stressed controls with each exposed stress tube. Upon environmental exposure the stress tubes were checked at frequent intervals. When a failure was encountered it was replaced with a stainless steel dummy bar, and the tube was re-stressed. The time for the first three failures was noted and the average taken. The control and subsequent intact stressed specimens were tested to failure to correlate retained strength and the effect of stress. All fracture surfaces were evaluated in order to establish the mode of failure.

4.2.1 Initial Strength

The average initial lap shear strengths were taken from a batch size of 6, are given in Table 4.2, and represented graphically in Figure 4.1. Specimens were tested with fillets intact. The alumina grit blast + primer and alumina grit blast specimens performed best with apparent shear strength values of 8.33 and 8.20kN respectively. For non-treated samples the 2B and 2D adhesive joints gave the highest tensile shear values of 7.95 and 7.55kN respectively. Specimens constructed with BA adherends gave the worst failure load, with an average of 5.02kN. In all cases the level of scatter is low.

Table 4.2 *– Initial overlap shear strength*

Surface Finish	Mean Failure Load	Standard Deviation (kN)	Mean Apparent Shear Strength (N/mm^2)	Standard Deviation (N/mm^2)
Bright Annealed (BA)	5.04	0.42	16.13	1.33
Semi Bright (2B)	7.95	0.16	25.44	0.51
Matt Finish (2D)	7.55	0.39	24.16	1.26
Alumina Grit Blast	8.20	0.30	26.2	0.90
Alumina Grit Blast + Primer	8.33	0.27	26.35	0.89

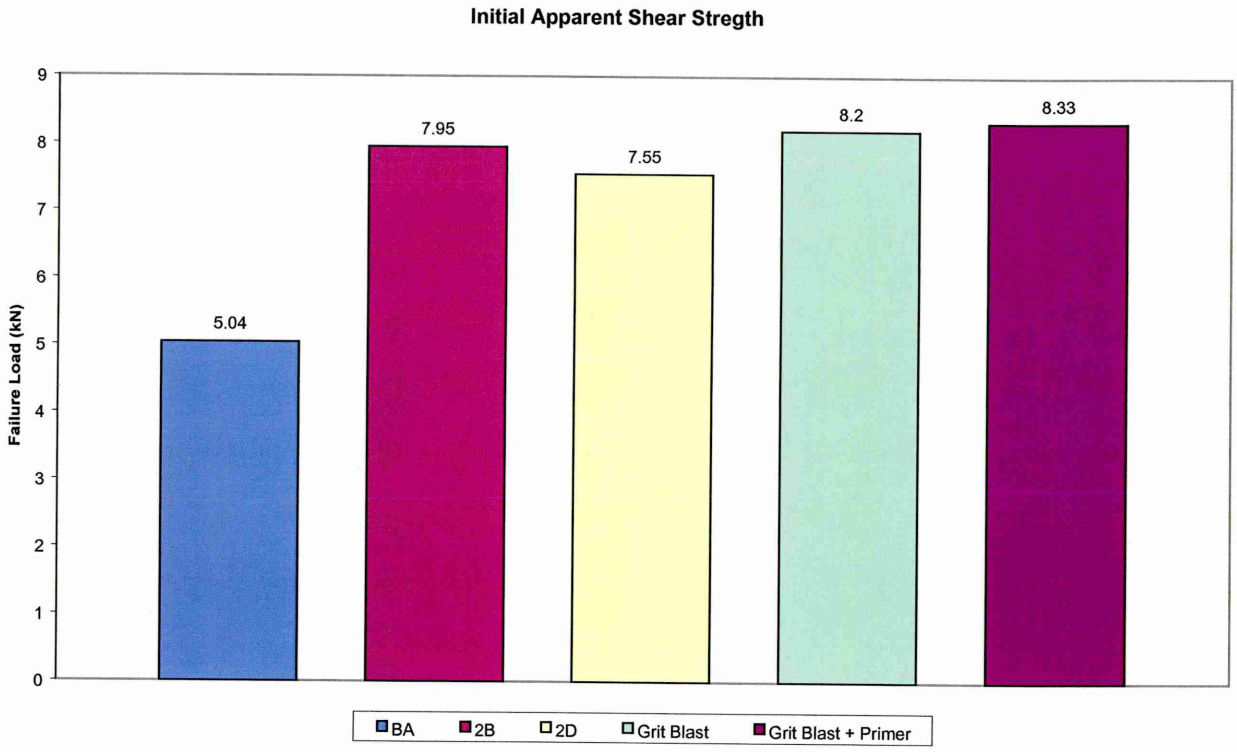

Figure 4.1 *– Initial overlap shear strength*

4.2.2 Stressed Durability

The results of the stressed durability tests for adhesive joints exposed to 60°C and 100% relative humidity are given in Table 4.3, and presented graphically in Figure 4.2.

***Table 4.3** – Stressed durability test results, 60°C and 100%RH (survival time in hours)*

	Applied Load (kN)					
Surface Finish	1.6	2.5	3.0	3.5	4.0	5.0
2B	256	211	122.3	-	-	-
2D	362	208	138.5	-	-	-
BA	213.1	147.5	98.6	-	-	-
Grit Blast	>5350	>5350	>5350	154.3	139.3	48
Grit Blast + Primer	>5350	-	-	-	30	-

Considering Figure 4.2, at all load levels the 2B and 2D surface finishes out perform the BA specimens. The difference in sustained load life between the three surface finishes is reduced when higher loads are imposed. As the applied load is reduced the improved performance offered by the 2B and 2D samples is clearly apparent. Environmental durability is enhanced considerably with the alumina grit blast and alumina grit blast + primer specimens, at applied loads of 1.6, 2.5 and 3.0kN there was no failures recorded. As the applied load is increased failure did occur, but at loads that are not characteristic of realistic in-service conditions.

The times to failure of adhesive joints exposed to natural outdoor weathering conditions are given in Table 4.4.

***Table 4.4** – Stressed durability test results, outdoor conditioning*

	Applied Load (kN)		
Surface Finish	**1.6**	**2.5**	**3.0**
2B	>8760	>8760	>8760
2D	>8760	>8760	>4300

No failures were observed for any load or surface finish combination.

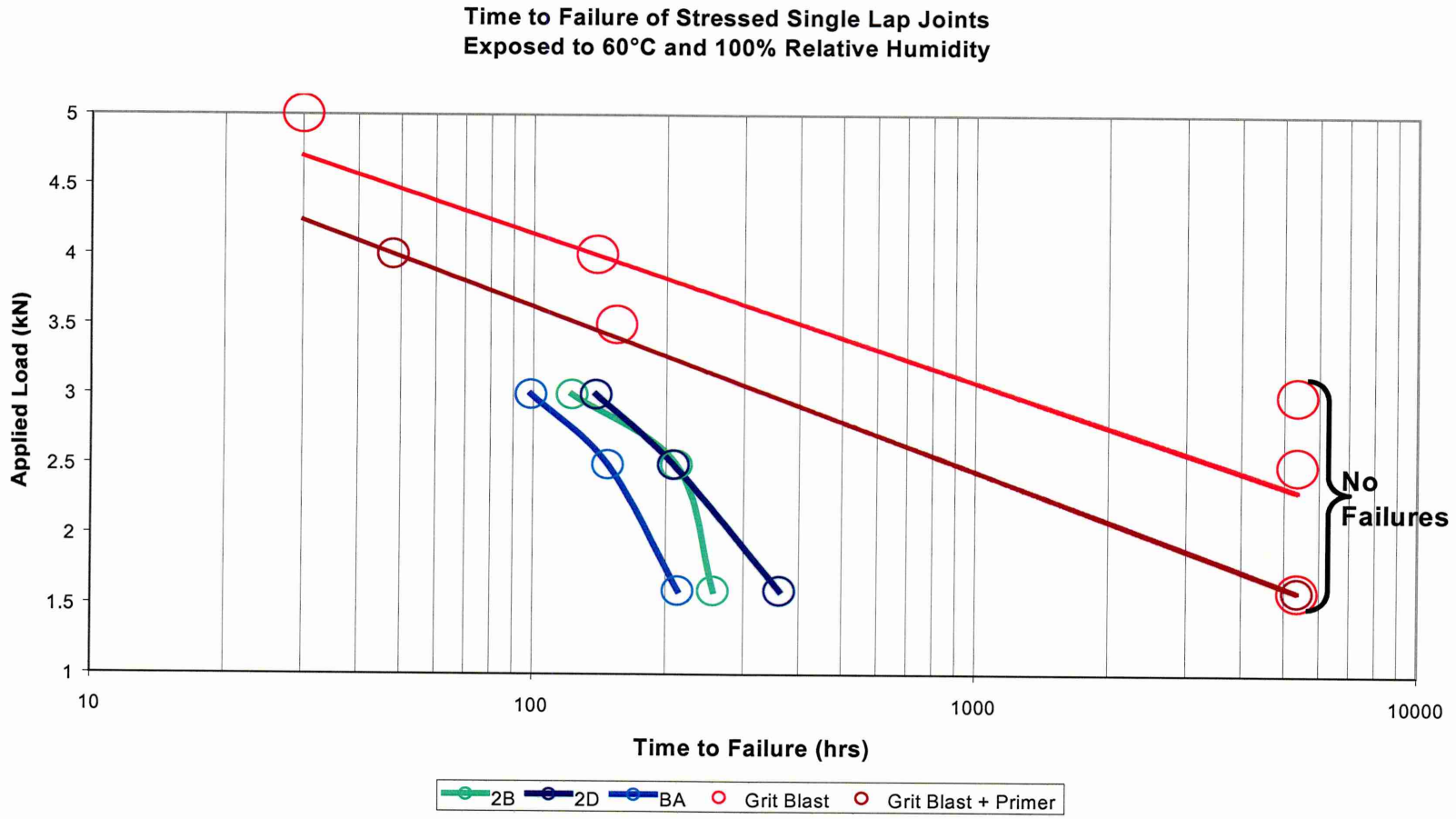

Figure4.2–*Time to failureof stressed lap pjoints,exposed to 60°C and 100%RH*

4.2.3 Residual Strength

The residual strength of non-stressed controls and non-failure specimens exposed to 60°C and 100% relative humidity are shown in Table 4.5.

Table 4.5 – Residual strength of non-stressed and non-failed single lap joints, 60°C and 100%RH

	Applied Load (kN)					
	1.6		2.5		3.0	
Surface Finish	Control	Non-Failure	Control	Non-Failure	Control	Non-Failure
BA	3.35	1.79	3.52	2.06	3.38	3.46
	3.99	1.97	3.05	2.89	3.91	2.83
	3.09	2.15	3.18	2.67	3.76	3.31
Average	**3.47**	**1.97**	**3.25**	**2.55**	**3.68**	**3.20**
Retained strength	**69.59%**	**39.40%**	**65%**	**51%**	**73.4%**	**64%**
2B	5.43	3.37	6.27	5.36	5.69	5.84
	4.98	4.56	5.91	5.15	6.54	5.77
	5.61	3.89	5.28	6.14	6.40	5.16
Average	**5.34**	**3.94**	**5.82**	**5.55**	**6.21**	**5.59**
Retained strength	**67.2%**	**49.6%**	**73.2%**	**69.8%**	**78.1%**	**69.93%**
2D	4.38	3.61	5.98	4.39	6.13	5.50
	4.77	3.22	6.46	5.02	7.23	5.92
	5.28	3.31	5.37	4.18	6.41	6.37
Average	**4.81**	**3.38**	**5.936**	**4.53**	**6.59**	**5.93**
Retained strength	**63.72%**	**44.8%**	**78.62%**	**60%**	**87.3%**	**78.5%**
Alumina Grit Blast	4.55	4.22	5.17	4.09	4.97	4.02
	4.66	4.46	4.44	4.18	5.34	4.14
	5.87	3.75	5.74	4.57	5.52	4.81
Average	**5.03**	**4.14**	**5.11**	**4.28**	**5.27**	**4.32**
Retained strength	**61.30%**	**50.52%**	**62.39%**	**52.19%**	**64.34%**	**52.72%**

	Applied Load (kN)					
	3.5		4.0		5.0	
	Control	Non-Failure	Control	Non-Failure	Control	Non-Failure
Alumina Grit Blast	-	5.97	-	5.64	-	6.27
	-	6.23	-	6.54	-	6.70
	-	6.79	-	6.55	-	7.10
Average		**6.33**		**6.24**		**6.69**
Retained strength	-	**77.16%**	-	**76.14%**	-	**81.56%**

Note that for alumina grit blast specimens loaded over 3kN, no control specimens were available. Also for alumina grit blast + primer joints no control specimens were available for all load levels tested.

The retained strength of un-stressed and non-failed specimens as a function of applied load will be considered first.

Bright Annealed BA, Figure 4.3

The retained strength of joints was adversely affected from the application of an applied load. For all load levels the retained strength of non-failures was lower than that of un-stressed controls. The observed trend implies the lower the imposed load the more depletion in strength occurred. For specimens loaded at 1.6kN the retained strength was 39.4%. For specimens loaded at 2.5kN and 3.0kN there was an increase in strength retention to 51% and 64% respectively

Semi-Bright Anneal 2B, Figure 4.4

A similar pattern emerged for stressed adhesive joints incorporating the 2B finish. Again the retained strength of all specimens was lower then the values attained by the un-stressed controls. Specimens stressed to the lowest load, 1.6kN, performed worst where only 46.9% of the initial strength was achieved. Again as the imposed load was increased so did the level of retained strength, where values of 69.8% and 69.93% were observed for loads of 2.5kN and 3.0kN respectively.

Dull Matt Finish 2D, Figure 4.5

Again the application of stress had a detrimental effects on strength retention. The inclination for specimens stressed at the minimum load to reap the lowest retained strength is evident. As the applied load was increased the retained strength for non-failures increased. For all load levels the retained strength of stressed specimens was worst than the un-stressed controls. The values of retained strength were 44.8%, 78.62% and 87.3% for joints stressed at 1.6kN, 2.5kN and 3.0kN respectively.

Alumina Grit Blast GB, Figure 4.6

For all load levels the retained strength for un-stressed controls and non-failure specimens is comparable. All specimens were exposure to the high humidity environment for 5350 hours. It has been observed the application of stress reduces the retained joint strength, where in all cases the specimens approximately ~52% of their initial strength. The un-stressed joints showed an increase in retained strength, where an average loss of ~38% was detected.

The effect of exposure to a high humidity environment as a function of time will now be considered for each surface finish and pre-treatment, with particular emphasis on un-stressed specimens.

Bright Annealed BA, Figure 4.7

All specimens exhibited a substantial loss in strength after a relatively short exposure time. For control specimens no further reduction in joint strength was observed for specimens aged in excess of 200 hours. Although the plotted stressed joints have had varying loads applied, it appears in a majority of cases the application of stress in high humidity environments reduces the amount of residual strength for single lap joints fabricated from bright annealed stainless steel.

Semi-Bright Annealed 2B, Figure 4.8

A sizeable reduction in lap shear strength has occurred during the first ~100 hours of environmental exposure. As the ageing time increases, there was not a significant decrease in joint strength. In comparison the application of stress in combination with high humidity increased the rate of strength loss.

Dull Matt Finish 2D, Figure 4.9

As the ageing time increases there was a reduction in residual strength for all specimens. For both control and stressed joints a similar pattern emerged, however the application of stress had a detrimental effect on retained strength.

Alumina Grit Blast, Figure 4.10

A reduction in lap shear strength was observed for all types of specimens. Joints were aged for over 5000 hours either in a stressed or non-stressed state. The application of stress did in general reduce the residual strength of the joints.

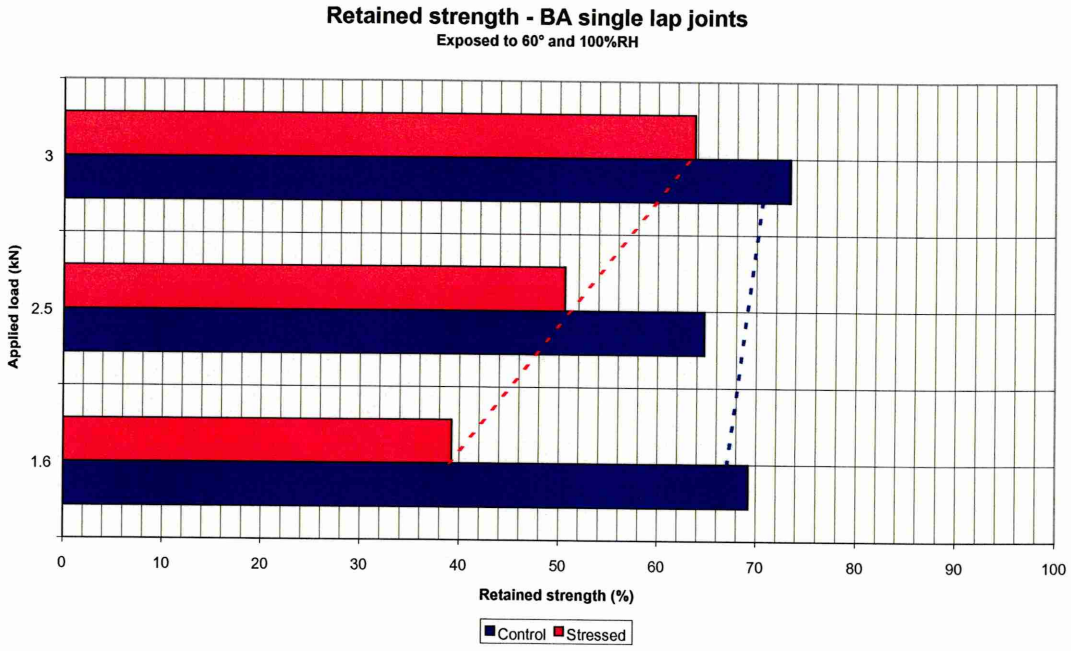

Figure 4.3 – *Retained strength of stressed and non-stressed BA lap joints as a function of load*

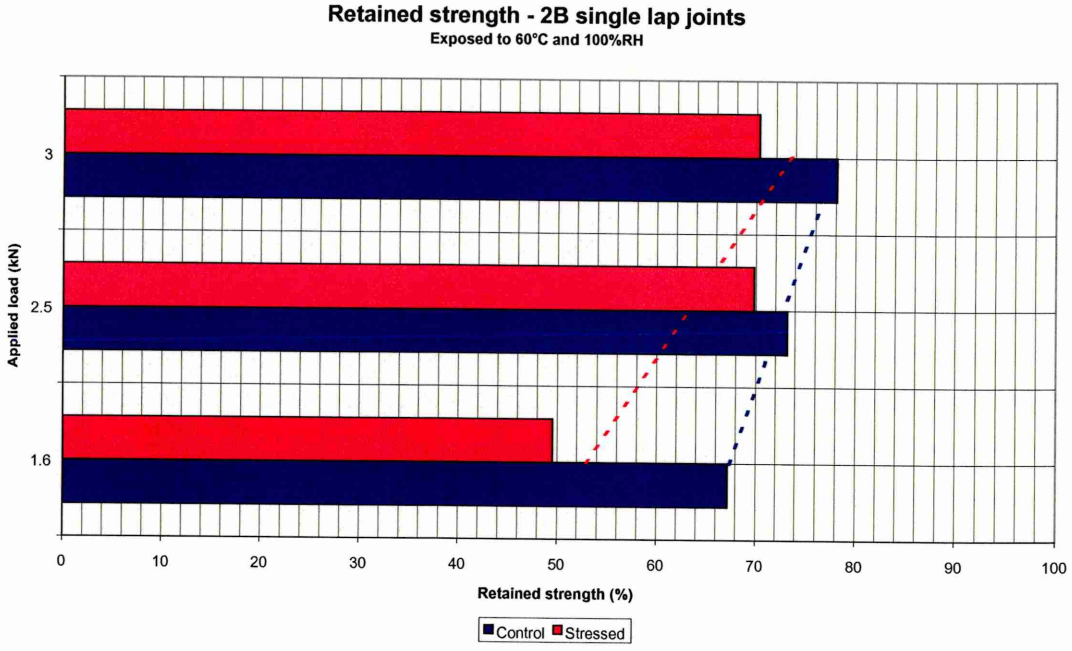

Figure 4.4 – *Retained strength of stressed and non-stressed 2B lap joints as a function of load*

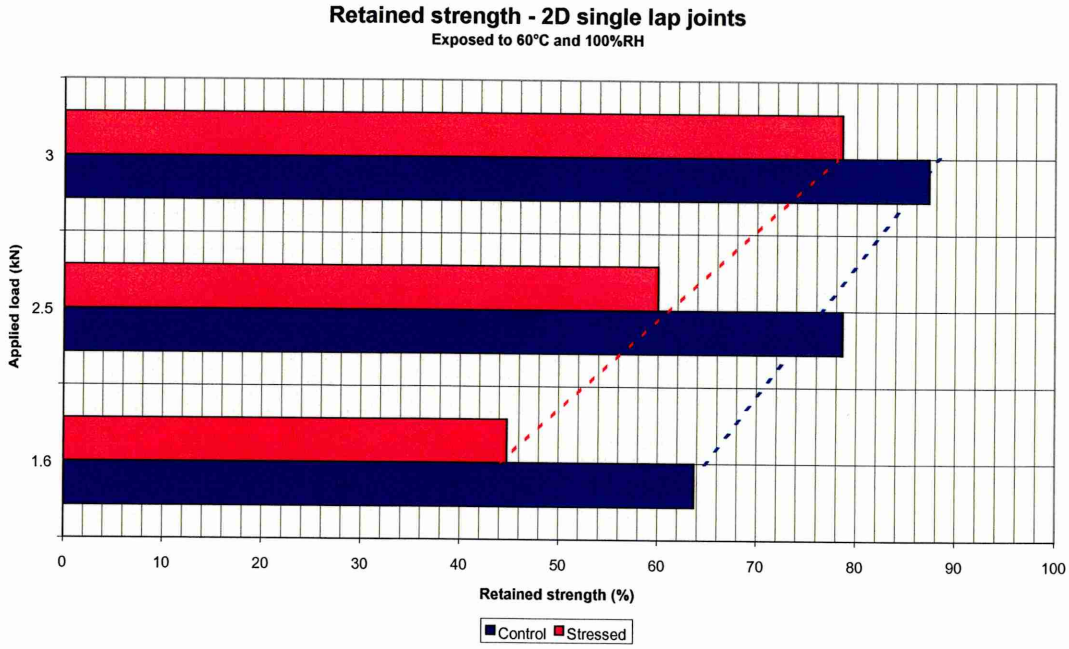

Figure 4.5 *– Retained strength of stressed and non-stressed 2D lap joints as a function of load*

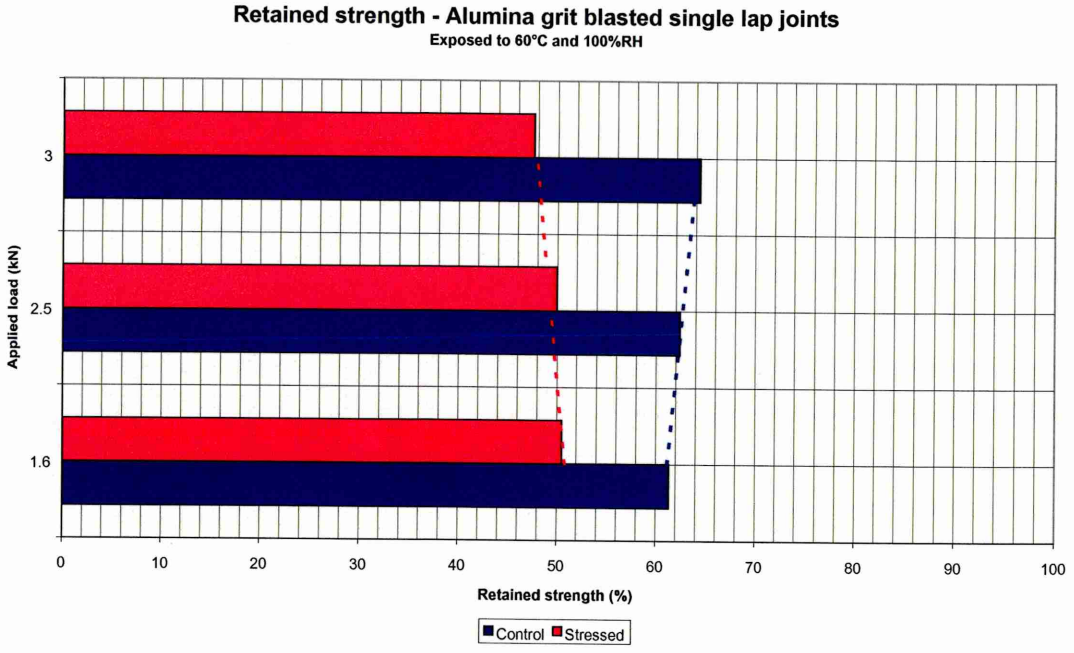

Figure 4.6 *– Retained strength of stressed and non-stressed alumina grit blasted lap joints as a function of load*

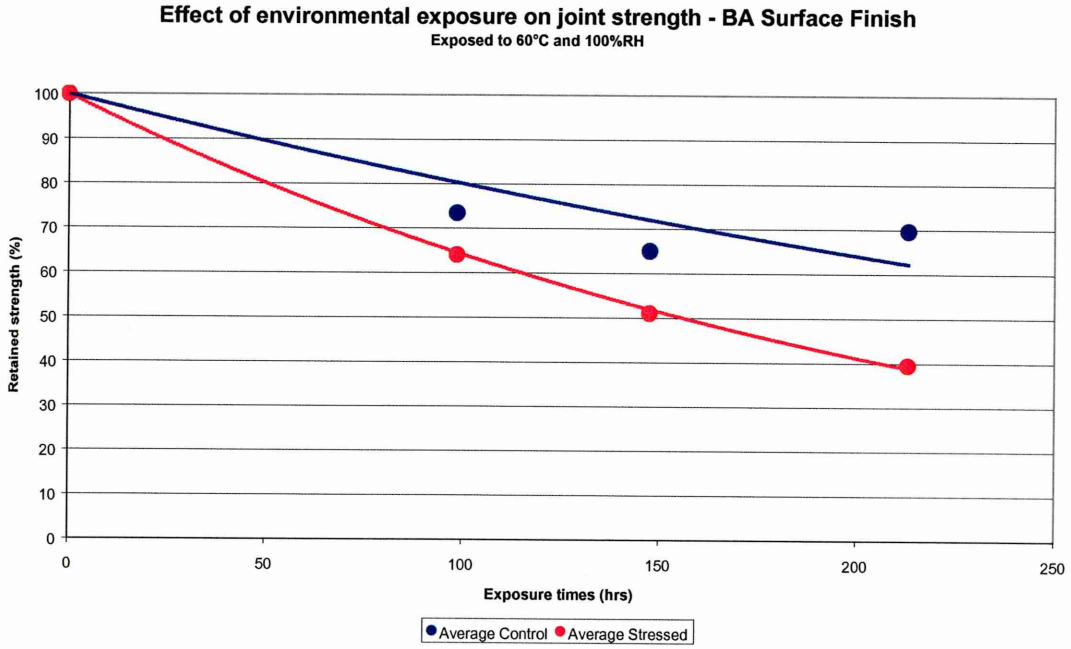

Figure 4.7 – *Effect of environmental exposure on BA lap joint strength*

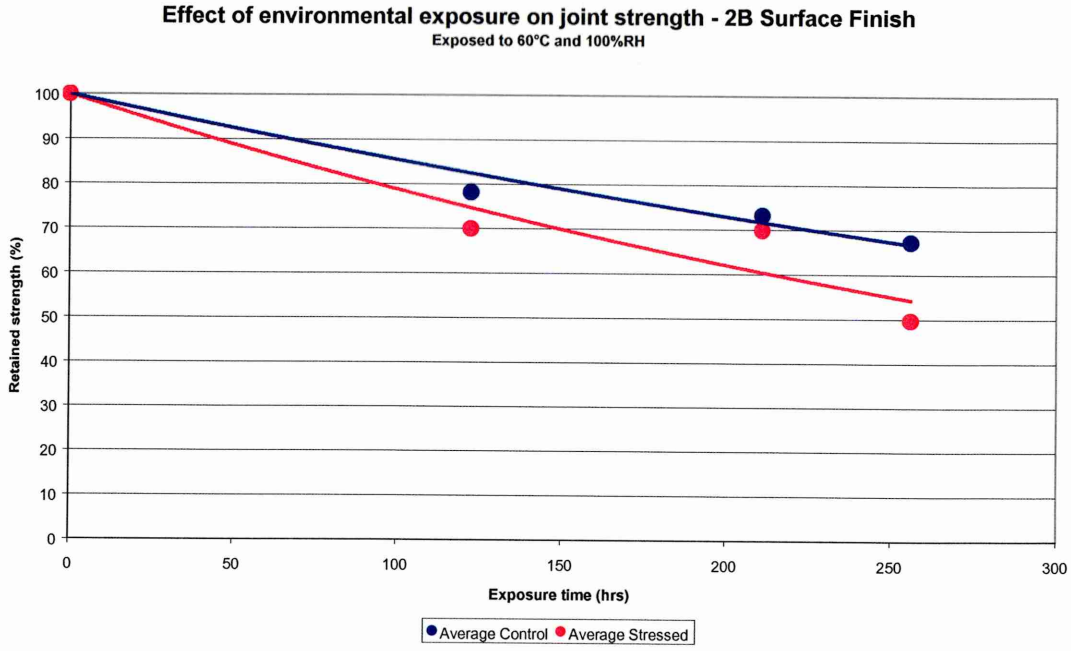

Figure 4.8 – *Effect of environmental exposure on 2B lap joint strength*

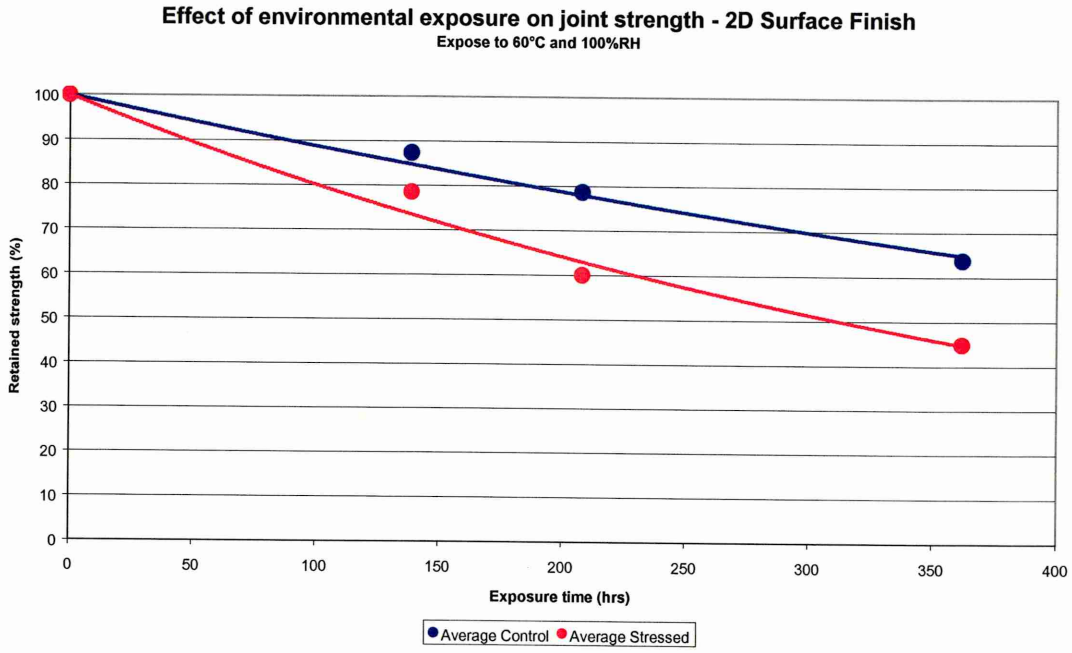

Figure 4.9 – *Effect of environmental exposure on 2D lap joint strength*

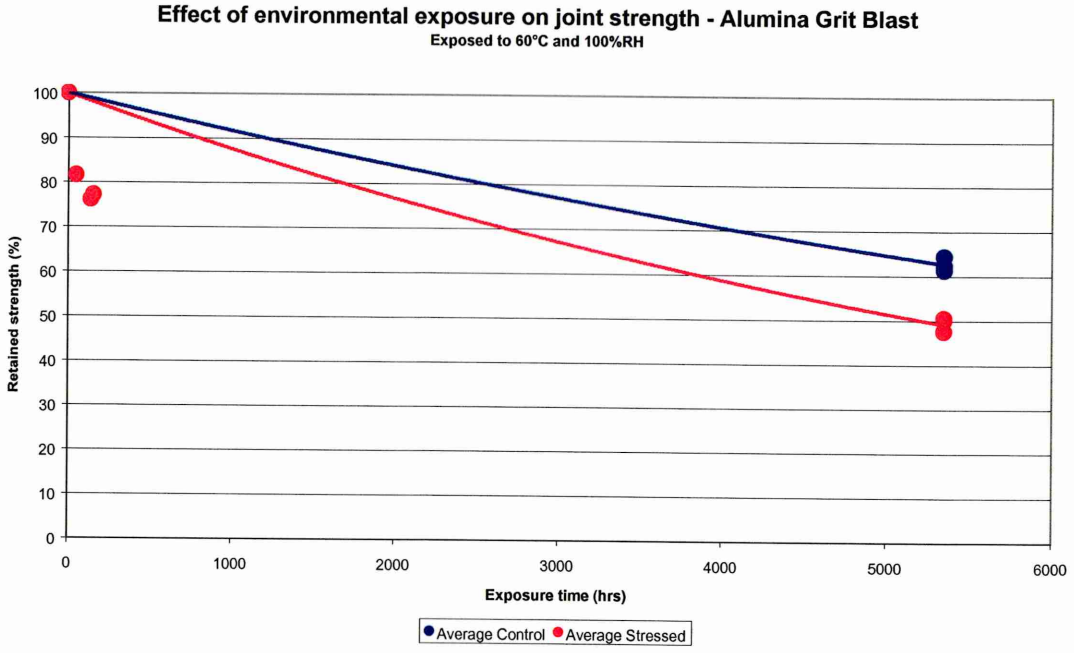

Figure 4.10 – *Effect of environmental exposure on alumina grit blasted lap joint strength*

The residual strength of un-stressed controls and non-failure specimens exposed to natural weathering conditions are given in Table 4.6 and represented graphically in Figure 4.11 and 4.12.

Table 4.6 *– Residual strength of non-stressed and non-failed single lap joints, exposed to natural weathering conditions*

	Applied Load (kN)					
	1.6		2.5		3.0	
Surface Finish	**Control**	**Non-Failure**	**Control**	**Non-Failure**	**Control**	**Non-Failure**
2B	7.41	6.91	7.30	6.82	7.59	6.61
	7.24	7.34	7.71	6.51	7.34	6.95
	7.93	7.29	7.10	6.93	7.11	7.18
Average	**7.53**	**7.18**	**7.37**	**6.75**	**7.35**	**6.91**
Retained strength	**94.67%**	**90.31%**	**92.70%**	**84.64%**	**92.42%**	**86.96%**
2D	6.78	6.33	7.15	7.09	7.26	6.21
	7.26	6.65	7.12	7.03	7.37	6.94
	7.24	7.37	7.33	6.88	6.64	6.62
Average	**7.09**	**6.78**	**7.20**	**7.00**	**7.09**	**6.59**
Retained strength	**93.95%**	**89.85%**	**95.36%**	**92.72%**	**93.91%**	**87.28%**

For both surface finishes the retained strength of the adhesive joints, whether stressed or unstressed, is very comparable for all load levels. The application of stress promotes a slight reduction in residual strength for both 2B and 2D joints.

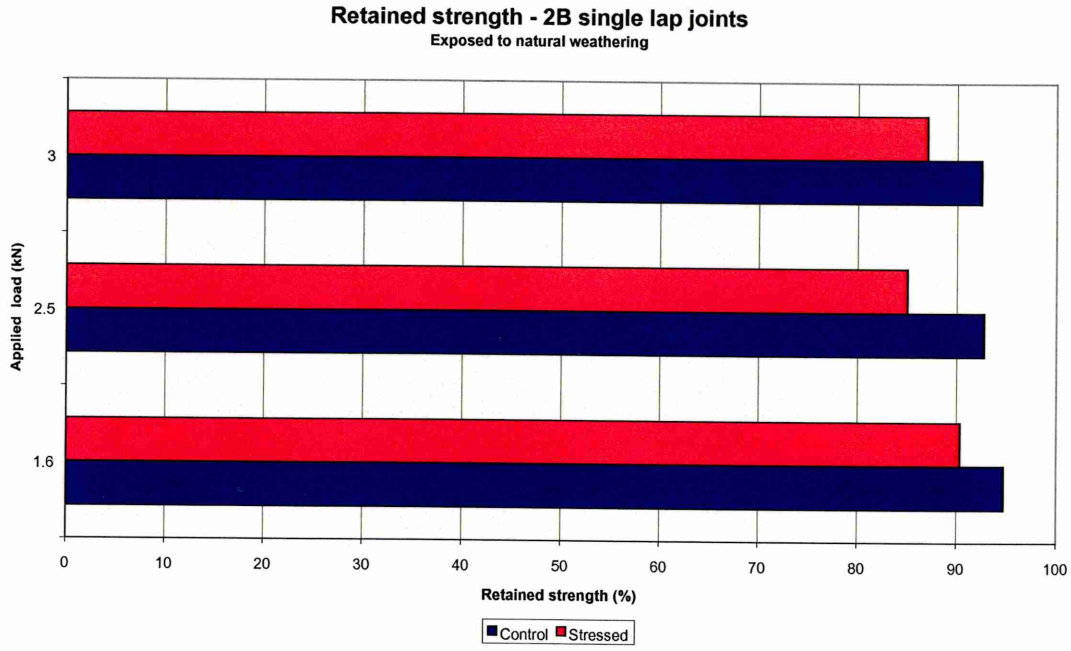

Figure 4.11 *– Retained strength of stressed and non-stressed 2B alkaline degreased lap joints as a function of load*

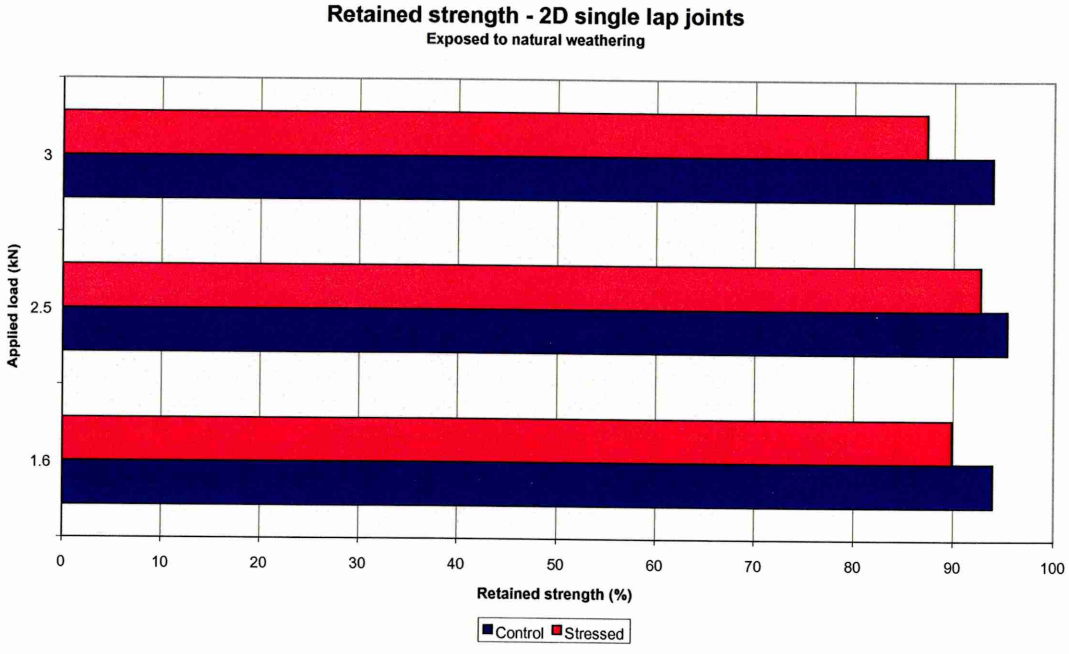

Figure 4.12 *– Retained strength of stressed and non-stressed 2D alkaline degreased lap joints as a function of load*

4.2.4 Closing Remarks

The surface finish of AISI 304L stainless steel influences the resistance to failure and retained strength of single lap shear specimens. For joints exposed to high humidity, the 2B and 2D surface finish out performs the BA product. However the sustained load life of joints was increased to in excess of 5000 hours at 60°C and 100% relative humidity, when adherends were either alumina grit blasted or alumina grit blasted and primed prior to bonding. For alkaline degreased only joints, the results indicate that increasing the applied load does not further reduced the retained strength. It has been shown that the residual strength of joints is worse when a low load-long exposure (to high humidity) regime is encountered. This observation is more apparent if the high humidity testing is compared with the natural weathering results. The residual strength of joints exposed to a natural climate is considerably higher that those exposed to high humidity, implying the performance of stainless steel-epoxy single lap joints is adversely affected by the presence of moisture. It would be reasonable to assume that the interfacial region of the bond has weakened as a result of water impregnation.

4.3 Effect of Surface Pre-Treatment

4.3.1 Introduction

As outlined in the *Review of Literature*, the need to suitably treat adherends prior to bonding is a prerequisite to aid in the resistance against environmental attack. To evaluate pre-treatments with respect to environmental durability the following surface treatments were assessed ;

1. Alumina Grit Blasting
2. Alumina Grit Blasting + Silane Primer
3. Alumina Grit Blasting + Accomet C©
4. Sulpho-Dichromate Anodising
5. Nitric Acid Anodising
6. Oxalic Acid Etch
7. Ferric Chloride Acid Etch
8. Alkaline Degreased
9. Alumina Grit Blasting + CP30 treatment
10. Alumina Grit Blasting + AZS treatment
11. Sulphuric Acid Etch

In order to achieve some practical results in a reasonable time scale the dimensions of the joint were reconsidered, i.e. the surface area of the bonded joint was diminished by reducing the width and overlap length and by incorporating perforations. As shown in section 4.2.2, the alumina grit blasting surface pre-treatment considerably increased environmental durability of standard single overlap joints. It is envisaged the incorporation of the above named pre-treatments will enhance adhesive joint durability, and if used in combination with the standard lap shear joint dimensions, excessively long exposure times will be required. In order to produce reliable durability data within a reasonable time scale the single overlap shear specimen used for this evaluation were modified as detailed in section 3.4.2 *Perforated Shear Joint*. This type of specimen diminishes the length of the diffusion path of the attacking media, thus providing the basis for accelerated testing, whilst permitting the discrimination of surface pre-treatments. Initial strengths were obtained for each pre-treatment with a batch size of three. Specimens were bolted into strings of six and inserted into stress tubes then loaded and exposed to conditions outlined in Table 4.7. Three un-stressed samples were used to act as controls. Samples were checked at frequent intervals for failures, at which point dummy samples were inserted and the stress tube re-loaded. The test was terminated, when three specimens failed.

In addition wedge specimens were manufactured in accordance with the procedure outlined in section 3.4.3 *Wedge Test Specimens*. This type of durability testing was incorporated into the research programme to compliment the perforated lap shear experiments. The wedge crack extension test is another method of exposing joints to hydro-thermal conditioning. Previous work[3] used adherends with a thickness of 1.5mm, however, once the wedge was inserted considerable plastic deformation took place. For the current work substrate thickness was

increased to 3mm to prevent yielding and maintain a tensile load at the crack tip and sustain Mode I cleavage opening. All wedge test samples were manufactured from AISI 304L stainless steel with a 2B finish, and alkaline degreased prior to pre-treatment. The combination of pre-treatments appraised in the perforated lap shear tests was used with the exception of the oxalic acid, ferric chloride and sulphuric acid etched surfaces. A batch size of three was used for each surface condition. The wedge specimens were exposed to 60°C and 100% relative humidity. Crack extension measurements were made using a travelling optical microscope.

***Table 4.7** – Loading and exposure conditions for perforated lap joints*

Surface Pre-treatment	Applied Load (kN)	Environment
Alumina Grit Blast	0.5 1.0 2.0	60°C and 100% RH
Alumina Grit Blast + Silane Primer	0.5 1.0 2.0	60°C and 100% RH
Alumina Grit Blast +Accomet C	0.5 1.0 2.0	60°C and 100% RH
Sulpho-Dichromate Anodising	0.5 1.0 2.0	60°C and 100% RH
Nitric Acid Anodising	0.5 1.0 2.0	60°C and 100% RH
Oxalic Acid Etch	0.5 1.0 2.0	60°C and 100% RH
Ferric Chloride Acid Etch	0.5 1.0 2.0	60°C and 100% RH
Alkaline Degreased	0.5 1.0 2.0	60°C and 100% RH
Alumina Grit Blasting + CP30 Treatment	0.5 1.0 2.0	60°C and 100% RH
Alumina Grit Blasting + AZS Treatment	0.5 1.0 2.0	60°C and 100% RH
Sulphuric Acid Etch	0.5 1.0 2.0	60°C and 100% RH

4.3.2 Perforated Lap Joints

4.3.2.1 Initial Strength

The initial strengths for perforated lap joints incorporating all surface pre-treatments are represented in Table 4.8 and graphically in Figure 4.13.

***Table 4.8** – Initial strength of perforated lap joints*

Surface Pre-Treatment	Mean Failure Load (kN)	Standard Deviation (kN)	Mean Apparent Shear Strength (N/mm^2)	Standard Deviation (N/mm^2)
Alumina Grit Blast	4.203	0.405	19.79	1.907
Alumina Grit Blast + Silane Primer	4.009	0.383	18.89	1.804
Alumina Grit Blast + Accomet C	3.88	0.078	18.28	0.368
Sulphuric Acid Sodium Dichromate Anodising	4.535	0.435	21.36	2.002
Nitric Acid Anodising	4.024	0.396	18.95	1.865
Oxalic Acid Etch	3.786	0.296	17.83	1.395
Ferric Chloride Etch	3.972	0.553	18.71	2.606
Alkaline Degreased	3.198	0.127	15.06	0.599
Alumina Grit Blast + CP30 Treatment	4.163	0.057	19.61	0.254
Alumina Grit Blast + AZS Treatment	4.361	0.177	20.54	0.833
Sulphuric Acid Etch	4.067	0.356	19.16	1.679

Considering Table 4.8, the best performance in terms of mean apparent shear strength came from the joints incorporating the sulphuric acid sodium dichromate anodising pre-treatment where a mean strength of 4.535kN was achieved. Surprisingly, mechanically modified joints treated with alumina blast media only, AZS and CP30 attained a high level of initial strength, with values of 4.203, 4.361 and 4.163kN respectively. Joints incorporating the proprietary treatments, Accomet C and Silane primer, and the remaining chemically treated joints had similar initial strengths ranging from 3.786 to 4.067kN. The lowest mean apparent strength came from joints incorporating the alkaline degreased surfaces, where adherends were given minimal surface preparation.

A large degree of scatter was observed, because a variety of flaws and defects are commonly encountered within the bondline. For example, voids from air entrapment and residual stresses from shrinkage during curing. From the initial strength testing the lowest scatter was from joints constructed with alumina blast + CP30, alumina blast + Accomet C and alkaline degreased treated surfaces, where the standard deviations were 0.057, 0.078 and 0.127kN respectively. The author was surprised to find the lowest scatter came from joints made with relatively simple pre-treatments. Joints involving more complex treatments, for example sulphuric acid sodium dichromate anodising, nitric acid anodising and ferric chloride etch produced wide scatter bands where the standard deviations were 0.435, 0.396 and 0.553kN respectively.

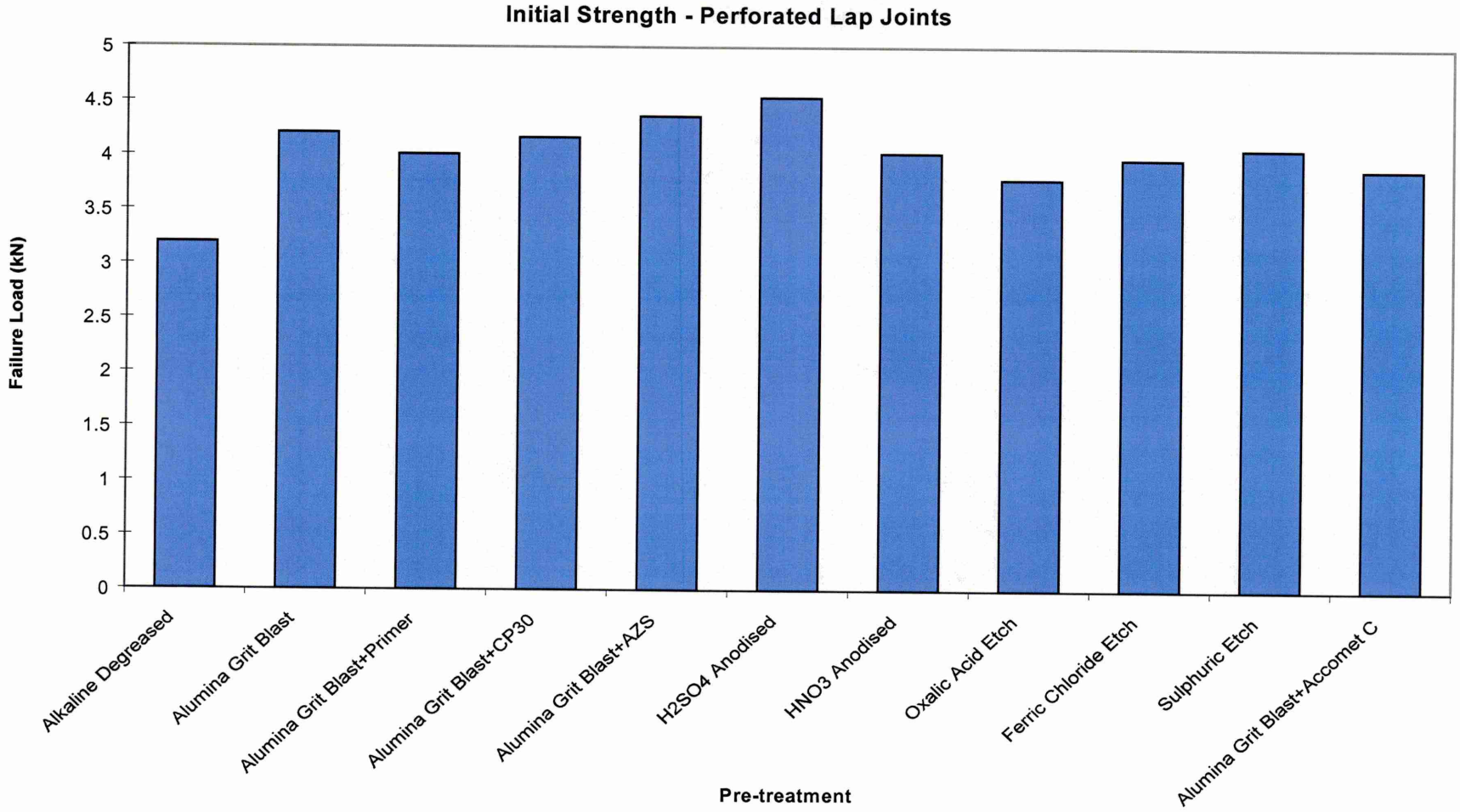

Figure 4.13 – *Initial joint strengths of perforated lap shear specimens*

4.3.2.2 Stressed and Perforated Lap Joints

Table 4.9 details the average lifetime of three failures with respect to different applied loads and surface pre-treatments. The results are represented graphically in Figure 4.14.

***Table 4.9** – Time to failure (hrs) for perforated lap joints exposed to 100%RH 60°C*

Pre-treatment	Load (kN)	Time to Failure (hrs)
Alkaline Degreased	0.5 1.0 2.0	168 120 49
Alumina Grit Blast	0.5 1.0 2.0	360 144 63.5
Alumina Grit Blast + Silane Primer	0.5 1.0 2.0	660 374 200
Alumina Grit Blast + CP30 Treatment	0.5 1.0 2.0	88 63 28
Alumina Grit Blast + AZS Treatment	0.5 1.0 2.0	224 166 52
Sulpho-Dichromate Anodising	0.5 1.0 2.0	>2520 424 330
Nitric Acid Anodising	0.5 1.0 2.0	>2520 320 196
Oxalic Acid Etch	0.5 1.0 2.0	228 203 148
Ferric Chloride Etch	0.5 1.0 2.0	788 196 130
Sulphuric Acid Etch	0.5 1.0 2.0	196 127 44
Alumina Grit Blast + Accomet C	0.5 1.0 2.0	>2520 992 567

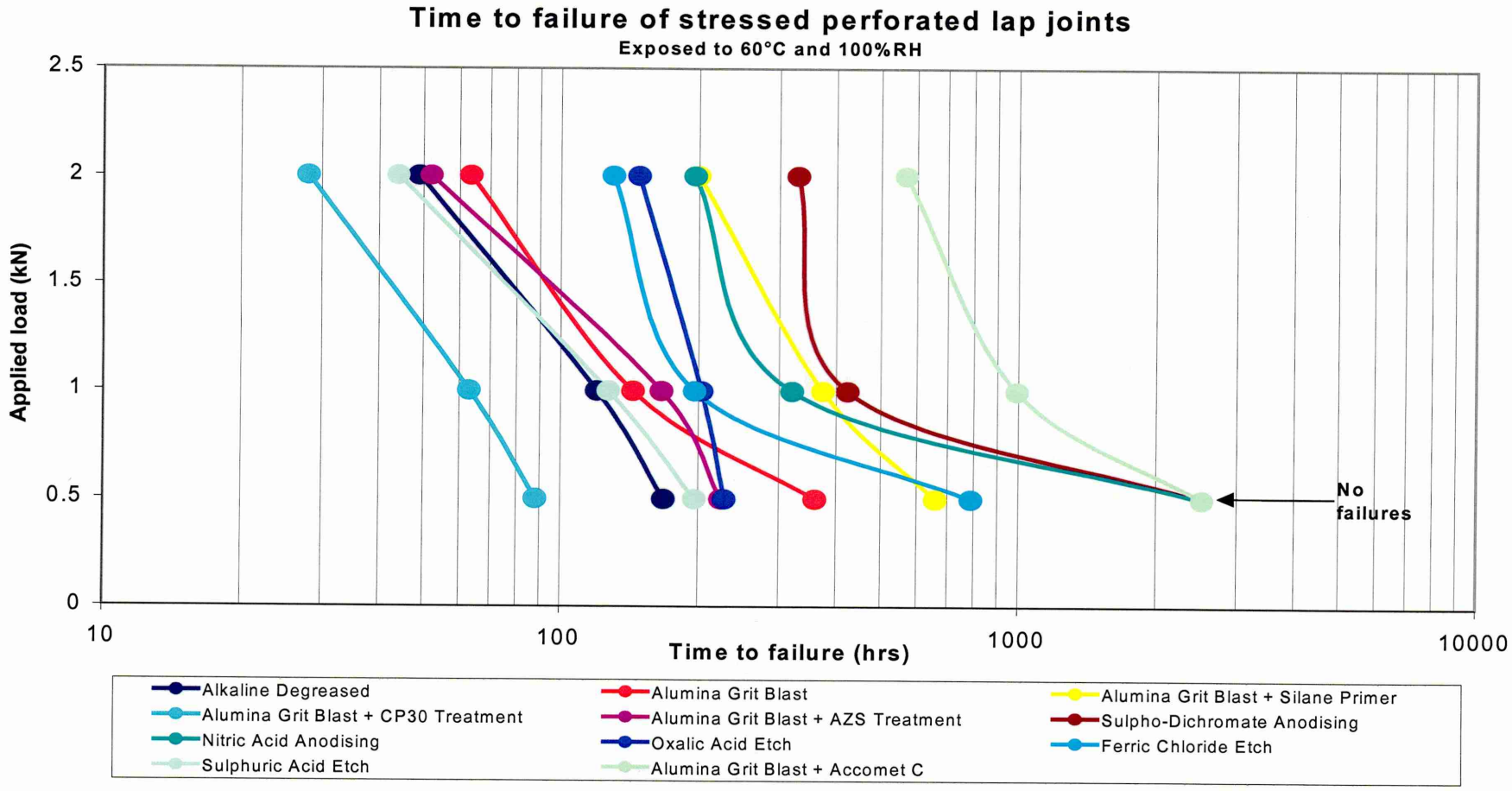

Figure 4.14 – *Time to failure of perforated lap shear joints exposed to 60°C and 100%RH*

Considering Table 4.9, the bonding systems that gave the highest resistance to the hydro-thermal stress regime at all levels of applied load were joints incorporating sulphuric acid sodium dichromate anodising, nitric acid anodising and alumina grit blasting + Accomet C pre-treatments. For each of these three systems, stressed specimens survived in excess of 2520 hours without failure when a load of 0.5kN was applied. Joints constructed using alumina grit blast + Silane primer and ferric chloride etch accomplished moderate performance. The other outstanding pre-treatments produced poor durability, notable specimens incorporating the alumina grit blast + CP30 pre-treatment.

4.3.2.3 Residual Strength

To determine the combined effects of an applied stress and harsh environment on joint strength, the remaining un-stressed control and non-failed joints were tested to failure. Tables 4.10 and 4.11 below list the residual strengths obtained for both un-stressed and intact samples respectively. The values shown are an average of three measurements.

***Table 4.10** - Residual strength of non-stressed specimens*

Pre-treatment	Applied Load (kN)	Failure Load (kN)	Retained Strength (%)
Alkaline Degreased	0.5	1.98	61.94
	1.0	2.23	69.64
	2.0	2.14	66.82
Alumina Grit Blast	0.5	2.51	59.72
	1.0	2.82	67.09
	2.0	3.27	77.80
Alumina Grit Blast + Primer	0.5	2.14	53.43
	1.0	2.39	59.54
	2.0	2.53	63.21
Alumina Grit Blast + CP30	0.5	1.62	38.96
	1.0	1.86	44.75
	2.0	1.81	43.50
Alumina Grit Blast + AZS	0.5	1.74	39.88
	1.0	1.65	37.79
	2.0	1.67	38.29
Sulpho-Dichromate Anodising	0.5	2.18	48.11
	1.0	2.87	63.17
	2.0	2.66	58.65
Nitric Acid Anodising	0.5	2.55	63.37
	1.0	2.97	73.86
	2.0	3.04	75.55
Oxalic Acid Etch	0.5	1.95	51.4
	1.0	2.03	53.67
	2.0	1.85	48.73
Ferric Chloride Etch	0.5	1.56	39.38
	1.0	2.05	51.56
	2.0	1.88	47.43
Sulphuric Acid Etch	0.5	2.10	51.64
	1.0	2.51	61.59
	2.0	2.43	59.98
Alumina Grit Blast + Accomet C	0.5	2.78	71.73
	1.0	2.69	69.54
	2.0	2.85	73.38

Table 4.11 - Retained strength of non-failures

Pre-treatment	Applied Load (kN)	Failure Load (kN)	Retained Strength (%)
Alkaline Degreased	0.5	1.82	56.75
	1.0	2.34	73.10
	2.0	2.06	64.25
Alumina Grit Blast	0.5	2.12	50.51
	1.0	2.68	63.80
	2.0	2.33	55.46
Alumina Grit Blast + Primer	0.5	1.85	46.10
	1.0	2.05	51.01
	2.0	2.09	52.28
Alumina Grit Blast + CP30	0.5	1.33	31.95
	1.0	1.74	41.89
	2.0	1.51	36.25
Alumina Grit Blast + AZS	0.5	1.55	35.54
	1.0	1.46	33.55
	2.0	1.28	29.44
Sulpho-Dichromate Anodising	0.5	1.94	42.78
	1.0	2.64	58.21
	2.0	2.50	55.19
Nitric Acid Anodising	0.5	2.14	53.18
	1.0	2.54	63.12
	2.0	2.45	60.91
Oxalic Acid Etch	0.5	1.84	48.47
	1.0	1.78	46.88
	2.0	1.48	38.96
Ferric Chloride Etch	0.5	1.38	34.74
	1.0	1.48	37.19
	2.0	2.00	50.35
Sulphuric Acid Etch	0.5	2.57	66.31
	1.0	2.99	77.08
	2.0	2.73	70.46
Alumina Grit Blast + Accomet C	0.5	2.57	66.31
	1.0	2.99	77.08
	2.0	2.73	70.46

4.3.2.3.1 Effect of Applied Load

A reduction in lap shear strength was observed for both stressed and unstressed specimens after environmental exposure. The effect of applied load on retained strength will be considered for all pre-treatments evaluated.

Alkaline Degreased, Figure 4.15

There is no observant tend to suggest the level of applied load is directly linked to the amount of retained strength. For alkaline degreased specimens the application of load does not appear to influence the strength retention of lap joints.

Alumina Grit Blast, Figure 4.16

For loaded specimens there is no significant difference in retained strength between the load levels, where the average retained strength falls within 55-65% of the initial strength. As the load is increased to 2.0kN it appears the retained strength of control specimens increases.

Alumina Grit Blast + Primer, Figure 4.17

Assessing the average retained strength values, the general trend implies that the application of stress reduced the residual strength of the joint. Although aged for different lengths of time, the retained strength of stressed joints is similar for all load levels.

Alumina Grit Blast + CP30, Figure 4.18

The average values indicate the application of stress slightly reduces the retained strength. Assessing stressed joints there is no significant difference in retained strength between all three load levels.

Alumina Grit Blast + AZS, Figure 4.19

Looking at the average values, the application of stress produces an insubstantial reduction in retained strength. The level of applied load does not appear to affect the amount of retained strength, where the retained strength for stress specimens at all load levels is ~35%.

Sulphuric Acid Sodium Dichromate Anodised, Figure 4.20

The variance in retained strength for both stressed and non-stressed specimens is negligible at all load levels. For specimens associated with the 0.5kN regime, the retained strength for both stressed and non-stressed joints is lower than that of the 1 and 2kN load levels.

Nitric Acid Anodised, Figure 4.21

For all levels of applied load, the average retained strength of stressed joints is lower than their associated control specimens. The scatter bands are also much wider for stressed specimens.

Oxalic Acid Etch, Figure 4.22

Taking average values into account, the retained strength for stressed joints is marginally lower than that of un-stressed controls. No distinct pattern has emerged for strength retention with respect to load level, the retained strength is similar for all cases.

Ferric Chloride Etch, Figure 4.23

There is not sizeable difference in retained strength between either the stressed or un-stressed joints. Although for joints stressed to 0.5 and 1kN, their residual strength is lower then the associated un-stressed specimens. But at the 2kN regime the average value for the retained strength of the stressed joints is higher then the un-stressed controls.

Sulphuric Acid Etch, Figure 4.24

There is a high level of scatter between the stressed and un-stressed joints, and no pattern or trend has emerged. For all load levels the strength retention for stressed joints is very comparable.

Alumina Grit Blast + Accomet C, Figure 4.25

Assessing the average values, there is very little difference in strength retention between stressed and un-stresses joints at all load levels.

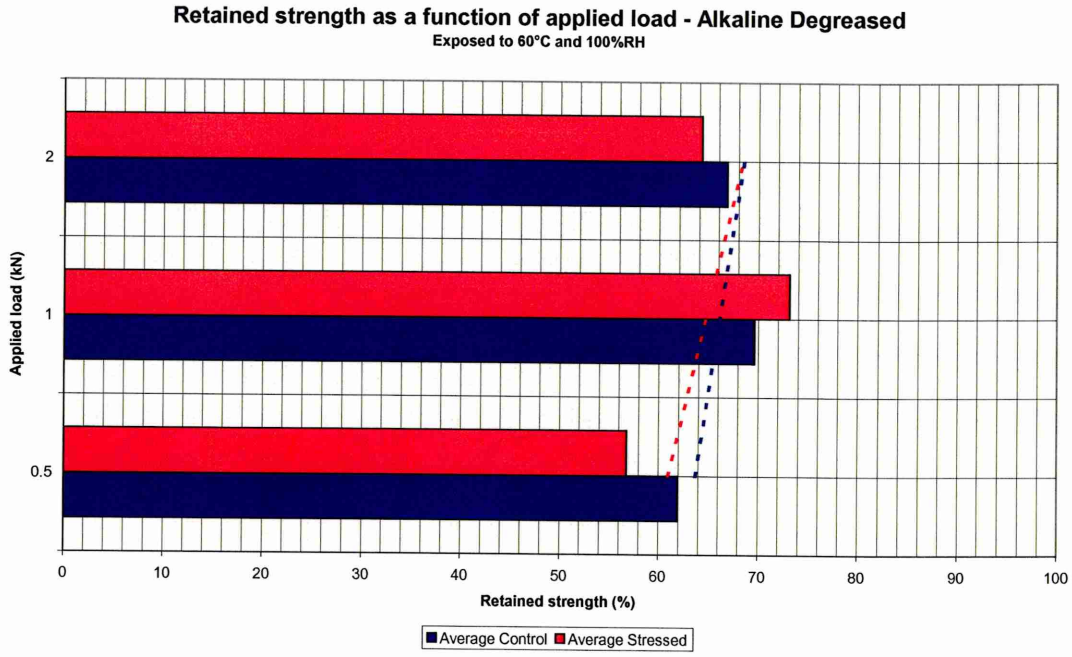

Figure 4.15 *- Retained strength of stressed and non-stressed alkaline degreased perforated lap joints as a function of load*

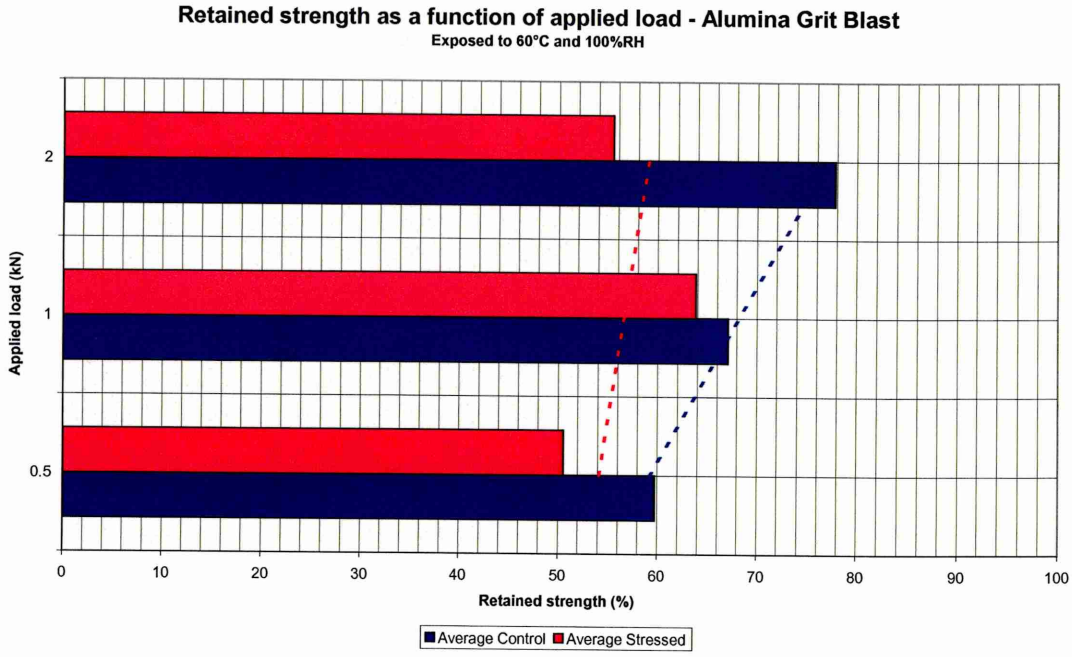

Figure 4.16 *- Retained strength of stressed and non-stressed alumina grit blasted perforated lap joints as a function of load*

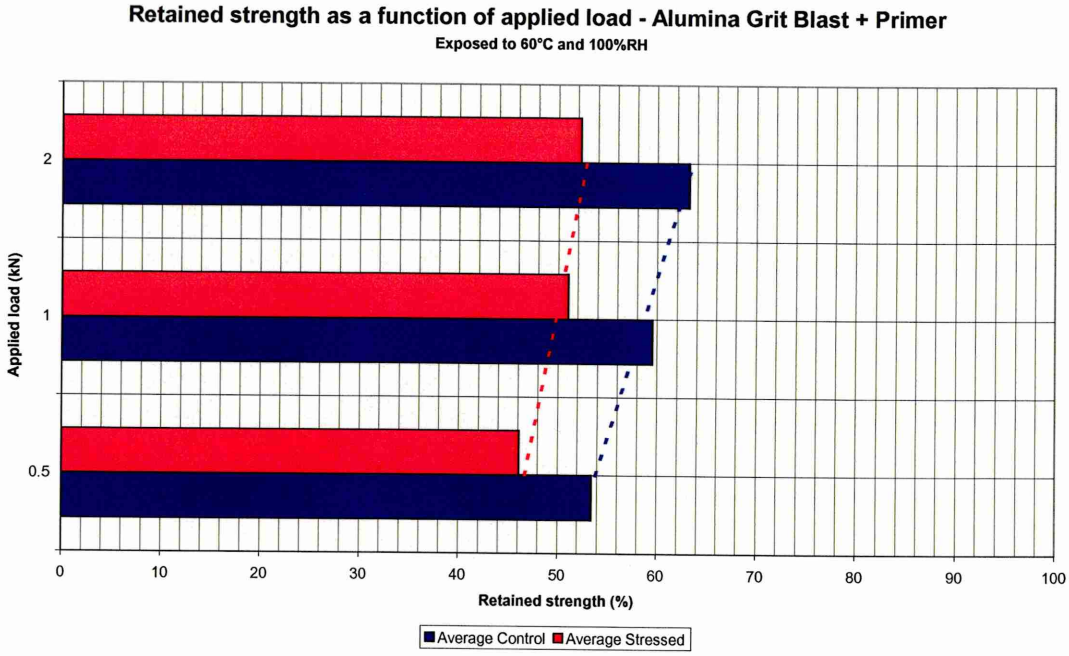

Figure 4.17 *- Retained strength of stressed and non-stressed alumina grit blast + primer perforated lap joints as a function of load*

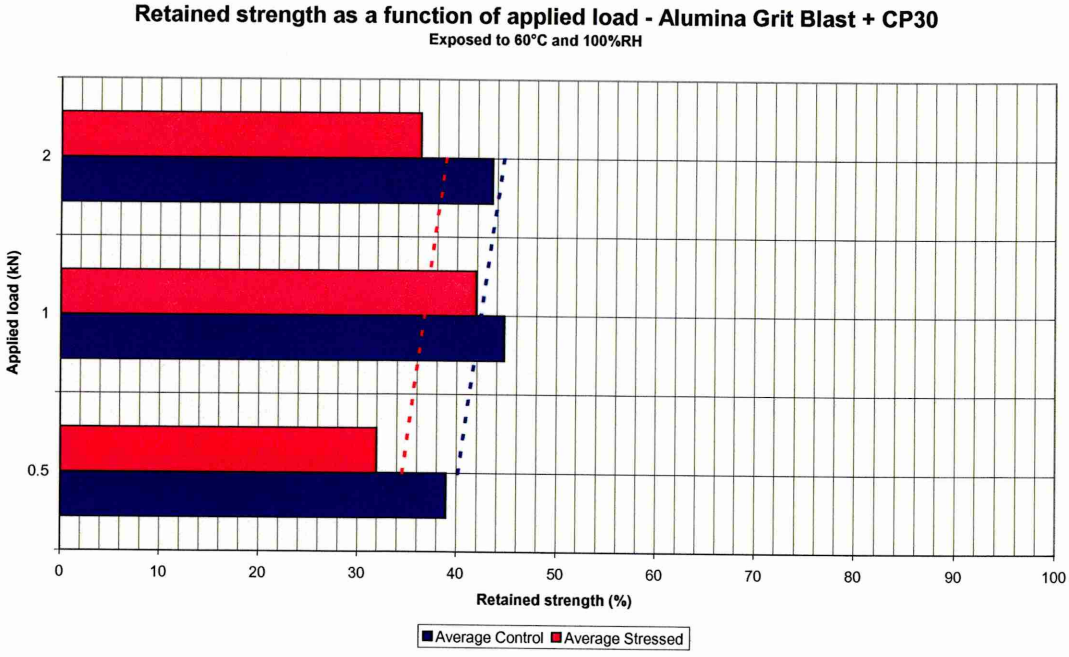

Figure 4.18 *- Retained strength of stressed and non-stressed alumina grit blast + CP30 perforated lap joints as a function of load*

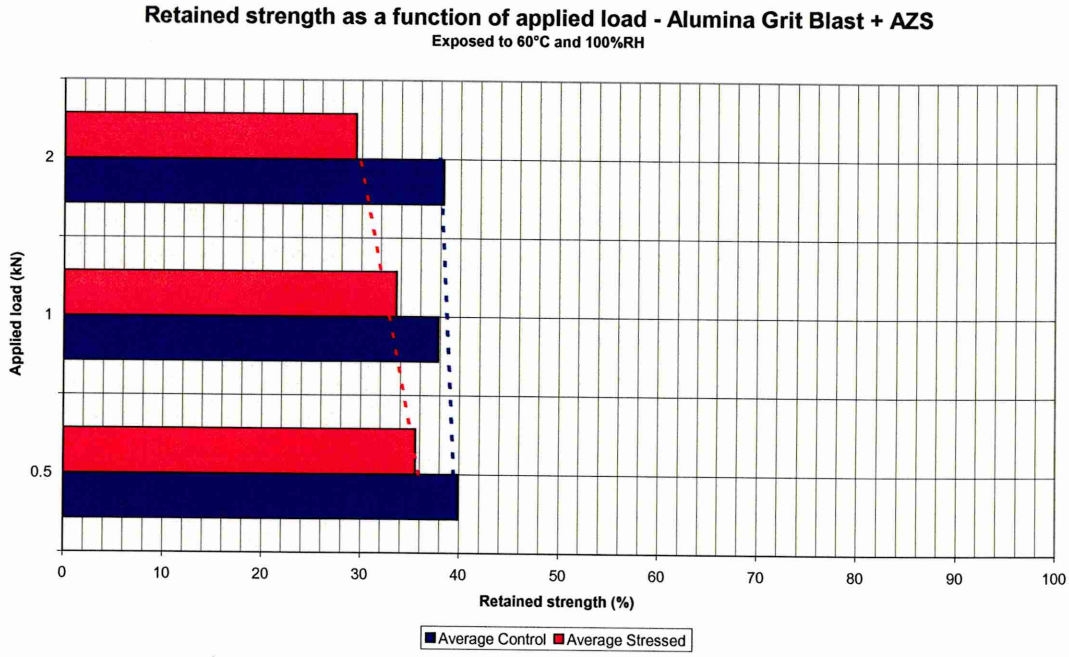

Figure 4.19 *– Retained strength of stressed and non-stressed alumina grit blast + AZS perforated lap joints as a function of load*

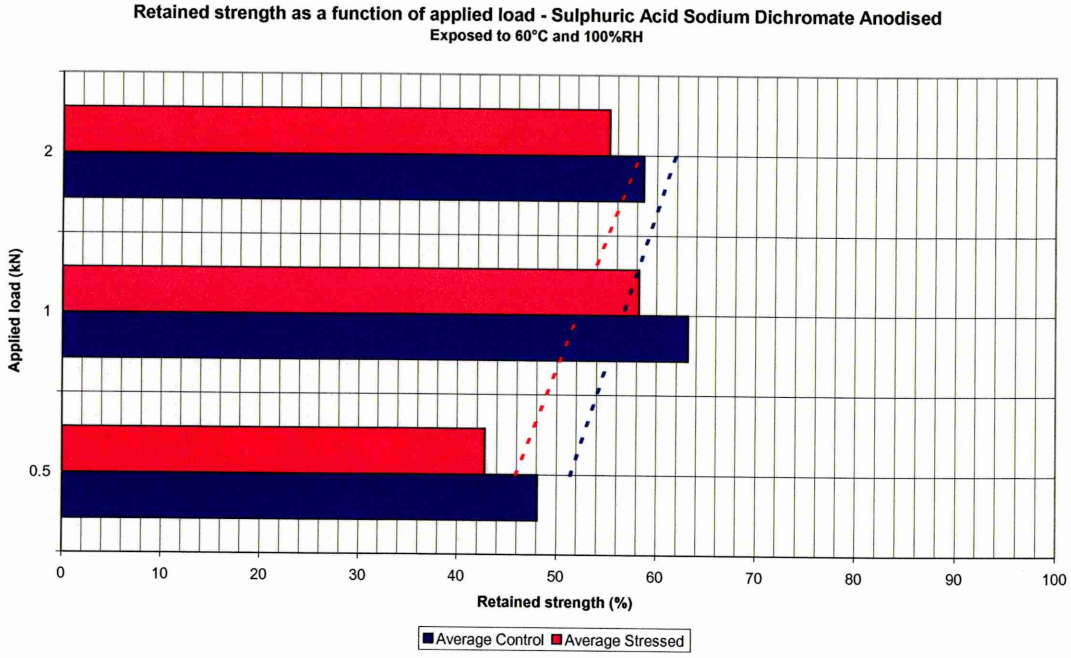

Figure 4.20 *- Retained strength of stressed and non-stressed sulphuric acid sodium dichromate anodised perforated lap joints as a function of load*

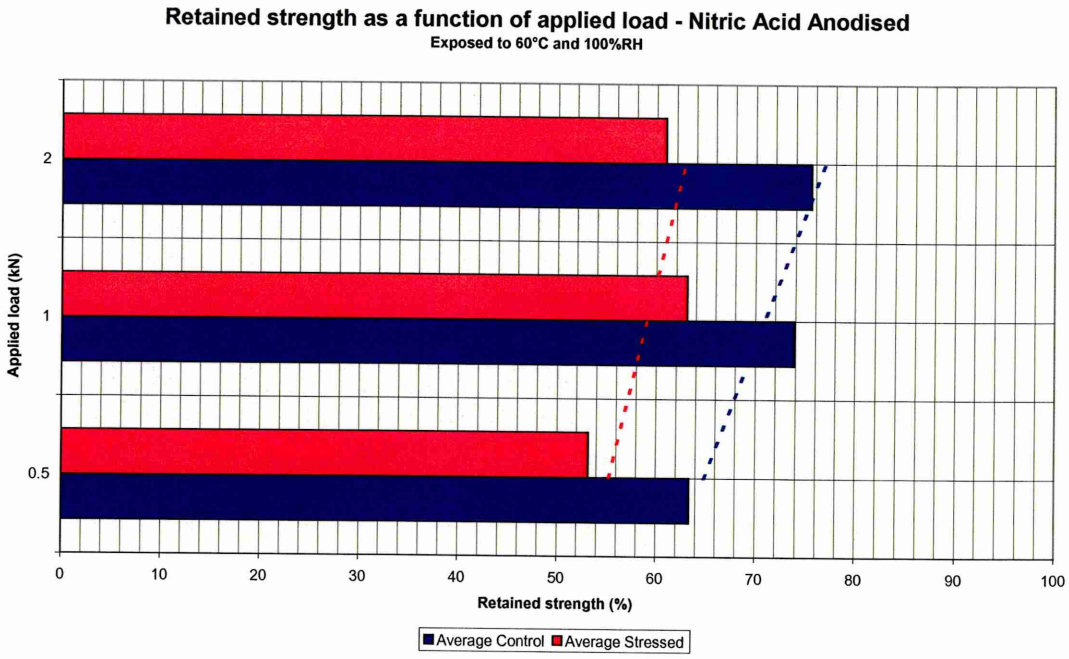

Figure 4.21 - *Retained strength of stressed and non-stressed nitric acid anodised perforated lap joints as a function of load*

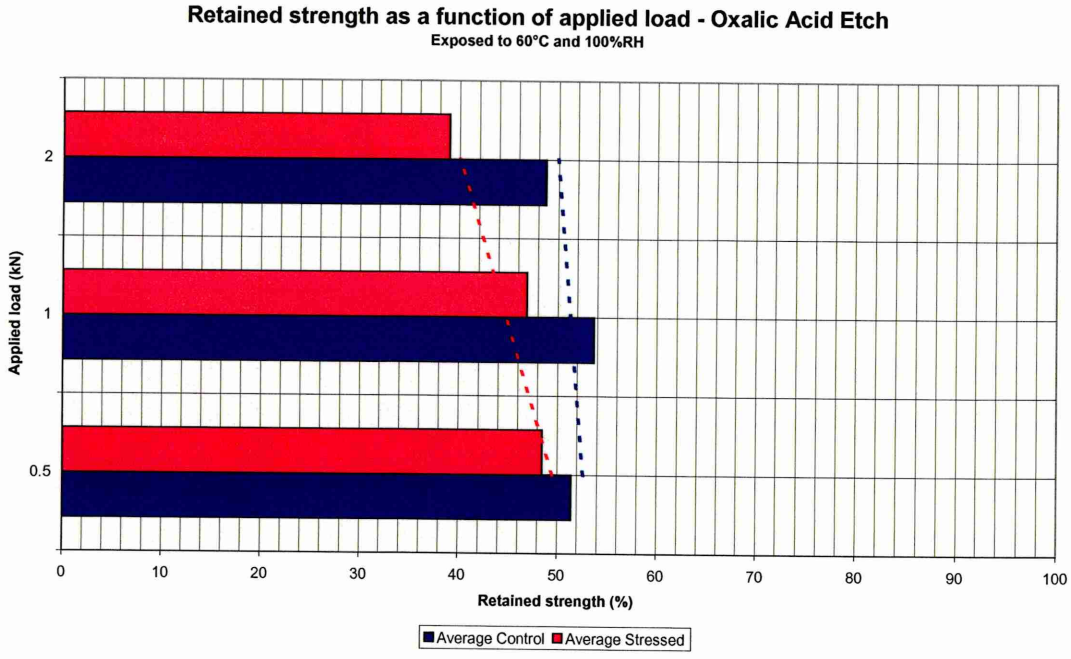

Figure 4.22- *Retained strength of stressed and non-stressed oxalic acid etched perforated lap joints as a function of load*

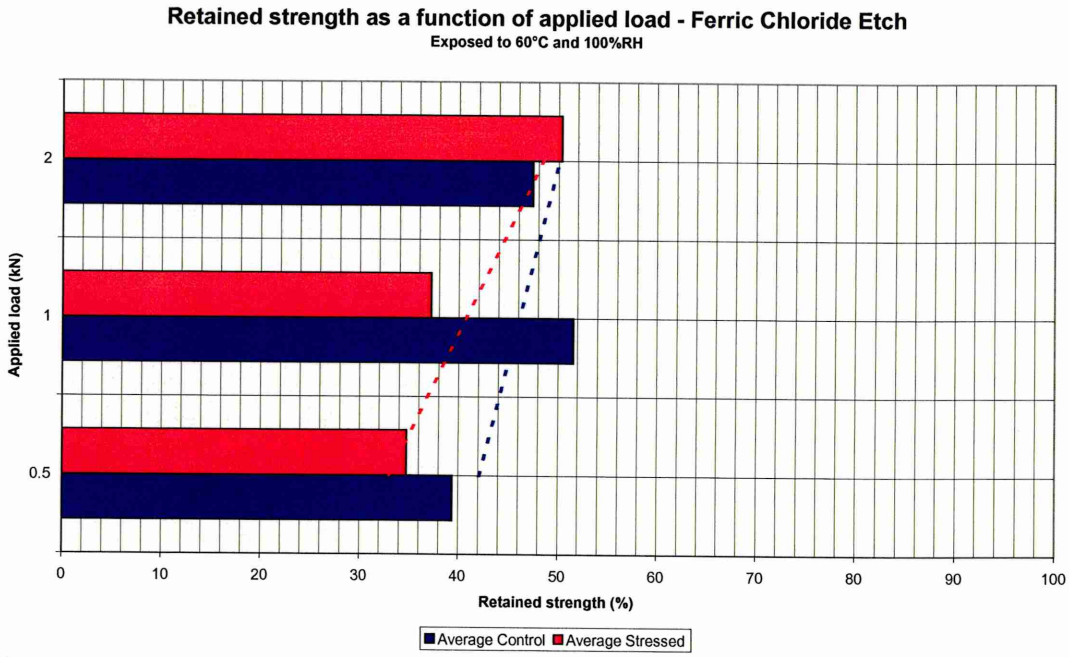

Figure 4.23 - *Retained strength of stressed and non-stressed ferric chloride etched perforated lap joints as a function of load*

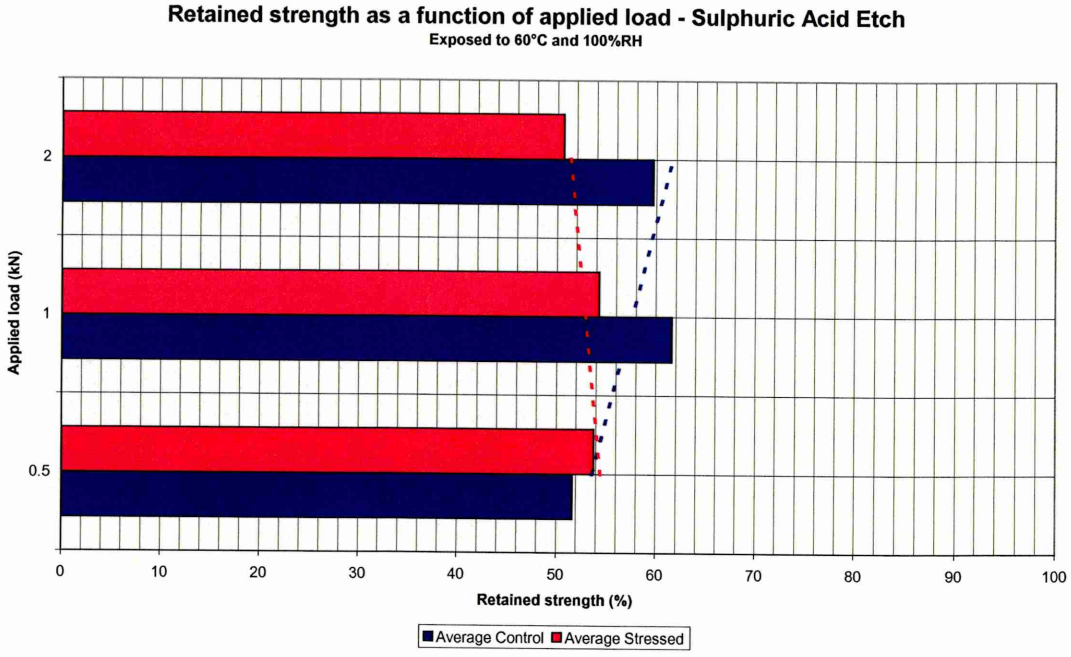

Figure 4.24 - *Retained strength of stressed and non-stressed sulphuric acid etched perforated lap joints as a function of load*

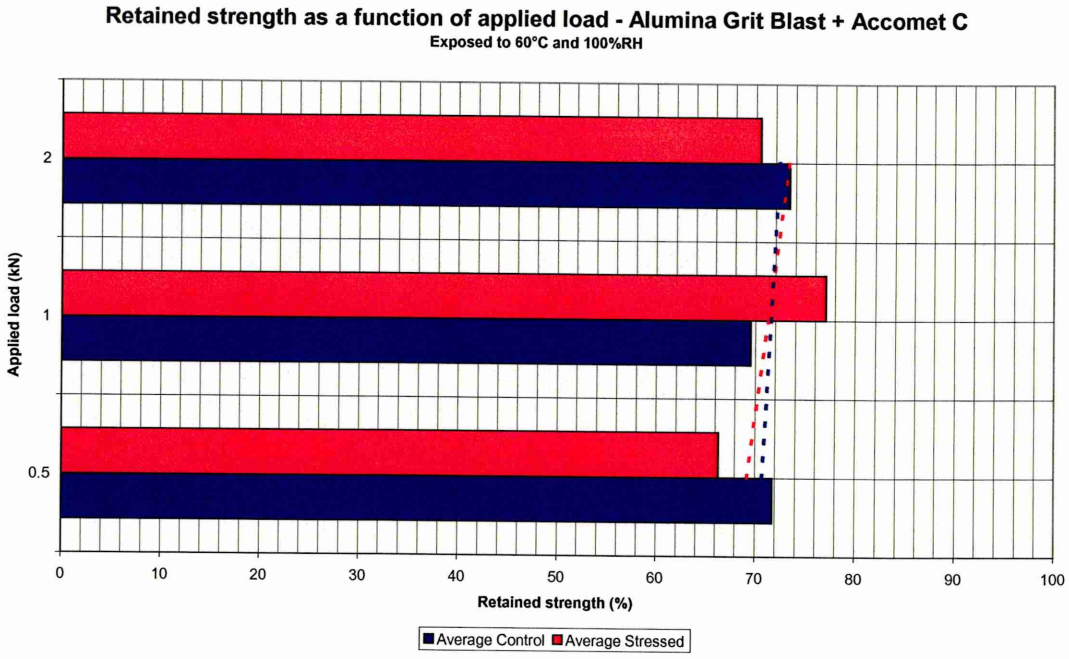

Figure 4.25 *- Retained strength of stressed and non-stressed alumina grit blast + Accomet C perforated lap joints as a function of load*

4.3.2.3.2 Influence of Environmental Exposure

The influence of exposure time on the retained strength for all pre-treatments will now be discussed, with particular emphasis on the strength retention of un-stressed control specimens.

Alkaline Degreased, Figure 4.26

A sharp loss of strength occurred after only ~50 hours of exposure. The continuation of ageing up to ~168 hours does incur further loss in strength. The results suggest that most of the joints load bearing capacity is lost soon after exposure commences.

Alumina Grit Blast, Figure 4.27

There was a continuous loss in strength as the exposure time increased. The specimens lost ~20% of their initial strength after approximately 66 hours exposure, this continued to deteriorate to ~40% loss in strength after ageing for over 350 hours.

Alumina Grit Blast + Primer, Figure 4.28

After ~200 hours exposure the specimens lost nearly 40% of their initial strength. Continued exposure only slightly affected the retained strength, where after over 650 hours of environmental conditioning there was close to 50% reduction in strength.

Alumina Grit Blast + CP30, Figure 4.29

The alumina grit blast + CP30 treatment produced the least durable joints, with a considerably loss in strength of nearly 60% after only 28 hours of exposure. Further ageing did not significantly deteriorate joint strength.

Alumina Grit Blast + AZS, Figure 4.30

After just over 50 hours of exposure to high humidity, the joints had loss 60% of their load bearing capacity. There was little change in strength loss even when the specimens have been aged for over 200 hours, it appears the majority of strength loss occurred in the early stages of exposure.

Sulphuric Acid Sodium Dichromate Anodised, Figure 4.31

It has taken between 330 and 424 hours of environmental conditioning for a loss of ~40% in strength. Further ageing does weaken the joint further, where after 2520 hours only a additional 12% loss in strength is observed.

Nitric Acid Anodised, Figure 4.32

A 27% loss in strength was observed after 320 hours of high humidity exposure. As the exposure continues there is an associated loss in strength, however after 2520 hours of ageing there is only an additional 10% loss in load bearing capacity.

Oxalic Acid Etch, Figure 4.33

Approximately half the initial strength was loss after 150 hours of exposure. After additional ageing the average shear strength increases insignificantly, where after 228 hours of exposure an average of 50% loss in strength was observed.

Ferric Chloride Etch, Figure 4.34

There is a substantial loss in strength , ~54%, after 130 hours exposure. Prolonged ageing reduced the retained strength further to 40% of the initial value after 788 hours of exposure.

Sulphuric Acid Etch, Figure 4.35

Sulphuric acid etching proved to be a less successful pre-treatment, where after only 44 hours of exposure their was a 40% loss in strength recorded. There is no notable reduction in strength for up to 196 hours of ageing.

Alumina Grit Blast + Accomet C, Figure 4.36

A ~27% loss in strength was observed after 567 hours of exposure. There is no subsequent loss in strength even when joints are aged for 2520 hours.

Figure 4.37 shows the effect of humidity exposure on the retained strength of unstressed joints, plotted on a logarithmic axis. The graph illustrates how the more durable pre-treatments retain a higher proportion of their initial strength after exposure to a high humidity environment.

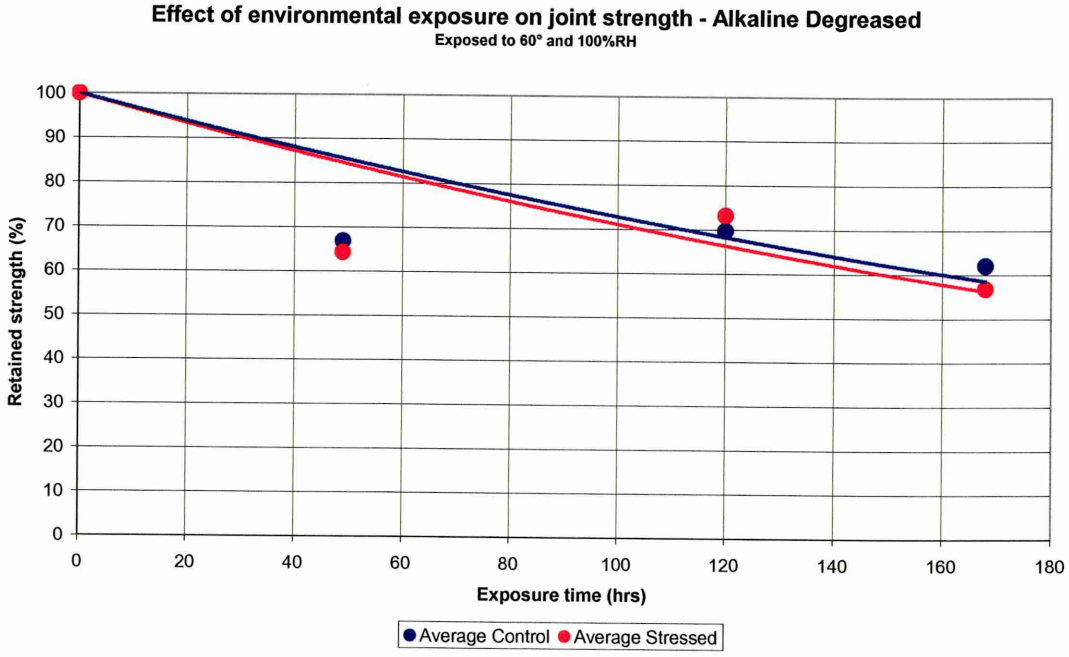

***Figure 4.26** – Effect of environmental exposure on alkaline degreased perforated lap joints*

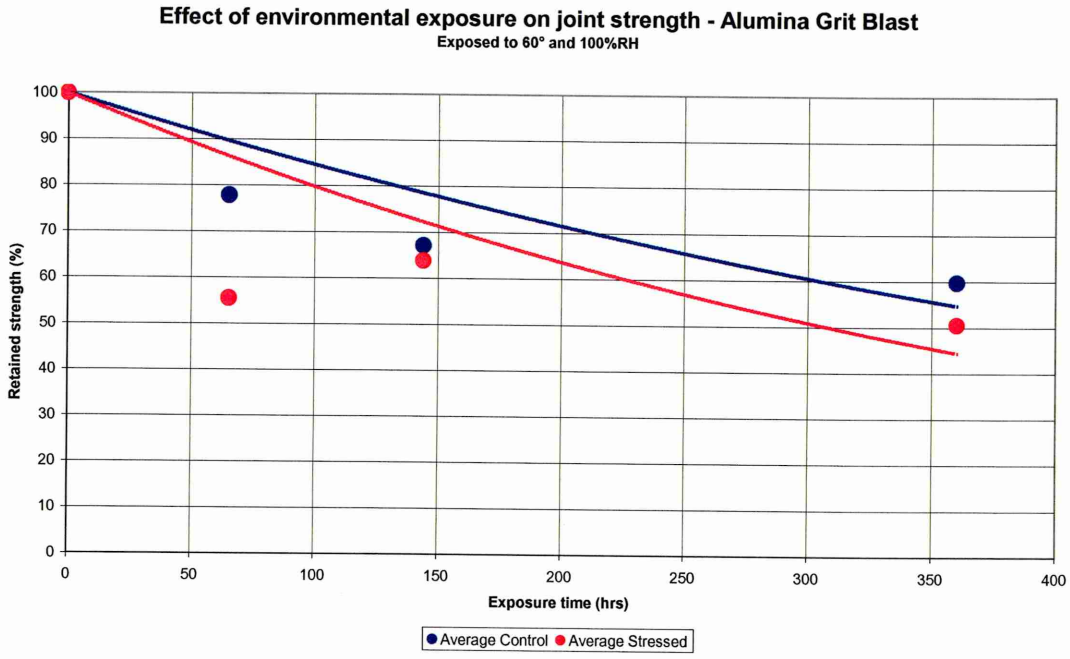

Figure 4.27 *– Effect of environmental exposure on alumina grit blasted perforated lap joint*

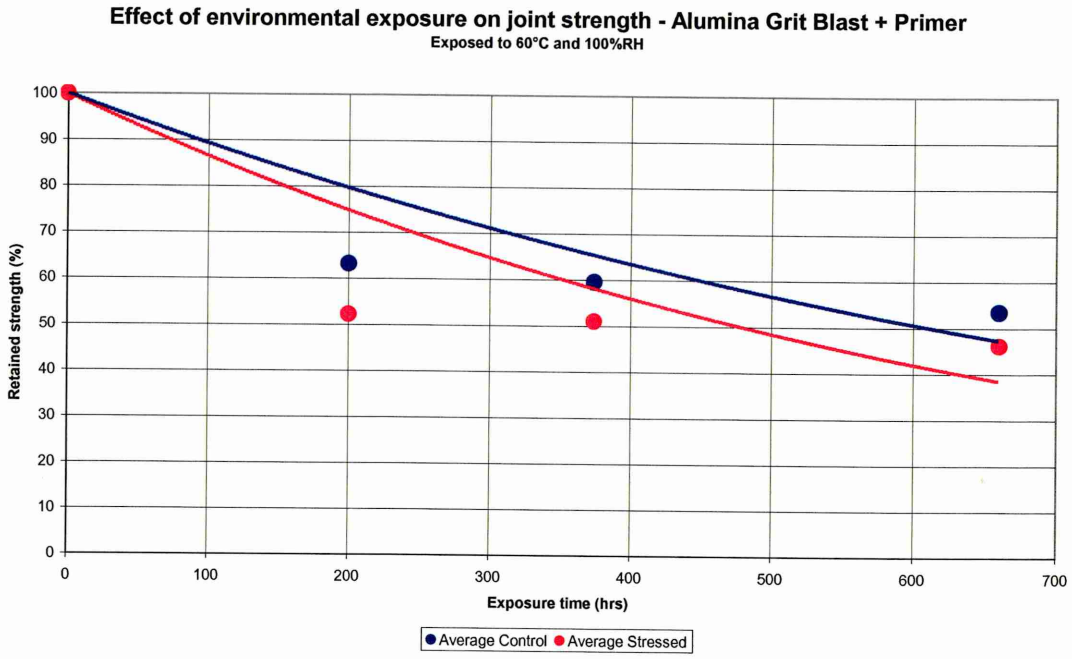

Figure 4.28 *– Effect of environmental exposure on alumina grit blast + primer perforated lap joint*

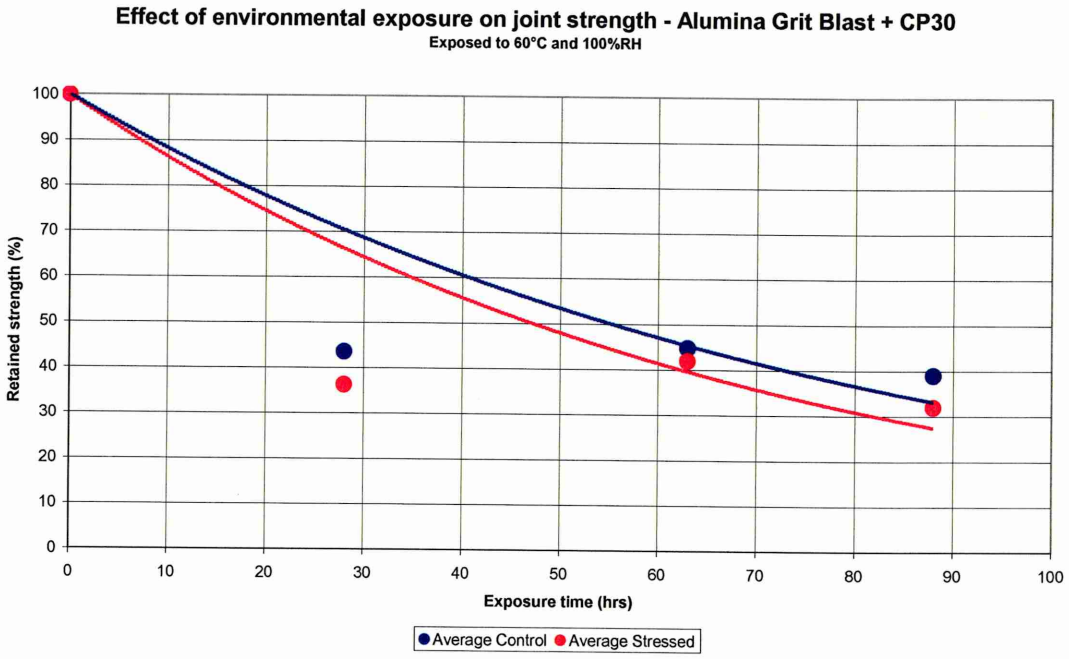

Figure 4.29 – *Effect of environmental exposure on alumina grit blast + CP30 perforated lap joint*

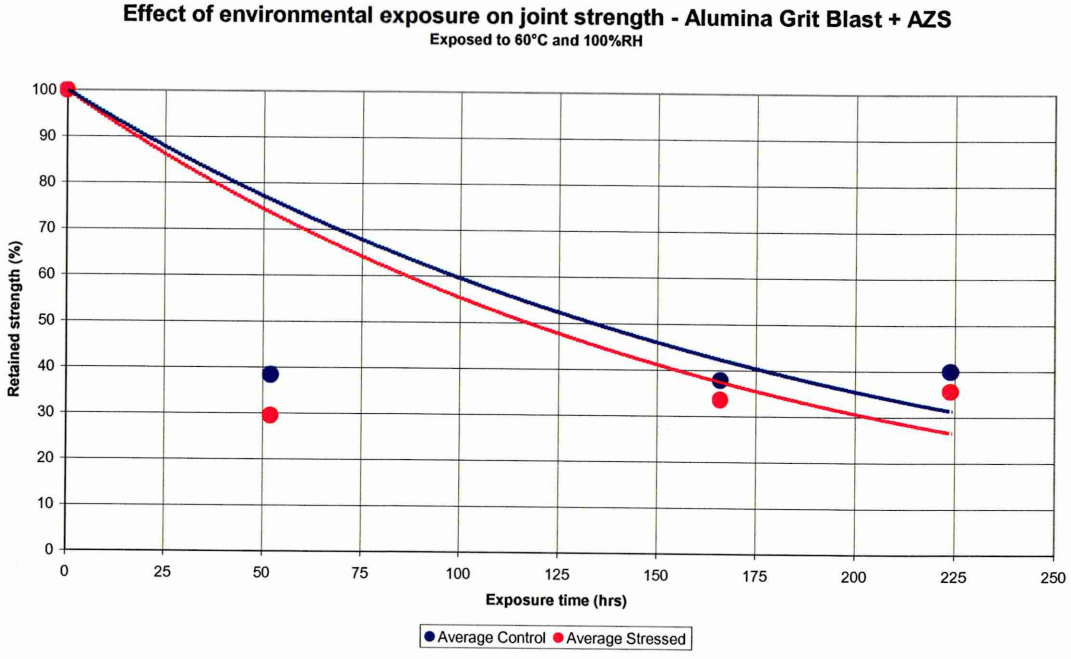

Figure 4.30 – *Effect of environmental exposure on alumina grit blast + AZS perforated lap joint*

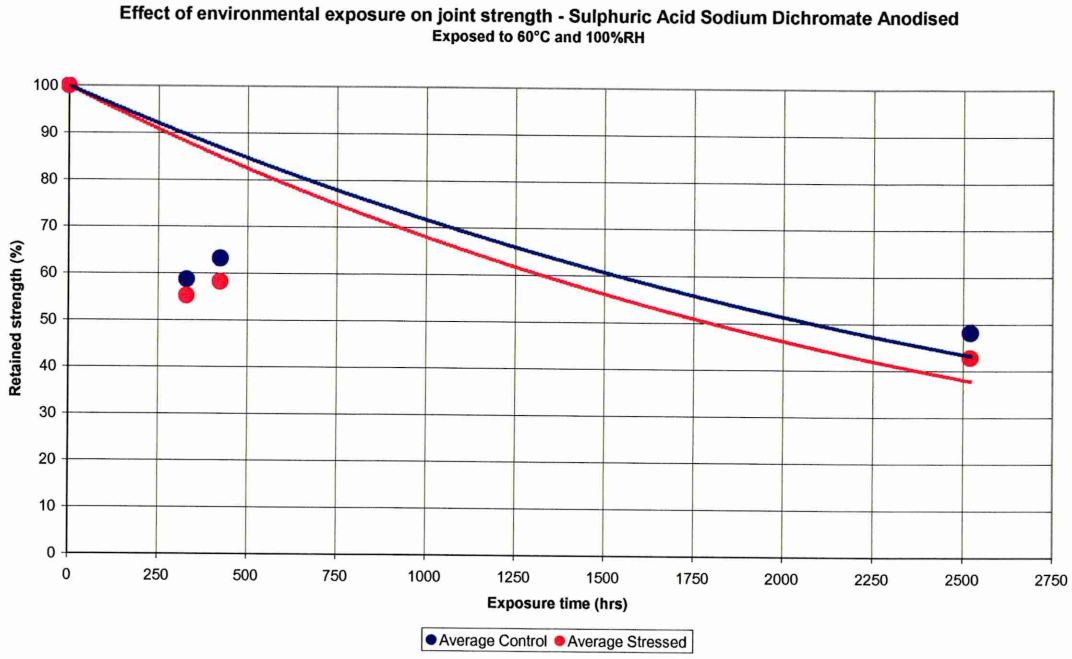

Figure 4.31 *– Effect of environmental exposure on sulphuric acid sodium dichromate anodised perforated lap joint*

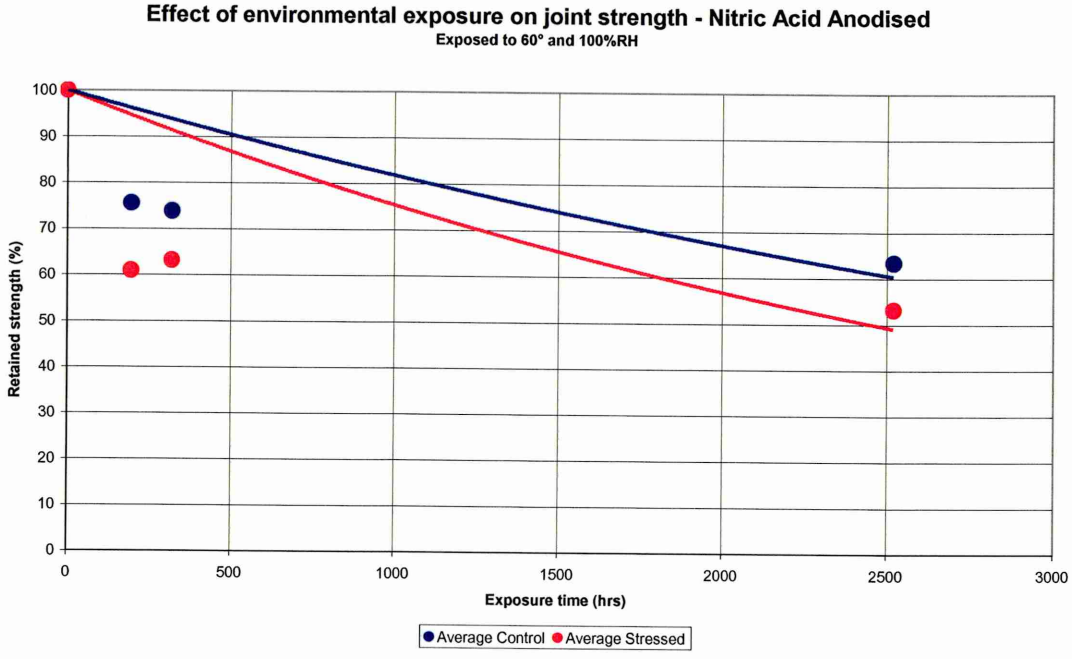

Figure 4.32 *– Effect of environmental exposure on nitric acid anodised perforated lap joint*

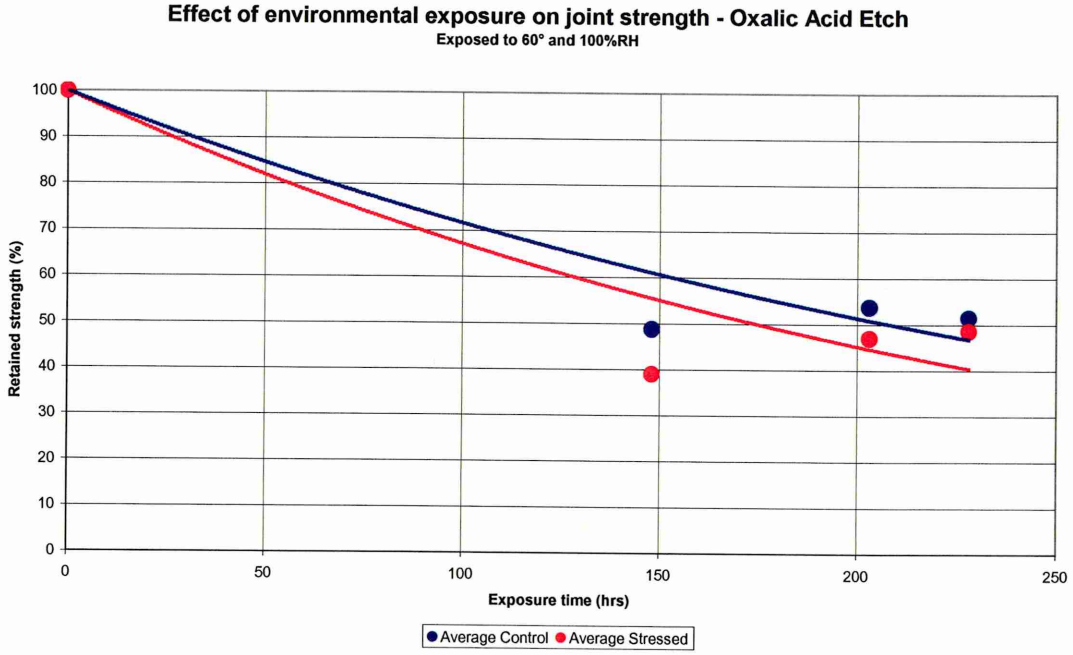

Figure 4.33 – *Effect of environmental exposure on oxalic acid etched perforated lap joint*

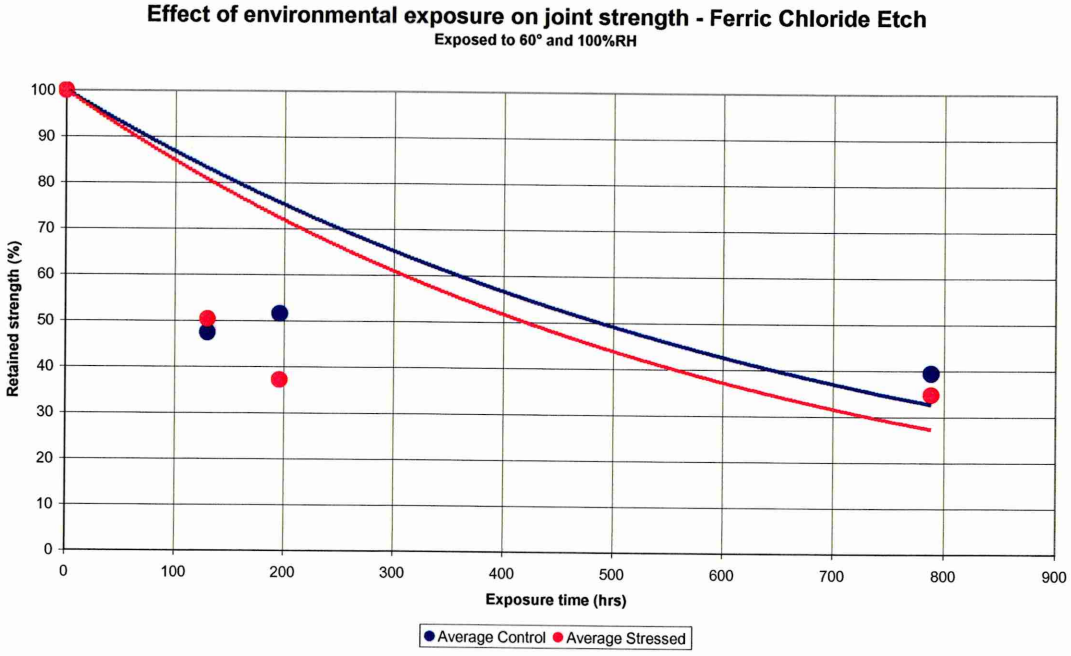

Figure 4.34 – *Effect of environmental exposure on ferric chloride etched perforated lap joint*

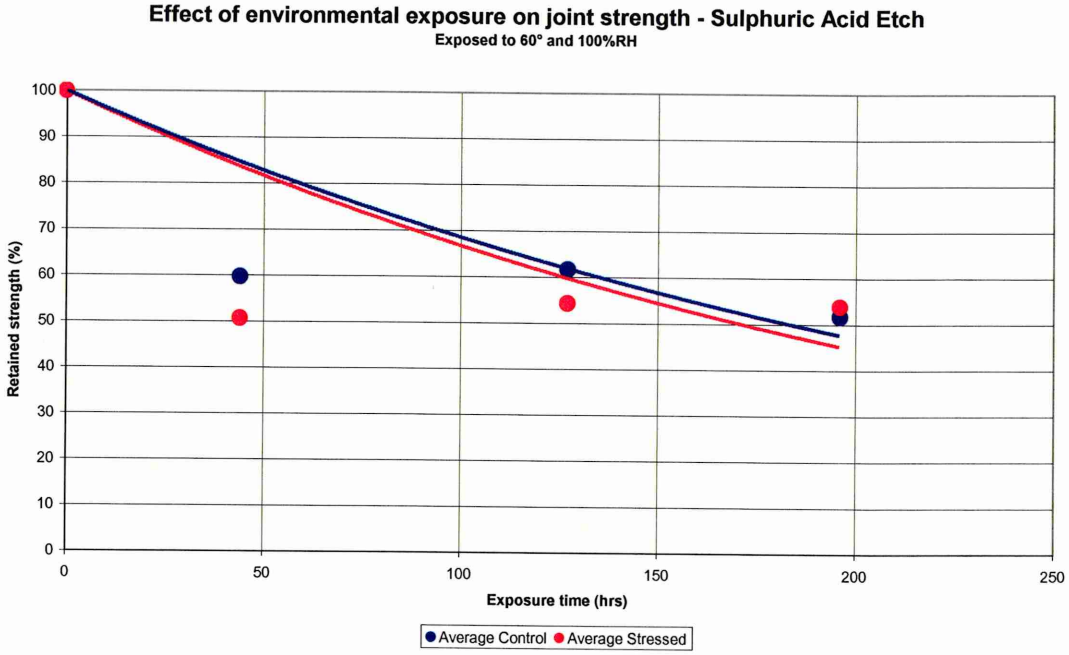

Figure 4.35 – *Effect of environmental exposure on sulphuric acid etched perforated lap joint*

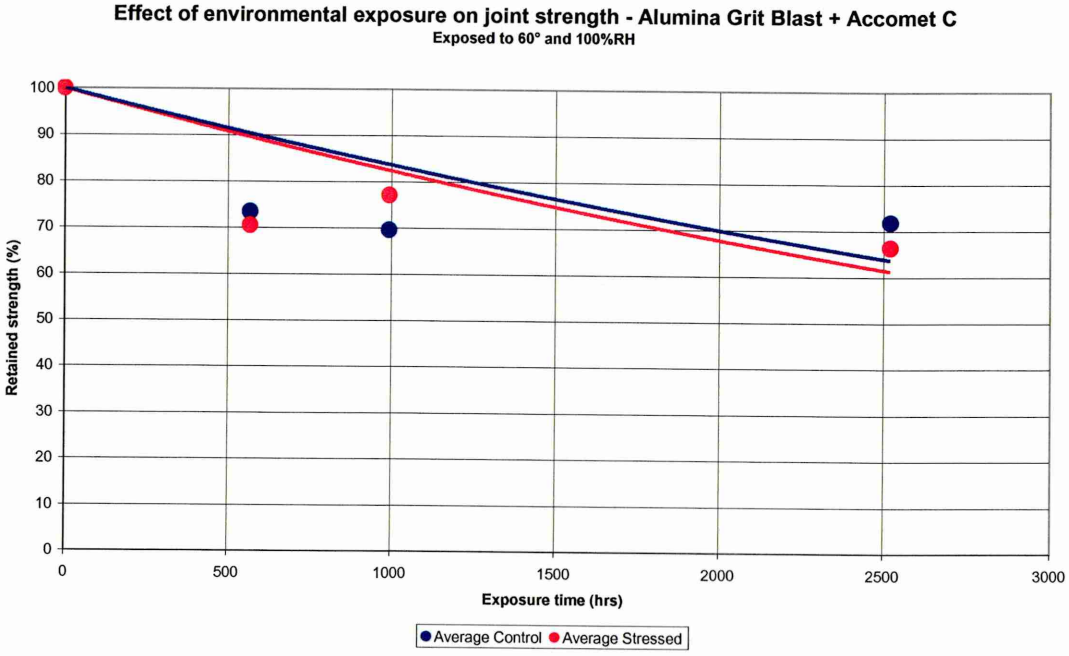

Figure 4.36 – *Effect of environmental exposure on alumina grit blast + Accomet C perforated lap joint*

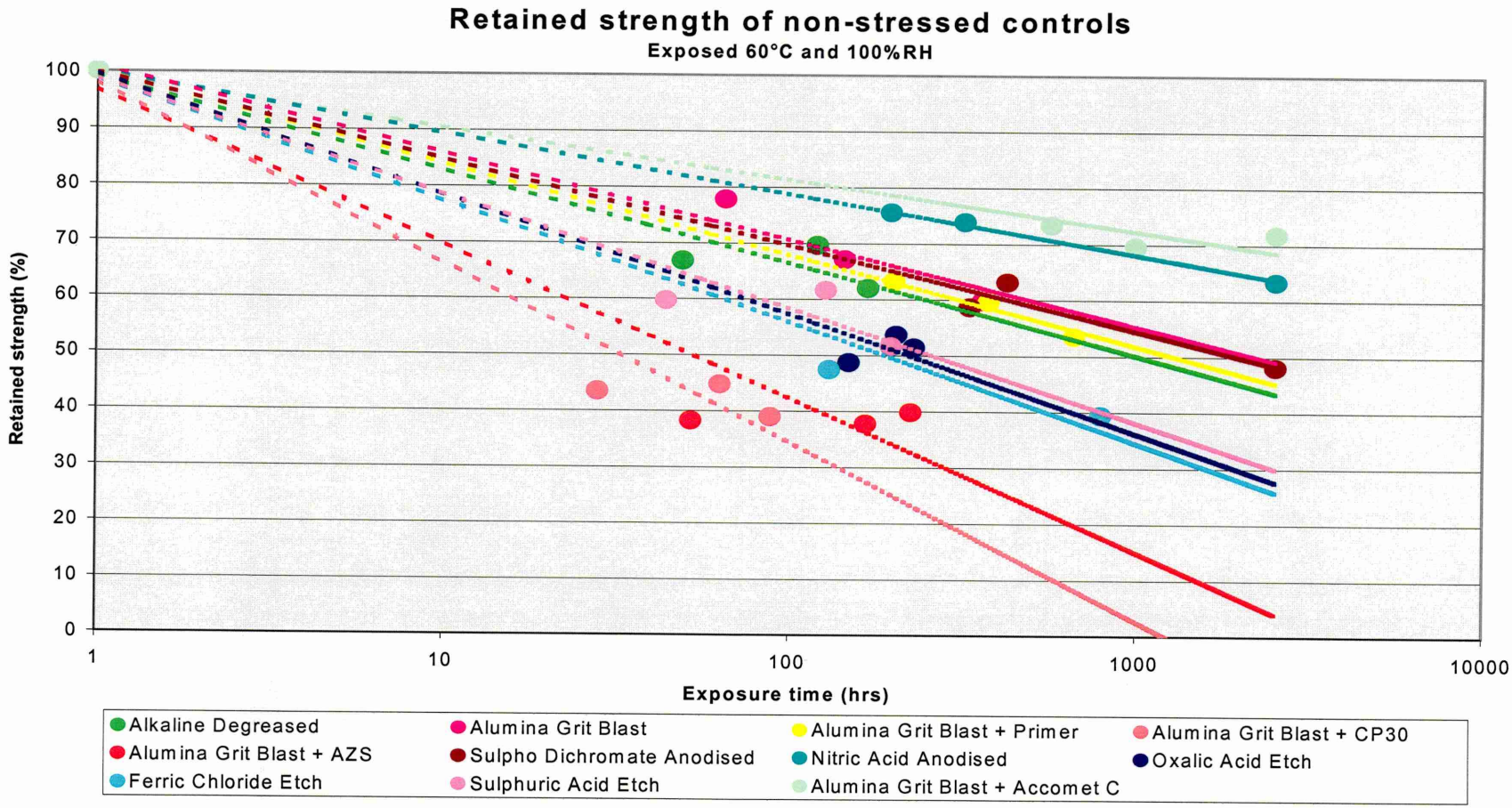

Figure 4.37 – *Retained strength of unstressed perforated lap joints*

4.3.3 Wedge Tests

To complement the environmental durability results obtained from the perforated lap shear tests, wedge crack extension test specimens were assembled, as described in Chapter 3 Section 3.4.3, and exposed to 60°C and 100% relative humidity. All previous pre-treatments were evaluated with the exception of oxalic acid etch, ferric chloride etch and sulphuric acid etch. A batch size of three was used for each pre-treatment, the results are shown in Figure 4.38. The specimens incorporating the alumina grit blast + Accomet C and sulphuric acid sodium dichromate anodising were the most durable pre-treatments, where crack lengths after 24 hours of exposure were 16.07 and 16.35mm respectively. For these two pre-treatments virtually no subsequent crack growth was observed after 1 weeks exposure. The nitric acid anodising treatment also produced durable results where crack growth after 24 hours was 31.41mm and no notable increase after 1 week's exposure. Moderate durability was exhibited from the alumina grit blast + primer, alumina grit blast and alumina grit blast + AZS treatments, where after 24 hours of exposure there was 36.5, 38.16 and 42.92mm of crack growth respectively. Wedge test incorporating the alkaline degreased and alumina grit blast + CP30 proved to be the least durable pre-bonding treatments, where rapid crack growth was observed after a 24 hour period. Upon completion of the experiment all specimens were pulled apart to assess the mechanisms and modes of failures using digital photography, SEM and XPS.

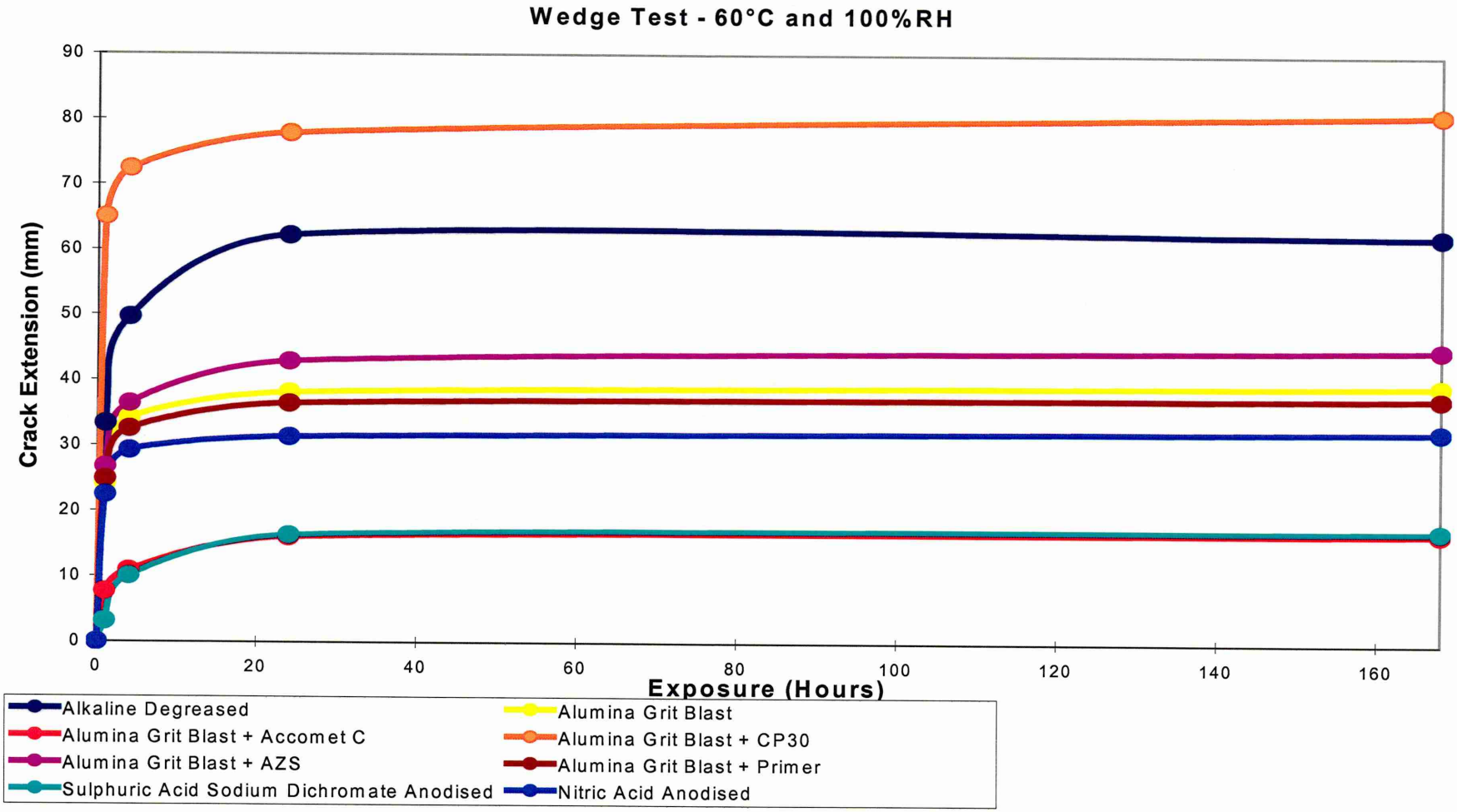

Figure 4.38 - *Wedge crack extension results, specimens exposed to 60°C and 100%RH*

4.4 Closing Remarks

The perforated lap shear joint has provided an effective method of assessing the influence of stainless steel pre-treatments on joint durability within a reasonable time period. The stressed durability performance for all pre-treatments has been shown in Figure 4.14; at low load levels the time difference between the least and most durable bonding systems is at its greatest, whilst at higher loads the survival times become clustered close together. This observation suggests that as the load is increased the adhesive joints may be dominated by the mechanical behaviour of the adhesive. At lower loads the survival time is dominated by the ability of the interfacial area to resist moisture ingression. Considering the effect of stress on strength retention, in a majority of cases the un-stressed joints retained a greater proportion of their initial strength. This is in contrast to work by Maddison[4] who reported that stressed perforated lap joints, manufactured from steel and epoxy resin, retained more strength than un-stressed controls. It was speculated the application of stress may act as a toughening mechanism. However, it can be easily explained why stressed joints have lower residual strengths, because they have been subjected to 3 un-loading and re-loading fluctuations. The wedge crack extension test has demonstrated that assemblies incorporating the more elaborate electro-chemical and proprietary treatments are more durable than those using physically unmodified adherends, such as alkaline degreasing. Joints made with the alumina grit blast + CP30 pre-treatment have been the least durable when assessed using either the perforated lap shear or wedge test specimens. For pre-treatments that are common to both test configurations, the ranking in terms of durability is the same. For this reason the author is confident that the resistance to interfacial weakening has been assessed and not the resistance to load, so a true measure of the durability of the treatments has been achieved.

4.4 Surface Characterisation

4.4.1 Introduction

The surface of the substrate is frequently modified prior to bonding. The treatments used in the experimental work include relatively simple degreasing practises to more complex electro-chemical techniques. For this reason it is necessary to characterise treated surfaces and investigate physical and chemical properties that contribute to enhanced environmental durability. SEM and surface profilometry were used to physically characterise adherends in terms of roughness and topography. XPS was used to chemically characterise substrates. The chemical and physical qualities of the adherends were investigated prior to bonding. Fractography of failed specimens was carried out using SEM and XPS to determine the loci of failure, as detailed later in 4.5 Failure Analysis. All characterising techniques were carried out as described in *3.6 Surface Characterisation*.

4.4.2 Surface Characterisation

4.4.2.1 Scanning Electron Microscopy

SEM was used to evaluate the morphological changes after the surfaces have undergone pre-bonding treatments.

2B Finish - Alkaline Degreased, Plate 4.1

The surface consists of re-crystallised equi-axed austenitic grains, between 5-15μm in size. The re-crystallisation occurs during the line annealing stage of the manufacturing process after the material has been cold rolled. The grain boundaries are visible as a result of grain boundary etching from the acid pickling process which defines the smooth grain surface region, to produce the typical 2B finish.

***Plate 4.1** – 2B finish alkaline degreased*

2D Finish – Alkaline Degreased, Plate 4.2

The 2D surface is produced via the same production route as the 2B material, except the it is not 'skin passed' to further brighten the steel. The 2D finish comprises of pronounced roughened grains and lands. The surface of the grains has a porous form from etch pitting and etching of the grain boundaries that has taken place during the pickling process.

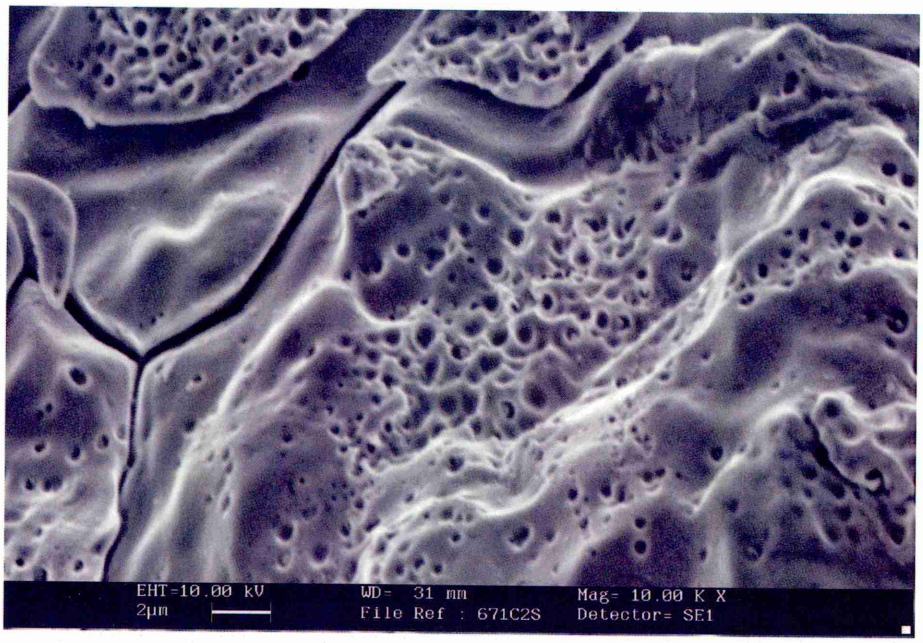

***Plate 4.2** – 2D finish alkaline degreased*

BA Finish - Alkaline Degreased, Plate 4.3

This finish differs significantly from the 2B and 2D surfaces. The annealing stage after cold rolling takes place in a controlled atmosphere that prevents the strip's surface oxidising. The softened surface retains a smoothness level similar to that of the final cold rolled strip. The surface is bright and reflective, and predominately featureless except for the surface striations running diagonally that are associated with the rolling process.

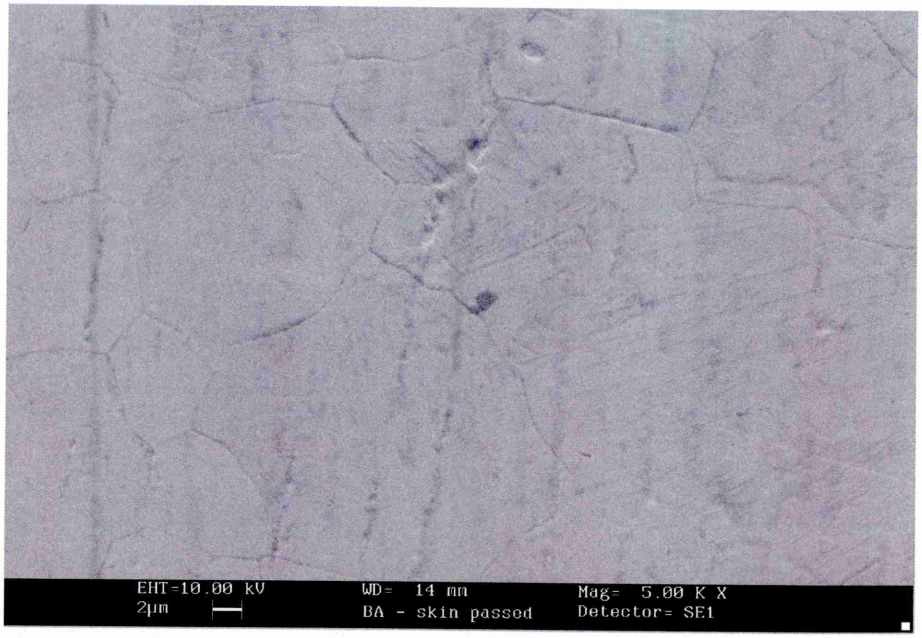

***Plate 4.3** – BA finish alkaline degreased*

Alumina Grit Blasted, Plate 4.4

The surface consists of heavily deformed material in a random flake-like manner. The new surface has evolved from the bombardment of adamantine alumina particles. The available area for adhesive bonding has been increased.

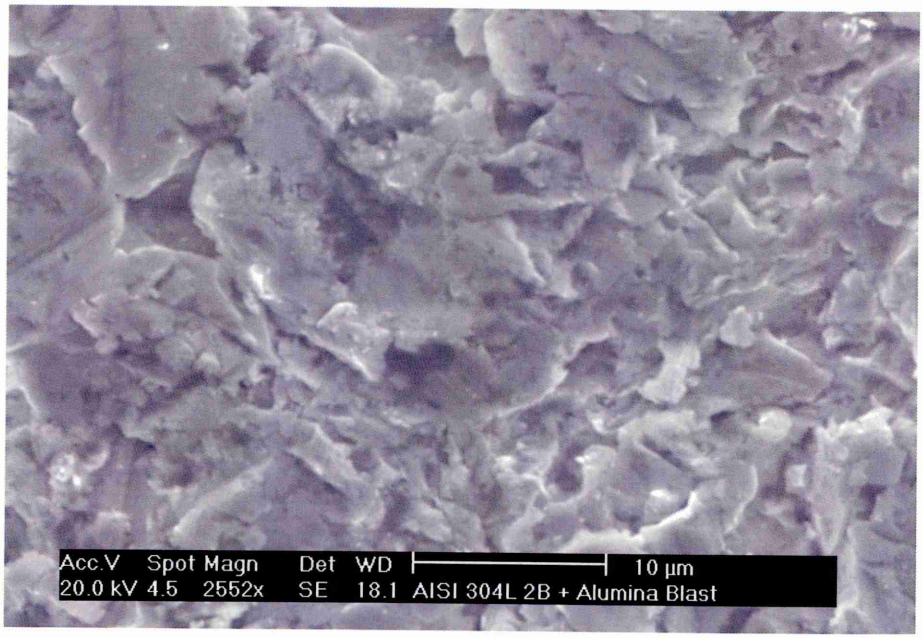

***Plate 4.4** – Alumina grit blasted surface*

Sulphuric Acid Sodium Dichromate Anodising, Plate 4.5 and 4.6

The surface showed increased corrosion along grain boundaries and also pitting which has occurred on the grain itself. The surface area and micro-roughness has increased from the chemical attack. The grains have a mottled appearance from the vigorous temperament of the anodising process.

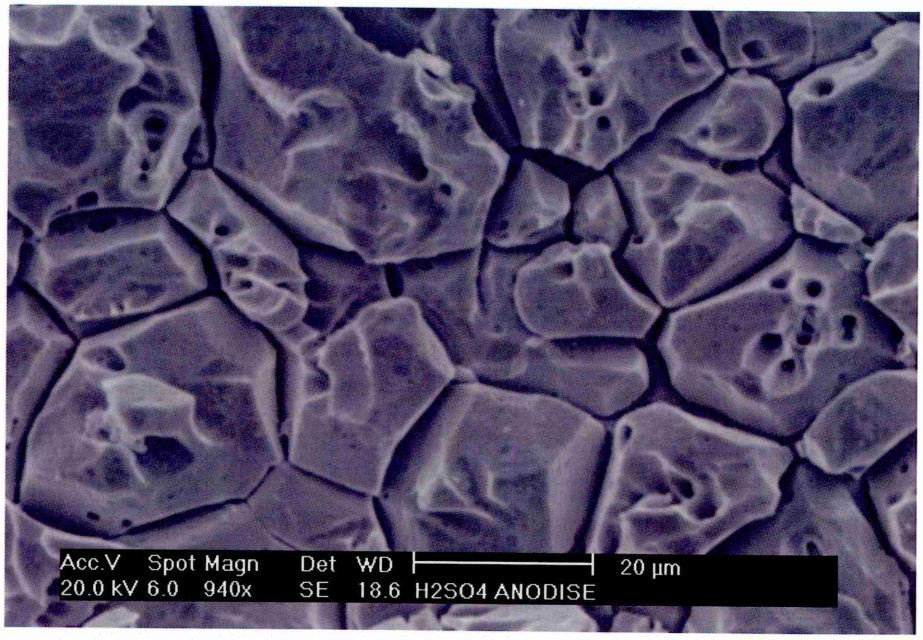

***Plate 4.5** – Sulphuric acid sodium dichromate anodised surface*

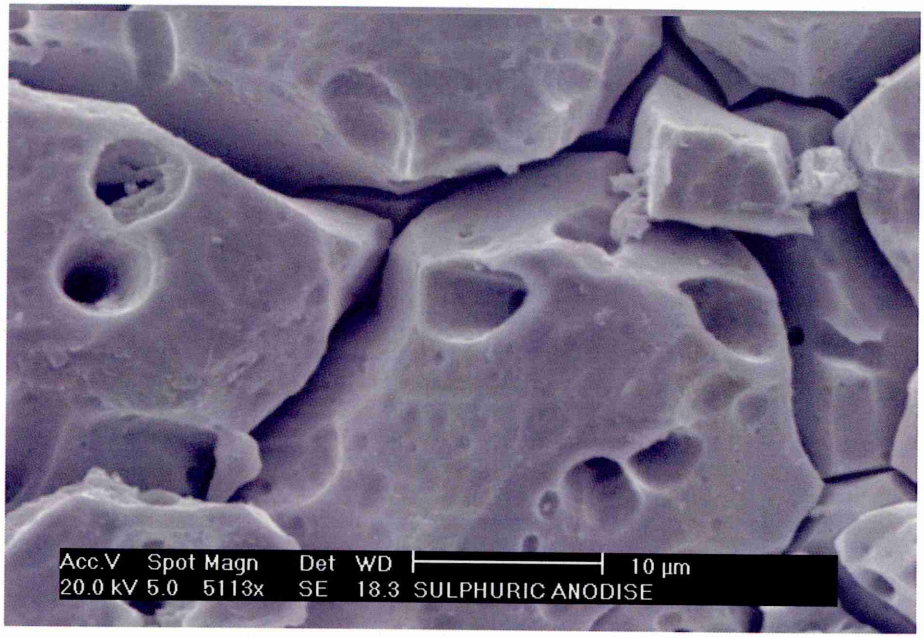

***Plate 4.6** – Sulphuric acid sodium dichromate anodised surface*

Nitric Acid Anodising, Plate 4.7 and 4.8

The grain boundary corrosion is not as severe as the sulphuric acid sodium dichromate anodising treatment. In addition there is evidence of pitting corrosion on the grain's surface. The available bonding area and micro-roughness has been increased.

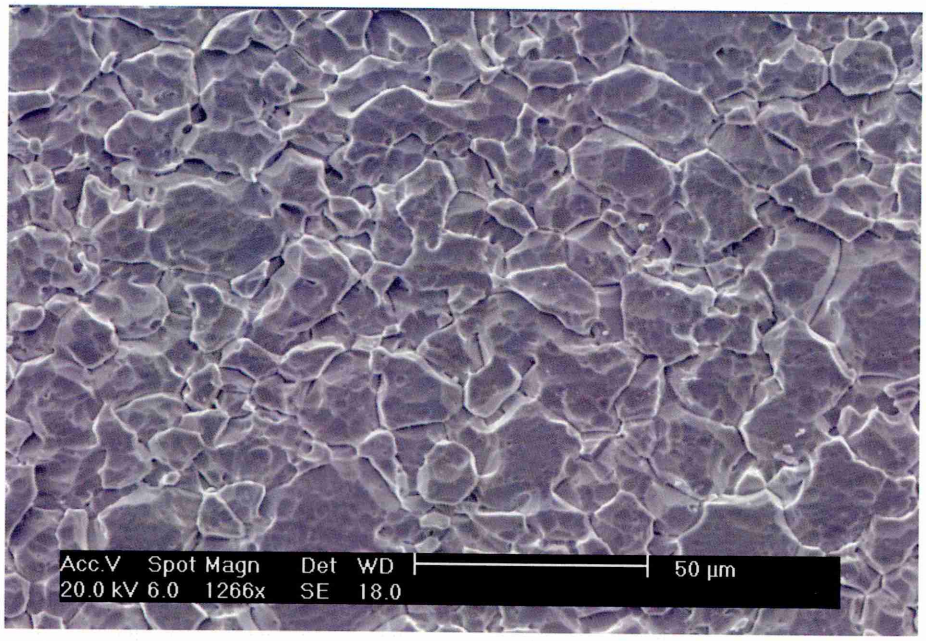

***Plate 4.7** – Nitric acid anodised surface*

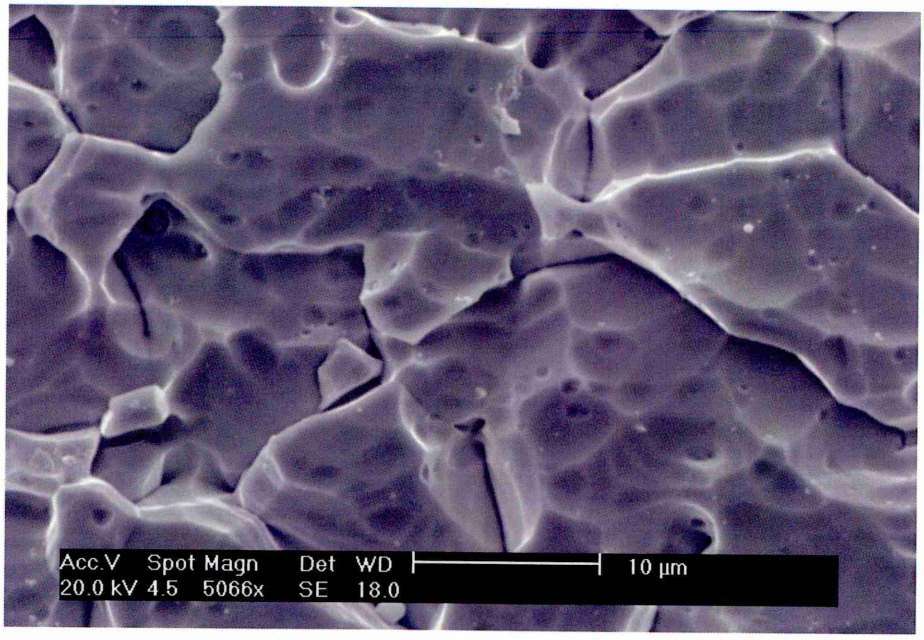

***Plate 4.8** – Nitric acid anodised surface*

Oxalic Acid Etch, Plate 4.9

The grain boundaries are still visible but a featured layer exists that appears to protrude in places. The area available for bonding has also been increased.

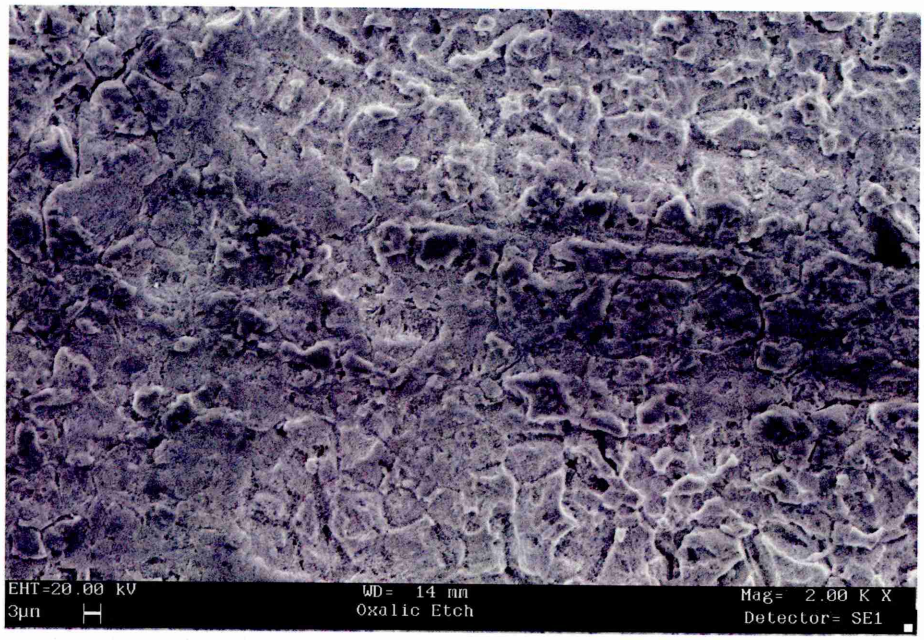

***Plate 4.9** – Oxalic acid etched surface*

Ferric Chloride Etch, Plate 4.10

The treated surface is visible different from the other etched/anodised surfaces where the acidic attack appears less vigorous. The surface has sharp angular features that stand out. Again the surface area has increased.

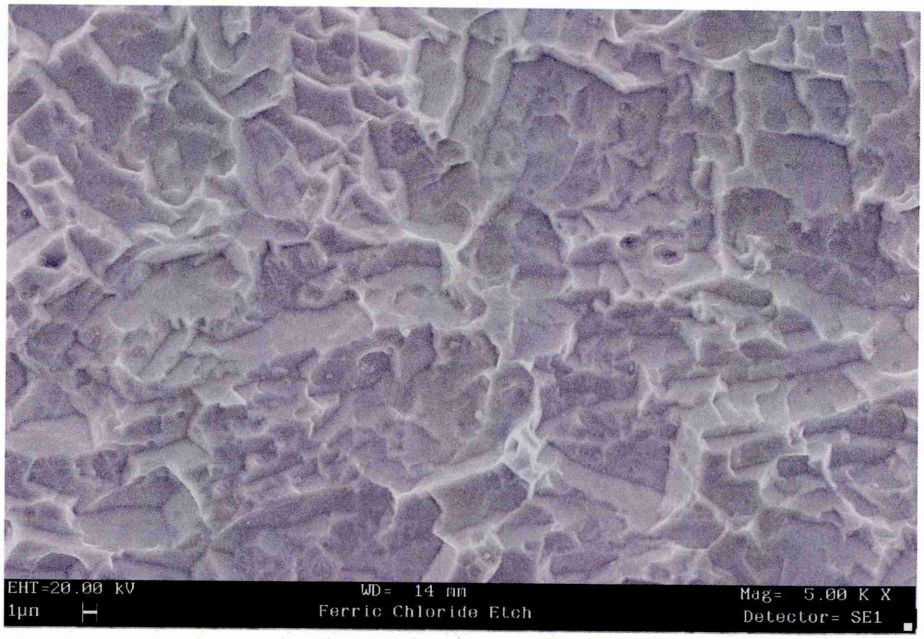

***Plate 4.10** – Ferric chloride etched surface*

Sulphuric Acid Etch, Plate 4.11 and 4.12

The surface is very similar in semblance to the alkaline degreased 2B surface. The surface of the grains do appear to have been modified slightly as indicated in Plate 4.12, but no significant modification has taken place.

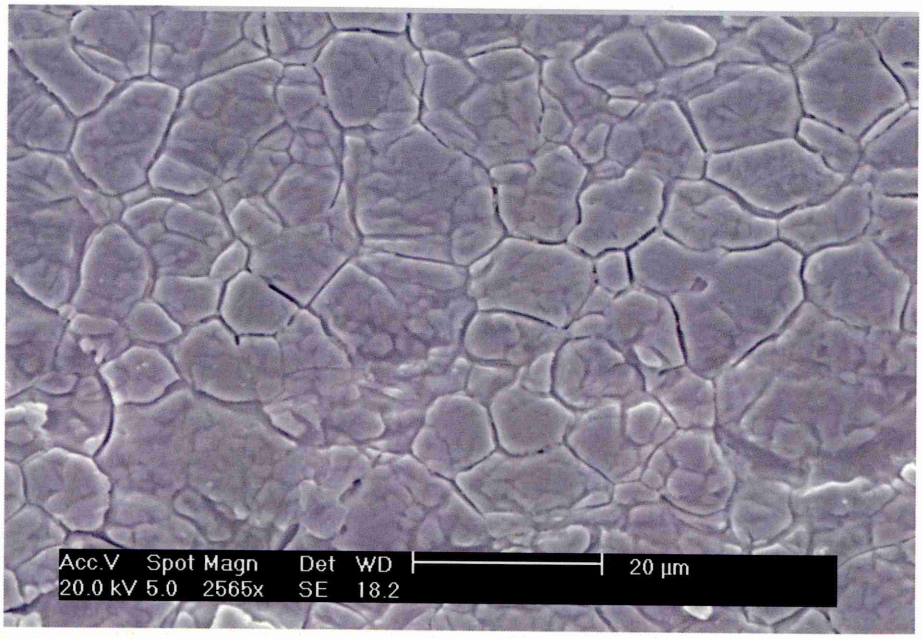

***Plate 4.11** – Sulphuric acid etched surface*

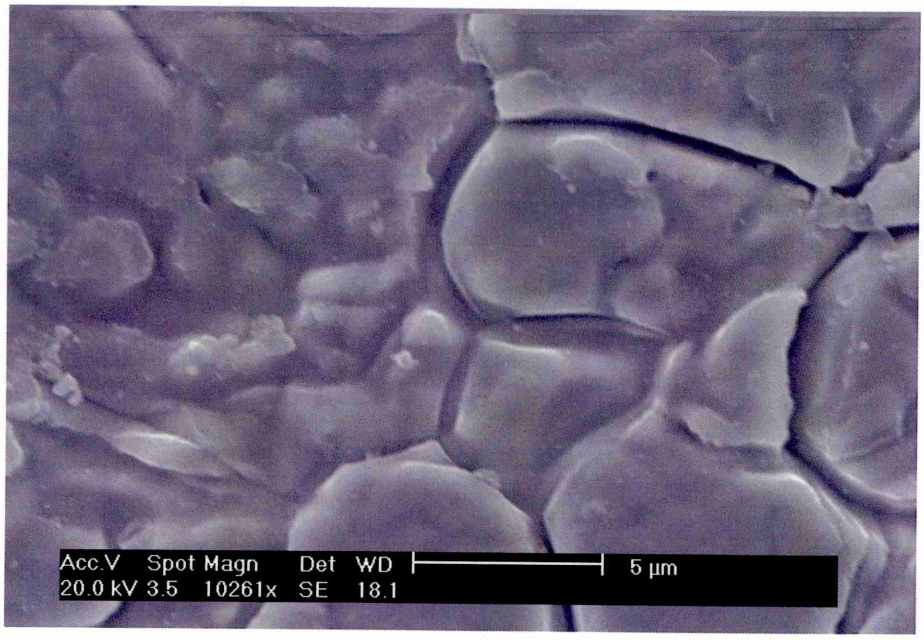

***Plate 4.12** – Sulphuric acid etched surface*

Alumina Grit Blast + Accomet C, Plate 4.13 and 4.14

The faceted topography of the grit blasted surface is visible, but there is evidence of the Accomet C coating which has smoothed out the sharp angular edges of the deformed surface. Plate 4.14 indicates regions where the Accomet C has cracked from the curing process. The coating uniformly covers the substrate and appears to be well adhered to the blasted surface.

***Plate 4.13** – Alumina grit blast + Accomet C surface*

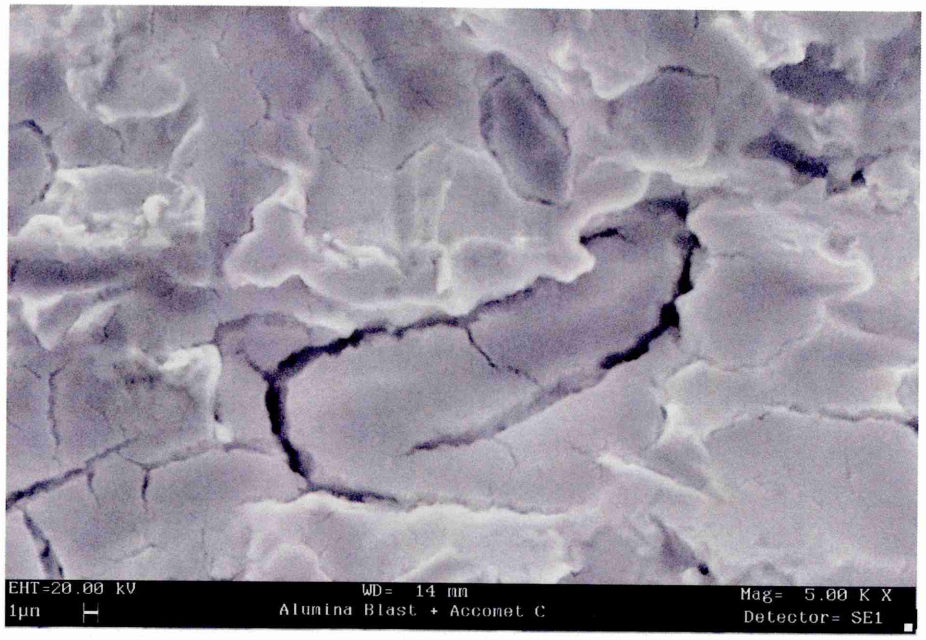

***Plate 4.14** – Alumina grit blast + Accomet C surface*

Alumina Grit Blast + Silane Primer, Plate 4.15

Evidence of primer on the surface has not been observed due to the resolution limitations of the SEM. The surface resembles that of an alumina grit blasted surface.

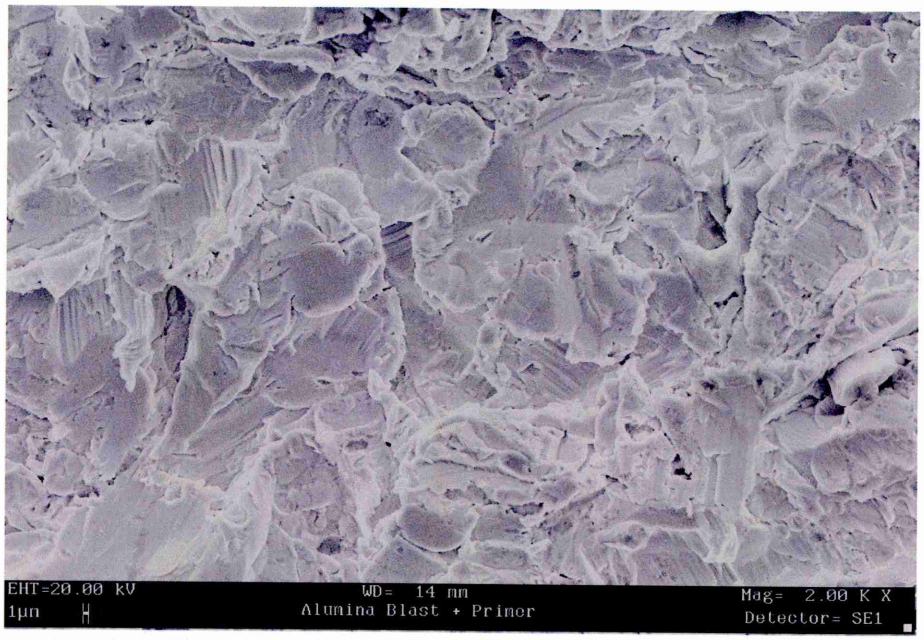

***Plate 4.15** – Alumina grit blast + silane primer surface*

Alumina Grit Blast + AZS, Plate 4.16

The surface detail shows no indication of the AZS coating. As with the primed surface the micrograph reveals heavy deformation only from the grit blasting process.

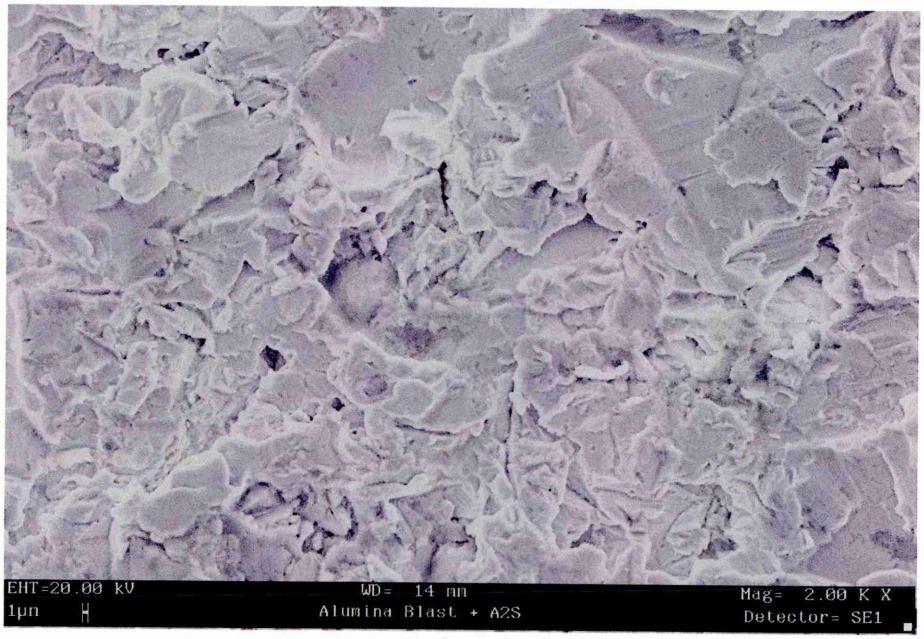

***Plate 4.16** – Alumina grit blast + AZS surface*

Alumina Grit Blast + CP30, Plate 4.17

The CP30 coating was applied in such a low weight, ~0.01% w/w, which produces a covering of one mono layer of the material therefore it was not expected that any artefacts would be observed from the SEM micrographs. The surface topography is reminiscent of an alumina grit blasted surface.

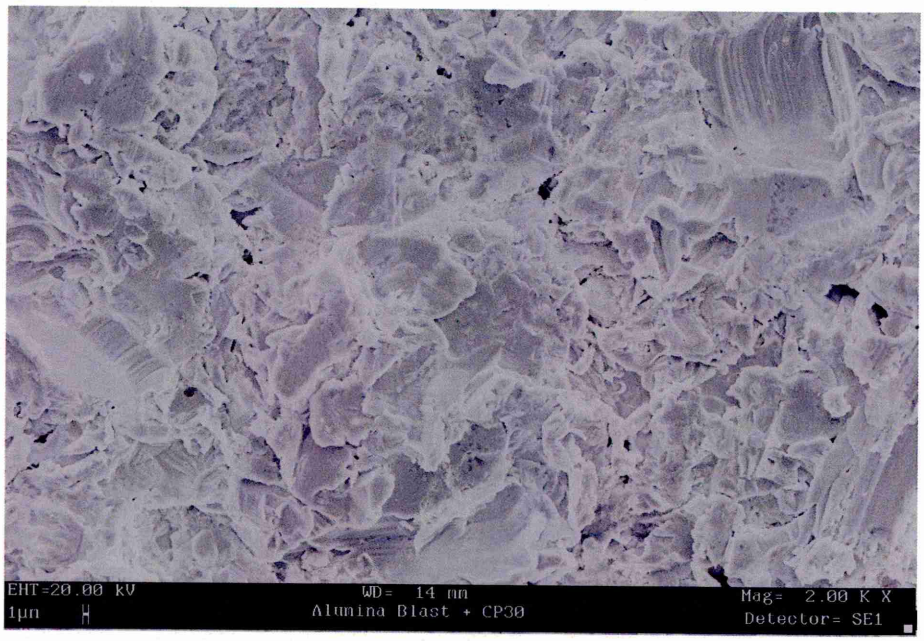

***Plate 4.17** – Alumina grit blast + CP30 surface*

4.4.3 Surface Profilometry

The surface roughness and texture parameters were evaluated for each of the treated surfaces considered in this chapter, using two-dimensional and three-dimensional surface profilometry.

4.4.3.1 Two-Dimensional Surface Profilometry

The results from the two-dimensional profilometry are detailed in Table 4.12.

Table 4.12 - 2D Surface roughness results.

Surface	Roughness Parameters				
	Ra (μm)	Rt (μm)	Rz (μm)	Rsk (μm)	Rku (μm)
2B Finish	0.17	2.21	1.45	0.80	5.40
2D Finish	0.21	3.21	2.23	1.56	8.55
BA Finish	0.03	0.22	0.16	-0.14	3.32
Alumina Grit Blast	2.43	19.45	-	-0.14	3.04
Alumina Grit Blast + CP30	2.45	23.09	-	-0.04	3.45
Alumina Grit Blast + AZS	2.62	20.25	-	0.06	2.95
Alumina Grit Blast + Accomet C	2.81	18.66	-	0.03	2.91
H_2SO_4-$Na_2Cr_2O_7$ Anodise	1.99	15.28	-	0.68	3.16
Nitric Acid Anodise	0.15	2.82	-	-2.08	13.39
Ferric Chloride Etch	0.60	6.34	-	-0.83	5.15
Oxalic Acid Etch	1.09	14.01	-	-0.82	6.63
Sulphuric Acid Etch	0.17	1.54	-	-0.93	4.45
Alumina Grit Blast + Primer	2.57	24.88	-	-0.27	3.94

The surfaces will be appraised in terms of the arithmetic mean, Ra, value, which is a useful parameter for detecting general variations in overall profile height. When the Ra value changes it signifies the resultant change in average roughness for the entirety of the surface. The smoothest surface was obtained from the bright annealed, BA, specimen where Ra = 0.03μm. Surprisingly the nitric acid anodised surface was relatively smooth, where Ra = 0.15μm. The 2B and sulphuric acid etch surfaces both received Ra = 0.17μm, it appears this etching treatment

had no effect on the average roughness of the surface. The 2D surface was slightly rougher then the 2B surface, Ra = 0.21μm, this can be attributed to manufacturing process where 2D material does not get 'skin passed'. Both the ferric chloride and oxalic acid etching treatments produced rougher surfaces, where Ra values of 0.60μm and 1.09μm were obtained respectively. The sulphuric acid sodium dichromate anodised surface attained Ra = 1.99μm, a considerable increase in roughness compared with the 2B finish. A high level of macro-roughness was also achieved by the alumina grit blasted surface, where Ra = 2.43μm. A slight increase was also observed for the specimens treated with alumina grit blast + CP30, alumina grit blast + silane primer and alumina grit blast + AZS, where Ra = 2.45μm, 2.57μm and 2.62μm respectively. The roughest surface was obtained by the alumina grit blast + Accomet C surface, with Ra = 2.81μm.

4.4.3.2 Three-Dimensional Surface Profilometry

3-D surface profiles were made of the treated surfaces, by making a series of transverse scans over a pre-determined area. Figures 4.39 to 4.51 reveal the 3-D profiles for the 13 surfaces detailed above in Table 4.12. The profiles give a visual indication and representation for the calculated average roughness, Ra. For example the 3-D profile for the BA surface represents a flush surface in comparison to the 2D and 2B profiles where the undulations on the surface can be seen. The macro-roughening effects of grit blasting are highlighted, where the profiles depict the surface craters formed from the bombardment of high velocity alumina particles.

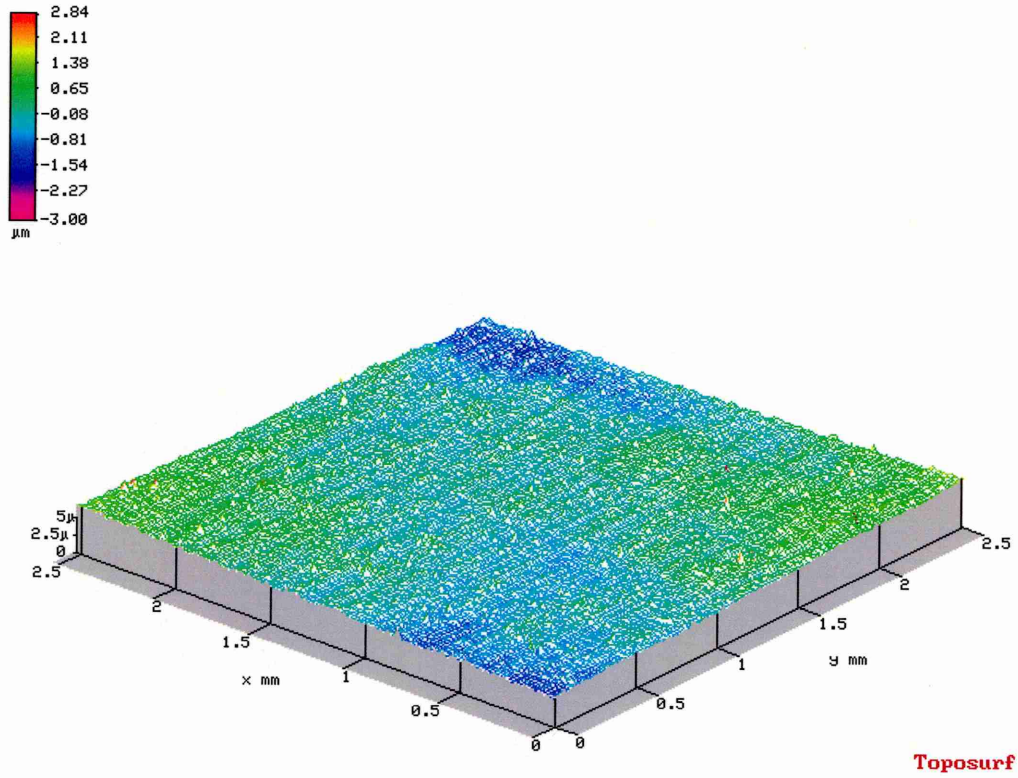

Figure 4.39 - *3D surface profile of 2B finish*

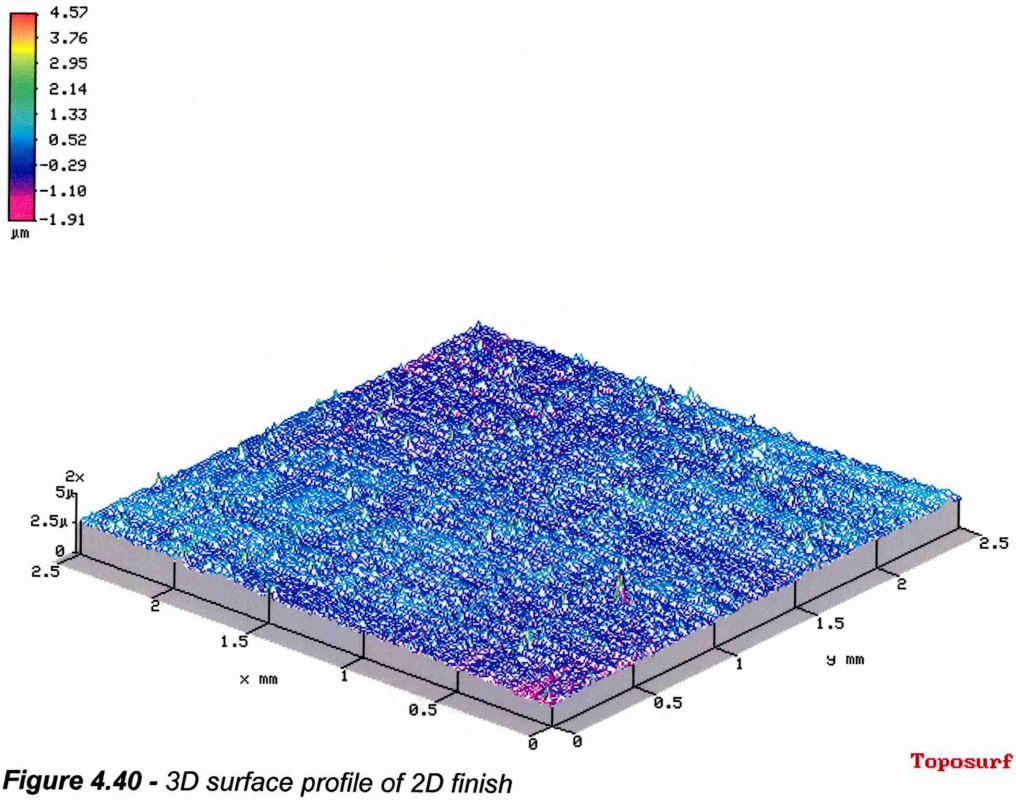

Figure 4.40 - *3D surface profile of 2D finish*

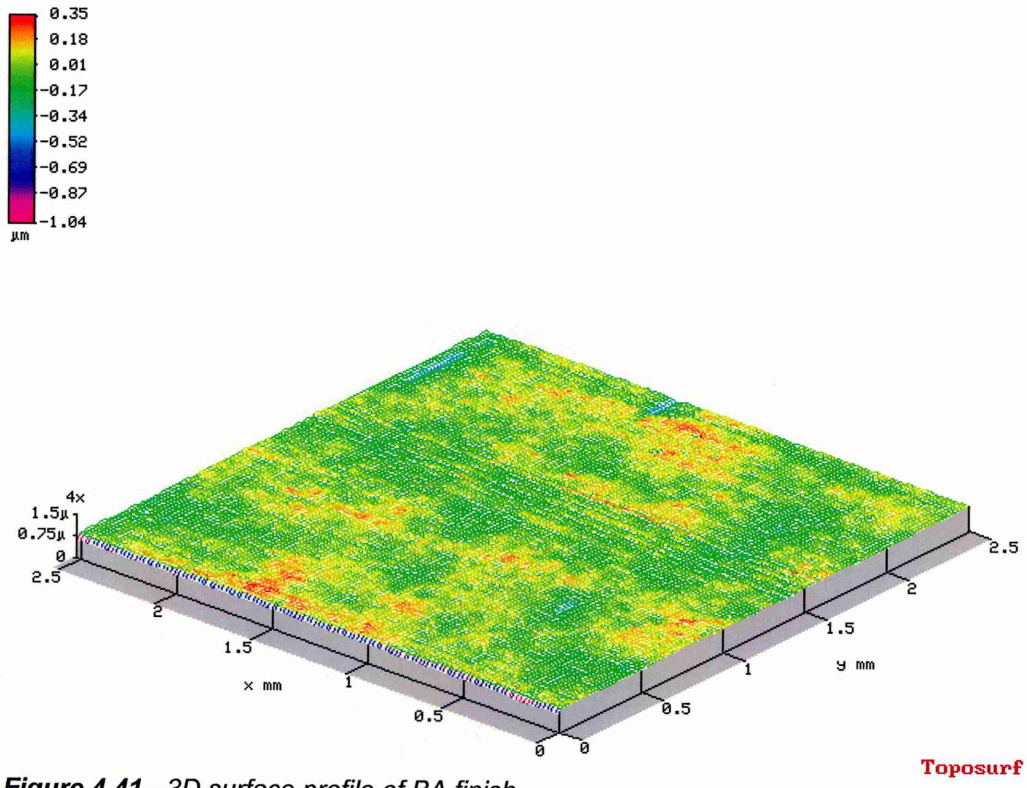

Figure 4.41 - *3D surface profile of BA finish*

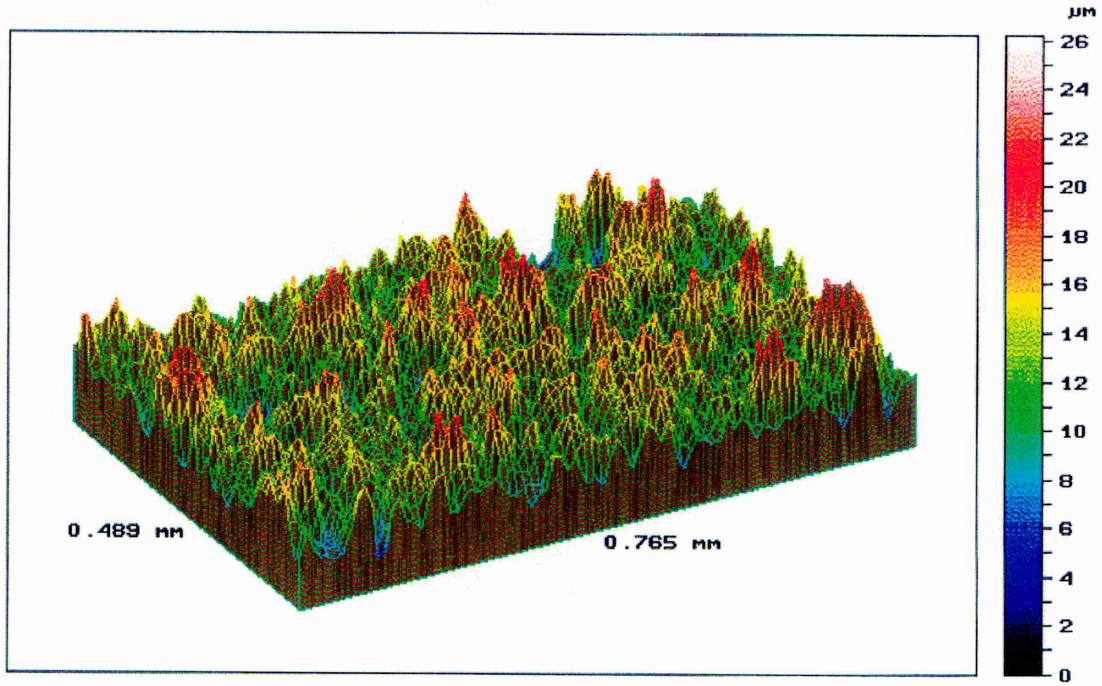

Figure 4.42 - *3D surface profile of alumina grit blast surface*

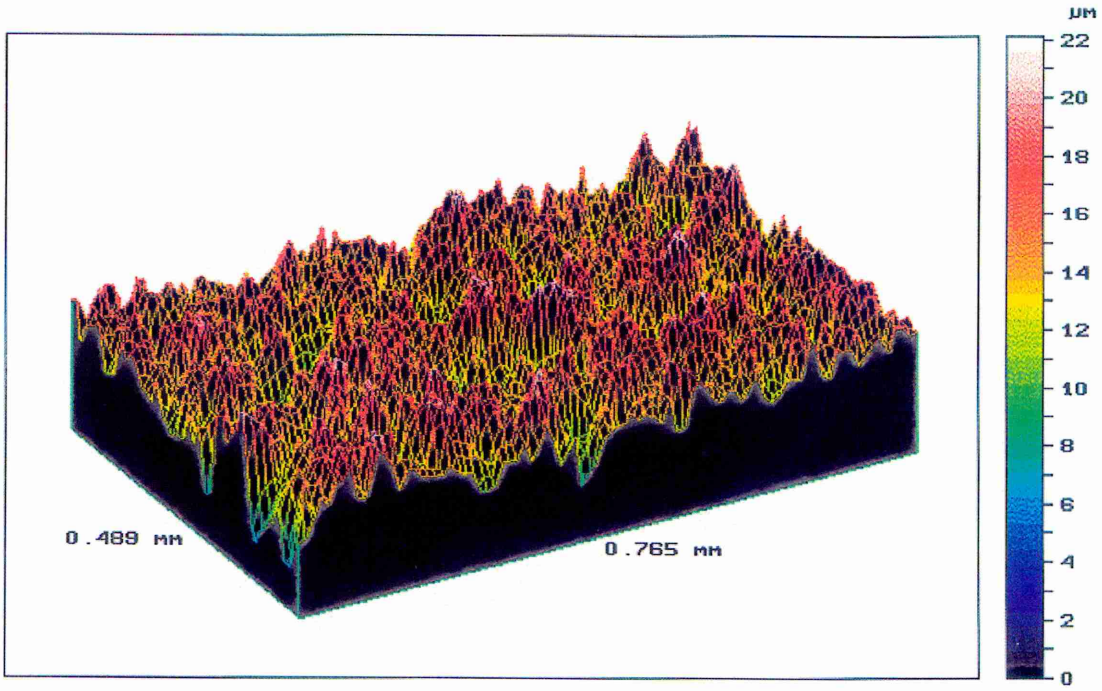

Figure 4.43 - *3D surface profile of alumina grit blast + CP30 surface*

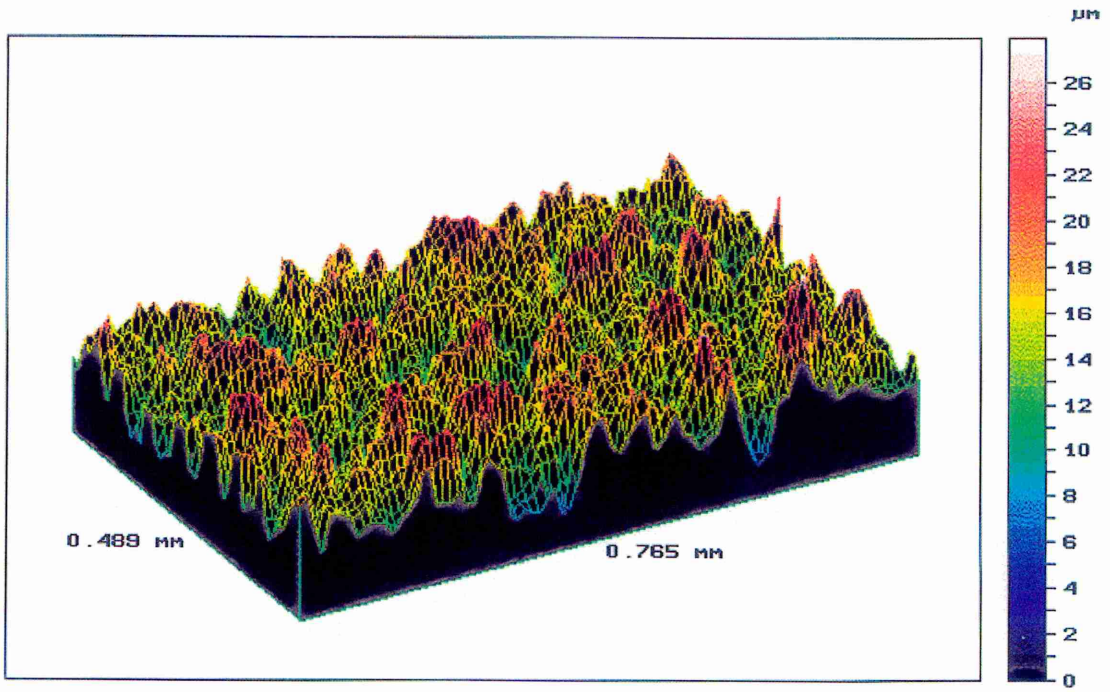

Figure 4.44 - *3D surface profile of alumina grit blast + AZS surface*

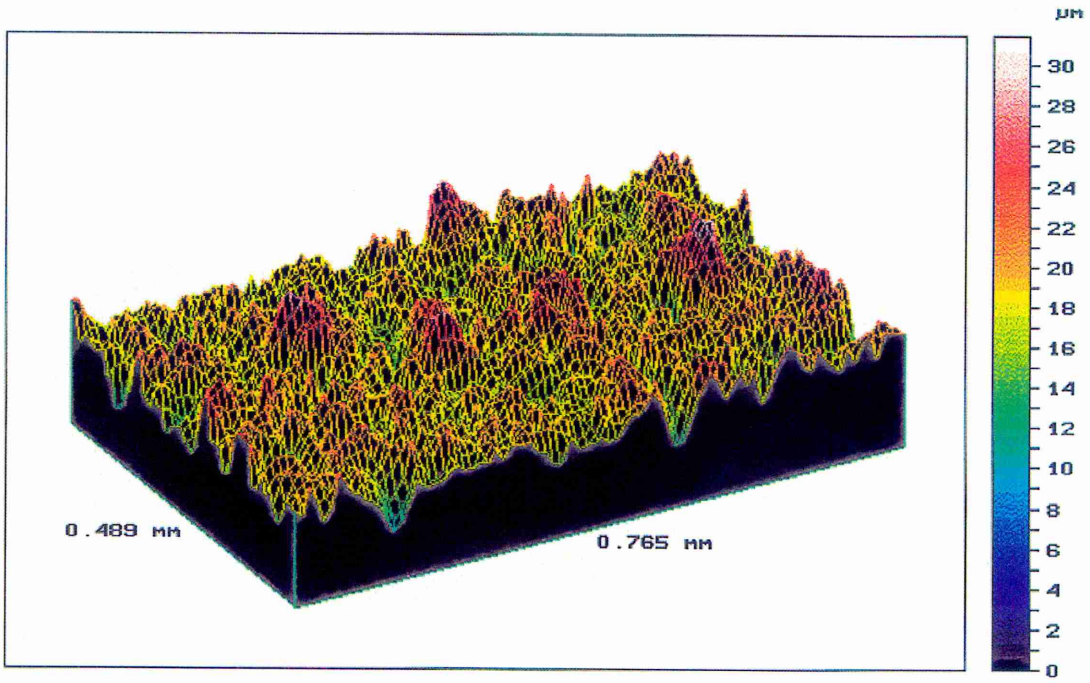

Figure 4.45 - *3D surface profile of alumina grit blast + Accomet C surface*

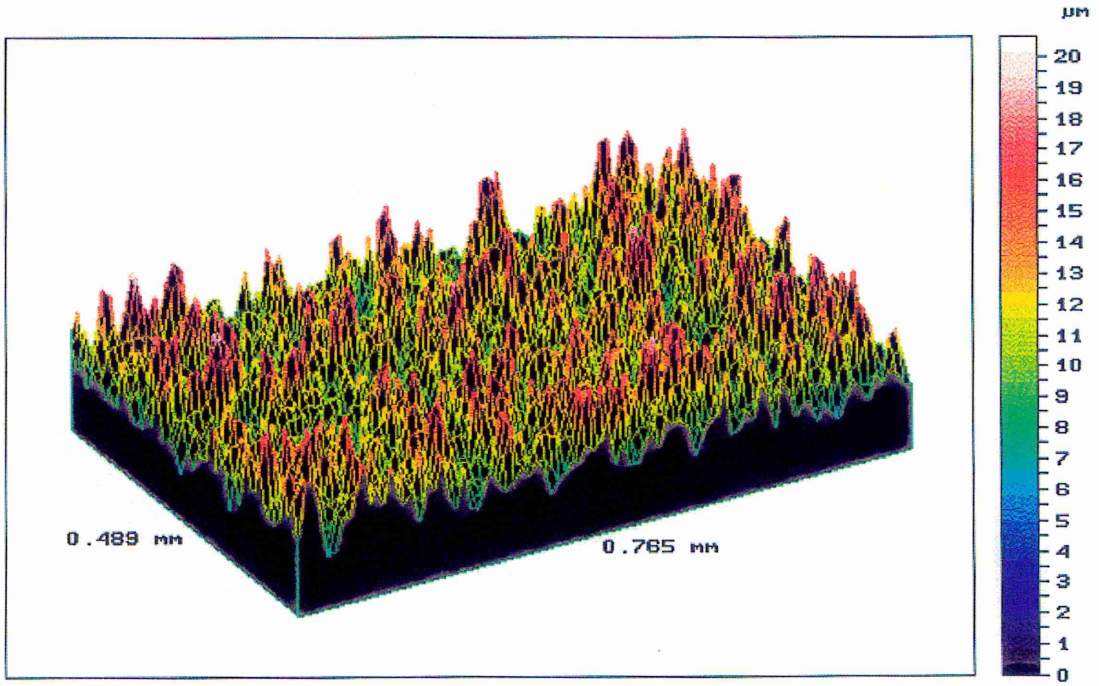

Figure 4.46 - *3D surface profile of sulphuric acid sodium dichromate anodised surface*

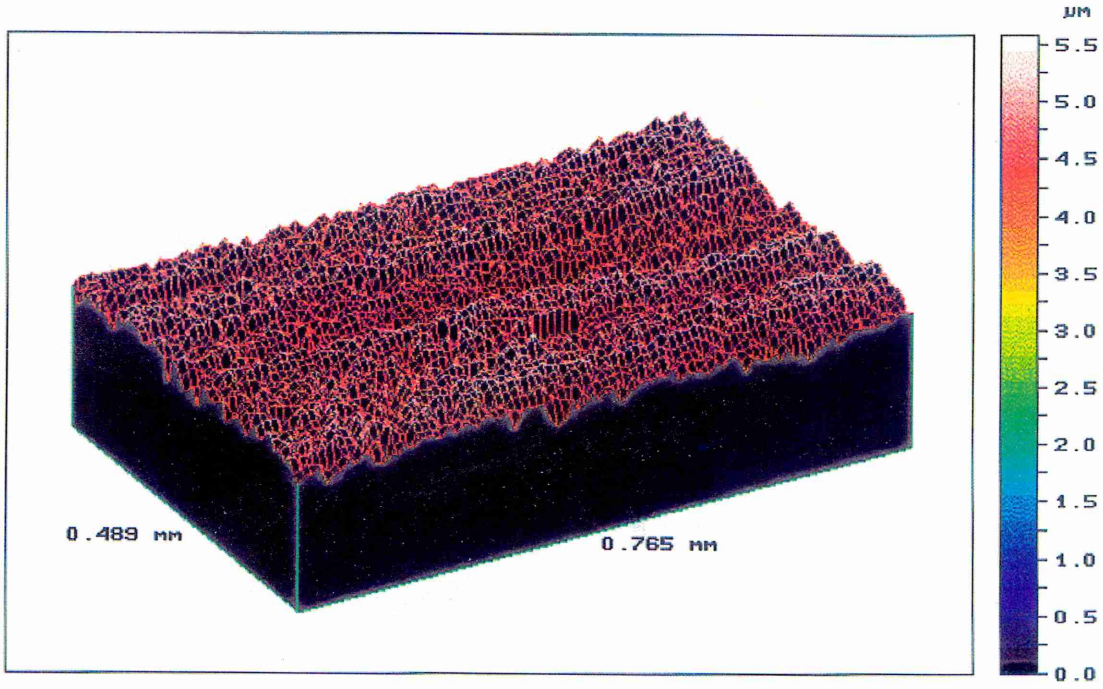

Figure 4.47 - *3D surface profile of nitric acid anodised surface*

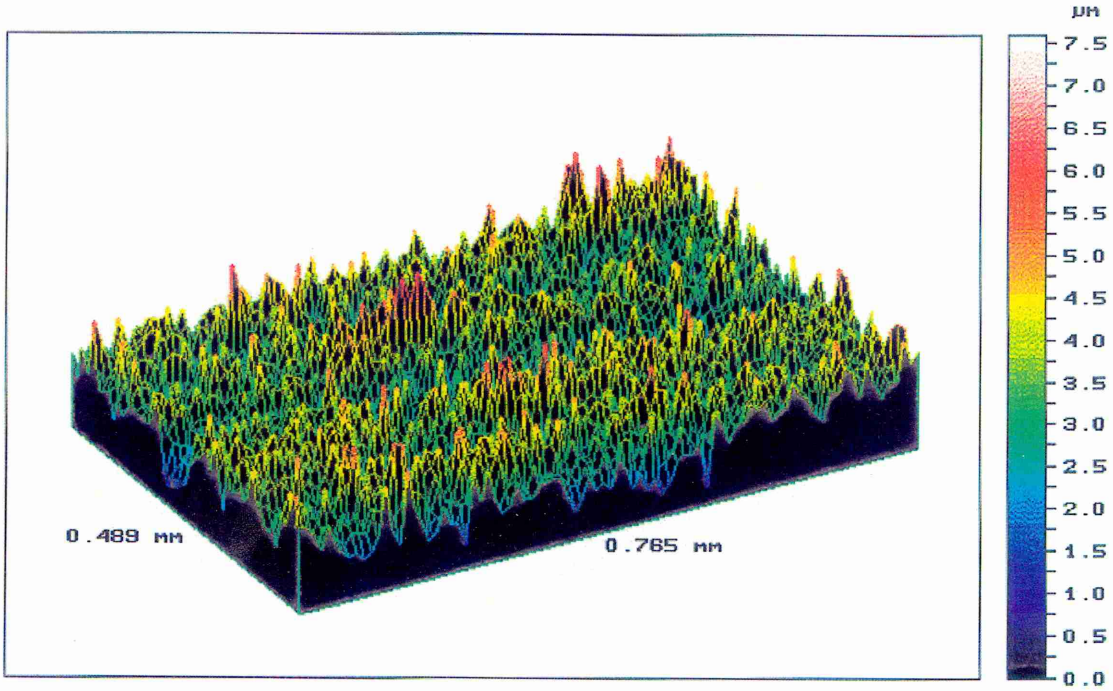

Figure 4.48 - *3D surface profile of ferric chloride etched surface*

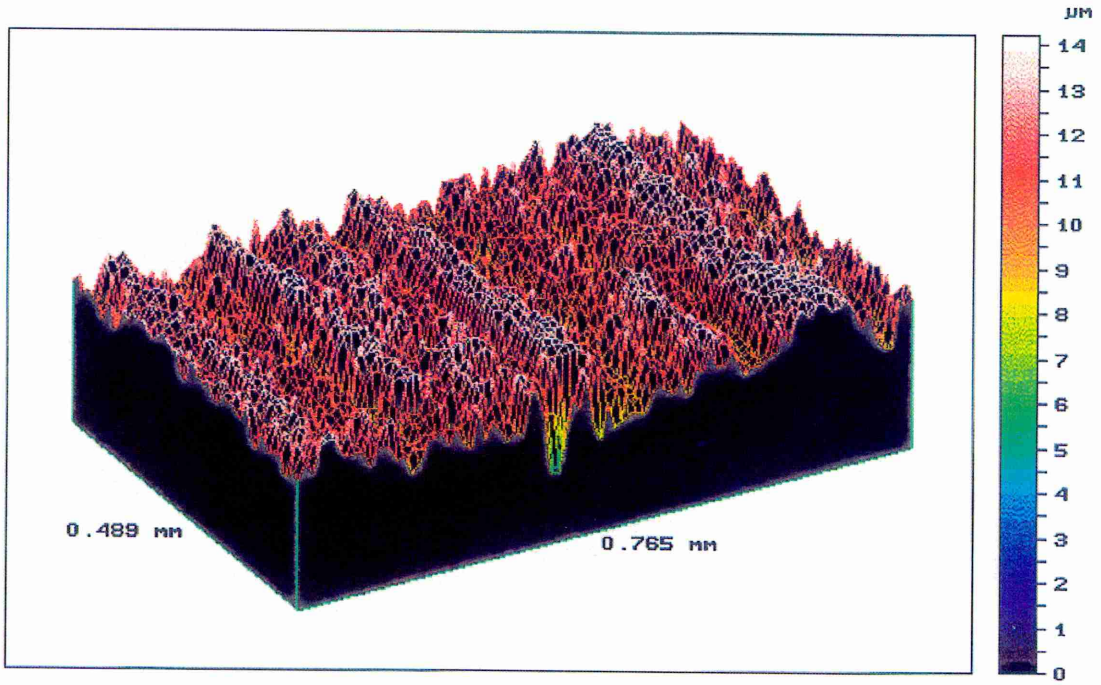

Figure 4.49 - *3D surface profile of oxalic acid etched surface*

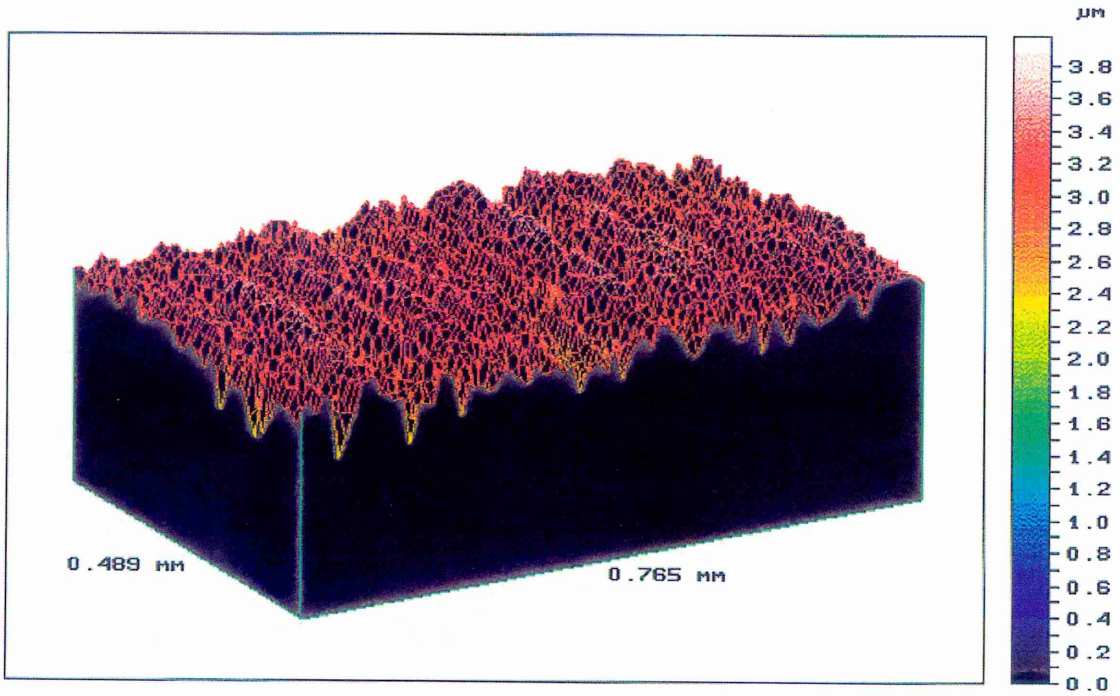

Figure 4.50 - *3D surface profile of sulphuric acid etched surface*

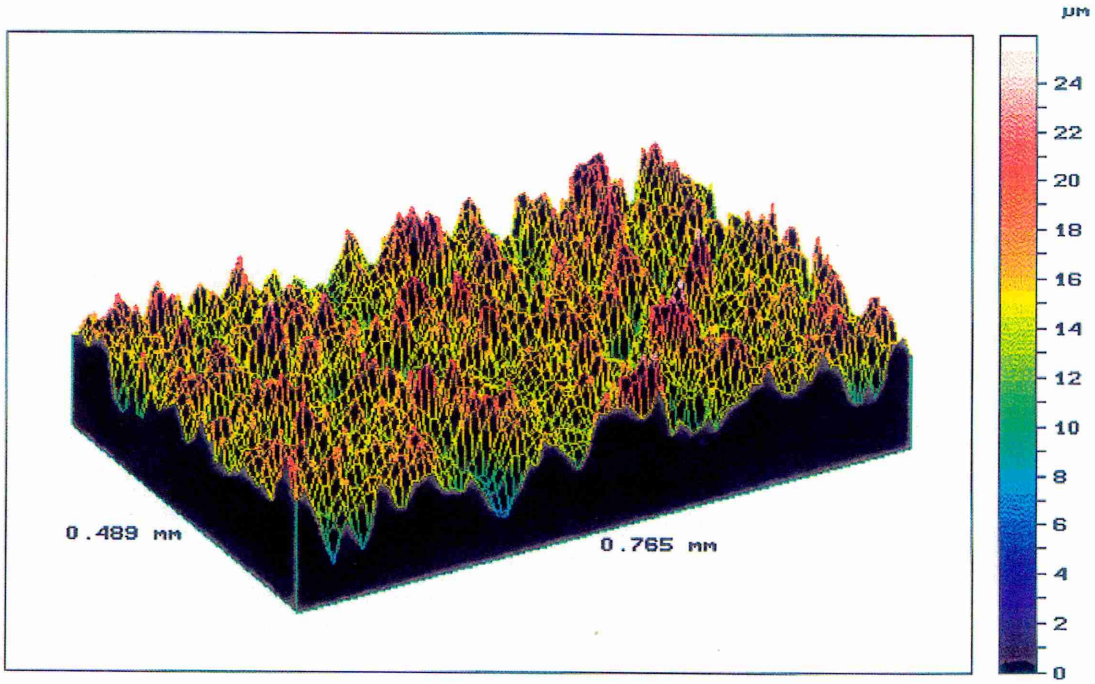

Figure 4.51 - *3D surface profile of alumina grit blast + silane primer surface*

4.4.4 X-Ray Photoelectron Spectroscopy, XPS

XPS was used to evaluate the atomic concentration of elements on the surface of newly treated adherends and the DP490 structural epoxy adhesive. All pre-treatments used in this chapter were analysed with the exception of sulphuric acid etch and alumina grit blast + CP30 treatments. The analysis was carried out as detailed in 3.6 Surface Characterisation, 3.6.2.2 X-Ray Photoelectron Spectroscopy.

Alkaline Degreased – 2B, BA and 2D commercial finishes

The elemental composition of the 2B, BA and 2D finishes are shown in Table 4.13, where mainly oxygen and carbon dominate the surface. The calcium content on the 2B finish has been introduced to the surface from the alkaline degreasing process. Chromium and iron were detected as they form the bulk of the metallic oxide. Figure 4.52 shows the XPS wide survey scan.

***Table 4.13** - XPS analysis of 2B surface.*

Element	% Concentration			Binding Energy (eV)
	2B	BA	2D	
Oxygen, O1s	36.384	35.8	31.2	532
Carbon, C1s	46.474	39.6	56.2	285
Chromium, Cr2p	3.819	5.4	4.1	576.5
Iron, Fe2p3/2	4.502	10.3	5.5	710.5
Manganese, Mn2p	1.336	-	-	641
Fluorine, F1s	1.052	-	-	684.5
Zinc, Zn2p	0.785	-	-	1023
Sodium, Na1s	2.046	-	-	1072
Nitrogen, N1s	1.043	3.7	2.9	400.5
Calcium, Ca2p	0.399	-	-	348
Chlorine, Cl2p	0.741	-	-	198.5
Sulphur, S2p	0.717	-	-	169.5
Silicon, Si2p	0.702	-	-	102

Alumina Grit Blast

The elemental composition of the alumina grit blasted surface is detailed in Table 4.14. When compared to the alkaline degreased surface, there is a reduction in the amount of surface contamination, represented by carbon. However aluminium has been introduced from the mechanical treatment. The XPS wide survey scan is shown in Figure 4.53.

***Table 4.14** - XPS analysis of alumina grit blasted surface.*

Element	% Concentration	Binding Energy (eV)
Oxygen, O1s	44.285	532
Carbon, C1s	36.926	285.5
Chromium, Cr2p	3.59	576.5
IronFe2p3/2	5.847	710.5
Manganese, Mn2p	0.738	639.5
Zinc, Zn2p	0.682	1022
Sodium, Na1s	2.258	1072.5
Calcium, Ca2p	0.99	348
Sulphur, S2p	0.31	170
Aluminium, Al2s	3.427	120
Silicon, Si2p	0.947	100

Alumina Grit Blast + Silane Primer

The application of the primer has introduced a higher concentration of silicon and nitrogen to the surface. The primer has masked the chromium, iron and other elements associated with a stainless steel surface. Aluminium was detected from residual material left from the grit blasting process. The XPS wide survey scan is shown in Figure 4.54.

***Table 4.15** - XPS analysis of the alumina grit blast + silane primer*

Element	% Concentration	Binding Energy (eV)
Oxygen, O1s	26.802	532.5
Carbon, C1s	54.9	285.5
Chromium, Cr2p	1.046	576.5
Iron, Fe2p3/2	1.481	710.5
Zinc, Zn2p	0.331	1022.5
Sodium, Na1s	0.261	1072.5
Nitrogen, N1s	6.728	400
Calcium, Ca2p	0.431	348.5
Chlorine, Cl2p	0.621	198.5
Silicon, Si2p	3.735	103
Sulphur, S2p	0.411	169.5
Aluminium, Al2s	3.253	119.5

Alumina Grit Blast + AZS

The AZS proprietary treatment has masked the substrate surface. All elements affiliated with stainless steel have been removed, suggesting the treatment has been generously applied. AZS is primarily a silicon based product, which is confirmed from the high concentration of silicon on the surface. In addition the AZS treatment has increased the phosphorus content. The low level detection of aluminium suggests it is from the application of AZS rather than from the grit blasting process. The surface is also heavily dominated by oxygen. The XPS wide survey scan is shown in Figure 4.55.

***Table 4.16** - XPS analysis of the alumina grit blast + AZS surface*

Element	% Concentration	Binding Energy (eV)
Oxygen, O1s	52.759	533.5
Carbon, C1s	20.156	285.5
Sodium, Na1s	0.499	1072
Nitrogen, N1s	1.065	402.5
Phosphorus, P2p	3.171	134.5
Silicon, Si2p	20.533	104
Aluminium, Al2s	1.817	120

Sulphuric Acid Sodium Dichromate Anodising

The XPS elemental analysis of the sulphuric acid sodium dichromate anodised surface is shown below in Table 4.17. Comparing with the analysis of the alkaline degreased surface there is a substantial increase in the chromium content at the surface. The level of surface contamination has decreased. The XPS wide survey scan is shown in Figure 4.56.

***Table 4.17** - XPS analysis of sulphuric acid sodium dichromate anodised surface*

Element	% Concentration	Binding Energy (eV)
Oxygen, O1s	47.675	531.5
Carbon, C1s	33.321	285
Chromium, Cr2p	11.17	577.5
Iron, Fe2p3/2	4.781	707
Manganese, Mn2p	1.409	641
Nitrogen, N1s	0.994	398.5
Sulphur, S2p	0.651	169

Nitric Acid Anodising

Table 4.18 details the XPS analysis of the nitric acid anodised surface. Comparing the surface with the alkaline degreased variant the pre-treatment has increased the oxygen and chromium content. The carbon level has been reduced, suggesting surface contamination has been minimised. The treatment has introduced phosphorus. The XPS wide survey scan is shown in Figure 4.57.

***Table 4.18** - XPS analysis of nitric acid anodised surface*

Element	% Concentration	Binding Energy (eV)
Oxygen, O1s	52.912	532
Carbon, C1s	28.079	285
Chromium, Cr2p	8.868	577
Manganese, Mn2p	0.896	640
Iron, Fe2p3/2	4.087	707.5
Nitrogen, N1s	1.301	400.5
Sulphur, S2p	1.089	168.5
Chlorine, Cl2p	0.853	198.5
Phosphorus, P2p	1.139	133.5
Silicon, Si2p	0.777	100

Oxalic Acid Etch

Table 4.19 shows the XPS analysis of the oxalic etched surface. Both the chromium and iron content has increased to some extent in contrast to the alkaline degreased surface. Interestingly the nitrogen level has appreciably amplified. The XPS wide survey scan is shown in Figure 4.58.

***Table 4.19** - XPS analysis of the oxalic acid etched surface*

Element	% Concentration	Binding Energy (eV)
Oxygen, O1s	39.647	532
Carbon, C1s	42.979	285.5
Chromium, Cr2p	5.132	576.5
Iron, Fe2p3/2	5.158	707
Manganese, Mn2p	1.01	640
Sodium, Na1s	1.03	1072
Nitrogen, N1s	4.082	400.5
Calcium, Ca2p	0.193	348
Chlorine, Cl2p	0.651	198.5
Sulphur, S2p	0.118	168.5

Ferric Chloride Etch

Table 4.20 constituents the XPS analysis of the ferric chloride etched surface. The etchant has deposited both chlorine and phosphorus onto the surface. In addition the chromium and iron content of the surface has increased, whilst the degree of surface contamination has stayed in a similar range to the alkaline degreased surface. The XPS wide survey scan is shown in Figure 4.59.

***Table 4.20** - XPS analysis of the ferric chloride etched surface*

Element	% Concentration	Binding Energy (eV)
Oxygen, O1s	44.058	531.5
Carbon, C1s	34.383	285
Chromium, Cr2p	7.583	577
Iron, Fe2p3/2	7.807	707
Manganese, Mn2p	1.067	640.5
Sodium, Na1s	0.598	1071.5
Nitrogen, N1s	2.111	397.5
Chlorine, Cl2p	1.701	198.5
Sulphur, S2p	0.477	168.5
Phosphorus, P2p	0.214	133

Alumina Grit Blast + Accomet C

From Table 4.21 below, the Accomet C process has altered the surface of the stainless steel substrate. The proprietary coating has introduced a high silicon content onto the surface. Accomet C also contains chromium which has been deposited to an extent matching that of the alkaline degreased substrate. The carbon and iron content have been notably diminished, whilst the oxygen content has been increased. The XPS wide survey scan is shown in Figure 4.60.

Table 4.21 *- XPS analysis of the alumina grit blast + Accomet C surface*

Element	% Concentration	Binding Energy (eV)
Oxygen, O1s	63.296	534
Carbon, C1s	16.387	286
Chromium, Cr2p	4.591	579
Iron, Fe2p3/2	0.646	701
Silicon, Si2p	15.08	104.5

DP490 Structural epoxy adhesive

Table 4.22 details the concentration of elements on the surface of the epoxy adhesive used throughout the research. The surface is dominated by carbon and to a much lesser extent by oxygen. There are no metallic species present. The evidence of silicon on the surface is a result of silica particulate been used as filler material, to enhance product volume and reduce manufacturing costs. The XPS wide survey scan is shown in Figure 4.61.

Table 4.22 *– XPS analysis of the DP490 structural epoxy adhesive surface*

Element	% Concentration	Binding Energy (eV)
Oxygen, O1s	17.4	534
Carbon, C1s	74.2	286
Chromium, Cr2p	-	579
Sulphur, S2p	0.2	
Nitrogen, N1s	4.2	397.5
Iron, Fe2p3/2	-	701
Silicon, Si2p	4.0	104.5

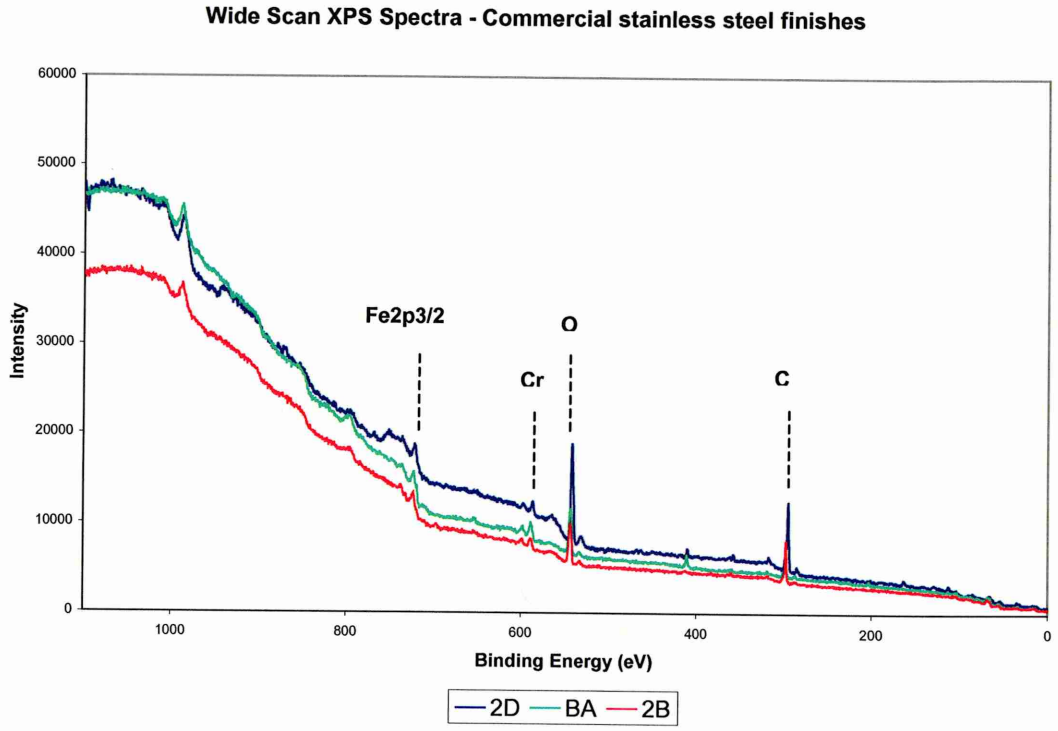

Figure 4.52 - *Wide scan XPS spectra of 2B, BA and 2D alkaline degreased commercially available surfaces*

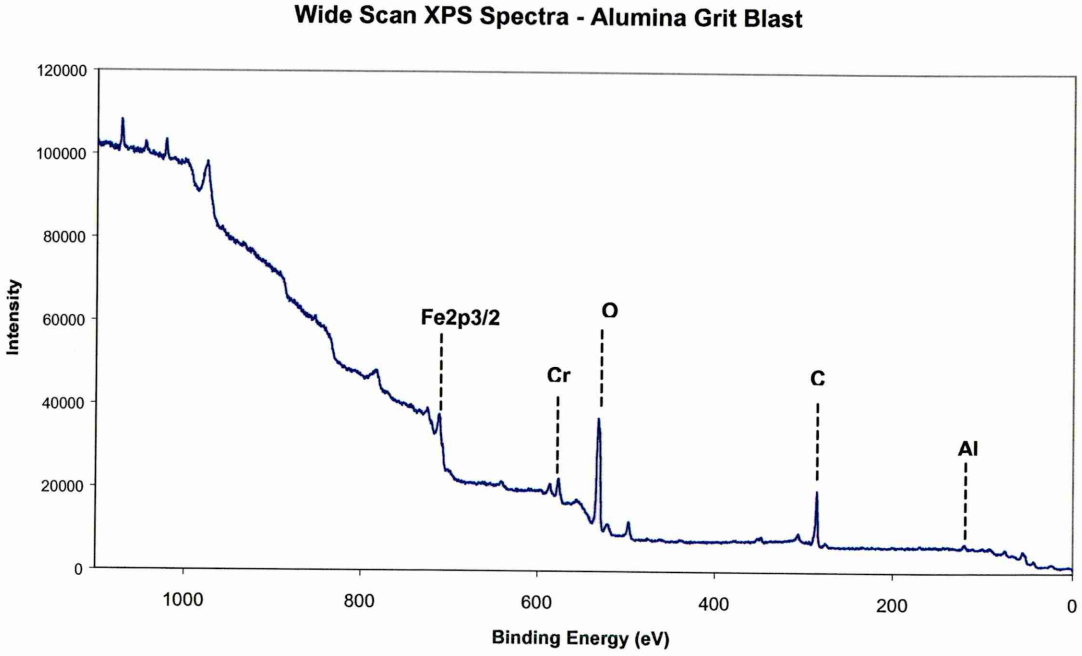

Figure 4.53 - *Wide scan XPS spectra of alumina grit blasted surface*

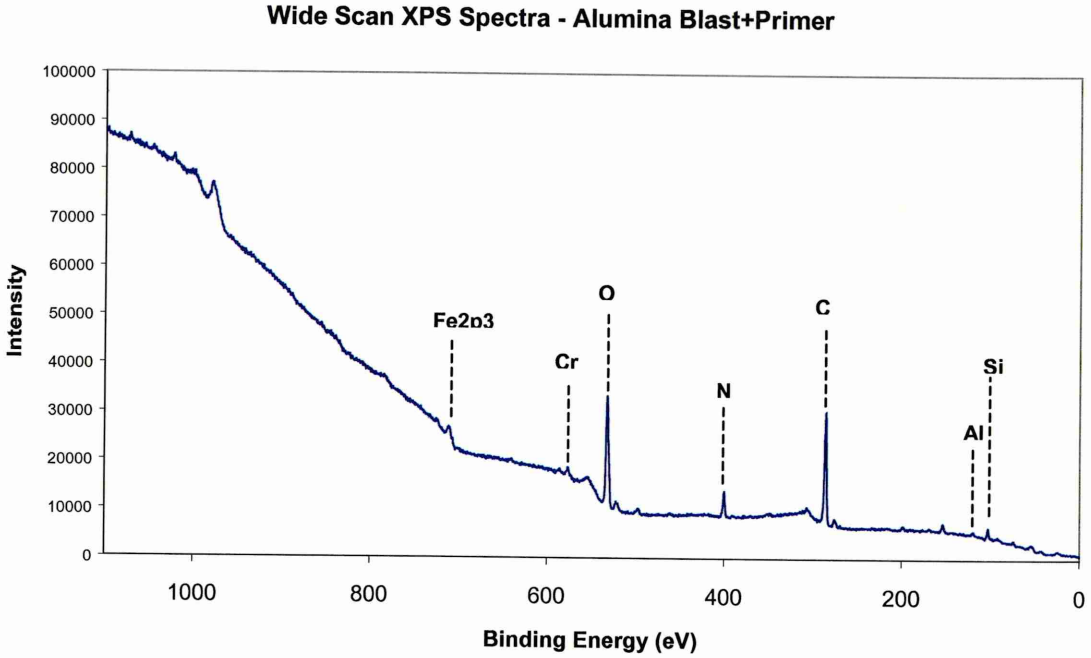

Figure 4.54 - *Wide scan XPS spectra of alumina grit blast + primer surface*

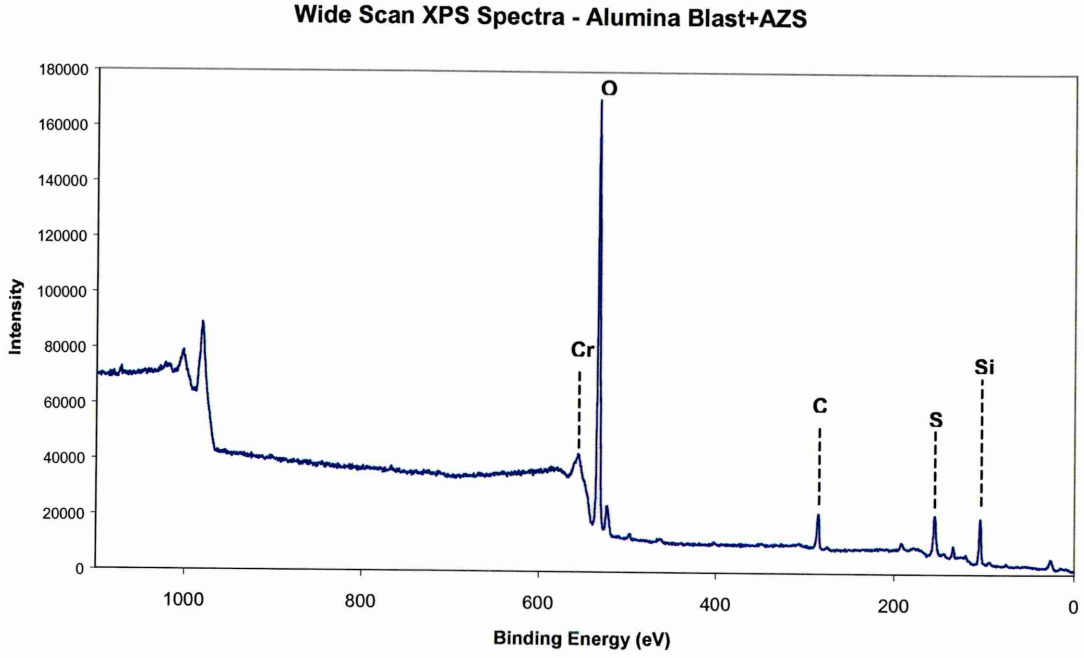

Figure 4.55 - *Wide scan XPS spectra of alumina grit blast + AZS treated surface*

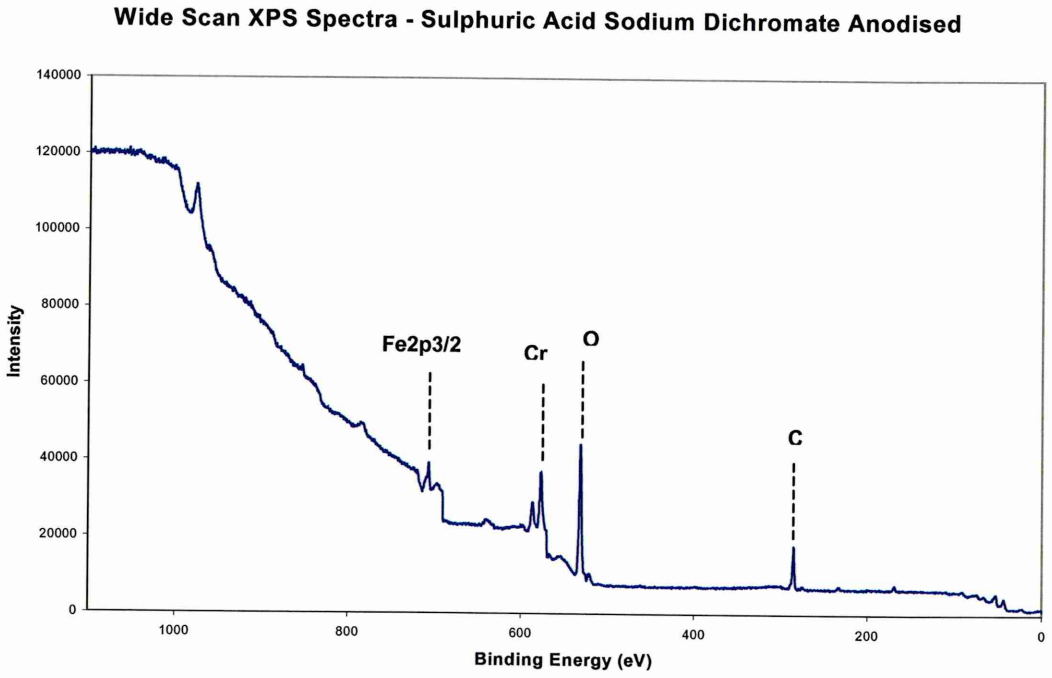

Figure 4.56 - *Wide scan XPS spectra of sulphuric acid anodised surface*

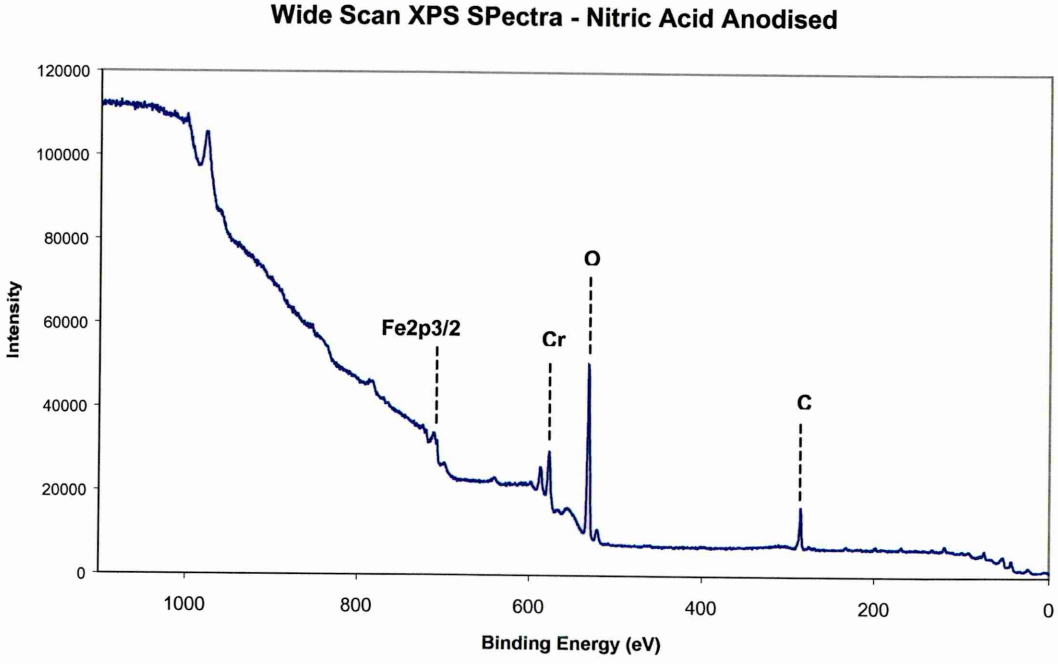

Figure 4.57 - *Wide scan XPS spectra of nitric acid anodised surface*

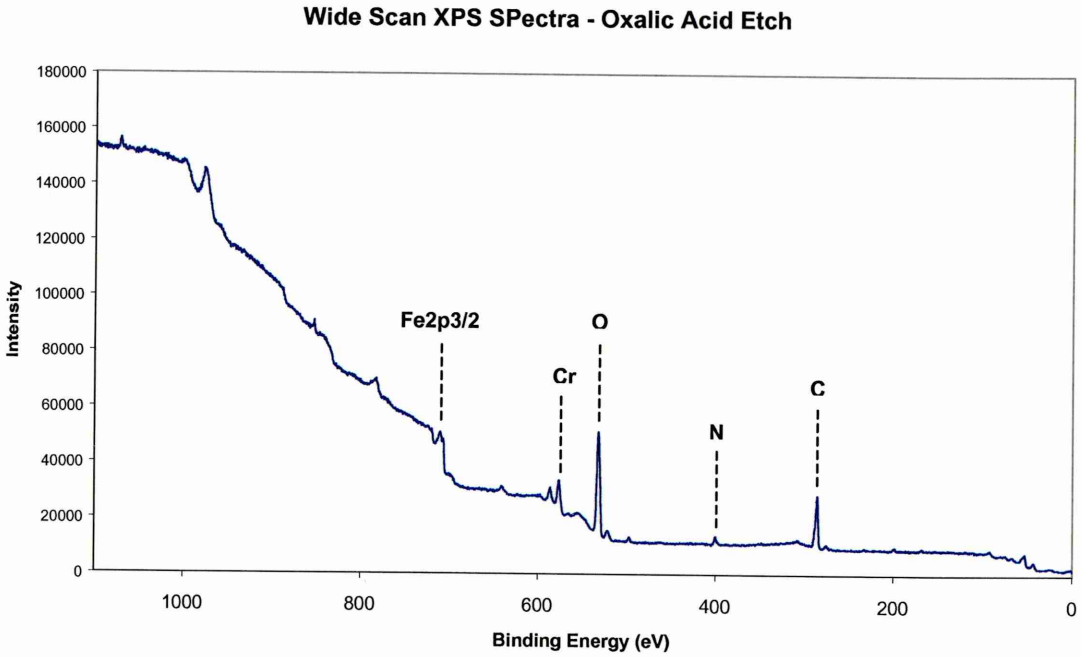

Figure 4.58 - *Wide scan XPS spectra of oxalic acid etched surface*

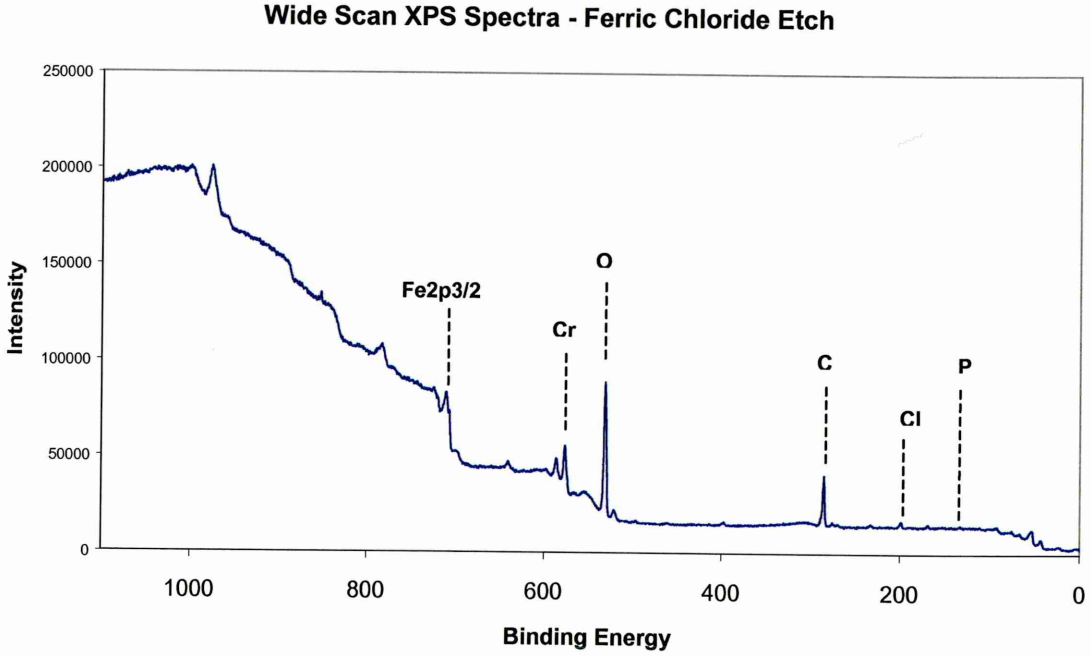

Figure 4.59 - *Wide scan XPS spectra of ferric chloride etched surface*

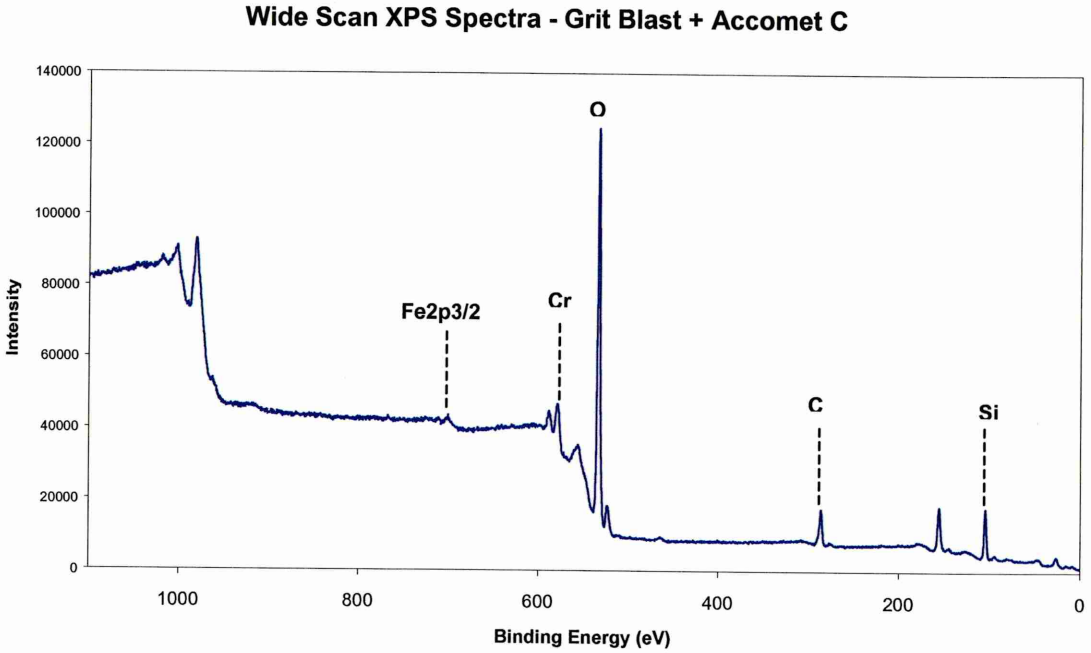

Figure 4.60 *- Wide scan XPS spectra of alumina grit blast + Accomet C treated surface*

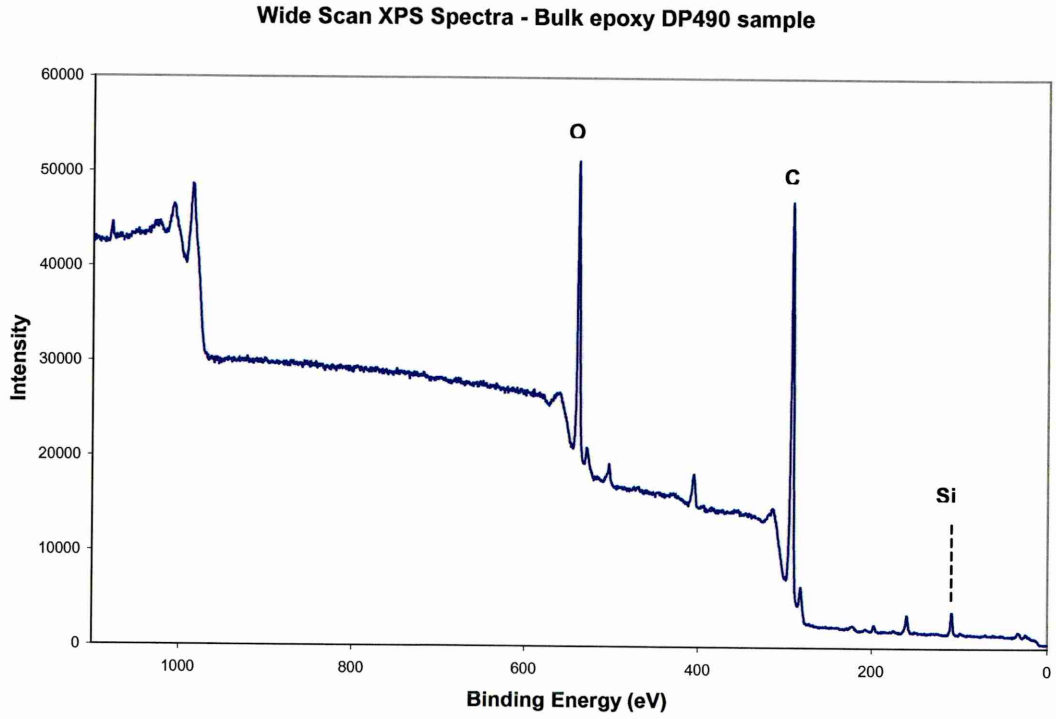

Figure 4.61- *Wide scan XPS spectra of DP490 structural epoxy adhesive surface*

4.4.5 Closing Remarks

The physical and chemical analysis of treated adherends prior to bonding has been achieved using SEM, surface profilometry and XPS. SEM has provided useful information on the surface topography of the stainless steel substrates as a function of pre-treatment. Whilst surface profilometry has demonstrated it is a useful tool for assessing surface roughness, and works well as a complementary technique. For example the 3D surface profiles of the alumina grit blasted surfaces reveal 'crater' like undulations from the high velocity impact of particles, resulting in a characteristic macro-roughening affect. The micro-roughening effect of the sulphuric acid sodium dichromate anodised surface is exhibited as a very fine network of relatively high peak to trough spikes. XPS analysis has yielded information on the chemical composition of the treated surfaces, which may relate to bond performance. The carbon levels on the treated surfaces are an indication of surface contamination. The alkaline degreased surface generally has the highest level of contamination. The carbon concentration is reduced on all other treated surfaces, and notably low on the alumina grit blast + Accomet C where the carbon concentration is 16.38%.

4.5 Failure Analysis

4.5.1 Introduction

An adhesive joint can fail in a variety of ways. If the mode of failure is attained this can yield useful information on the performance of individual 'adhesive systems' when exposed to high humidity environments. Visual and optical micrograph analysis has been carried out on perforated lap shear and wedge test specimens. The failure mode investigations have then been taken a stage further to include SEM and XPS analysis on the fracture surfaces of wedge specimens.

4.5.2 Visual and Optical Macrograph Analysis

4.5.2.1 Perforated Lap Shear Joints

4.5.2.1.1 Initial Lap Shear Strength

For all the pre-treatments evaluated the fracture surfaces of the perforated lap shear joints were mainly cohesive failure within the adhesive. Visual analysis of the specimens revealed equal amounts of adhesive on both sides of the fracture faces, suggested failure has taken place through the adhesive and not at the metal oxide-adhesive interface.

4.5.2.1.2 After Environmental Exposure

Exposure to the 100% relative humidity environment incurred changes in the observed failure mode, each surface treatment will be discussed individually.

Alkaline Degreased

For all joints, whether stressed or unstressed, the resulting fracture surfaces revealed adhesive failure had occurred. Visual examination showed one fracture face had a complete covering of adhesive, whilst the other showed no evidence of adhesive. The effects of humidity and increased temperature have weakened the interface between the adhesive and the substrate, causing the adhesive to delaminate from the stainless steel surface. This is shown in Figure 4.62 below.

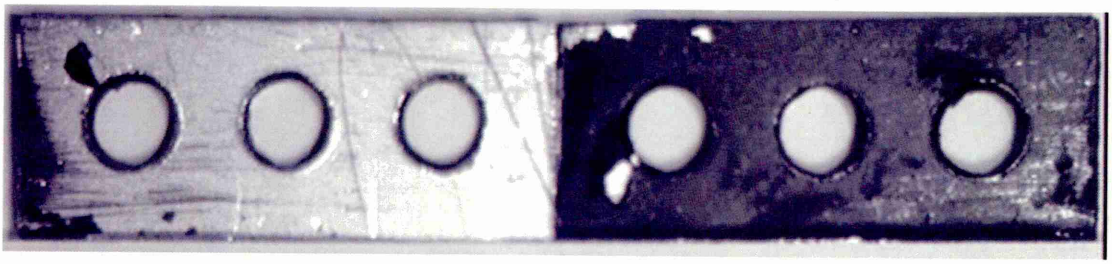

***Figure 4.62** - Alkaline degreased fracture surface after environmental exposure*

Alumina Grit Blast

After environmental exposure the failure mode, regardless if the joint was stressed or unstressed, was adhesive failure. Examination of the fracture surfaces showed each face

contained adhesive, whilst the corresponding region revealed only the alumina blasted surface. The fracture faces are shown in Figure 4.63.

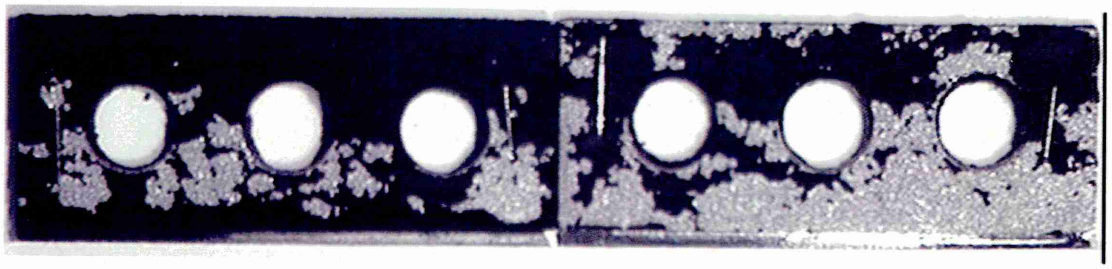

***Figure 4.63** - Alumina grit blast fracture surface after environmental exposure*

Alumina Grit Blast + Primer

The fracture surfaces appeared to display mixed modes of failure. The fracture faces examined contained both adhesive failure, and pockets of cohesive failure where thin layers of adhesive were still attached to one surface, as shown below.

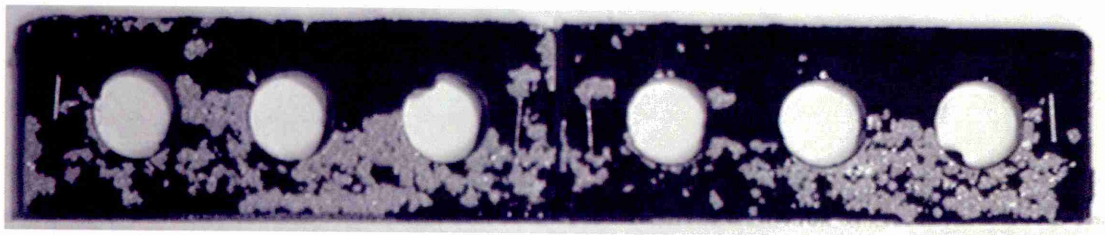

***Figure 4.64** - Alumina grit blast + primer fracture surface after environmental exposure*

Alumina Grit Blast + CP30

The fracture faces of the failed joints showed adhesive failure had taken place. It appears total delamination of the adhesive has taken place because there is no visual evidence of adhesive on the mating surface.

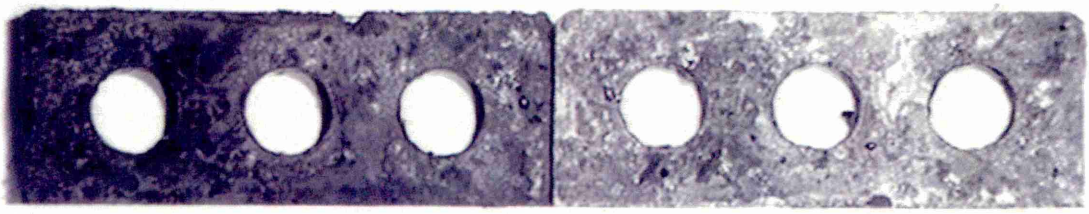

***Figure 4.65** - Alumina grit blast + CP30 fracture surface after environmental exposure*

Alumina Grit Blast + AZS

After environmental exposure examination of the fracture faces showed adhesive failure was the prominent mode of failure. The fracture surfaces are shown below in Figure 4.66. It appear delamination has occurred in a similar fashion to specimens treated with alumina grit blast + CP30.

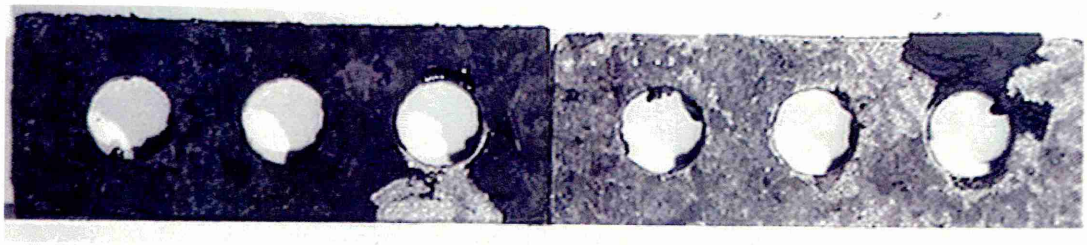

***Figure 4.66** - Alumina grit blast + AZS fracture surface after environmental exposure*

Sulphuric Acid Sodium Dichromate Anodising

Examination of the fracture surfaces revealed mixed mode failure had taken place. Fracture faces were a mixture of cohesive and interfacial failure. The areas of interfacial failure were located close to the edge of the overlap and the perforations, where moisture has been able to easily penetrate the joint, the fracture faces are shown in Figure 4.67.

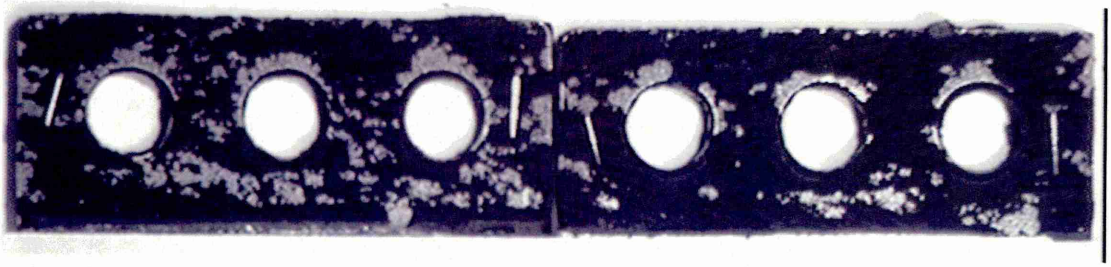

***Figure 4.67** - Sulphuric acid sodium dichromate anodised fracture surface after environmental exposure*

Nitric Acid Anodising

The majority of the fracture faces exhibited interfacial failure had taken place. The fracture faces were blotted with pockets of thin layers of adhesive that corresponded to bulkier layer on the opposing surface, as shown in Figure 4.68.

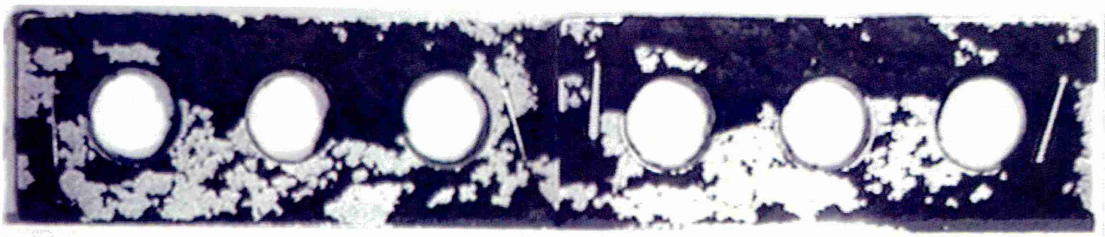

***Figure 4.68** - Nitric acid anodised fracture surface after environmental exposure*

Oxalic Acid Etch

The predominate mechanism of fracture was adhesive failure. Adhesive was observed only on one side of the joint, indicating complete adhesive delamination had taken place, as shown in Figure 4.69.

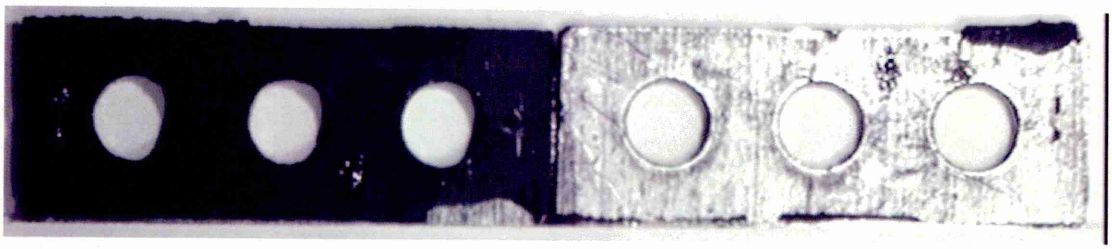

***Figure 4.69** - Oxalic acid etched fracture surface after environmental exposure*

Ferric Chloride Acid Etch

The fracture surfaces demonstrated mixed modes of failure had occurred, where predominately adhesive failure has taken place. Whilst to a lesser degree there were areas where a thin layer of adhesive was present that corresponded to a bulkier layer on the opposing face. The fracture surfaces are displayed below.

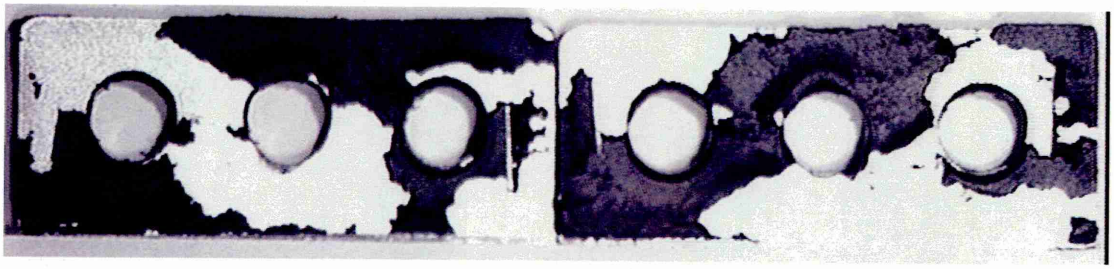

***Figure 4.70** - Ferric chloride etched fracture surface after environmental exposure*

Alumina Grit Blast + Accomet C

The fracture surfaces appeared to have a high proportion of interfacial and a lower proportion of cohesive within the adhesive failure. There was no evidence of adhesive failure taking place. The fracture faces are shown below.

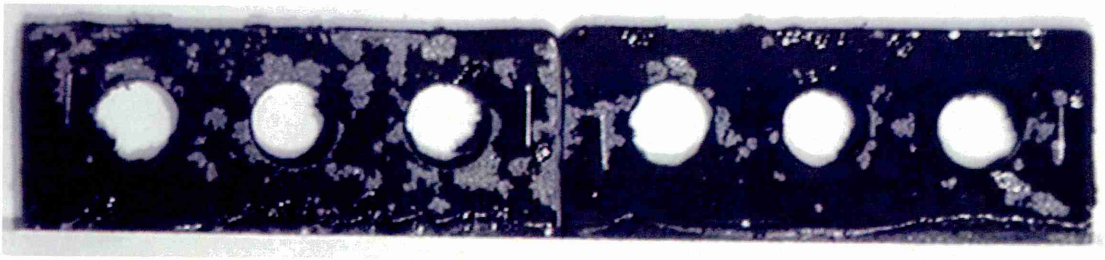

Figure 4.71 - *Alumina grit blast + Accomet C fracture surface after environmental exposure*

Sulphuric Acid Etch

The fracture surfaces where very similar to the alkaline degreased specimens. Visual examination revealed the adhesive had completely delaminated from one adherend. Upon closer inspection of the adhesive its surface was featureless and smooth with a glossy appearance.

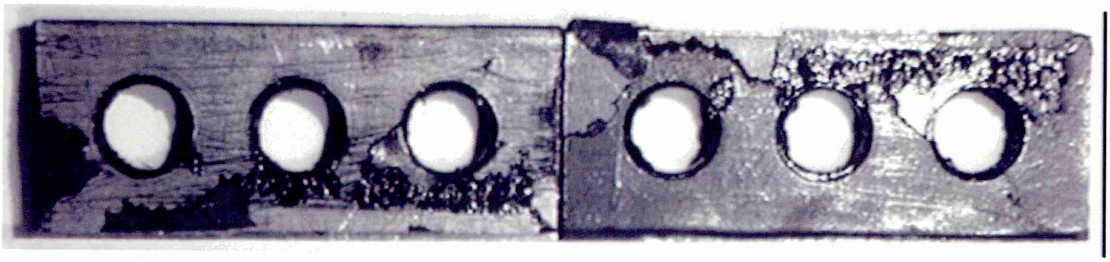

Figure 4.72 - *Sulphuric acid etched fracture surface after environmental exposure*

4.5.1.2 Wedge Tests

Alkaline Degreased

Figure 4.73 shows a typical macrograph of a fractured alkaline degreased wedge test specimen. The initial crack starts cohesively within the adhesive, however before arresting the crack then proceeds in an adhesive failure manner. There are large islands of adhesive on both adherends that correspond to areas of exposed metal. Once ageing commenced the crack advances along the adhesive-metal oxide interface causing adhesive failure. From the macrograph it can be seen rapid crack growth has occurred within 24 hours.

Alumina Grit Blast

Figure 4.74 shows a typical macrograph of a fractured alumina grit blasted wedge test specimen. The initial crack starts cohesively within the adhesive, however after a distance of ~17mm the mode of failure changes to adhesive with a small proportion of interfacial failure. As the environmental exposure commences the failure mode remains adhesive.

Alumina Grit Blast + Primer

The initial crack has developed in a mixture of cohesive and interfacial failure. Subsequent crack formation after environmental exposure has evolved between the adhesive and the substrate interface, resulting in apparent adhesive failure. This is shown in Figure 4.75.

Alumina Grit Blast + CP30

Figure 4.76 shows a typical macrograph of a fractured alumina grit blast + CP30 wedge test specimen. The initial crack propagated cohesively within the adhesive. As environmental exposure continued the fracture has occurred adhesively, where adhesive is only present on one substrate with the opposing surface revealing only the pre-treated surface. Crack growth has advanced rapidly within 24 hours.

Alumina Grit Blast + AZS

The fracture surfaces of alumina grit blast + AZS wedge test specimen are shown in Figure 4.77. After exposure to the high humidity environment the failure mode for a short distance, ~7mm, was cohesive within the adhesive, however the crack front has then advanced to the adhesive-substrate interface and proceeded rapidly within 24 hours.

Sulphuric Acid Sodium Dichromate Anodising

Figure 4.78 shows a typical macrograph of a fractured sulphuric acid sodium dichromate anodised wedge test specimen. The initial crack has advanced cohesively within the adhesive. The crack continues to propagate cohesively after environmental exposure has begun. The failure mode then changes to an apparent interfacial failure close to the adhesive-substrate interface.

Nitric Acid Anodising

The initial crack has propagated cohesively within the adhesive. Environmental exposure has led to a change in failure mode, where the crack has advanced close to the adhesive-substrate interface causing predominately adhesive failure coupled to a lesser extent with apparent interfacial fracture, as shown in Figure 4.79.

Alumina Grit Blast + Accomet C

Figure 4.80 shows a typical macrograph of a fractured alumina grit blast + Accomet C wedge test specimen. The initial crack has progressed cohesively within the adhesive. The crack front continues to advance cohesively once exposure to high humidity has started, this then changes to a mixture of cohesive and interfacial failure. The fracture faces are composed of pockets of adhesive, where the corresponding areas show evidence of thin layers of adhesive.

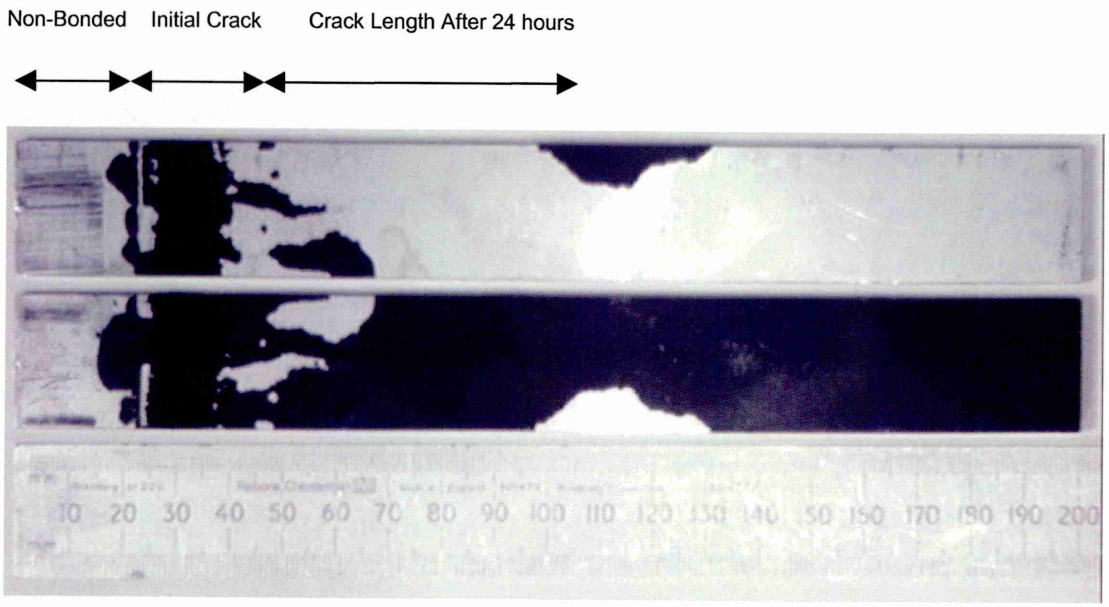

Figure 4.73 - *Alkaline degreased fractured wedge test specimen*

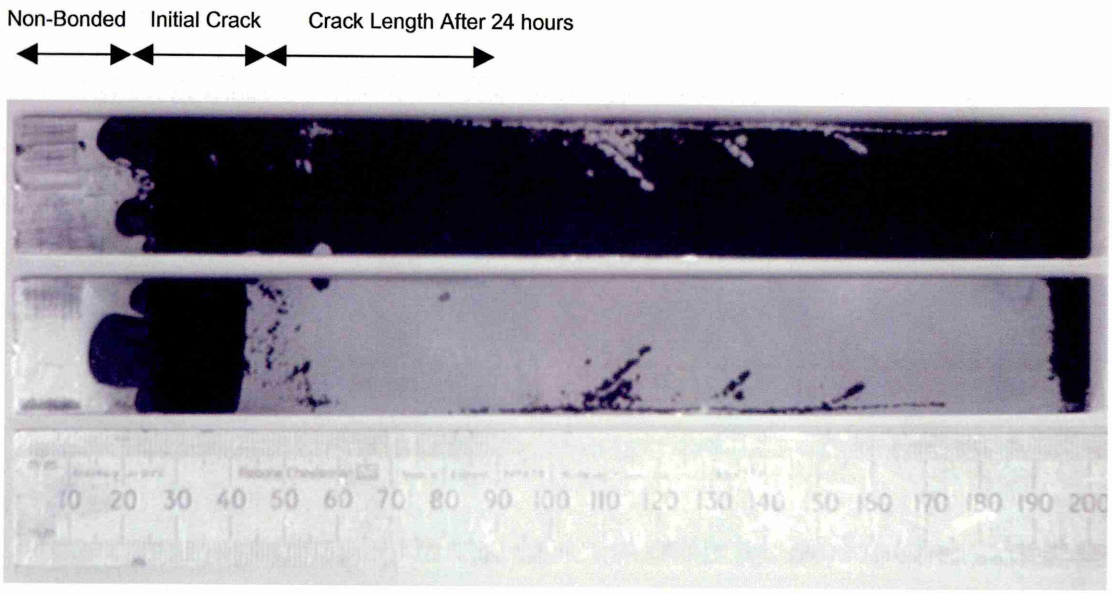

Figure 4.74 - *Alumina grit blast fractured wedge test specimen*

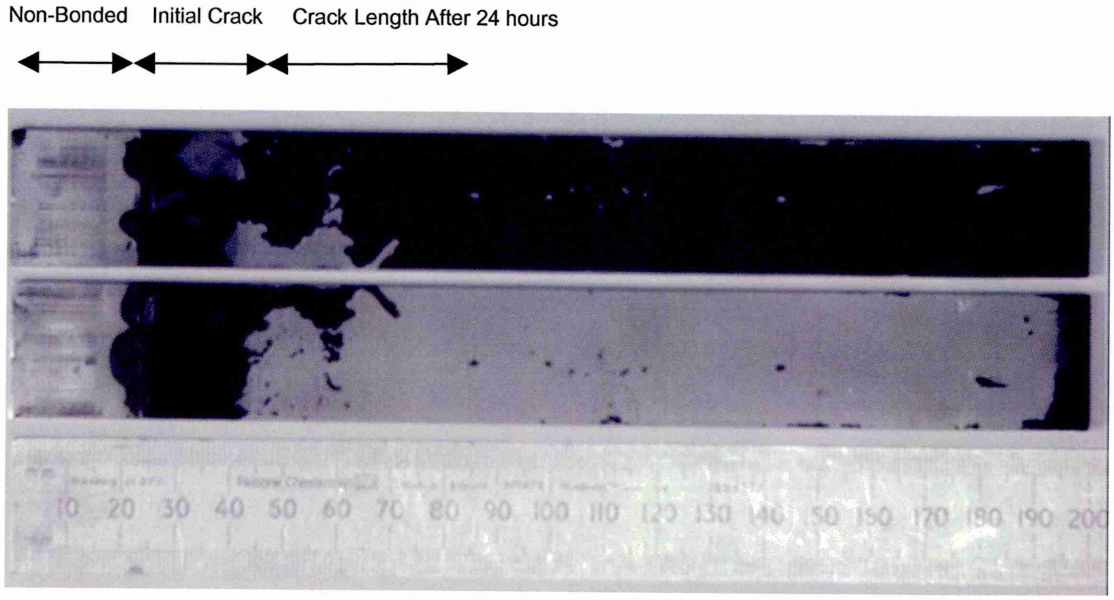

Figure 4.75 - *Alumina grit blast + primer fractured wedge test specimen*

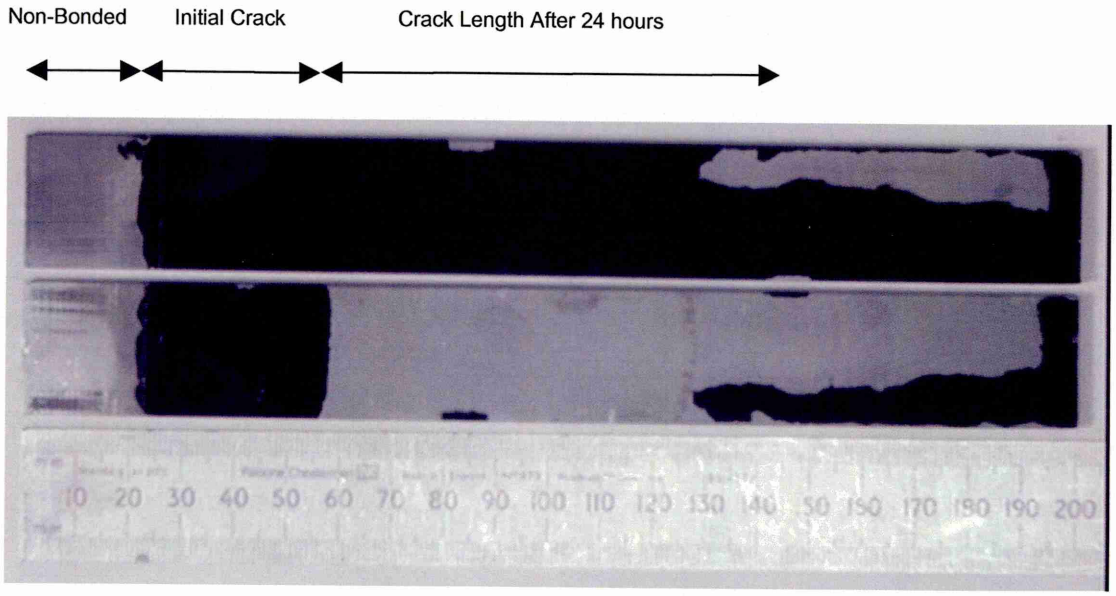

Figure 4.76 - *Alumina grit blast + CP30 fractured wedge test specimen*

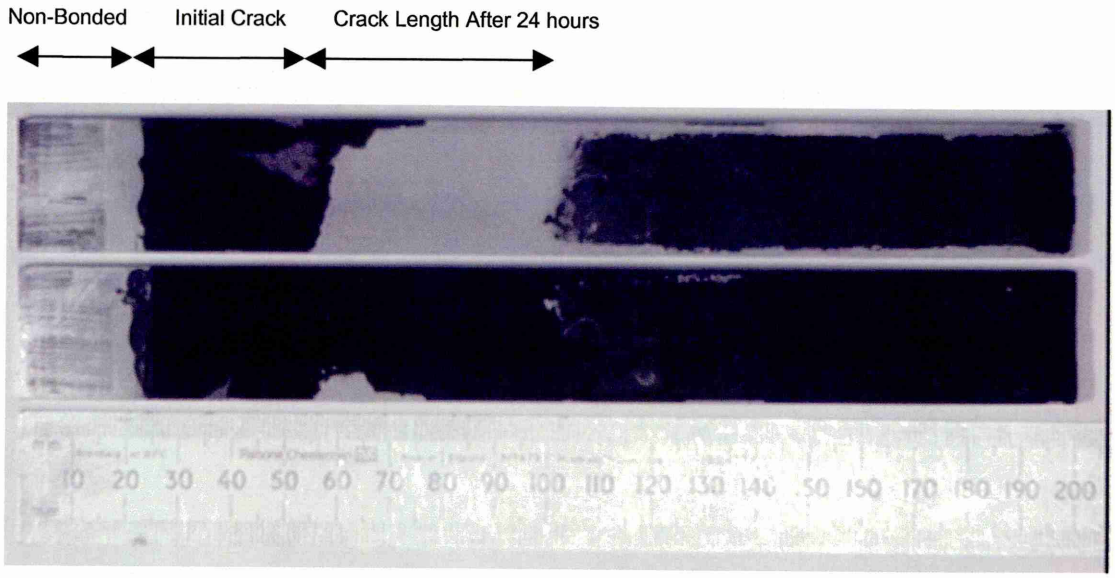

***Figure 4.77** - Alumina grit blast + AZS fractured wedge test specimen*

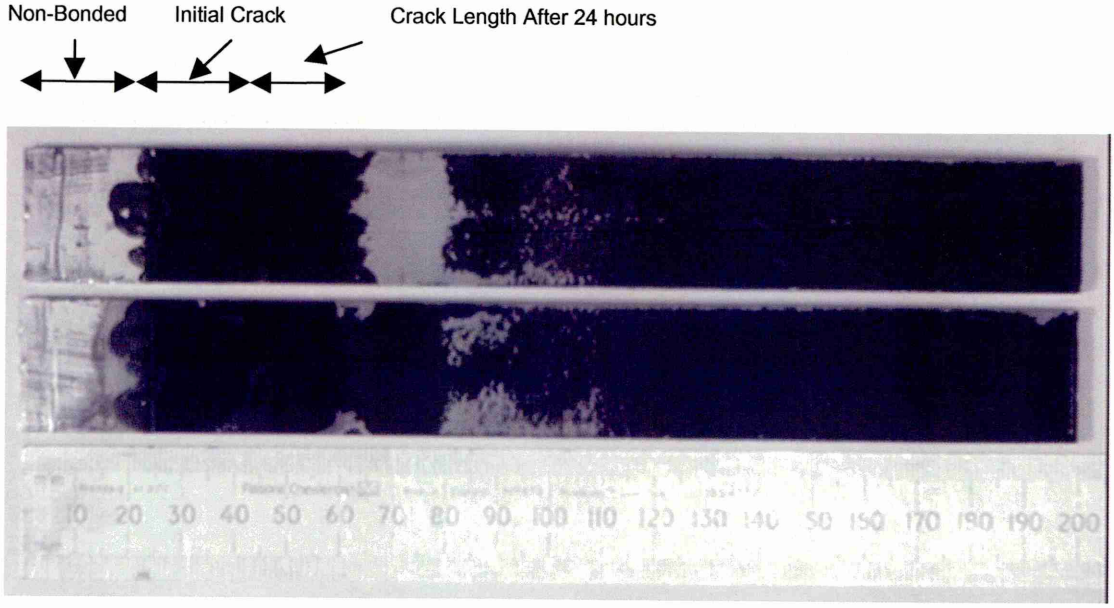

***Figure 4.78** - Sulphuric acid sodium dichromate anodised fractured wedge test specimen*

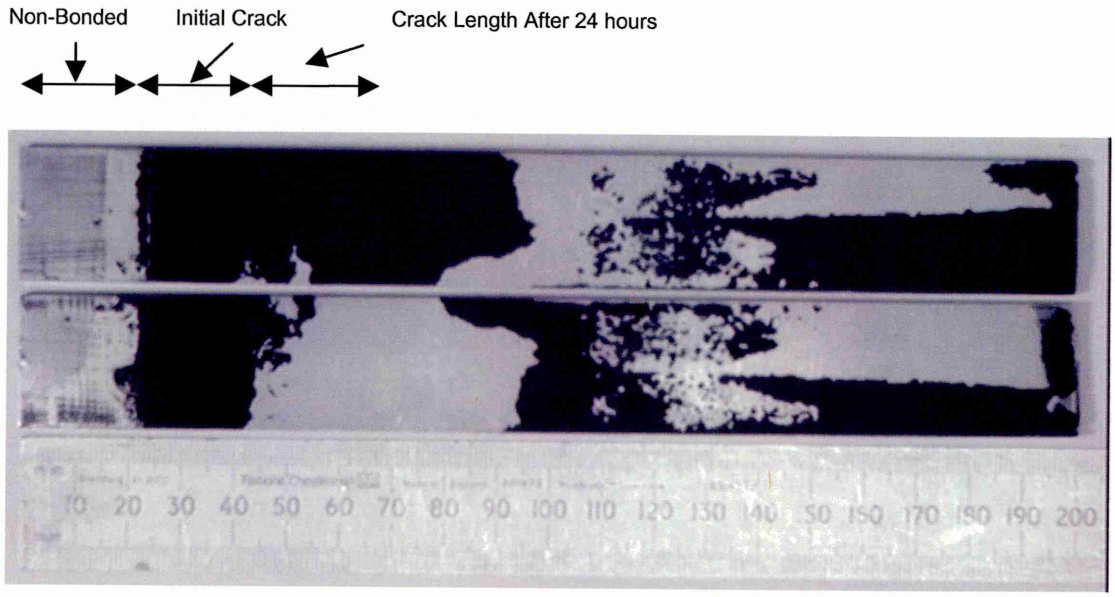

Figure 4.79 - *Nitric acid anodised fractured wedge test specimen*

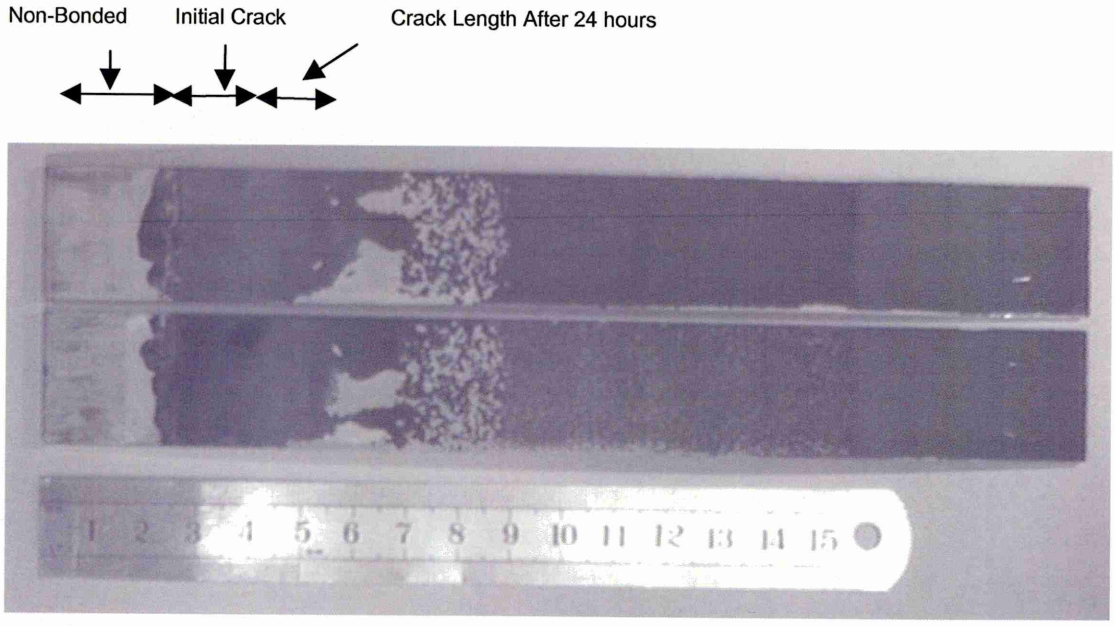

Figure 4.80 - *Alumina grit blast + Accomet C fractured wedge test specimen*

4.5.3 SEM Analysis

Fracture analysis using optical macrographs provides an indication of what type of failure has taken place but does not validate what has occurred close to surfaces, or uncover artefacts that are not visible to the human eye. Samples were obtained from fractured wedge test specimens and cut to appropriate sizes for SEM analysis. All specimens were taken from areas after the initial crack length, so they are indicative of the modes of failure that have taken place once environmental degradation has commenced.

Alkaline Degreased

Metal Side, Plate 4.18

There is no evidence of adhesive on the adherend surface. The surface is characteristic of the 2B finish where the grain boundaries are visible and have been flattened from the pinch pass production process.

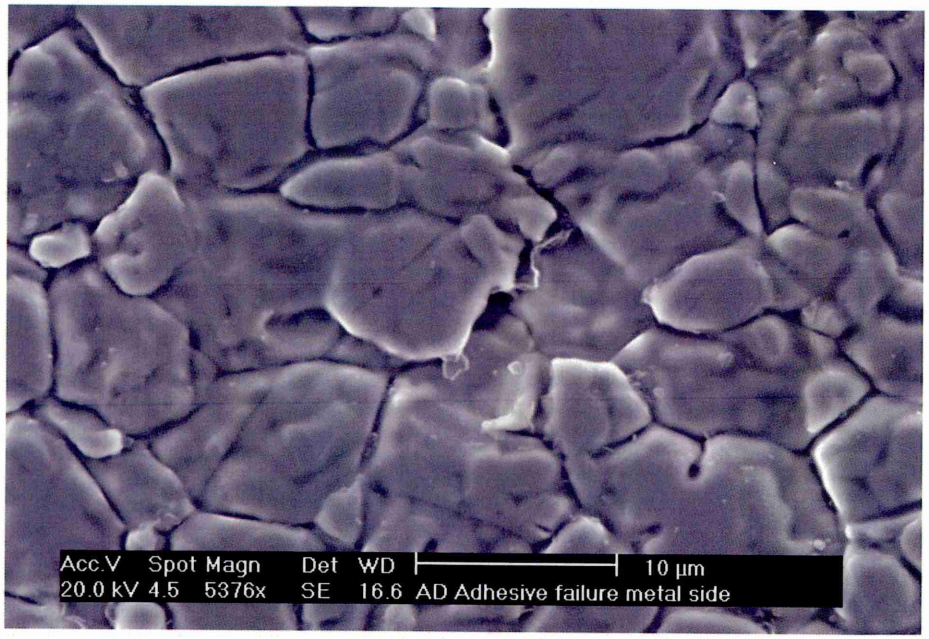

***Plate 4.18** - Metal side of apparent adhesive failure*

Adhesive Side, Plate 4.19

The features on the adhesive side of the failure denote how the adhesive has wetted the stainless steel surface, where replicas of the grain boundary patterns are clearly shown.

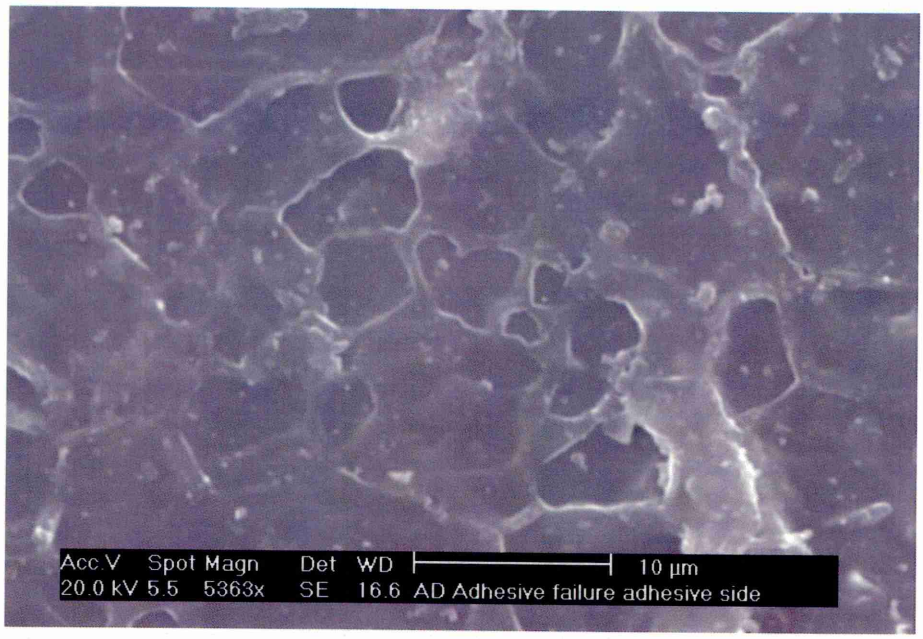

Plate 4.19 - *Adhesive side of apparent adhesive failure*

Alumina Grit Blast

Metal Side, Plate 4.20

The micrograph shows where the failure mode has changed from cohesive within the adhesive, on the left-hand side, to adhesive failure towards the bottom right-hand side. The crack initially propagated cohesively but has advanced towards the adhesive-substrate interface, and continued along this path. The exposed adherend region shows heavy deformation from the grit blasting process.

Adhesive Side, Plate 4.21 and 4.22

The surface of the adhesive is a duplicate of the alumina grit blasted surface. Plate 4.21 shows how the adhesive has effectively wetted the adherend and worked its way into the morphological features of the surface. This is further highlighted by Plate 4.22 showing the sharp angular features reproduced from the blast surface onto the cured adhesive. Environmental failure has occurred from moisture ingressing into the interface region and causing the adhesive to delaminate.

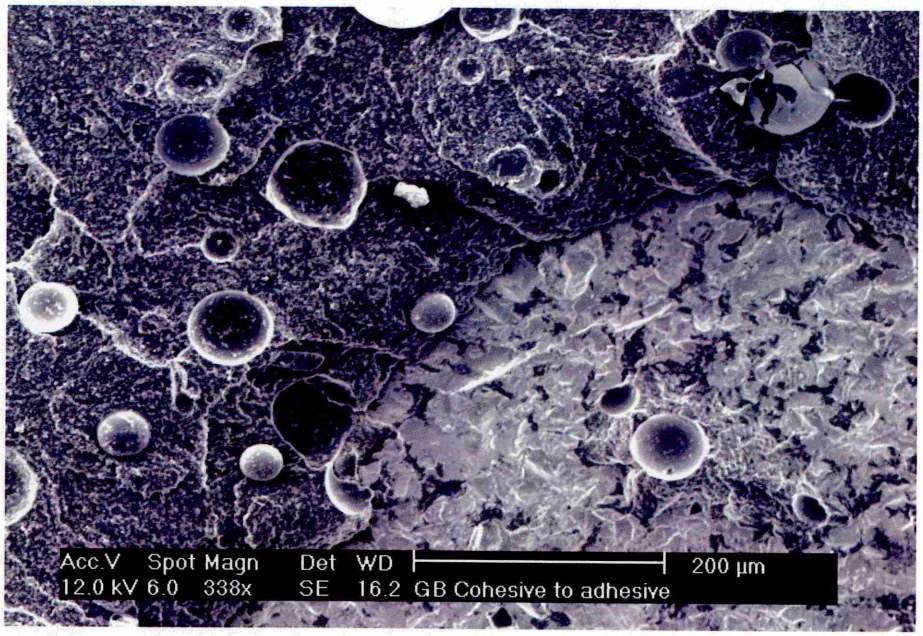

Plate 4.20 - *Metal side of the alumina grit blasted fracture specimen*

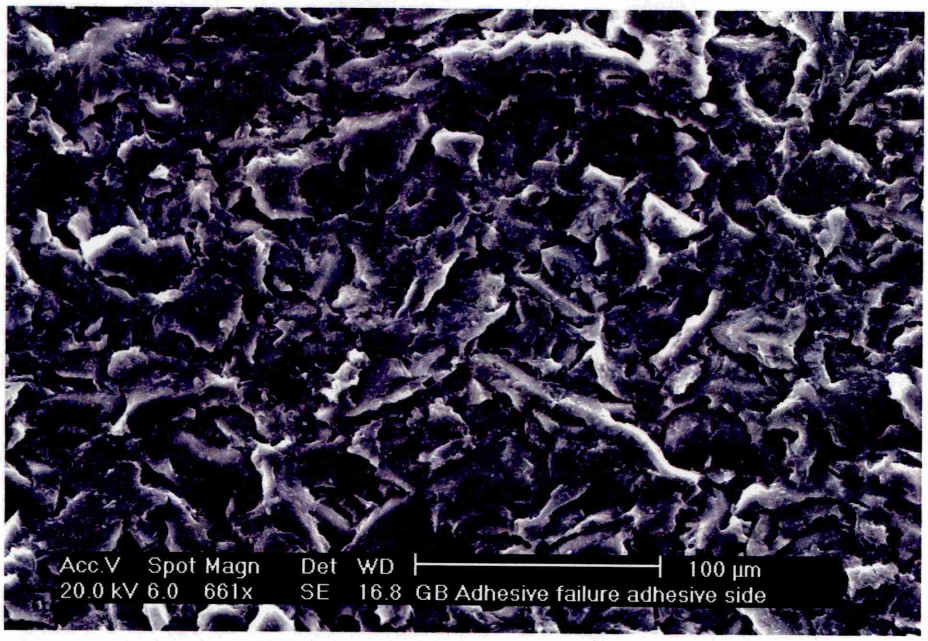

Plate 4.21 - *Adhesive side of alumina grit blasted fracture specimen*

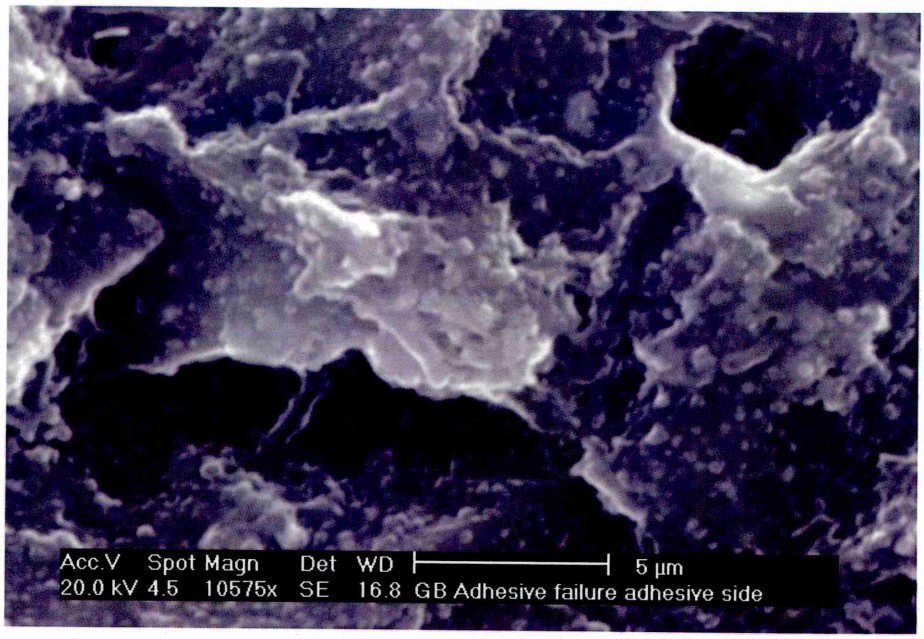

***Plate 4.22** - Adhesive side of alumina grit blasted fracture specimen*

Alumina Grit Blast + Silane Primer

Metal Side, Plate 4.23

The left-hand side of the fracture surface shows pockets of adhesive deposited on the surface. As the crack front proceeds from left to right the mode of failure becomes adhesive, where there is no evidence of adhesive on the surface but only the exposed grit blasted substrate.

Adhesive Side, Plate 4.24

The adhesive has wetted the primed surface and formed a replica of the adherend morphology. In the middle of the micrograph is a silicon filler particle that has been sheared by the advancing crack front close to the adhesive –substrate interface.

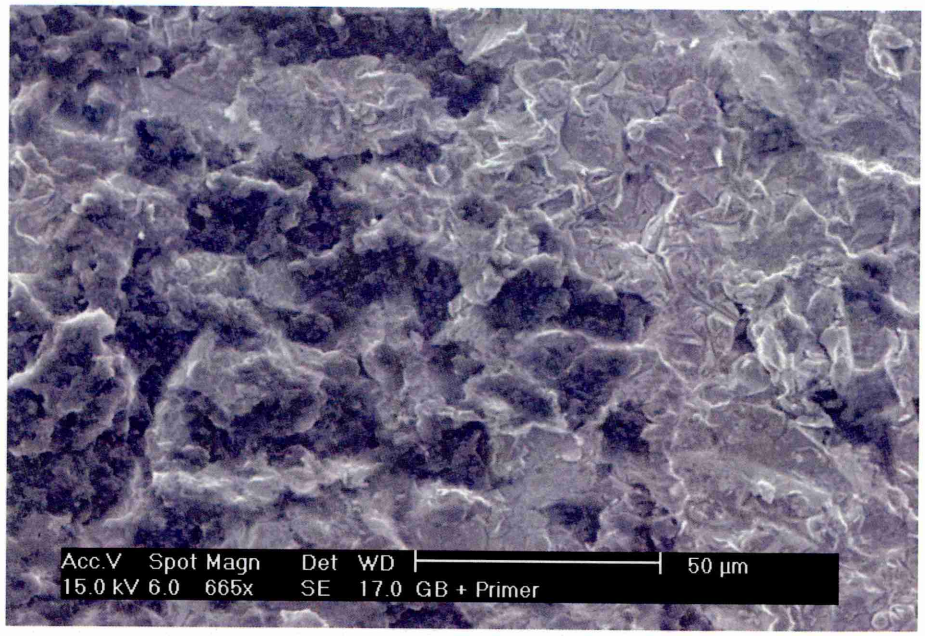

Plate 4.23 - *Metal Side of alumina grit blasted + primer fractured specimen*

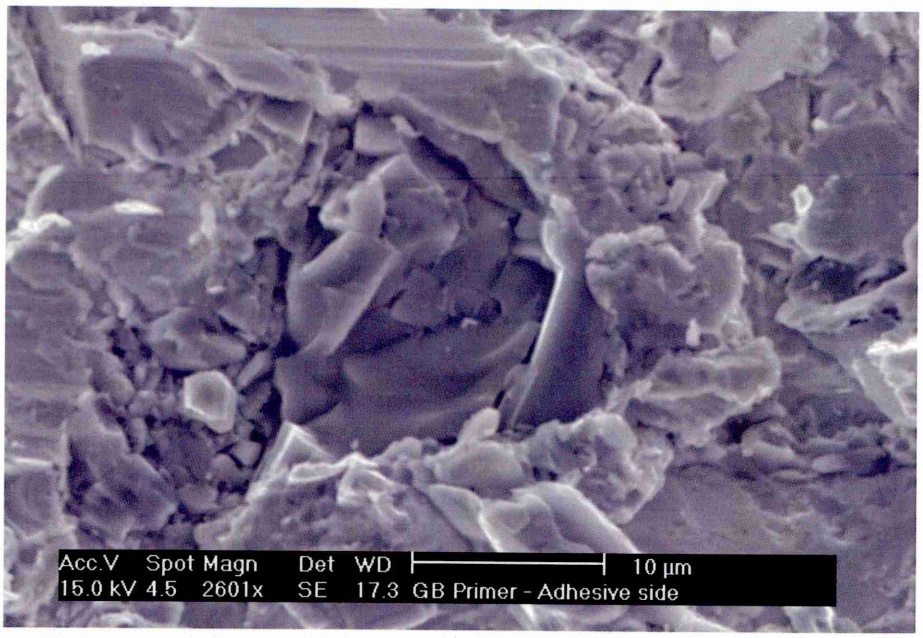

Plate 4.24 - *Adhesive side of alumina grit blasted + primer fractured specimen*

Alumina Grit Blast + CP30

Metal Side, Plate 4.25

The metal side of the fracture faces shows no evidence of adhesive on the surface. The specimen seems to have failed as a result of the crack advancing along the adhesive-CP30 coating interface.

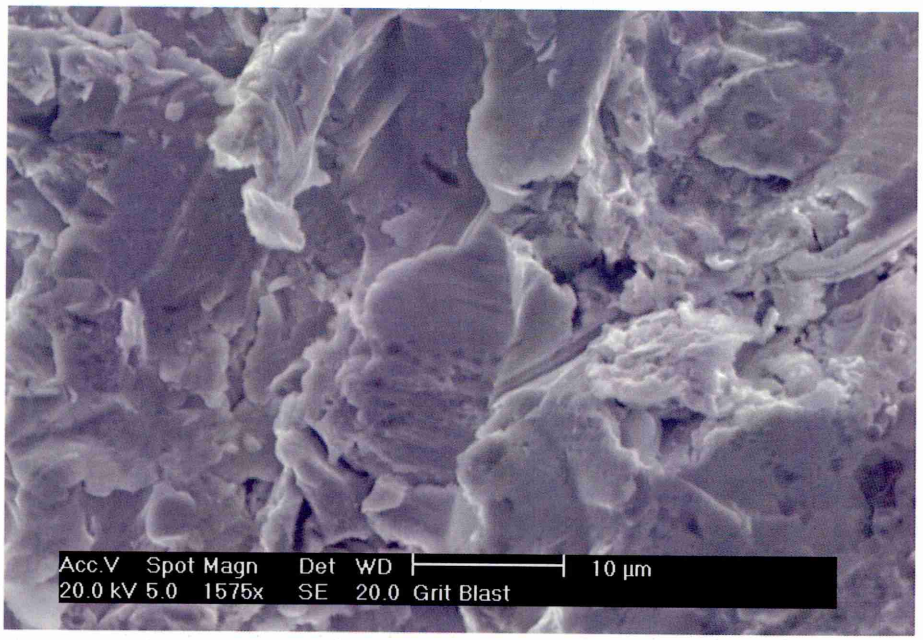

***Plate 4.25** - Metal side of alumina grit blast + CP30 fractured specimen*

Alumina Grit Blast + AZS

Metal Side, Plate 4.26

SEM has revealed no adhesive was evident on the metal side of the fracture surface. It would seem the likely mechanism of failure has occurred by the crack progressing between the adhesive-AZS interface.

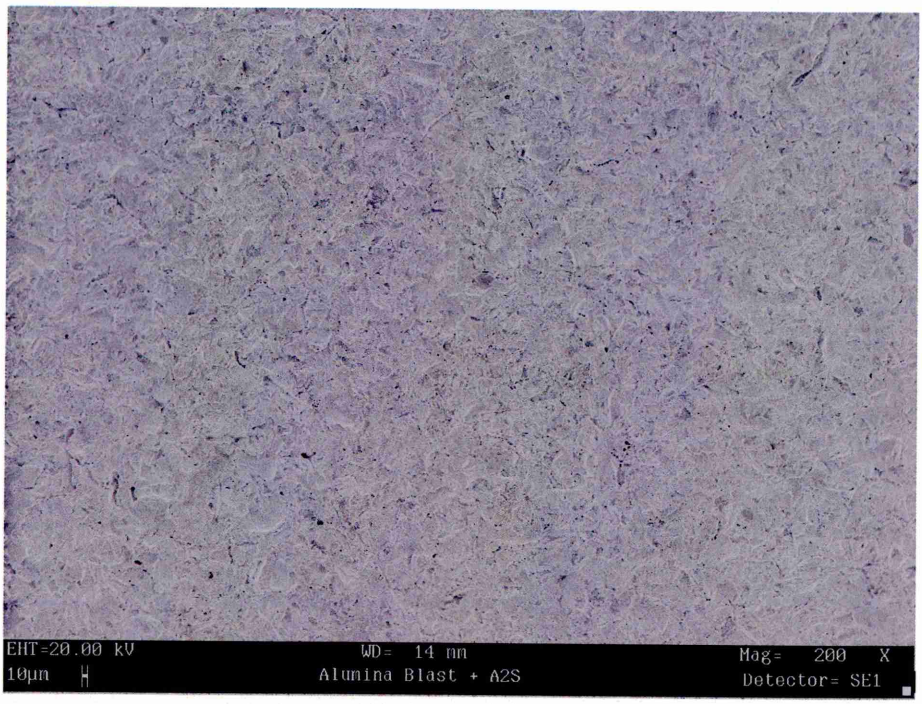

Plate 4.26 - *Metal side of alumina grit blast + AZS fractured specimen*

Sulphuric Acid Sodium Dichromate Anodised

Metal Side, Plate 4.27 and 4.28*

Adhesive has penetrated into the grain boundary network that has been exposed from the corrosion nature of the pre-treatment. Plate 4.28 shows the adhesive penetration at a higher magnification, and how the mechanism of mechanical interlocking between the adhesive and substrate has taken place.

Adhesive Side, Plate 4.29 , 4.30 and 4.31

The change in the mode of failure is identified in Plate 4.29, after exposure to the high humidity environmental the crack initially progressed cohesively within the adhesive – diagonally from the bottom right-hand corner of the micrograph. As environmental exposure continues the crack has advanced towards the adhesive-substrate interface, as depicted in the central area of the micrograph, and the morphology of the adhesive surface has changed dramatically. Plate 4.30 shows the adhesive surface and demonstrates how the adhesive had readily wetted the anodised surface and penetrated the available space surrounding the grain boundaries. The level of adhesive penetration is highlighted further in Plate 4.31, where columnar zones of adhesive protrude from the bulk of the adhesive layer.

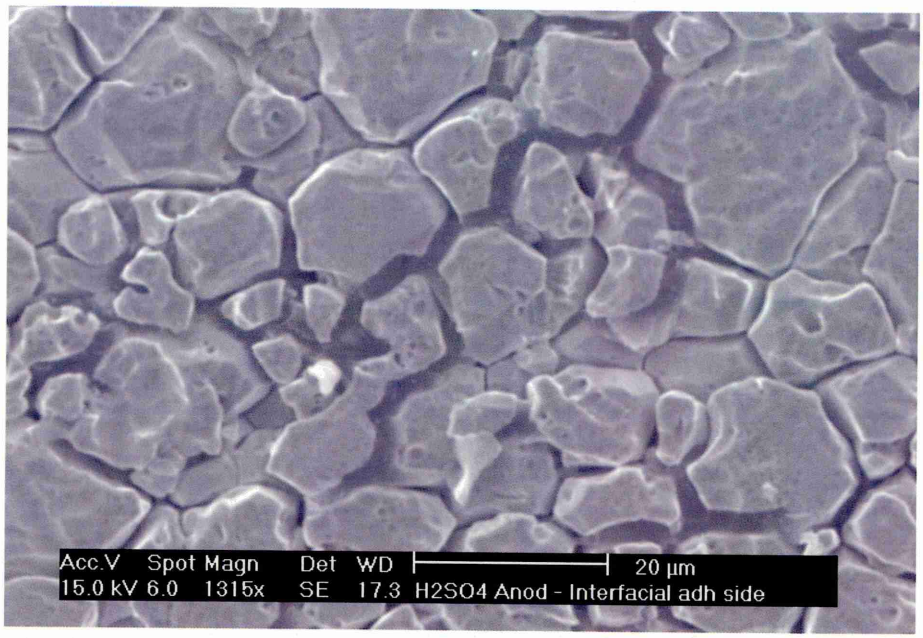

Plate 4.27 - *Metal side of sulphuric acid sodium dichromate anodised fractured specimen*

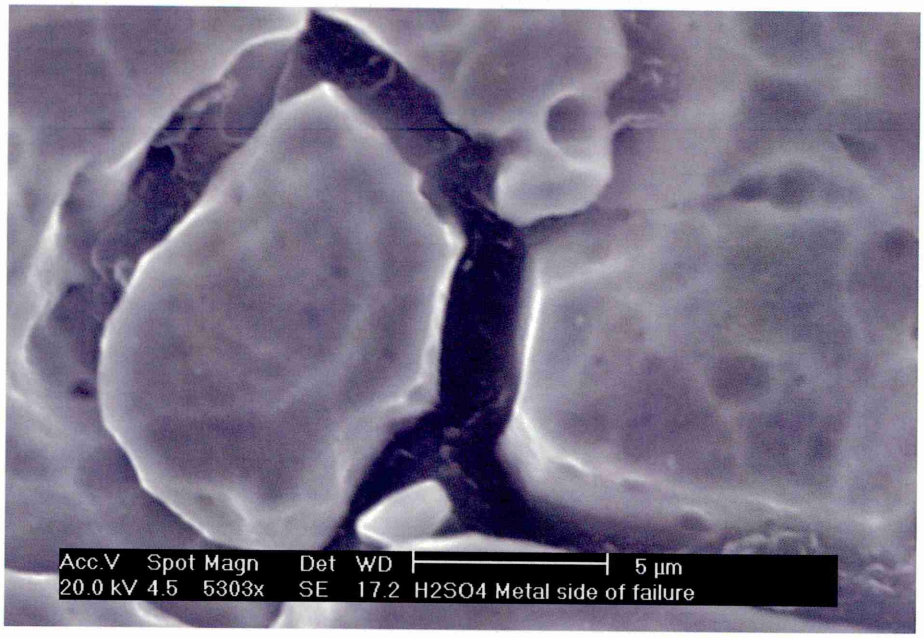

Plate 4.28 - *Metal side of sulphuric acid sodium dichromate anodised fractured specimen*

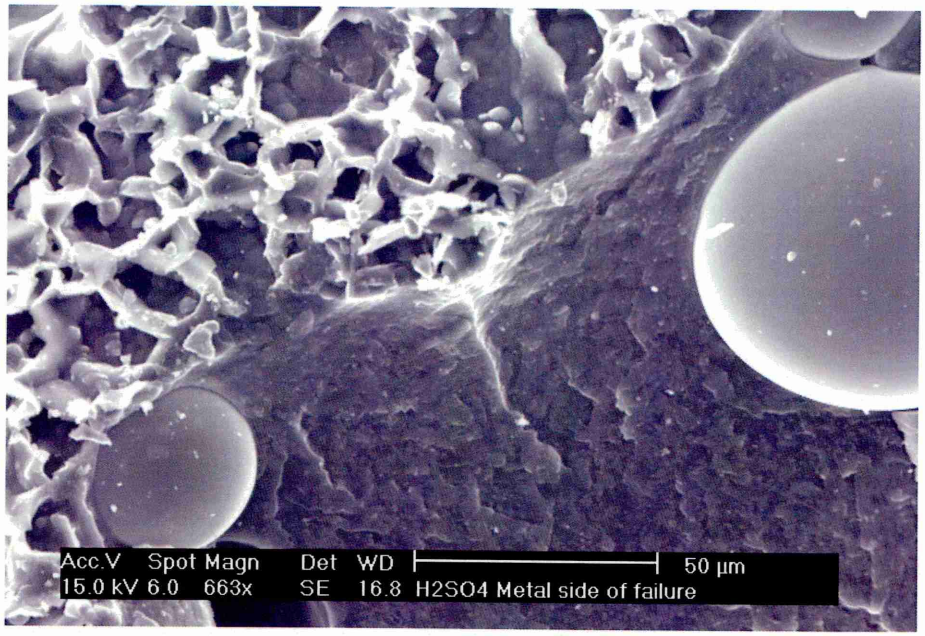

Plate 4.29 - *Adhesive side of sulphuric acid sodium dichromate anodise fractured specimen*

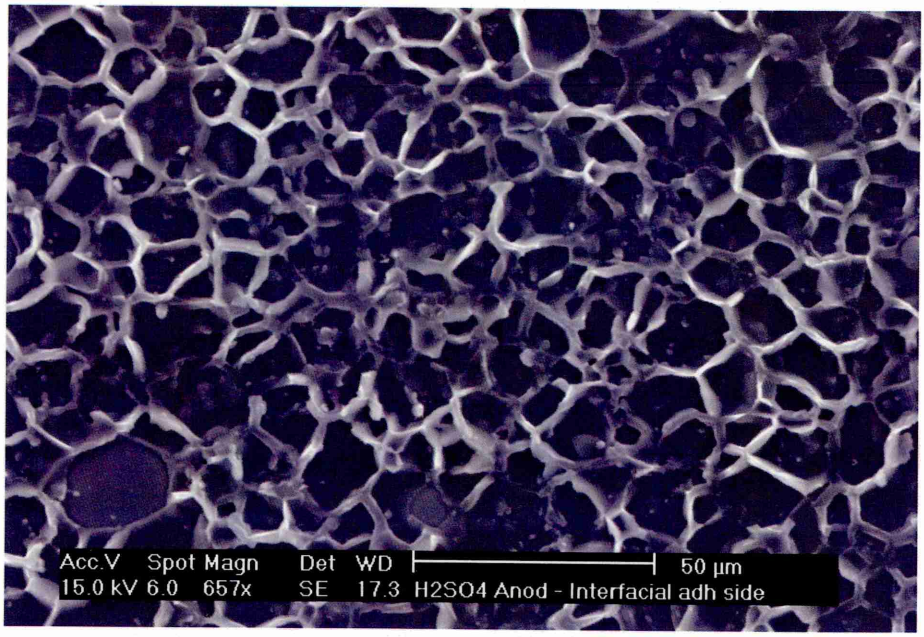

Plate 4.30 - *Adhesive side of sulphuric acid sodium dichromate anodise fractured specimen*

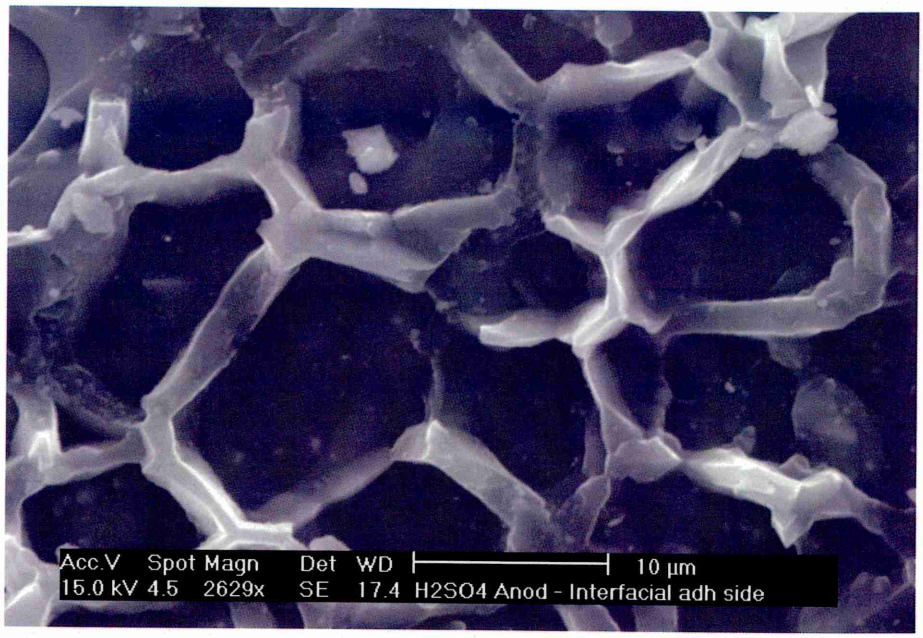

Plate 4.31 - *Adhesive side of sulphuric acid sodium dichromate anodise fractured specimen*

Nitric Acid Anodised

Metal Side, Plate 4.32, 4.33 and 4.34

Plate 4.32 reveals the mode of fracture that has occurred from environmental exposure. The grain boundary areas are surrounded by adhesive, which has penetrated into the porous structure. Mechanical interlocking has taken place between the adhesive and the anodised surface, suggesting the adhesive has facilely wetted the adherend. A back scattered electron image, Plate 4.33, attenuates the amount of interlocking that has occurred, the dark sections represent the adhesive.

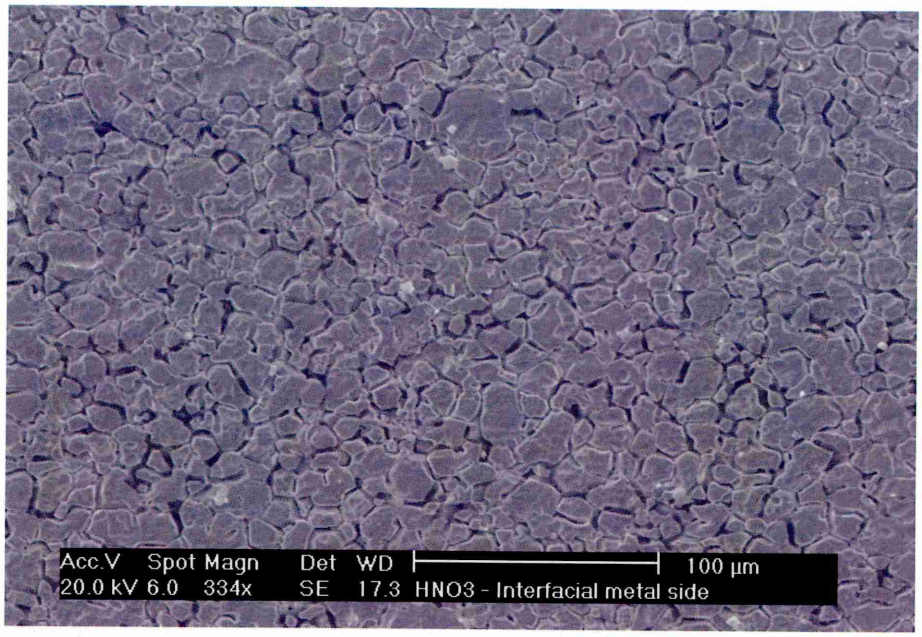

Plate 4.32 - *Metal side of nitric acid anodised fractured specimen*

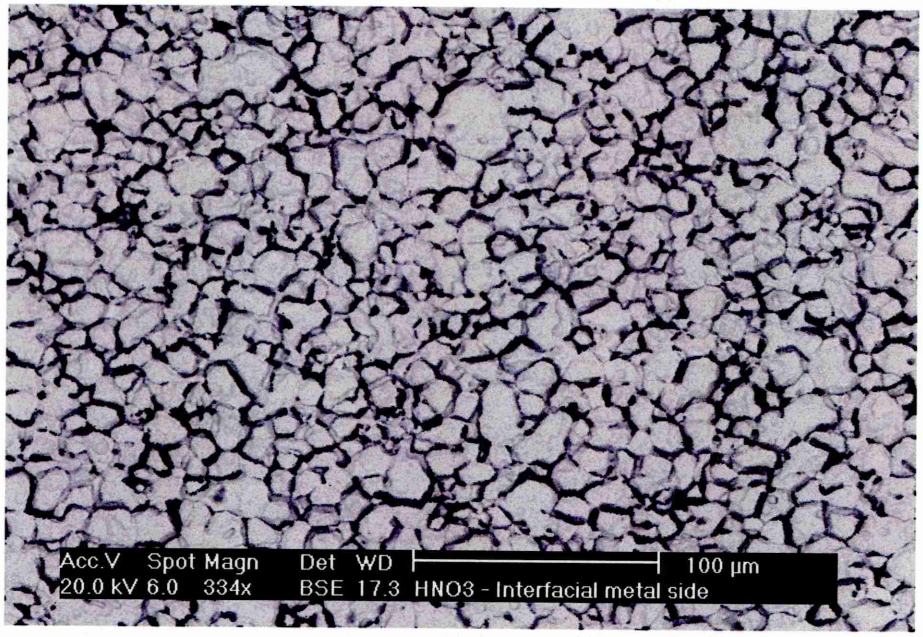

Plate 4.33 - *Metal side of nitric acid anodised fractured specimen*

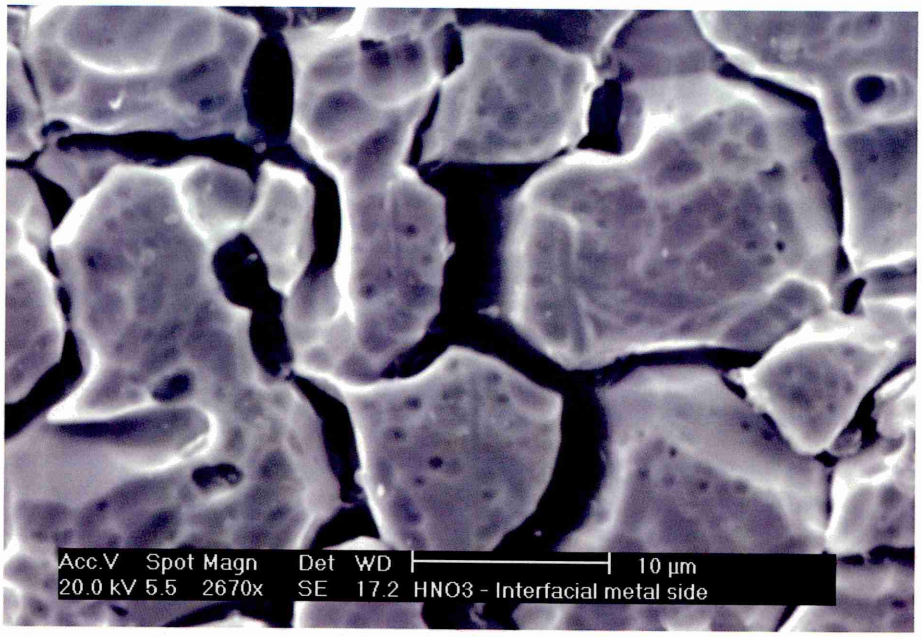

***Plate 4.34** - Metal side of nitric acid anodised fractured specimen*

Alumina Grit Blast + Accomet C

Metal Side, Plate 4.35 and Plate 4.36

The fracture surface shown in Plate 4.35 demonstrates how the crack has propagated by alternating between the adherends close to the adhesive-substrate interface. The crack advances from right to left, and the central region illustrates the step change of the crack. Closer examination of the substrate, Plate 4.36, unveils pockets of adhesive that has failed cohesively, indicating the Accomet C pre-treatment has attained localised areas of excellent adhesion between the surface and adhesive.

Adhesive Side, Plate 4.37

The morphology of the adhesive is identical to that of the adherend surface. However there is evidence of particulate material sporadically attached to the adhesive, which is presumably patches of Accomet C proposing that failure may have occurred between the adhesive-Accomet C and Accomet C-substrate interfaces.

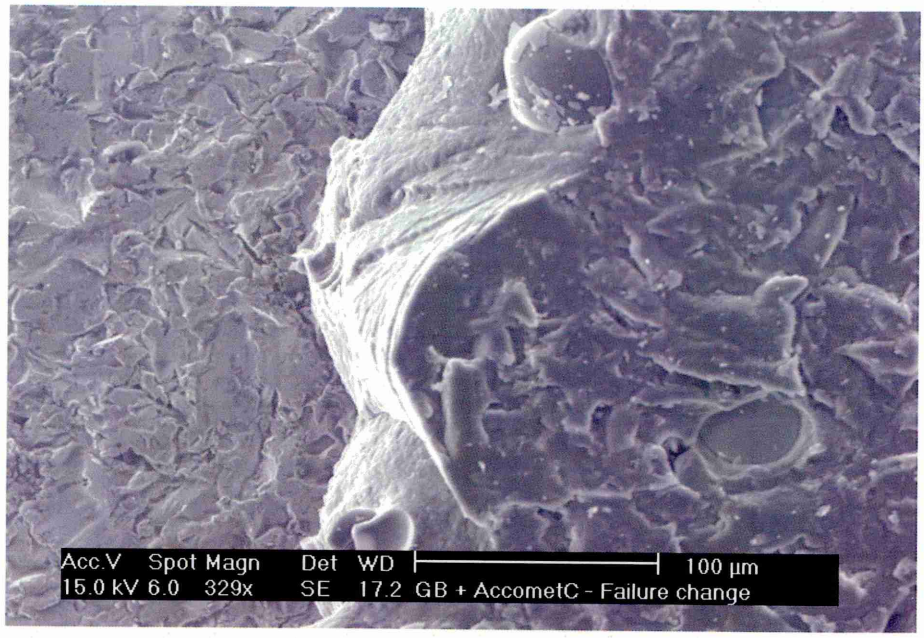

Plate 4.35 - *Metal Side of alumina grit blast + Accomet C fractured specimen*

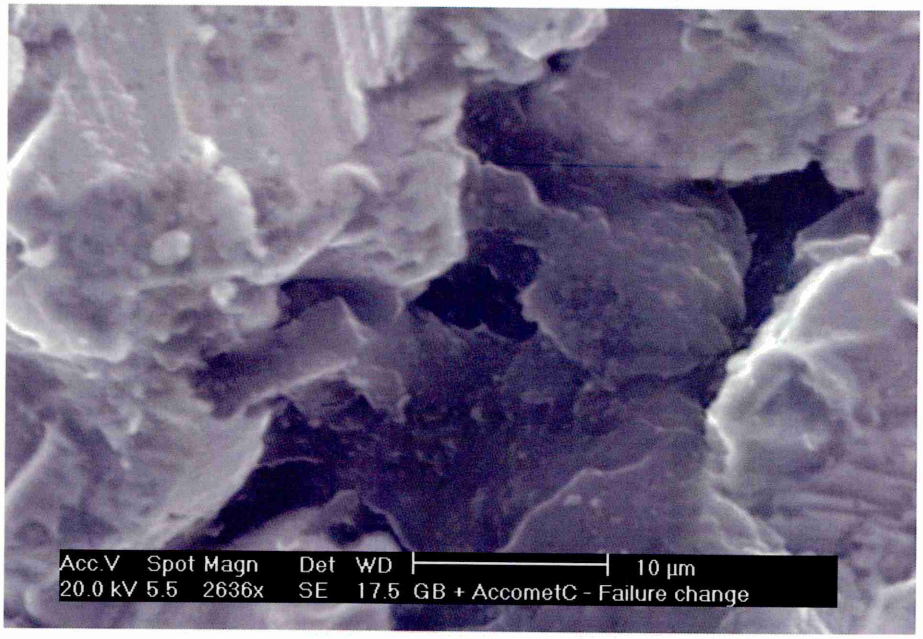

Plate 4.36 - *Metal Side of alumina grit blast + Accomet C fractured specimen*

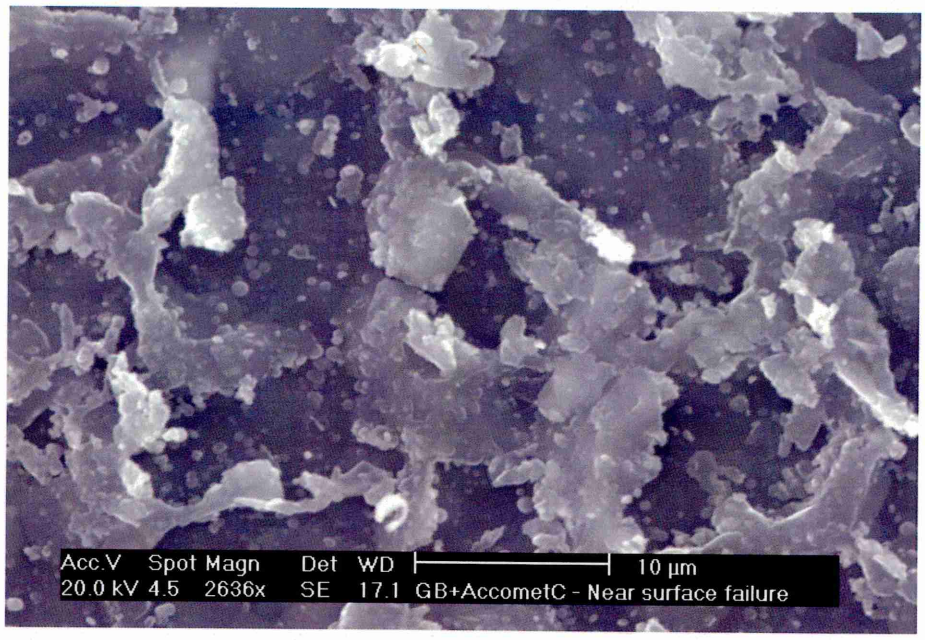

Plate 4.37 - *Adhesive side of alumina grit blast + Accomet C fractured specimen*

4.5.4 X-Ray Photoelectron Spectroscopy, XPS

For a comprehensive interpretation of the fracture mechanisms that have occurred in the wedge test specimens, XPS has been used to complement the SEM analysis and fully elucidate modes of failure. XPS was carried out on similar samples used for SEM to provide the physical and chemical characteristics of the failed surfaces.

Alkaline Degreased

Table 4.23 below details the quantified atomic concentration of elements found on the metal and adhesive sides of the fracture surface.

***Table 4.23** – Quantified XPS Data, alkaline degreased specimen*

Element	Concentration (Atomic %) Metal Side	Concentration (Atomic %) Adhesive Side
Nitrogen	4.1	1.2
Chromium	6.4	-
Iron	3.1	-
Carbon	57.8	76.4
Oxygen	26.3	19.1
Nickel	0.4	-
Silicon	2.0	3.3

Metal side, Figure 4.81

The presence of chromium, iron and nickel are an indication the metal side of the fracture surface is predominately made up of chromium oxide and resembles that of a AISI 304L stainless steel surface. High-resolution spectra of chromium (Cr2p) and iron (Fe2p3/2) are shown in Figure 4.82.

Adhesive side, Figure 4.83

The XPS results for the adhesive failure surface are equivalent to the concentrations found on the cured DP490 sample. The surface is dominated by carbon which constitutes the main elemental ingredient of an epoxy adhesive. The discrete filler phase material in DP490 is silica particles, which has been picked up by the XPS analysis. There is no evidence of iron or chromium on the adhesive side, suggesting the joint has failed adhesively between the adhesive-metal oxide interface. High resolution spectra of carbon and oxygen are shown in Figure 4.84.

Alumina Grit Blast

Table 4.24 details the relative atomic concentrations found on the metal and adhesive sides of the fracture surfaces.

***Table 4.24** – Quantified XPS Data, alumina grit blasted specimen*

Element	Concentration (Atomic %) Metal Side	Concentration (Atomic %) Adhesive Side
Nitrogen	1.6	3.0
Chromium	7.0	-
Iron	2.3	-
Carbon	50.7	71.2
Oxygen	33.7	20.7
Nickel	0.4	-
Silicon	3.7	4.6

Metal side, Figure 4.85

The XPS results reveal chromium, nickel and iron are on the surface of the specimen indicating the surface is covered by chromium oxide, high resolution spectra of chromium and iron are given in Figure 4.86. The concentration of carbon is typical for that found from atmospheric contamination. The surprising result is that no aluminium has been detected since the adherend had been mechanically treated using alumina as the blast media.

Adhesive side, Figure 4.87

The XPS results show no traces of elements associated with the components of the adherend surface. The concentrations of the elements identified are similar to that of the analysed cured DP490 sample, i.e. carbon and silicon are detected, high resolution scans are shown in Figure 4.88. It appears failure has occurred between the adhesive-metal oxide interface, resulting in total delamination of the adhesive from the mechanically treated surface.

Alumina Grit Blast + Primer

The quantified XPS analysis for the metal and adhesive sides of the fracture is shown in Table 4.25

***Table 4.25** – Quantified XPS Data, alumina grit blasted + primer specimen*

Element	Concentration (Atomic %) Metal Side	Concentration (Atomic %) Adhesive Side
Nitrogen	4.1	5.5
Chromium	3.2	-
Iron	6.0	-
Carbon	42.8	70.7
Oxygen	36.2	20.3
Nickel	0.1	-
Silicon	6.9	3.4
Zinc	0.6	-

Metal side, Figure 4.89

The increased concentration of silicon and low level of carbon suggest the surface does not contain any adhesive, but is covered with a discrete layer of silane primer. The presence of

chromium, iron and nickel signify that failure has occurred through the adhesive-primer interface. High resolution scans for chromium, iron and silicon are shown on Figure 4.90.

Adhesive side, Figure 4.91

There are no traces of chromium or iron therefore failure has not taken place cohesively through the oxide layer. The fracture face has similar concentrations to the cured DP490 specimen, thus implying that adhesive failure has occurred between the adhesive-primer interface. High resolution scans of carbon, oxygen and silicon are given in Figure 4.92.

Alumina Grit Blast + CP30

The XPS analysis of the alumina grit blast + CP30 fracture faces is shown below in Table 4.26.

***Table 4.26** – Quantified XPS Data, alumina grit blasted + CP30 specimen*

Element	Concentration (Atomic %) Metal Side	Concentration (Atomic %) Adhesive Side
Nitrogen	3.8	0.3
Chromium	5.6	0.3
Iron	9.5	4.7
Carbon	39.4	61.2
Oxygen	36.6	30.3
Nickel	0.6	-
Silicon	4.4	3.3
Zinc	-	-

Metal side, Figure 4.93

The low detection level of carbon and the presence of chromium and iron suggest there is no adhesive on the metal side of the failure. The high level of silicon could be attributed to handling contamination. High resolution scans of chromium and iron are shown in Figure 4.94.

Adhesive side, Figure 4.95

The adhesive 'identifiers', high carbon and silicon concentration, indicate the fracture face is predominately adhesive. However traces of chromium and iron propose that a mixed mode of failure has occurred, with a majority been adhesive failure and to a lesser degree cohesively within the metal oxide. Figure 4.96 depicts high resolution spectra for carbon and iron.

Alumina Grit Blast + AZS

The quantified XPS data is shown in Table 4.27.

Metal side, Figure 4.97

The pre-bonding XPS analysis of the AZS treated substrate revealed the surface was dominated by silicon, the main ingredient of the AZS coating. However on the metal side of the fracture the presence of silicon, chromium and iron suggest that a mixed mode of failure has

occurred through the coating and metal oxide. Chromium and iron was not detected on the pre-bonded AZS surface, high resolution scans of chromium and iron are shown in Figure 4.98.

***Table 4.27** – Quantified XPS Data, alumina grit blasted + AZS specimen*

Element	Concentration (Atomic %) Metal Side	Concentration (Atomic %) Adhesive Side
Nitrogen	0.8	3.7
Chromium	2.9	-
Iron	8.4	2.1
Carbon	36.6	62.7
Oxygen	42.4	24.9
Nickel	-	-
Silicon	9.0	6.6
Zinc	-	-

Adhesive side, Figure 4.99

The presence of iron and silicon on the surface of the adhesive add credibility to the fact mixed failure has occurred both through the adhesive-AZS interface and through the AZS-metal oxide interface. High resolution scans of carbon and iron are shown in Figure 4.100.

Sulphuric Acid Sodium Dichromate Anodised

Optical macrographs revealed the first stage of crack growth, for sulphuric acid sodium dichromate anodised wedge specimens, advanced cohesively through the adhesive. Table 4.28 gives the XPS data from analysis of the cohesive within the adhesive failure, and Figure 4.101 gives the wide scan XPS spectra.

***Table 4.28** – Quantified XPS Data, cohesive within the adhesive failure, H_2SO_4-$Na_2Cr_2O_7$ anodised specimen*

Element	Concentration (Atomic %) Cohesive Failure
Nitrogen	1.5
Chromium	-
Iron	-
Carbon	71.5
Oxygen	19.7
Nickel	-
Silicon	7.3
Zinc	-

As environmental exposure has commenced there was a notable change in failure mode from cohesive within the adhesive to interfacial between the metal oxide-adhesive interface. The results of the XPS analysis of the appropriate fracture surfaces are shown in Table 4.29.

***Table 4.29** – Quantified XPS Data, sulphuric acid sodium dichromate anodised specimen*

Element	Concentration (Atomic %) Metal Side	Concentration (Atomic %) Adhesive Side
Nitrogen	-	3.1
Chromium	2.7	0.3
Iron	4.9	-
Carbon	59.8	73.6
Oxygen	25.0	19.7
Nickel	2.2	-
Silicon	5.4	3.3
Zinc	-	-

Metal side, Figure 4.102

The detected concentrations of silicon and carbon imply adhesive is on the fracture surface. The presence of chromium and iron confirm the oxide layer has been exposed. Appropriate high resolution spectra of chromium and iron are shown in Figure 4.103.

Adhesive side, Figure 4.104

The data is almost identical to the cohesive failure analysis, confirming the surface is dominated with adhesive. There are low-level traces of chromium suggests the failure mode has been mixed. Taking the data from the metal side into consideration, it appears fracture has occurred both cohesively within the adhesive very close to the adhesive-oxide layer interface, and interfacially between the oxide layer and the adhesive. SEM examination clearly showed adhesive penetration into areas surrounding the grain boundaries, strengthening the fact mixed mode failure has occurred. High resolution spectra of carbon, oxygen, silicon and chromium are shown in Figure 4.105.

Nitric Acid Anodised

The XPS data for the nitric acid anodised surfaces is given in Table 4.30.

***Table 4.30** – Quantified XPS Data, nitric acid anodised specimen*

Element	Concentration (Atomic %) Metal Side	Concentration (Atomic %) Adhesive Side
Nitrogen	1.5	0.9
Chromium	7.4	1.6
Iron	5.7	1.8
Carbon	43.2	66.9
Oxygen	37.8	22.1
Nickel	0.8	-
Silicon	3.5	6.7
Zinc	-	-

Metal side, Figure 4.106

The relative concentrations of chromium and iron indicate the oxide layer has been analysed. The inclusion of silicon, filler material, to such a high level on the surface suggests adhesive is also present. High resolution spectra of applicable elements is shown in Figure 4.107.

Adhesive side, Figure 4.108

The common 'identifiers' of adhesive are present on the surface. However mixed failure may have occurred cohesively through the adhesive close to the oxide-adhesive interface and interfacially through the oxide due to the detection of chromium and iron on the surface of the adhesive. High resolution scans of chromium and iron are shown in Figure 4.109.

Alumina Grit Blast + Accomet C

The atomic concentrations of the fracture surfaces are given in Table 4.31.

***Table 4.31** – Quantified XPS Data, alumina grit blast + Accomet C specimen*

Element	Concentration (Atomic %) Metal Side	Concentration (Atomic %) Adhesive Side
Nitrogen	3.3	2.8
Chromium	3.4	-
Iron	1.1	-
Carbon	46.5	73.1
Oxygen	35.3	17.2
Nickel	0.1	-
Silicon	10.3	6.9
Zinc	-	-

Metal side, Figure 4.110

XPS analysis of the pre-bonded Accomet C surface revealed silicon and chromium were the major contributing elements of the surface. Similarly the metal side of the fracture also has a matching concentration of silicon and chromium, high resolution spectra of each are given in Figure 4.111.

Adhesive side, Figure 4.112

The surface is dominated by carbon and silicon, suggesting that the fracture face is covered with adhesive. There is no evidence of Accomet C (denoted by chromium) on the adhesive side of the fracture, suggesting that failure has occurred between the Accomet C-adhesive interface. This implies the Accomet C coating has adhered well to the stainless steel surface. High resolution spectra of carbon, oxygen and silicon are shown in Figure 4.113.

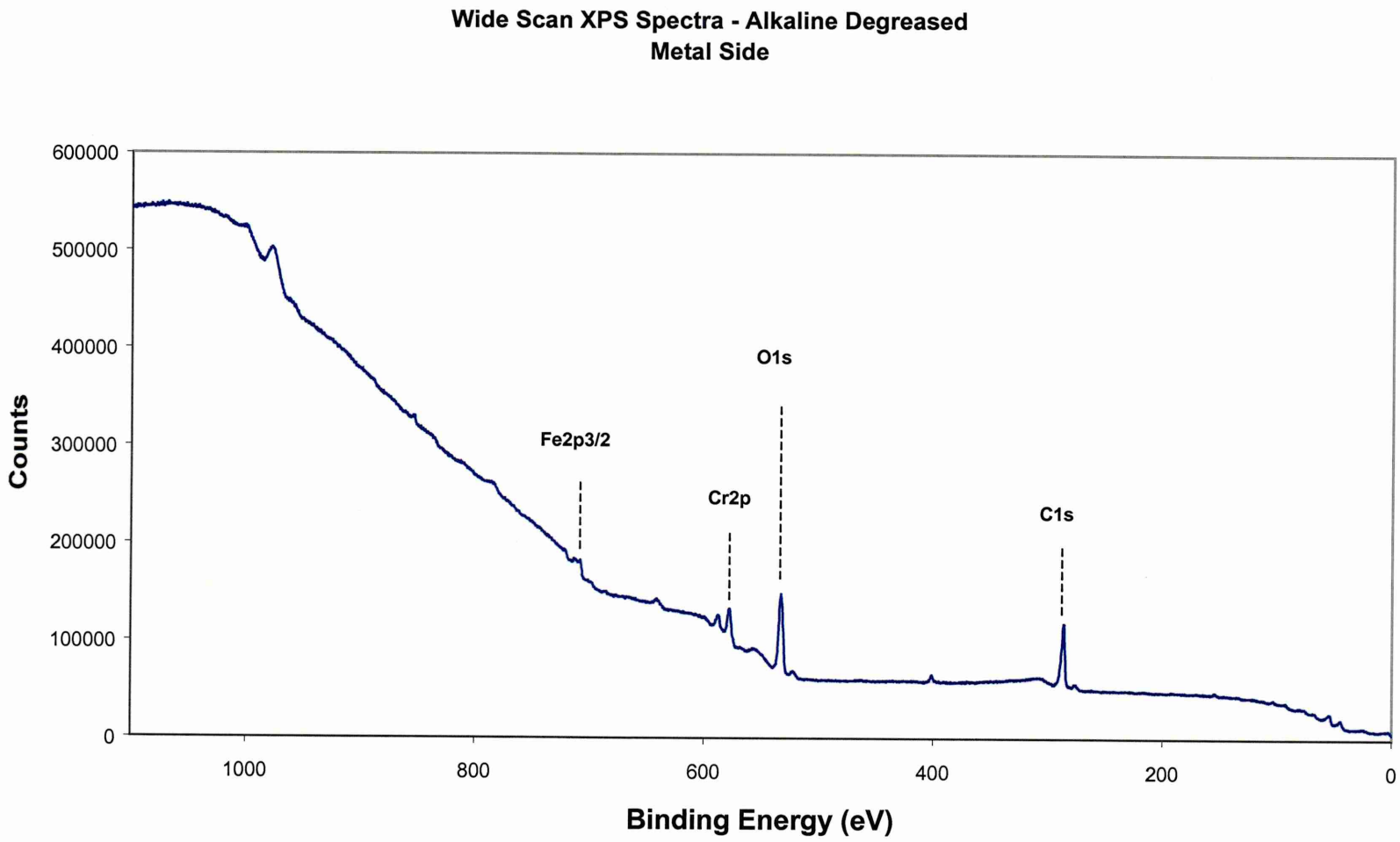

Figure 4.81 – *XPS wide scan spectra of metal side of alkaline degreased specimen*

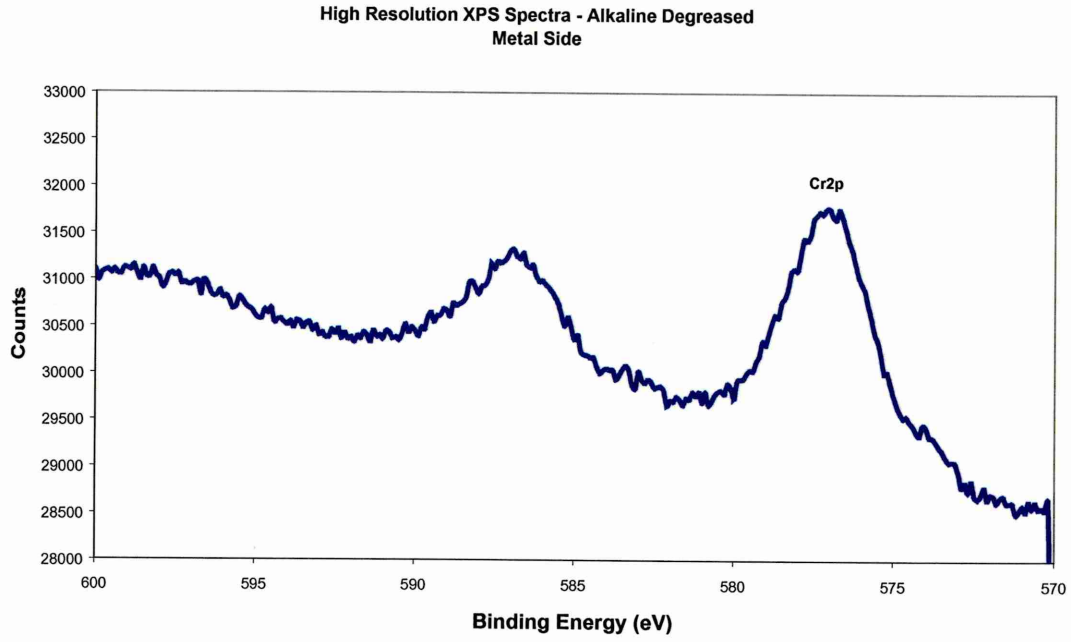

Figure 4.82(a) *– High resolution XPS spectra of chromium peak*

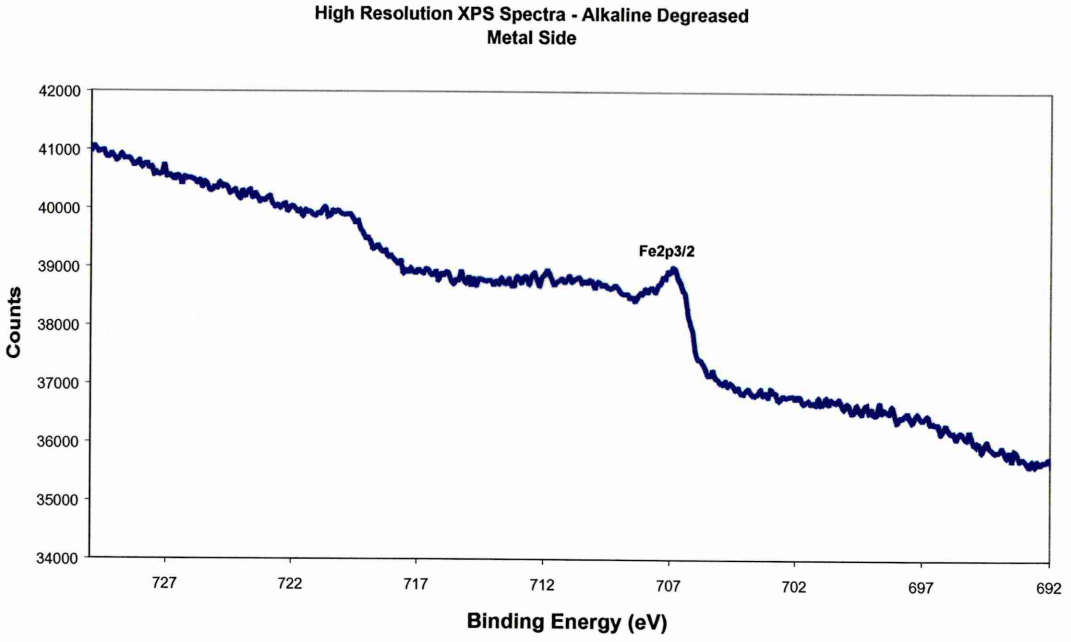

Figure 4.82(b) *– High resolution XPS spectra of iron peak*

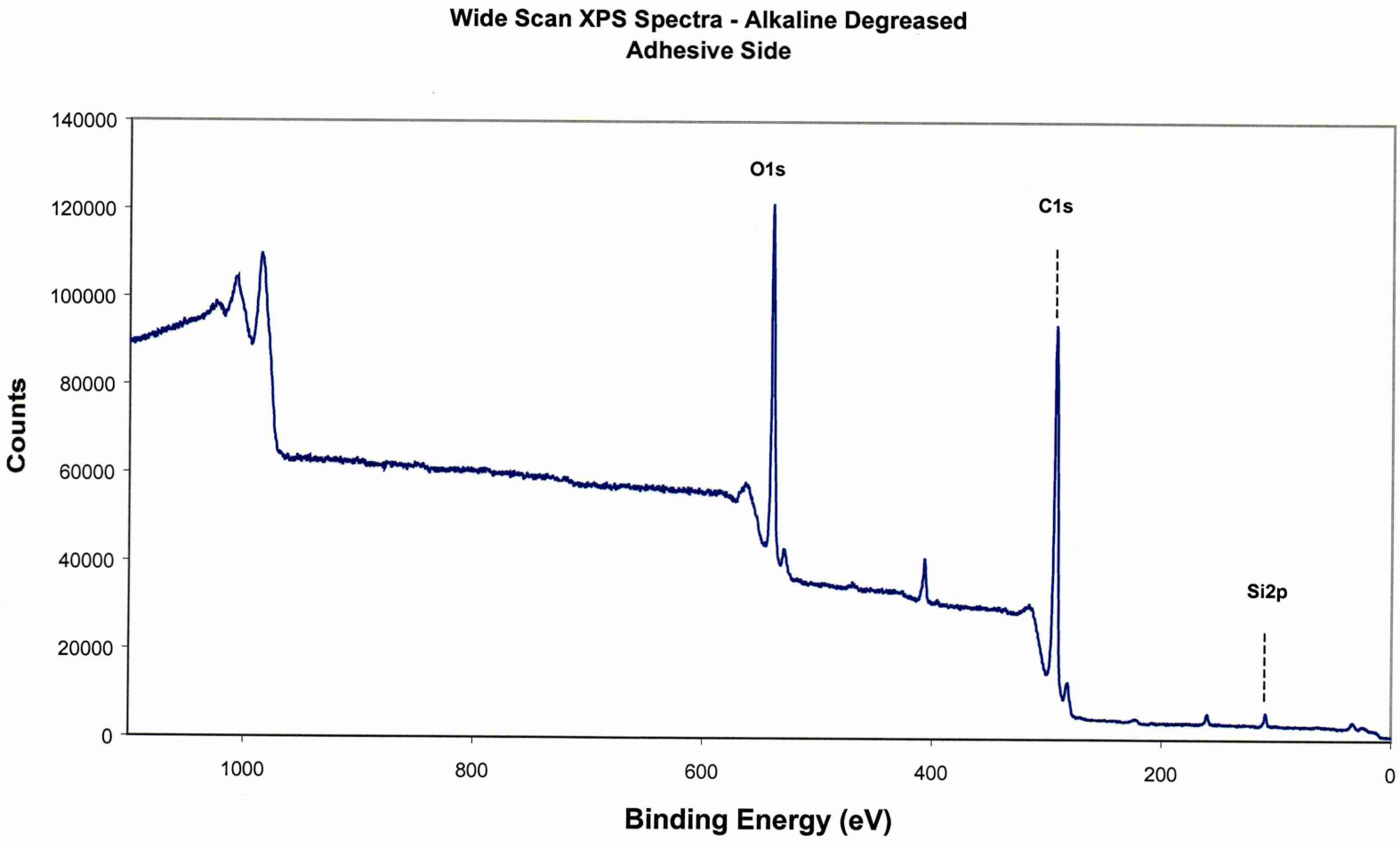

Figure 4.83 – *XPS wide scan spectra of adhesive side of alkaline degreased specimen*

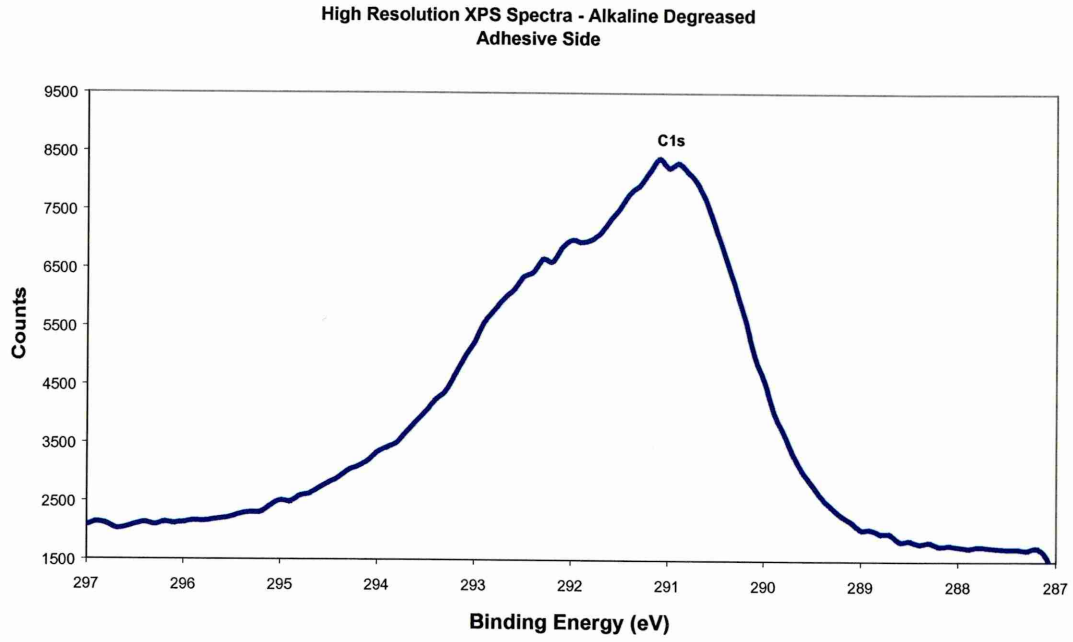

Figure 4.84(a) *– High resolution XPS spectra of carbon peak*

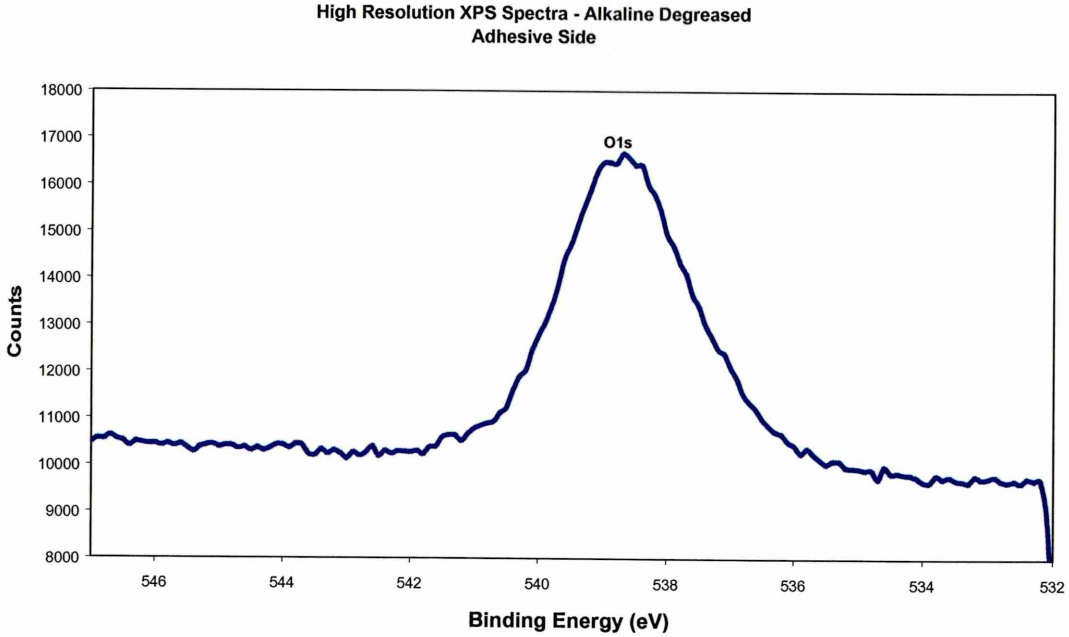

Figure 4.84(b) *– High resolution XPS spectra of oxygen peak*

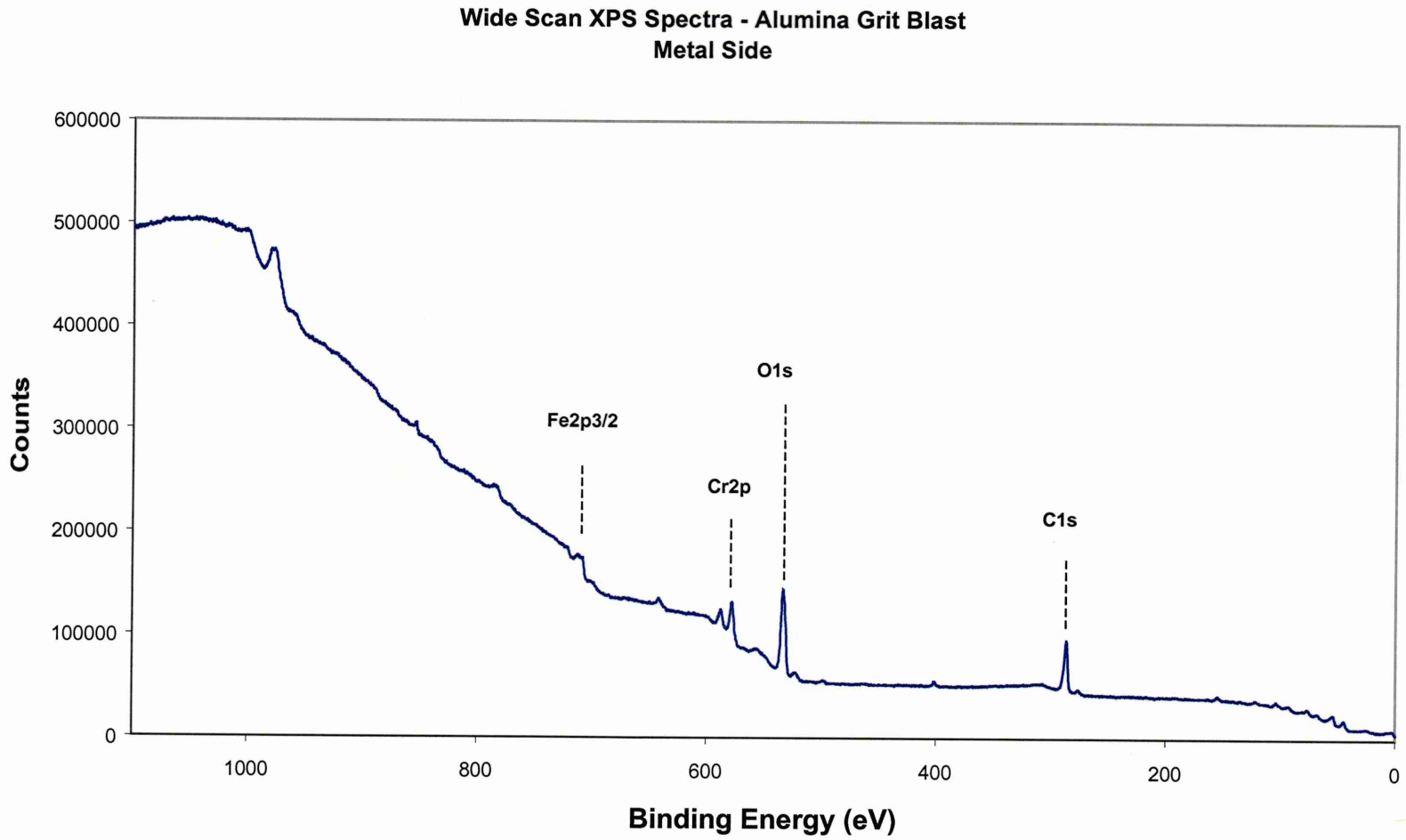

Figure 4.85 *– XPS wide scan spectra of metal side of alumina grit blast specimen*

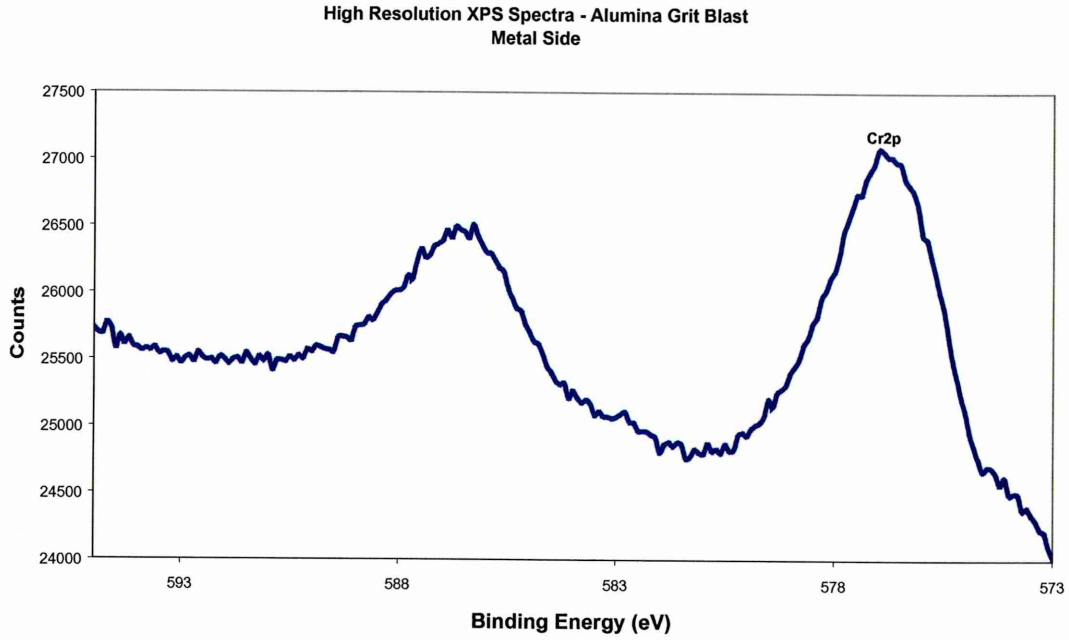

Figure 4.86(a) *– High resolution XPS spectra of chromium peak*

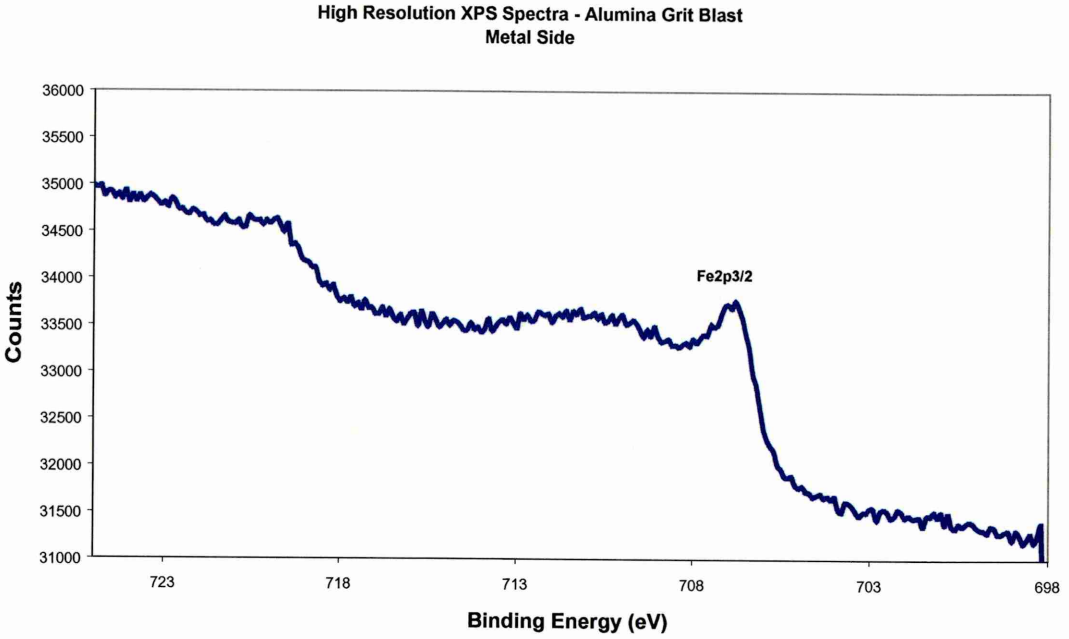

Figure 4.86(b) *– High resolution XPS spectra of iron peak*

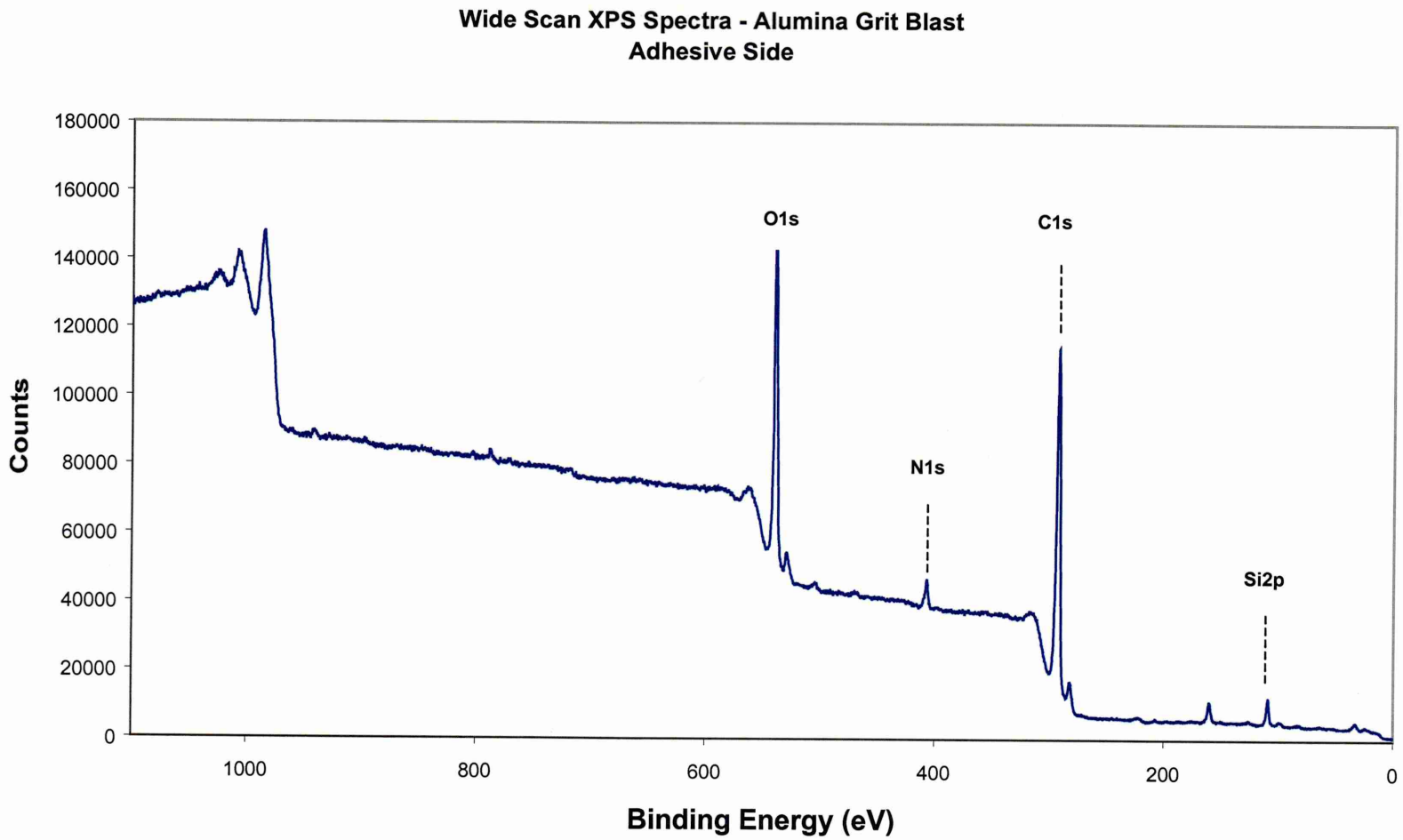

Figure 4.87 – *XPS wide scan spectra of adhesive side of alumina grit blast specimen*

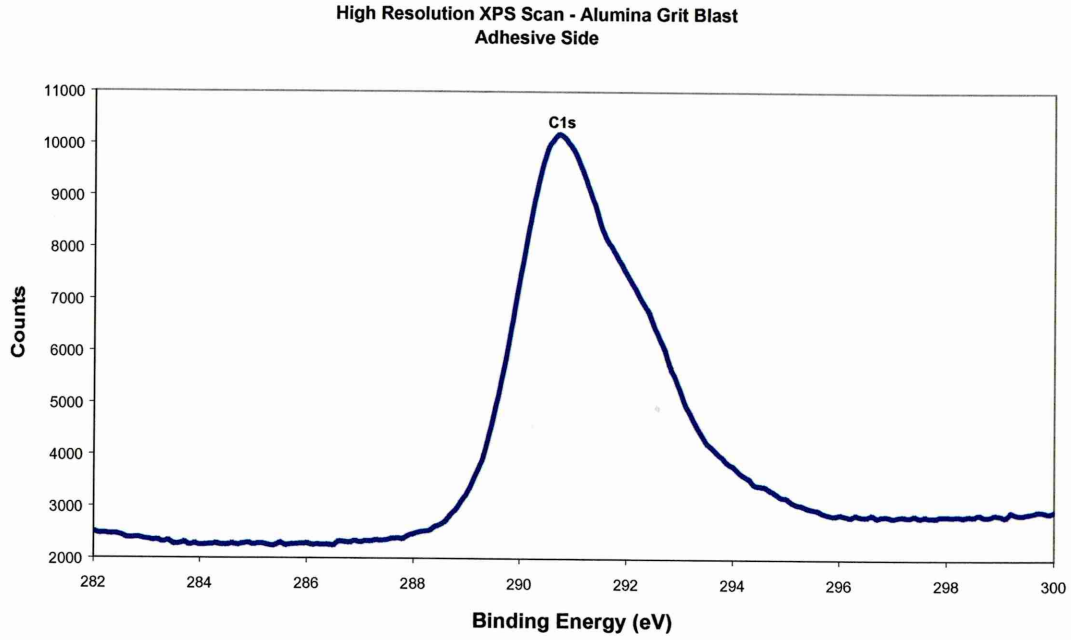

Figure 4.88(a) *– High resolution XPS spectra of carbon peak*

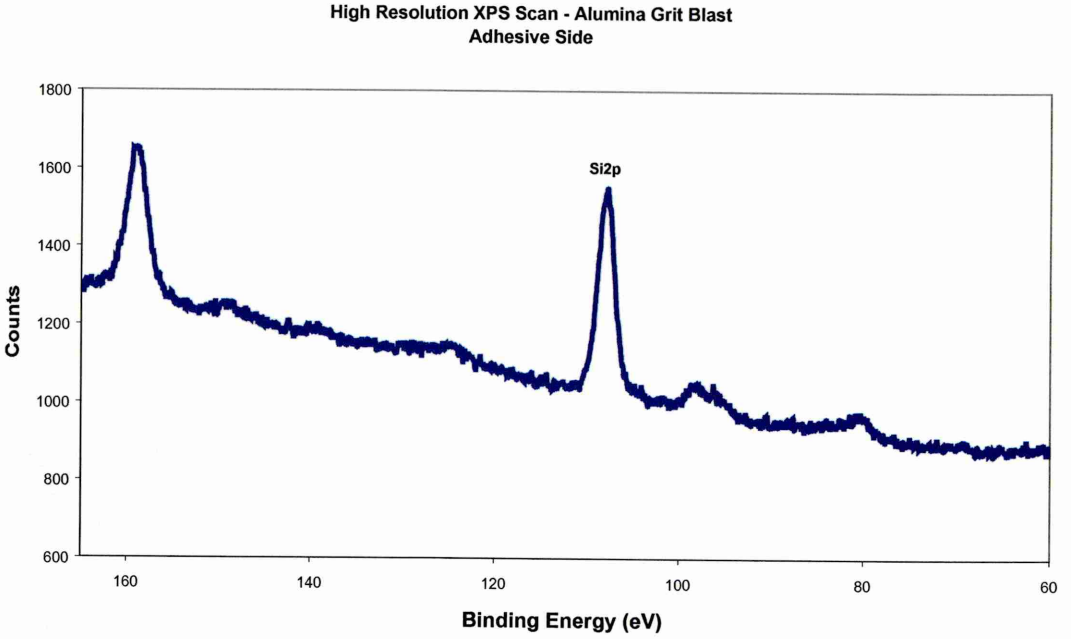

Figure 4.88(b) *– High resolution XPS spectra of silicon peak*

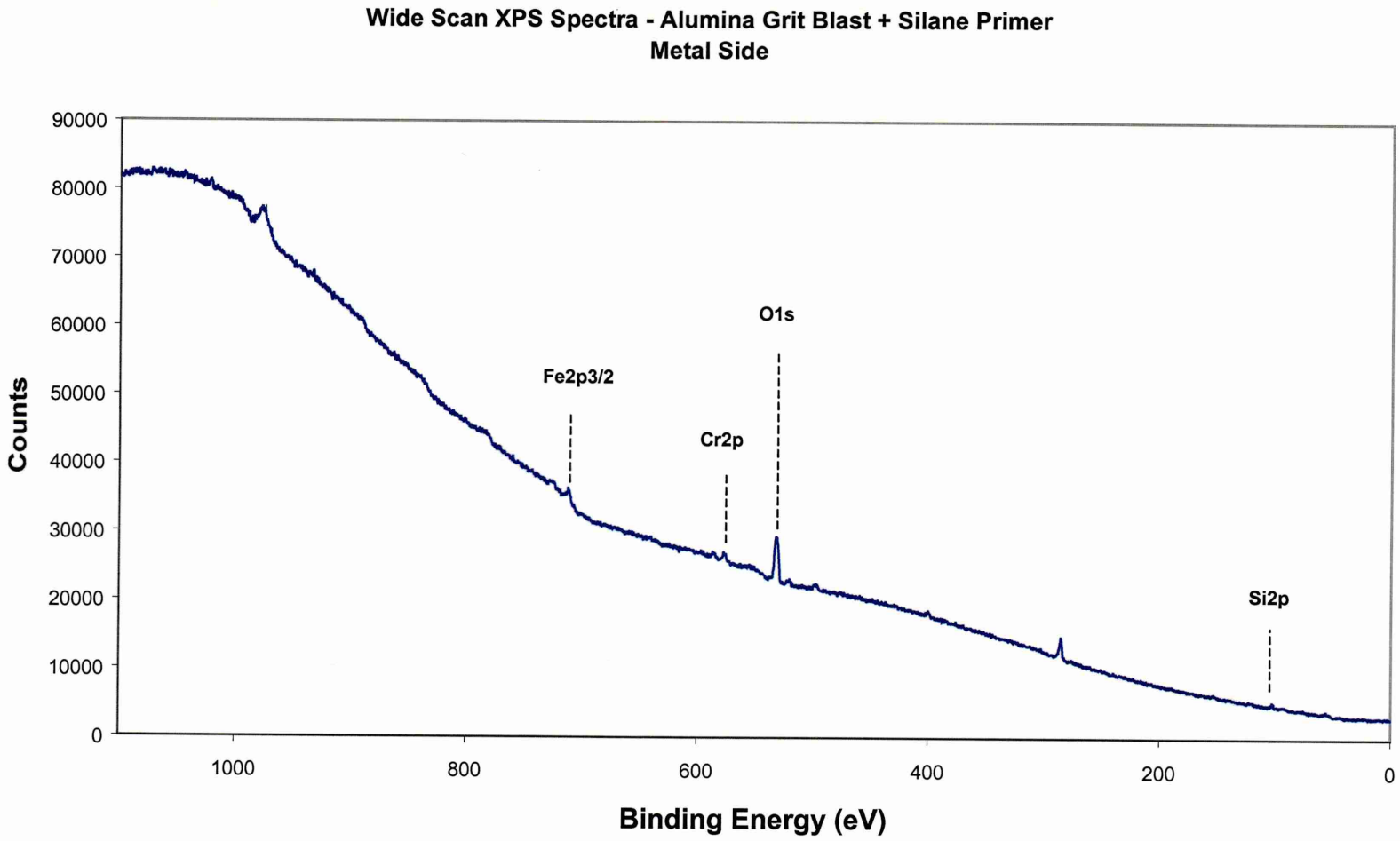

Figure 4.89 – *XPS wide scan spectra of metal side of alumina grit blast + silane primer specimen*

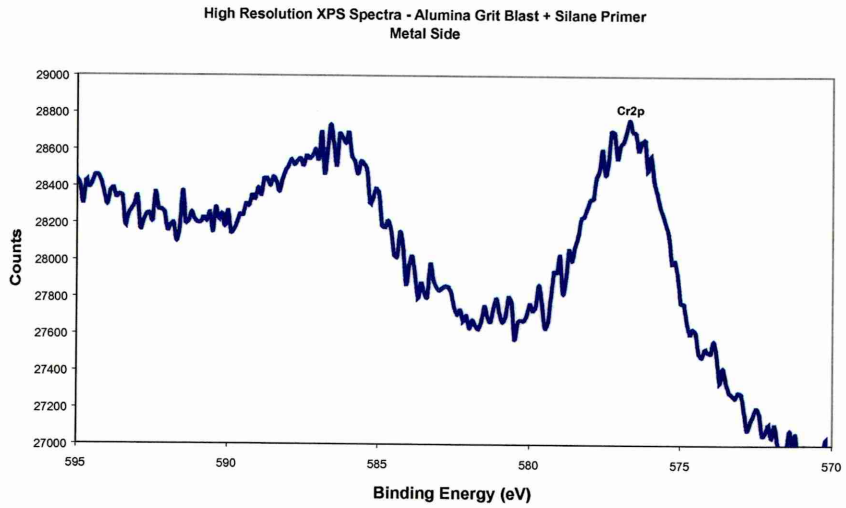

Figure 4.90(a) *– High resolution XPS spectra of chromium peak*

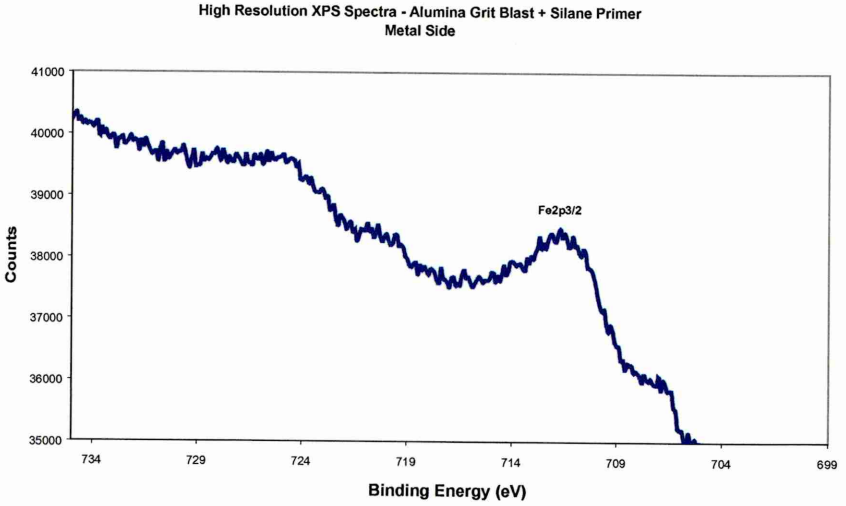

Figure 4.90(b) *– High resolution XPS spectra of iron peak*

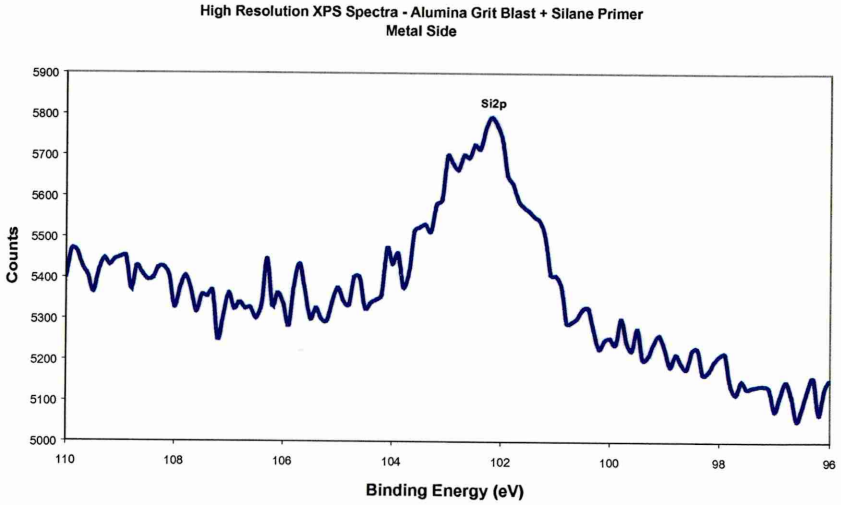

Figure 4.90© *– High resolution XPS spectra of silicon peak*

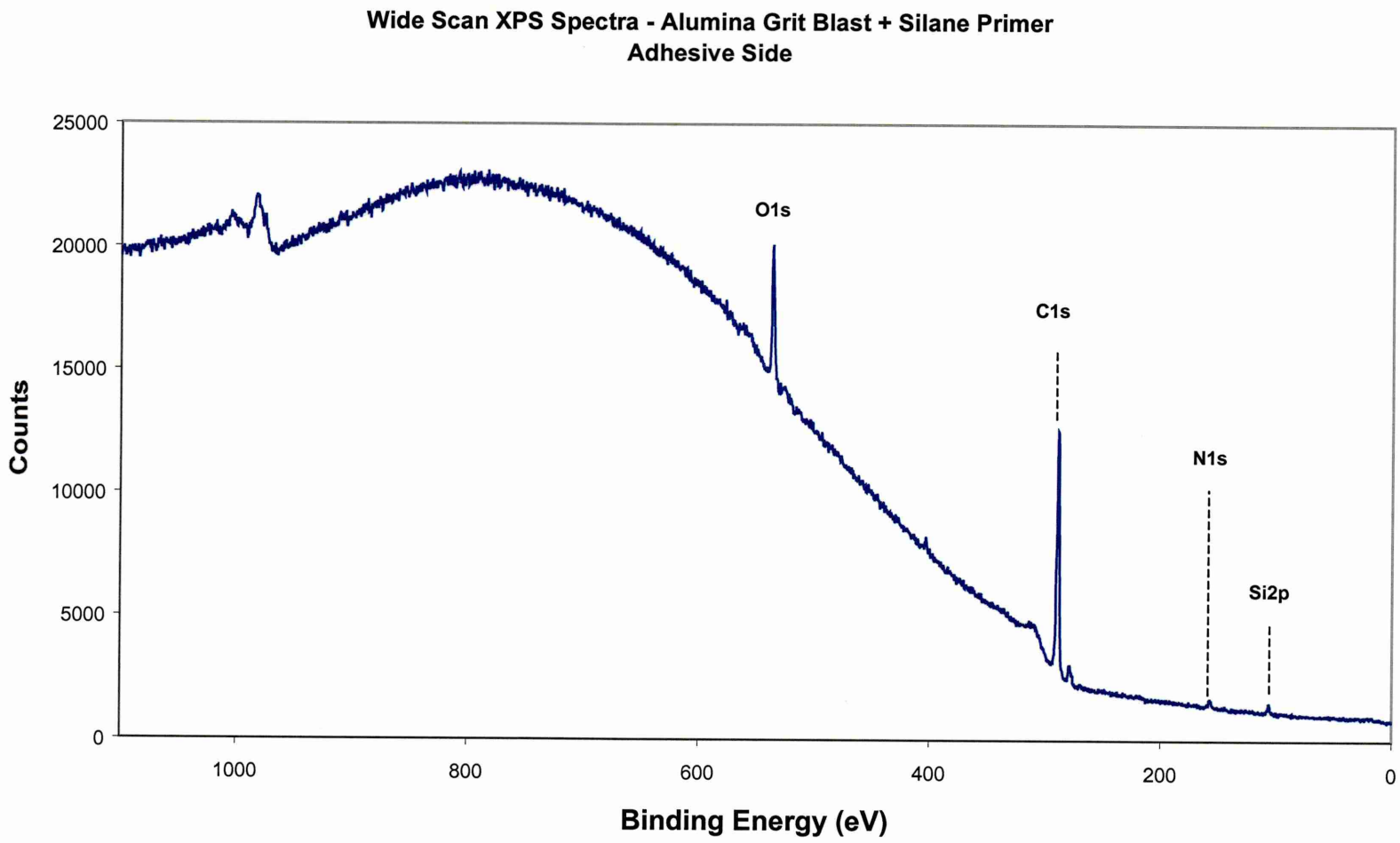

Figure 4.91 – *XPS wide scan spectra of adhesive side of alumina grit blast + silane primer specimen*

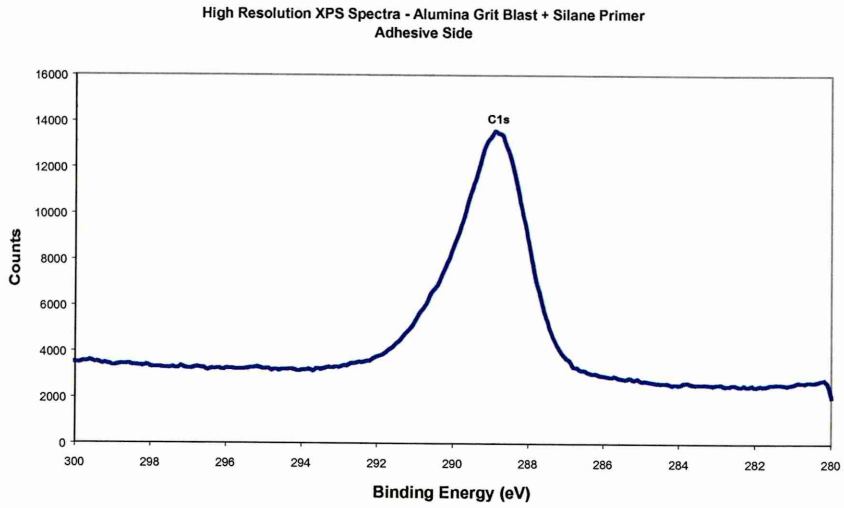

Figure 4.92(a) *– High resolution XPS spectra of carbon peak*

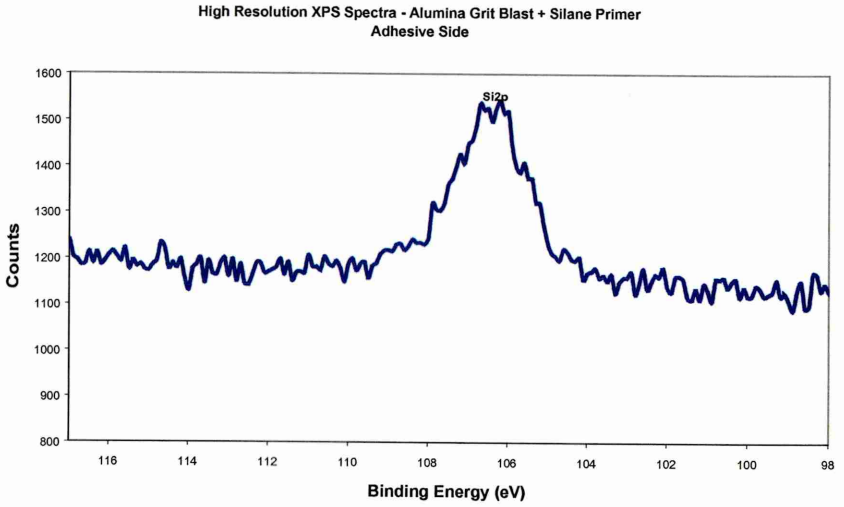

Figure 4.92(b) *– High resolution XPS spectra of silicon peak*

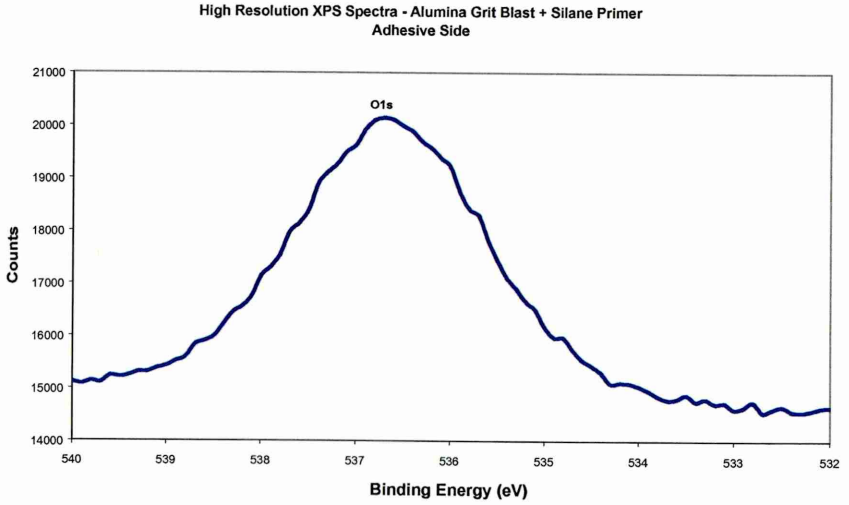

Figure 4.92© *– High resolution XPS spectra of oxygen peak*

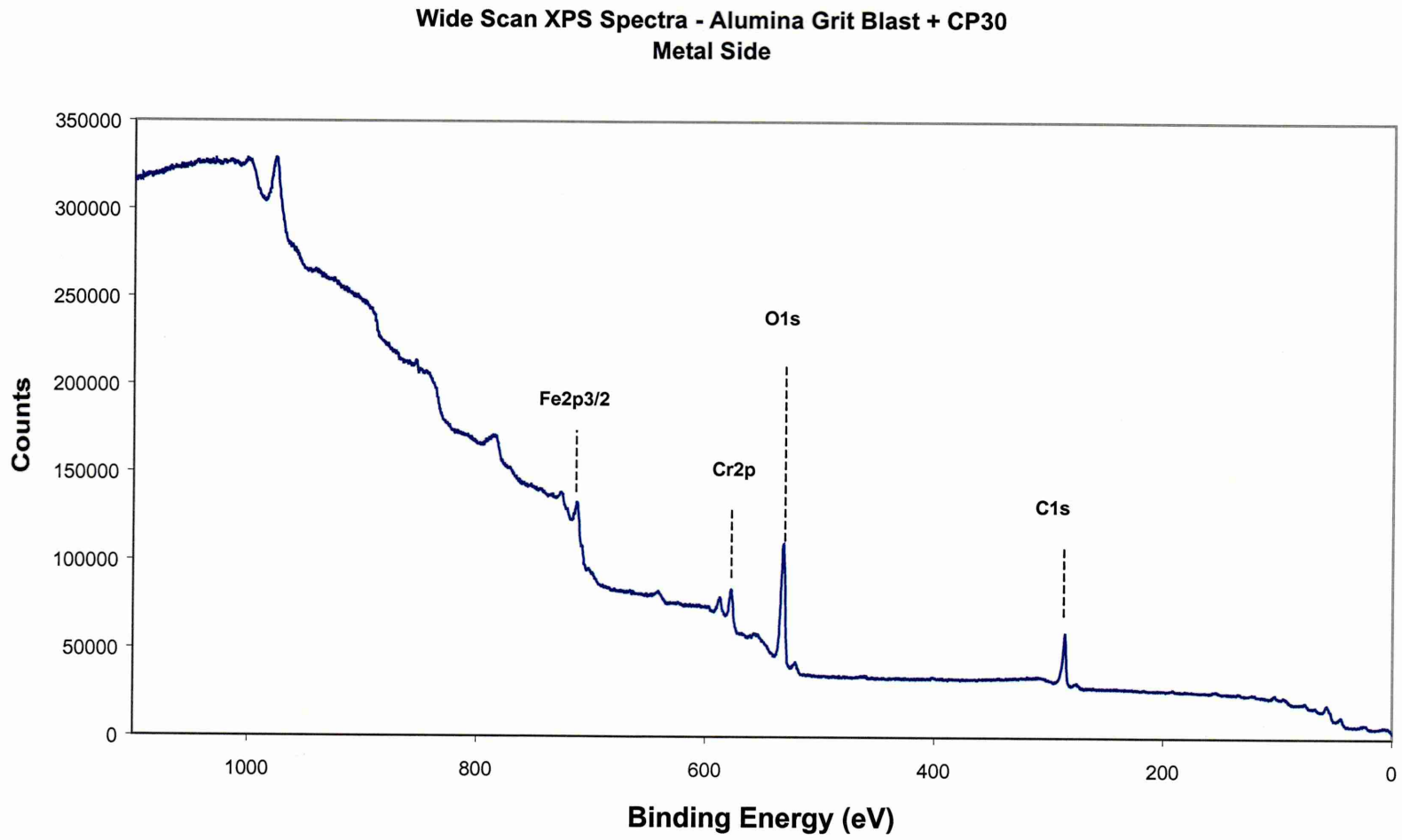

Figure 4.93 – *XPS wide scan spectra of metal side of alumina grit blast + CP30 specimen*

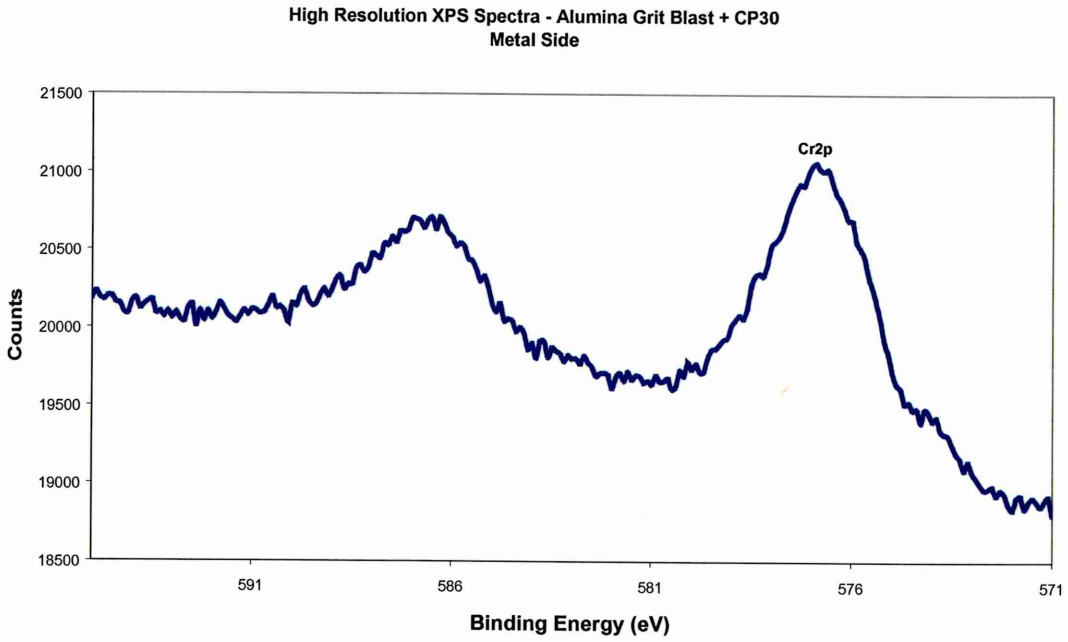

Figure 4.94(a) *– High resolution XPS spectra of chromium peak*

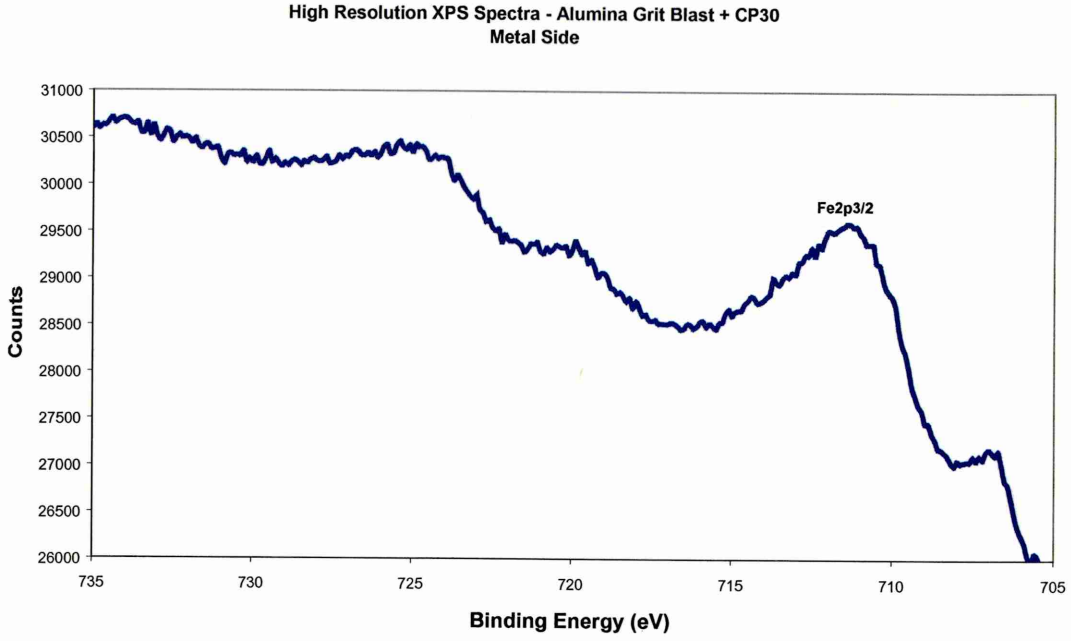

Figure 4.94(b) *– High resolution XPS spectra of iron peak*

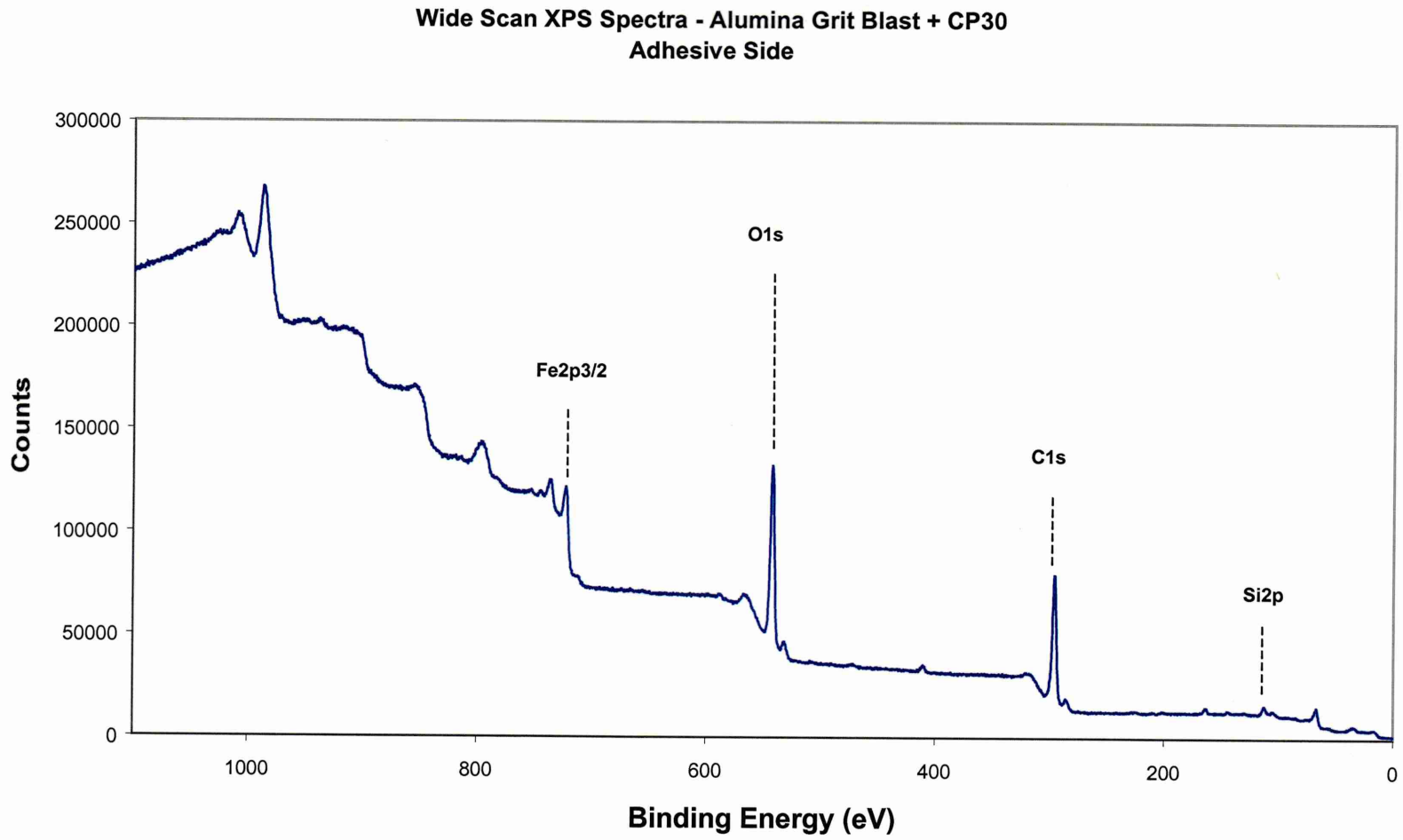

Figure 4.95 – *XPS wide scan spectra of adhesive side of alumina grit blast + CP30 specimen*

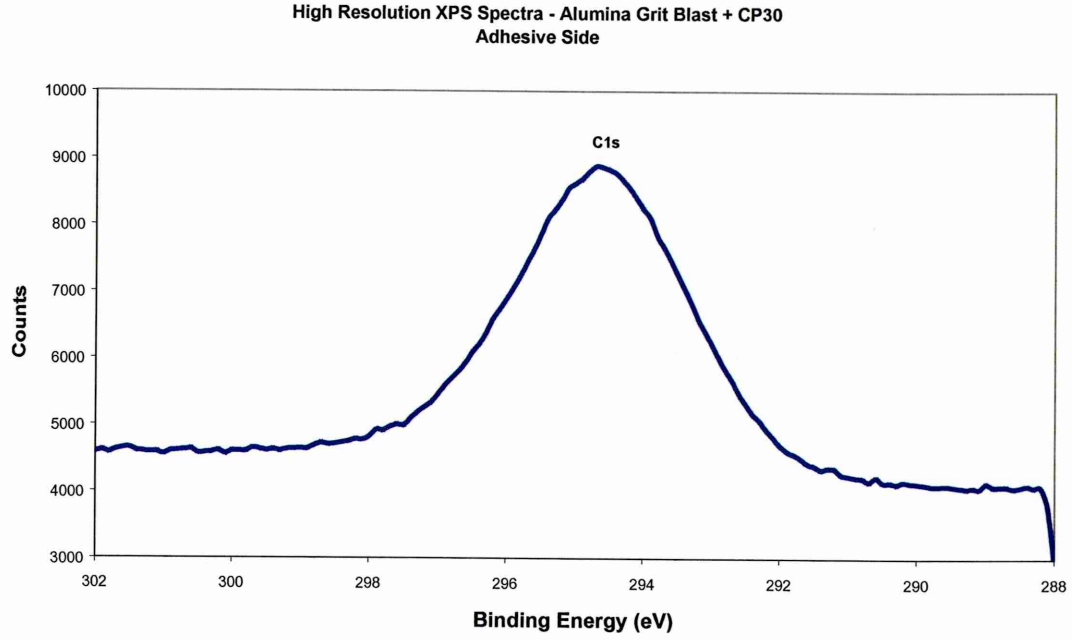

Figure 4.96(a) *– High resolution XPS spectra of carbon peak*

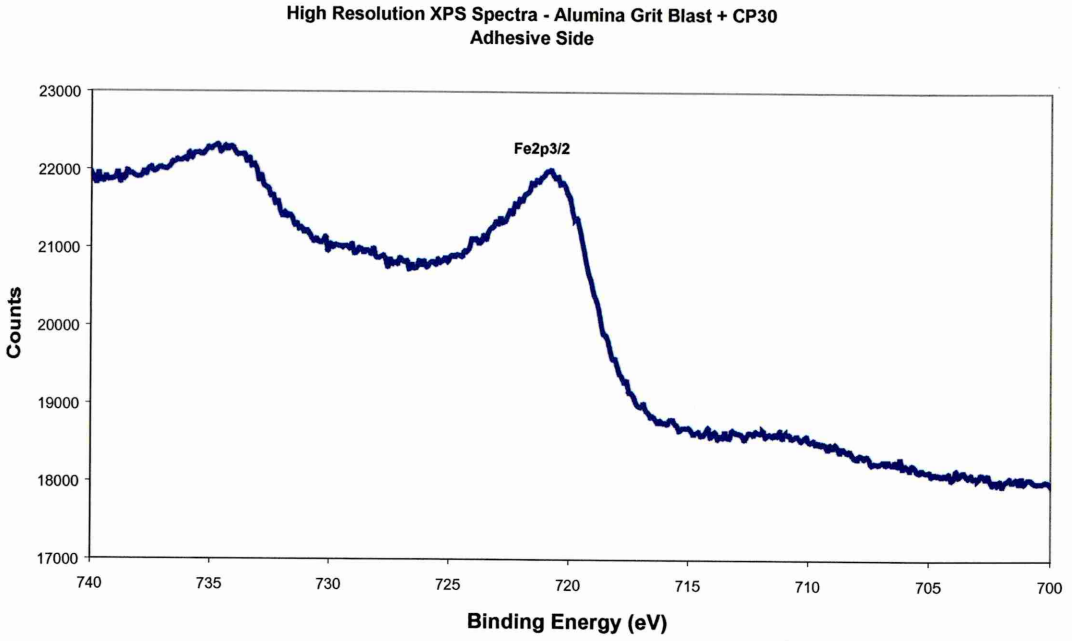

Figure 4.96(b) *– High resolution XPS spectra of iron peak*

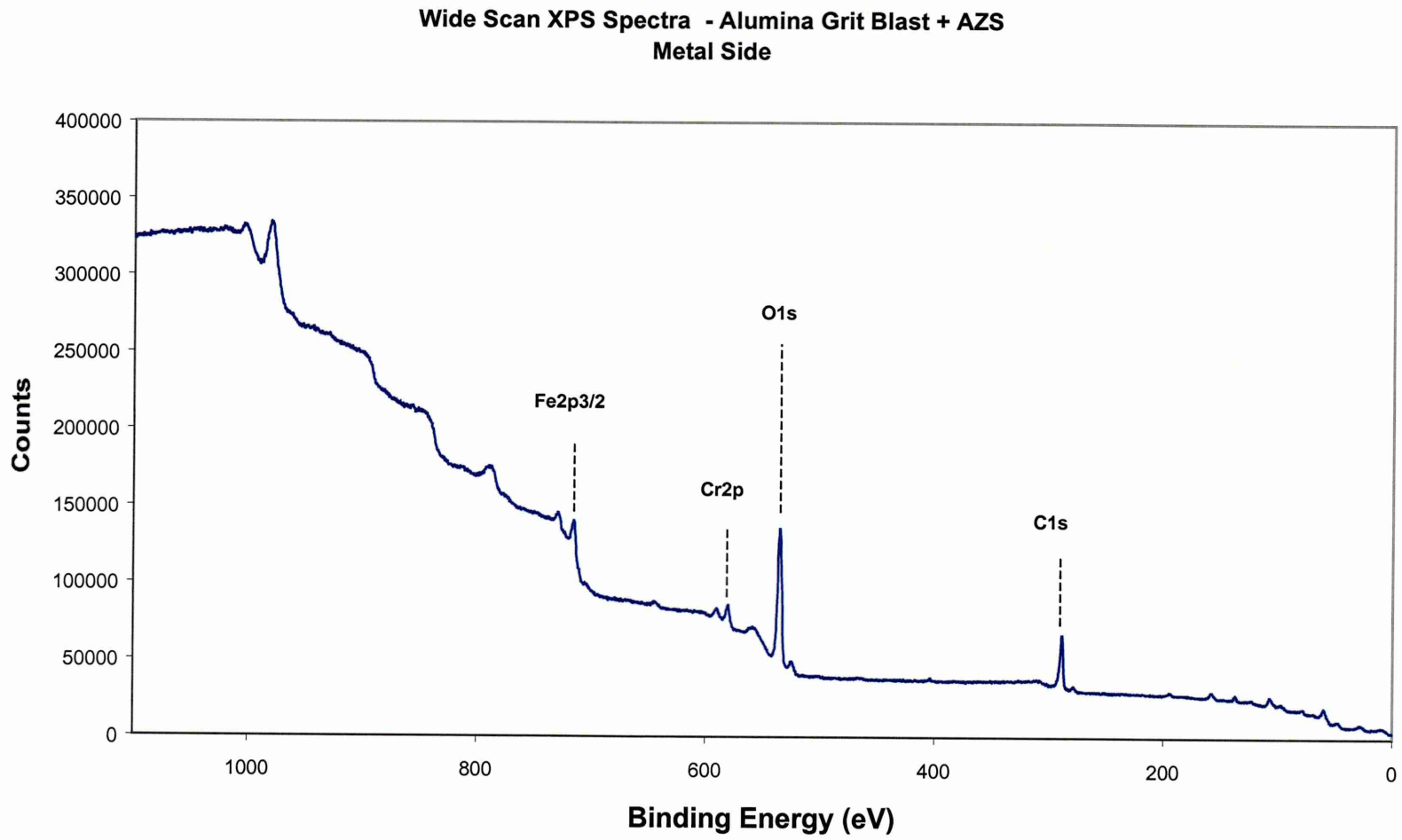

Figure 4.97 – *XPS wide scan spectra of metal side of alumina grit blast + AZS specimen*

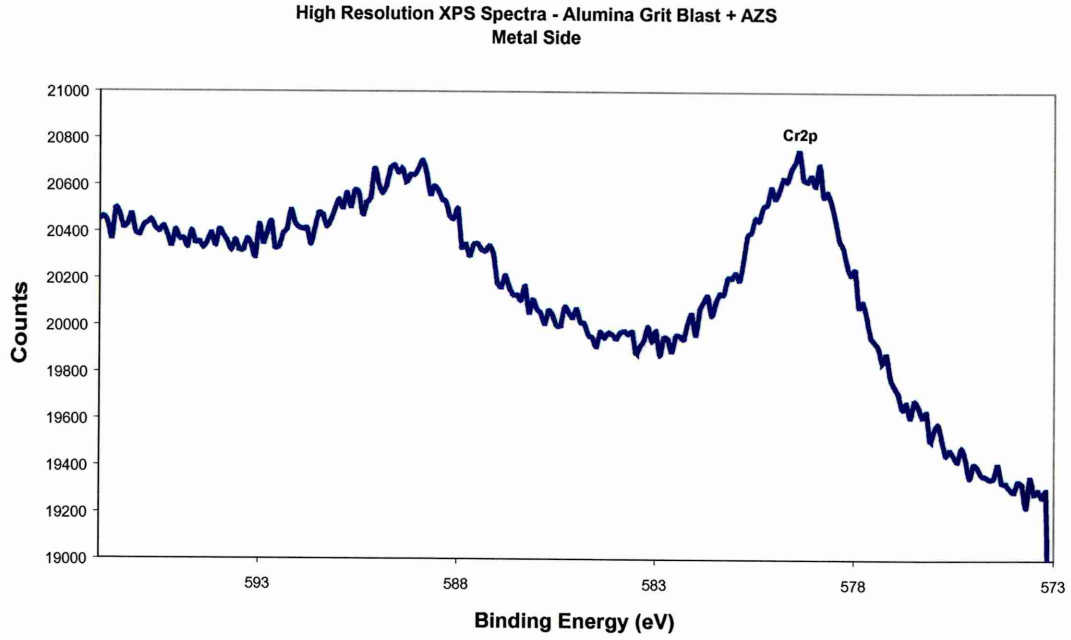

Figure 4.98(a) *– High resolution XPS spectra of chromium peak*

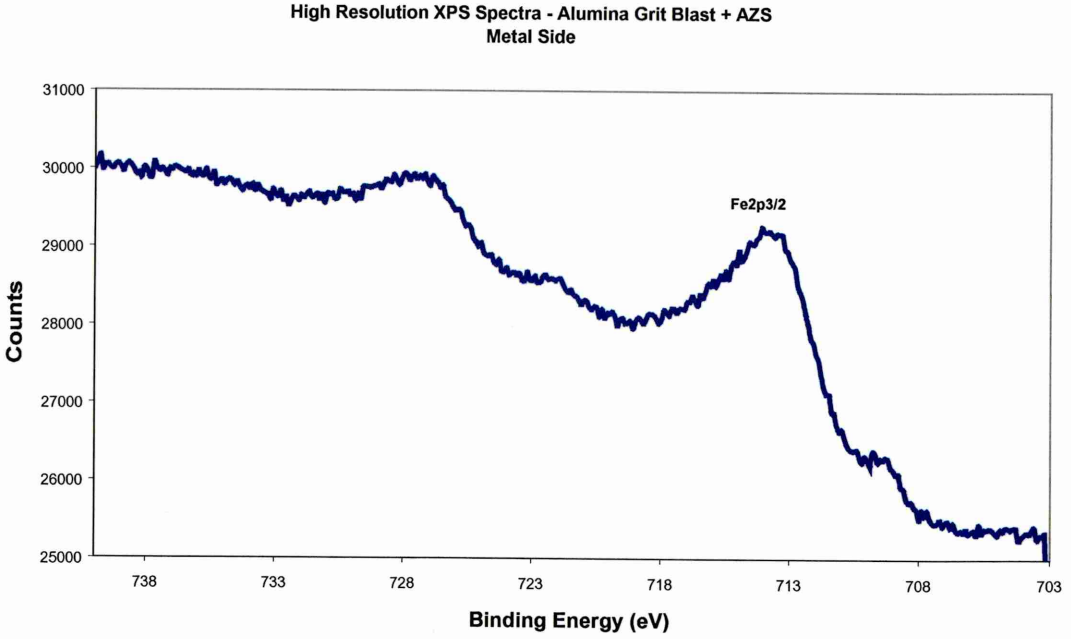

Figure 4.98(b) *– High resolution XPS spectra of iron peak*

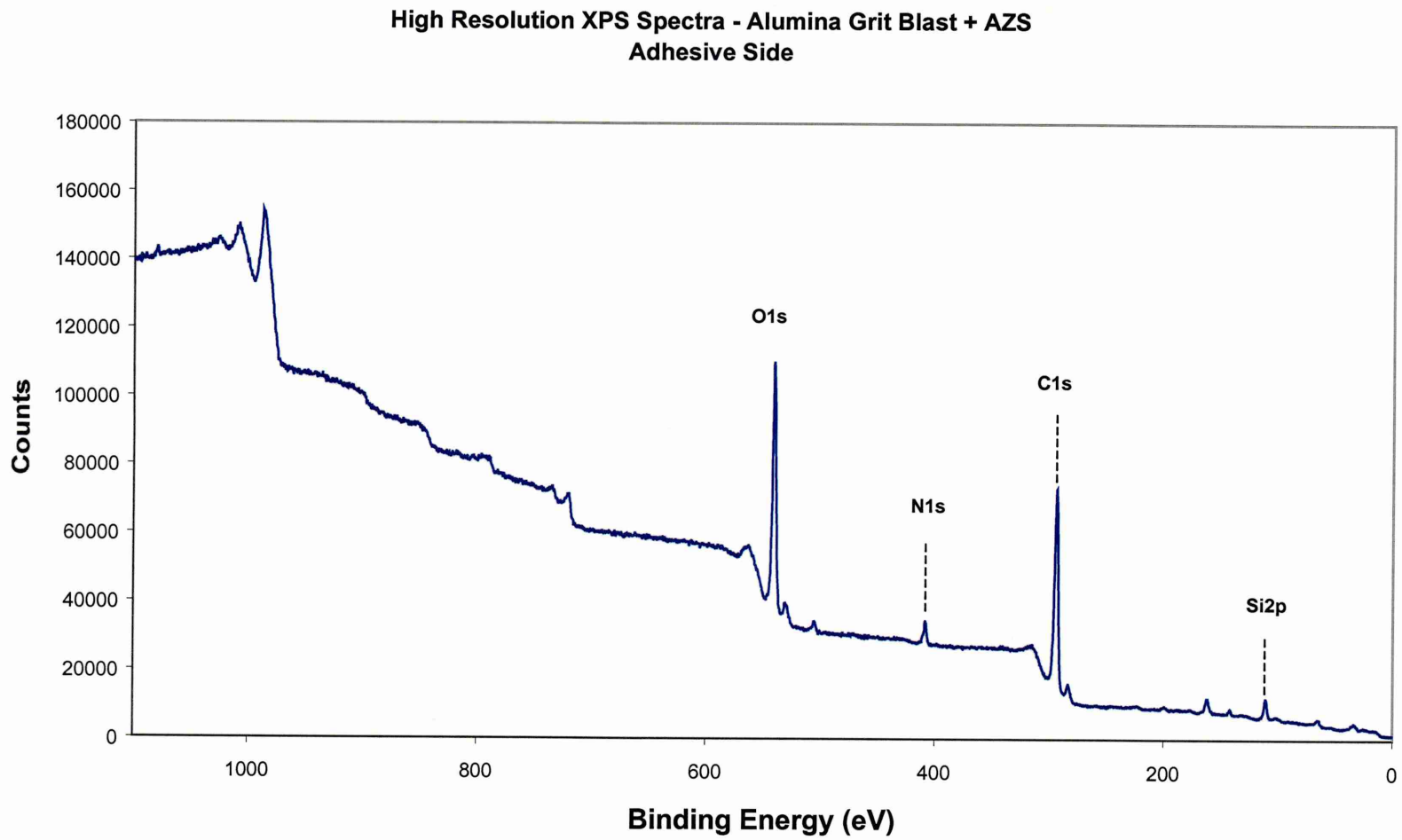

Figure 4.99 – *XPS wide scan spectra of adhesive side of alumina grit blast + AZS specimen*

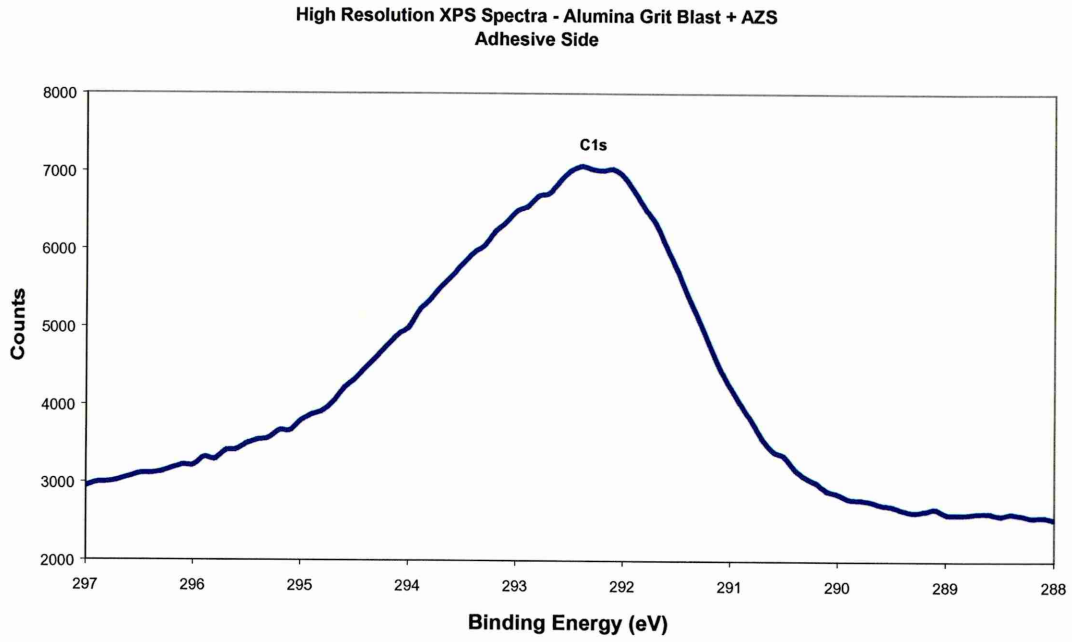

Figure 4.100(a) *– High resolution XPS spectra of carbon peak*

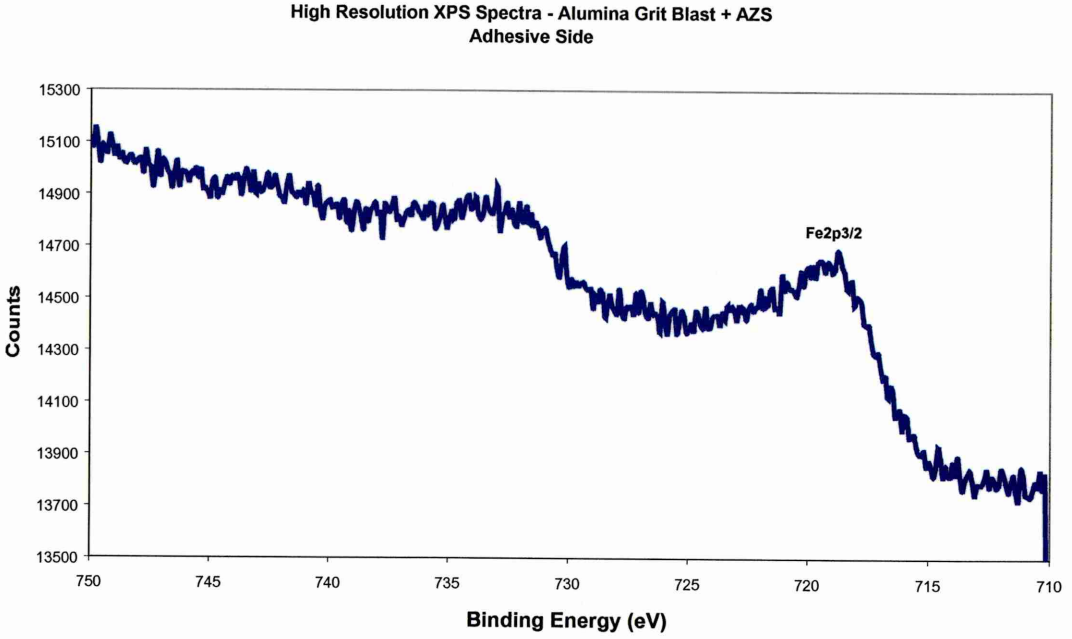

Figure 4.100(b) *– High resolution XPS spectra of iron peak*

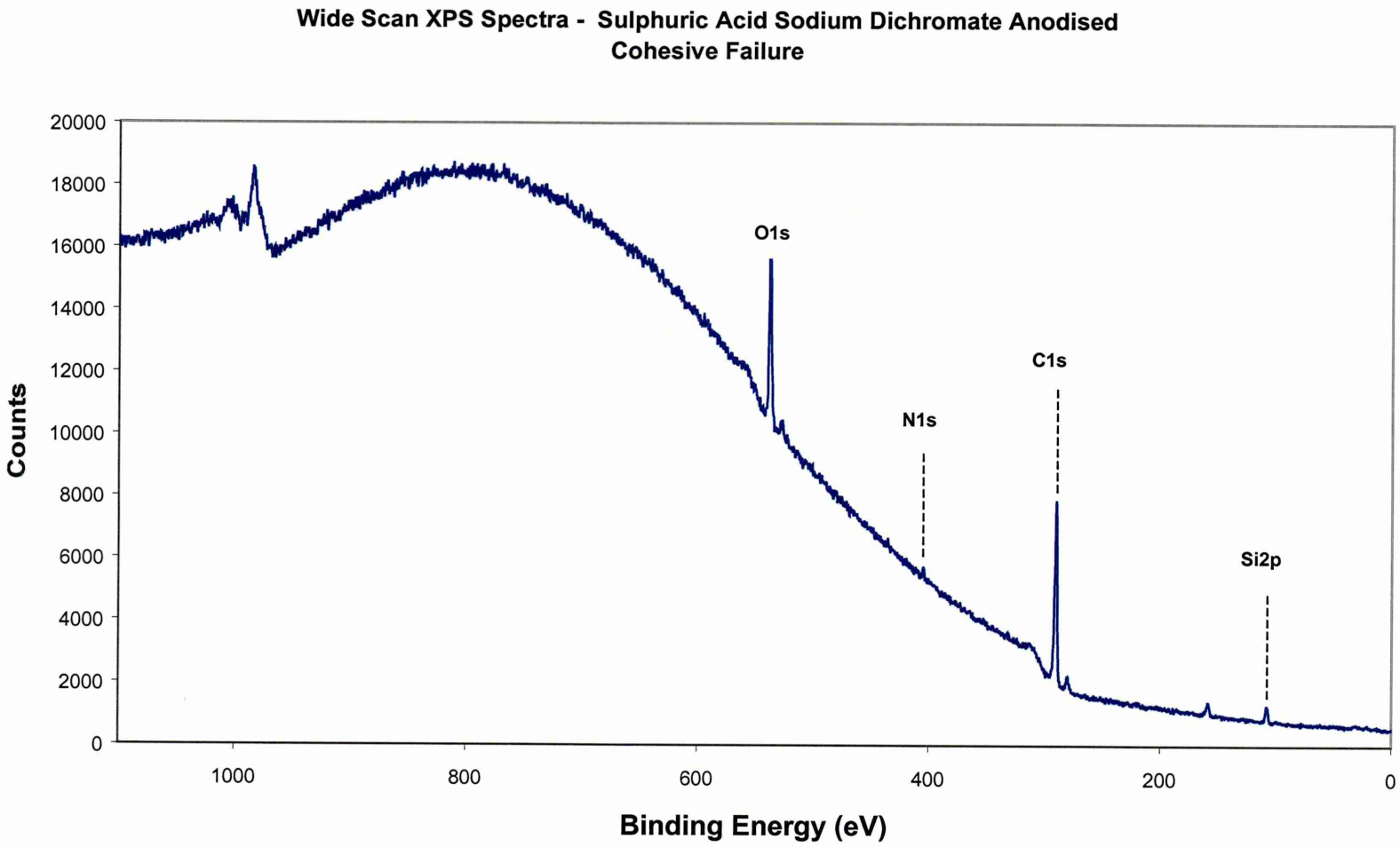

Figure 4.101 – *XPS wide scan spectra of adhesive in cohesive failure of sulphuric acid sodium dichromate anodised specimen*

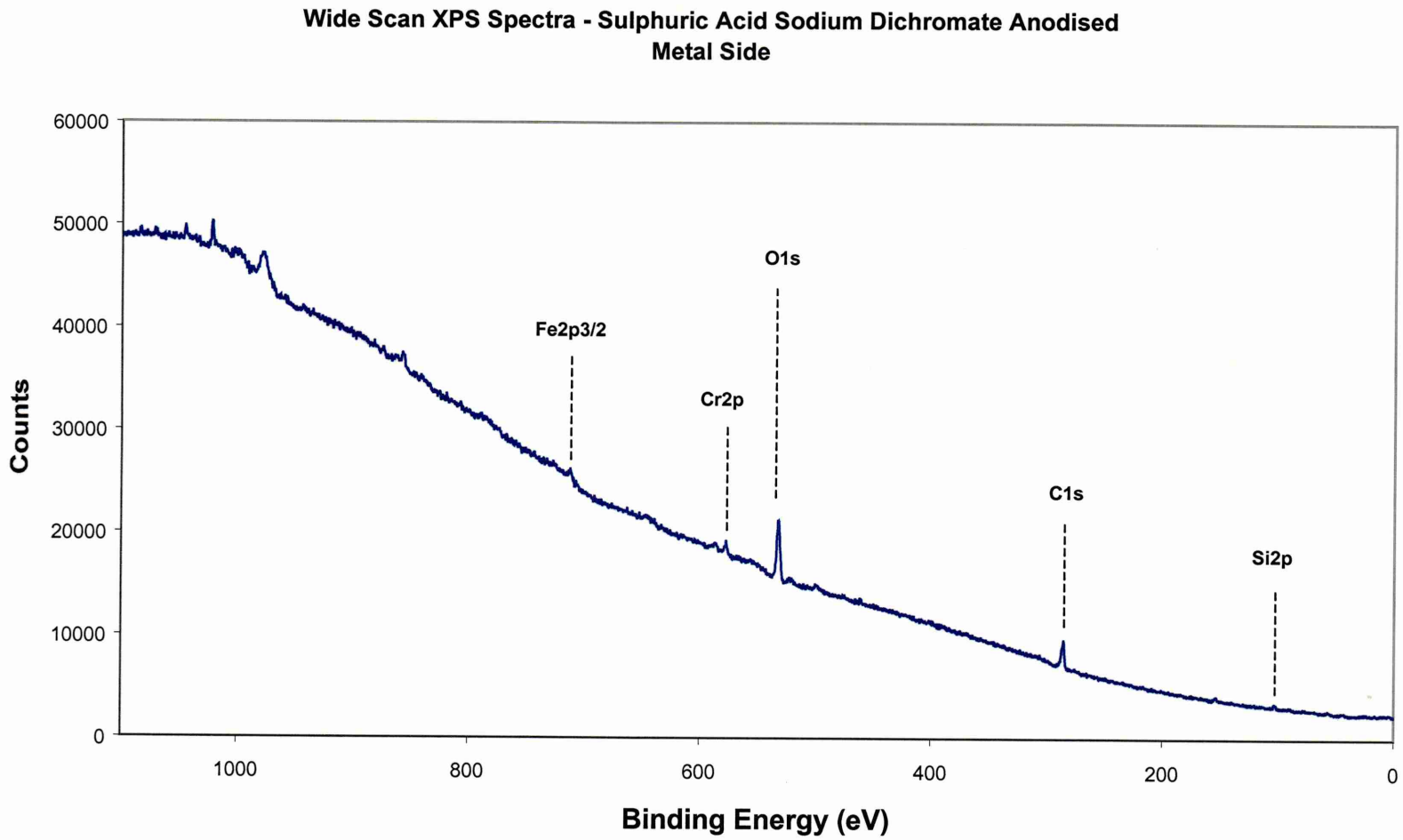

Figure 4.102 – *XPS wide scan spectra of metal side of sulphuric acid sodium dichromate anodised specimen*

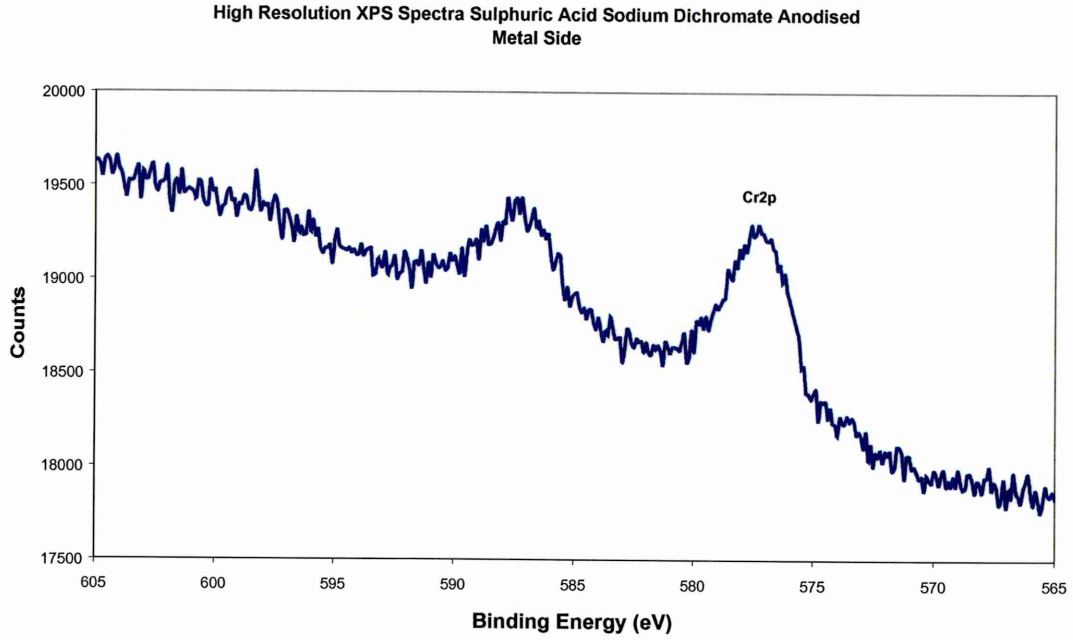

Figure 4.103(a) *– High resolution XPS spectra of chromium peak*

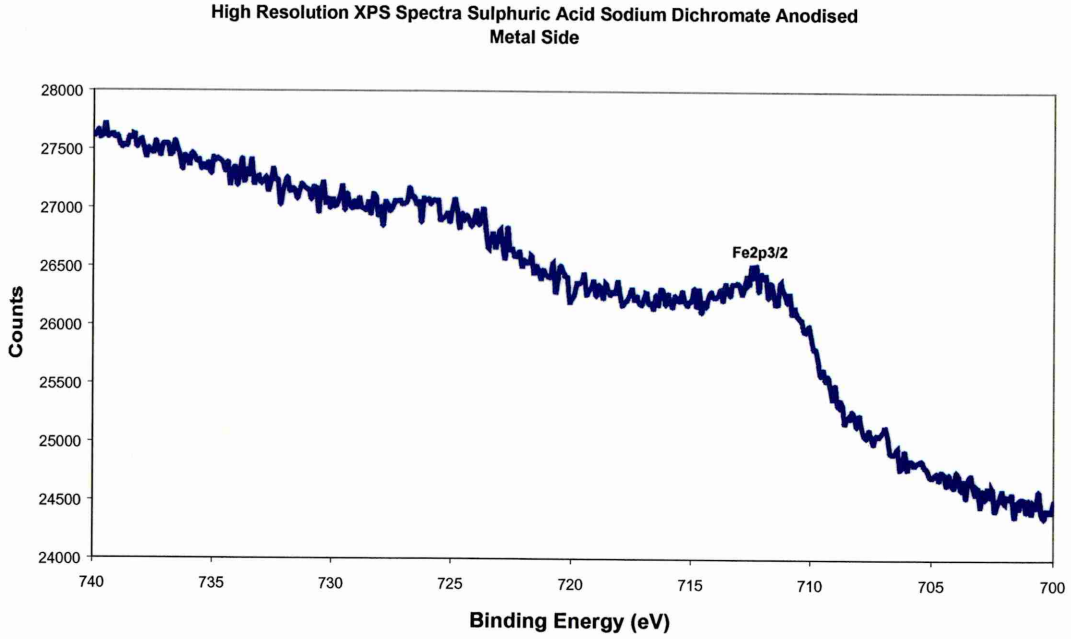

Figure 4.103(b) *– High resolution XPS spectra of iron peak*

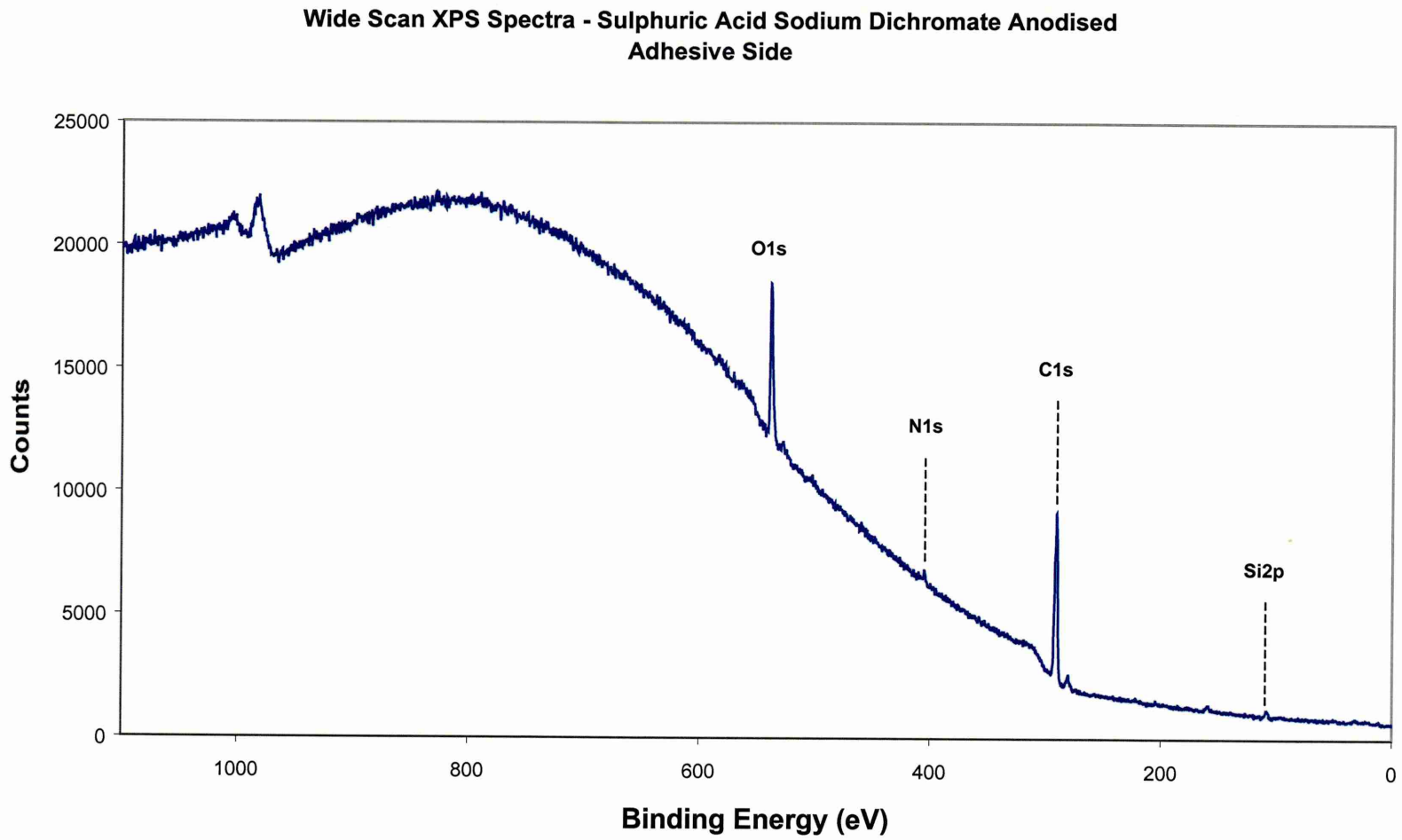

Figure 4.104 – *XPS wide scan spectra of adhesive side of sulphuric acid sodium dichromate anodised specimen*

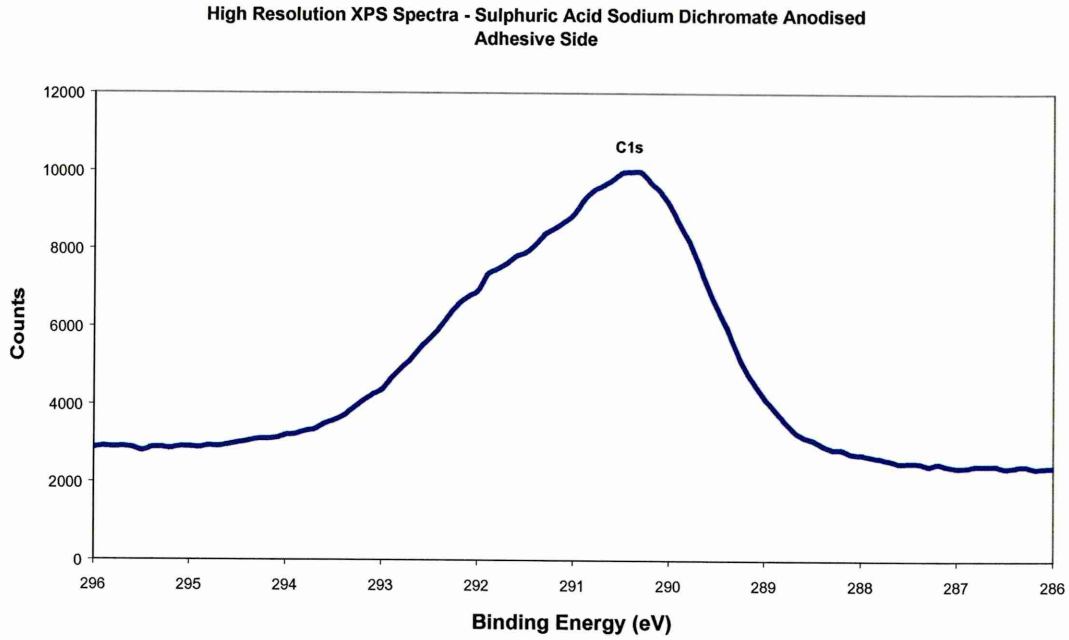

Figure 4.105(a) *– High resolution XPS spectra of carbon peak*

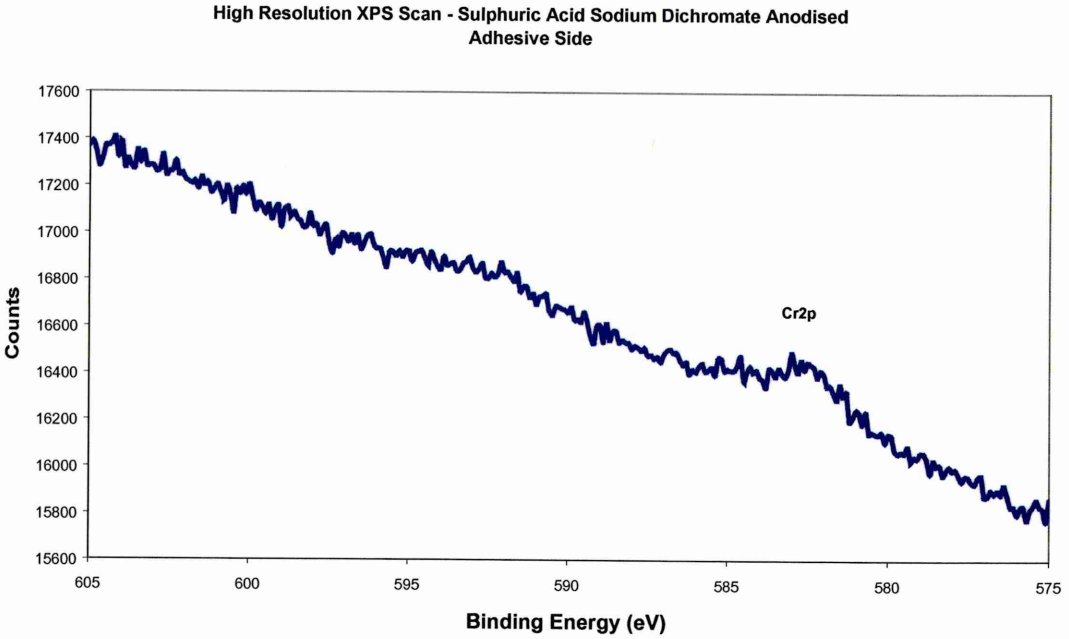

Figure 4.105(b) *– High resolution XPS spectra of chromium peak*

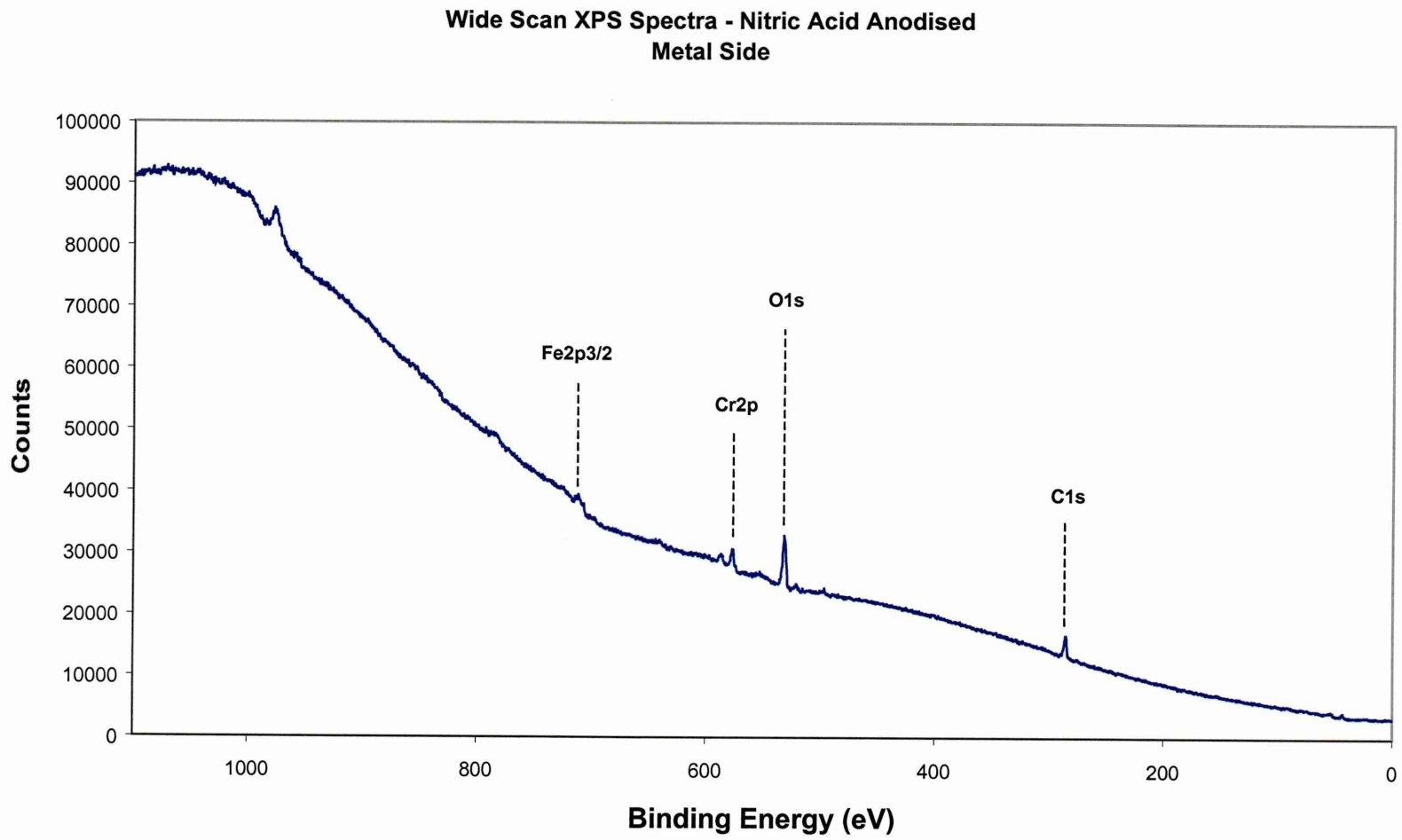

Figure 4.106 – *XPS wide scan spectra of metal side of nitric acid anodised specimen*

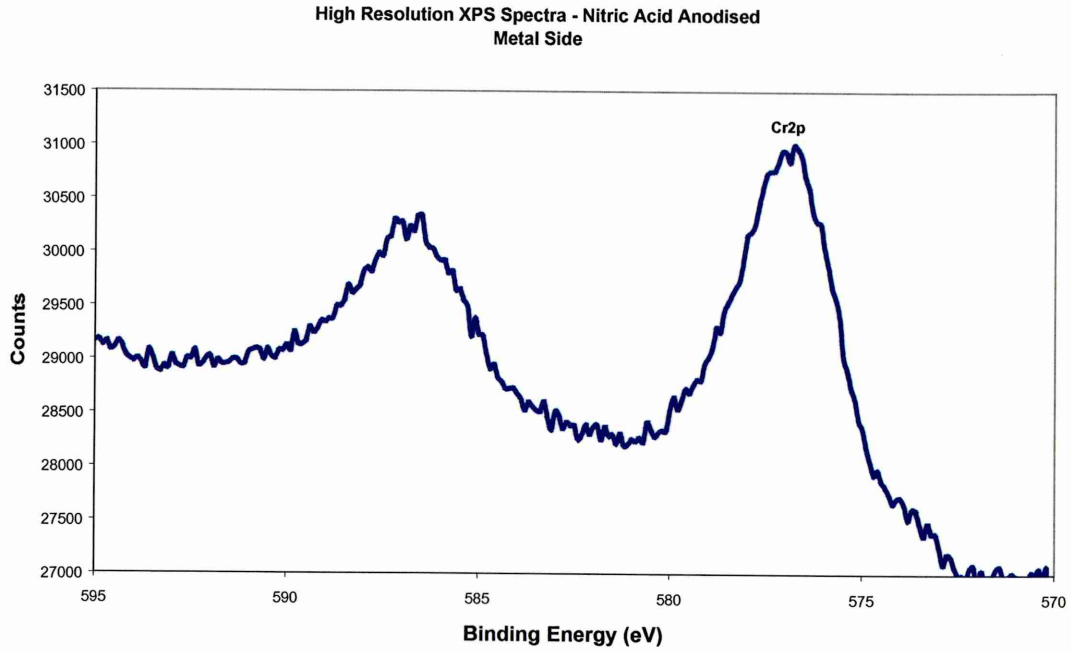

Figure 4.107(a) *– High resolution XPS spectra of chromium peak*

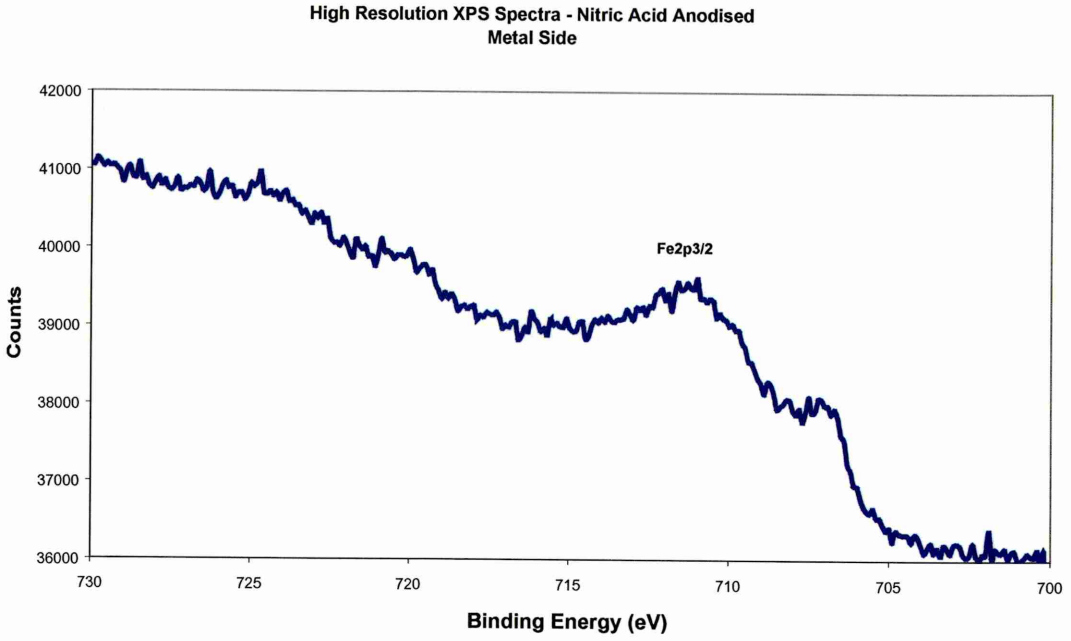

Figure 4.107(b) *– High resolution XPS spectra of iron peak*

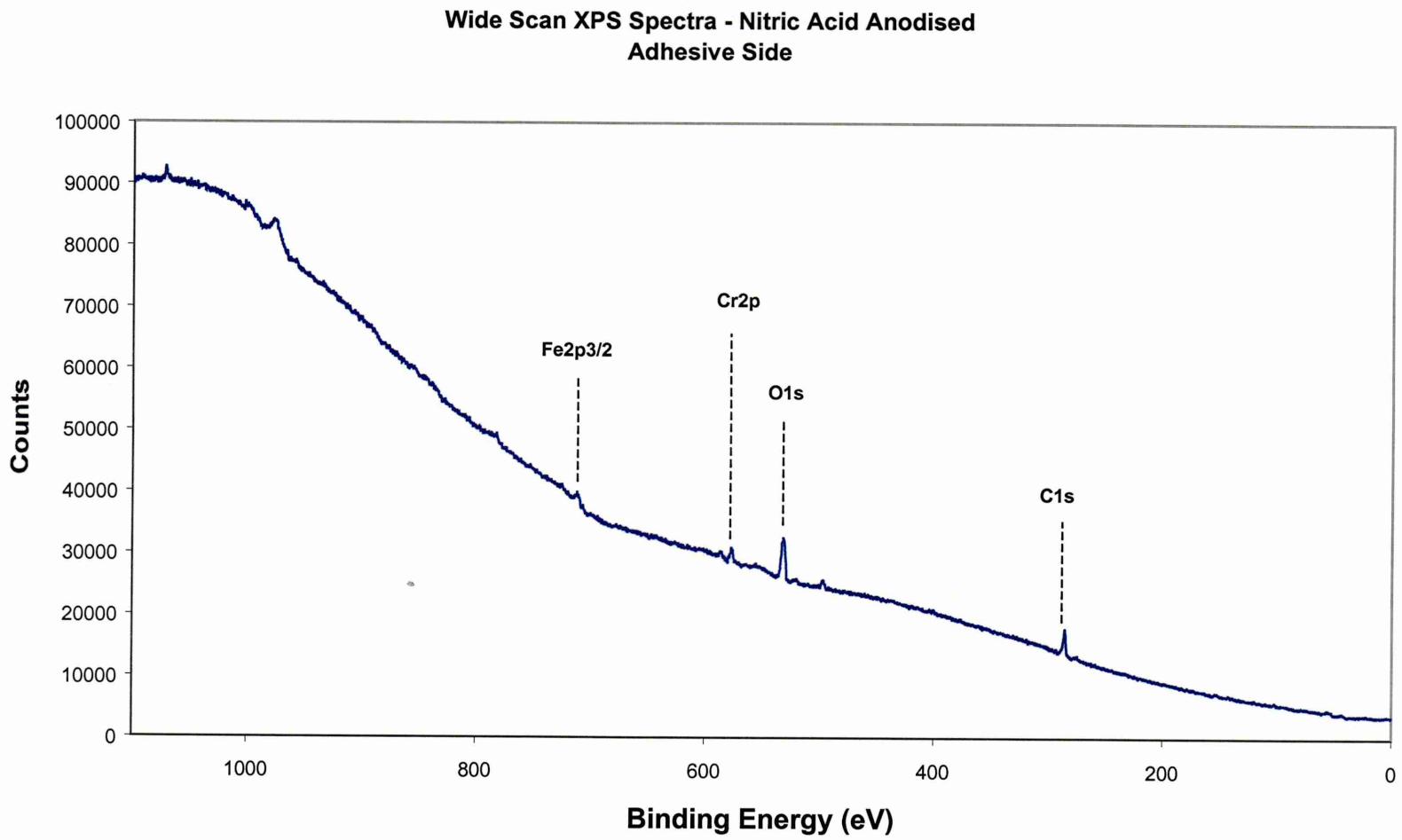

Figure 4.108 – *XPS wide scan spectra of adhesive side of nitric acid anodised specimen*

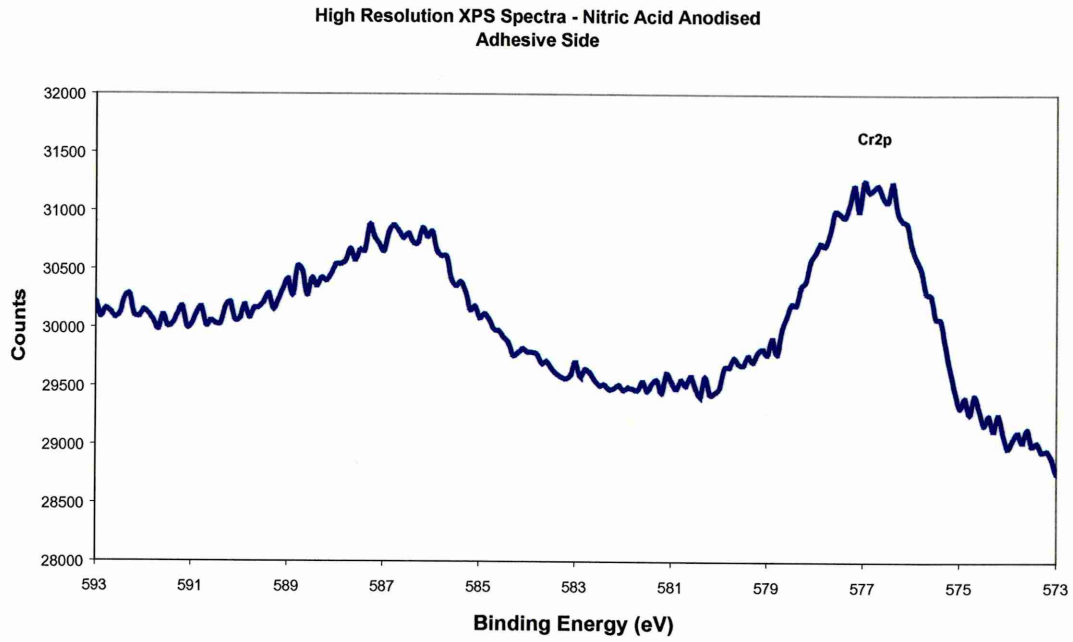

Figure 4.109(a) *– High resolution XPS spectra of chromium peak*

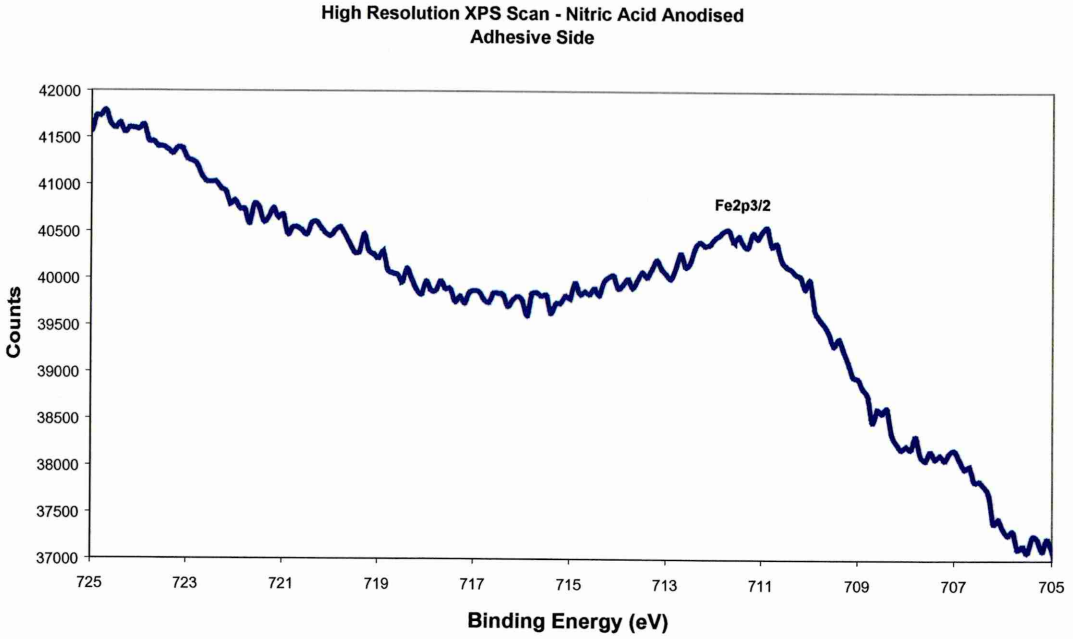

Figure 4.109(b) *– High resolution XPS spectra of iron peak*

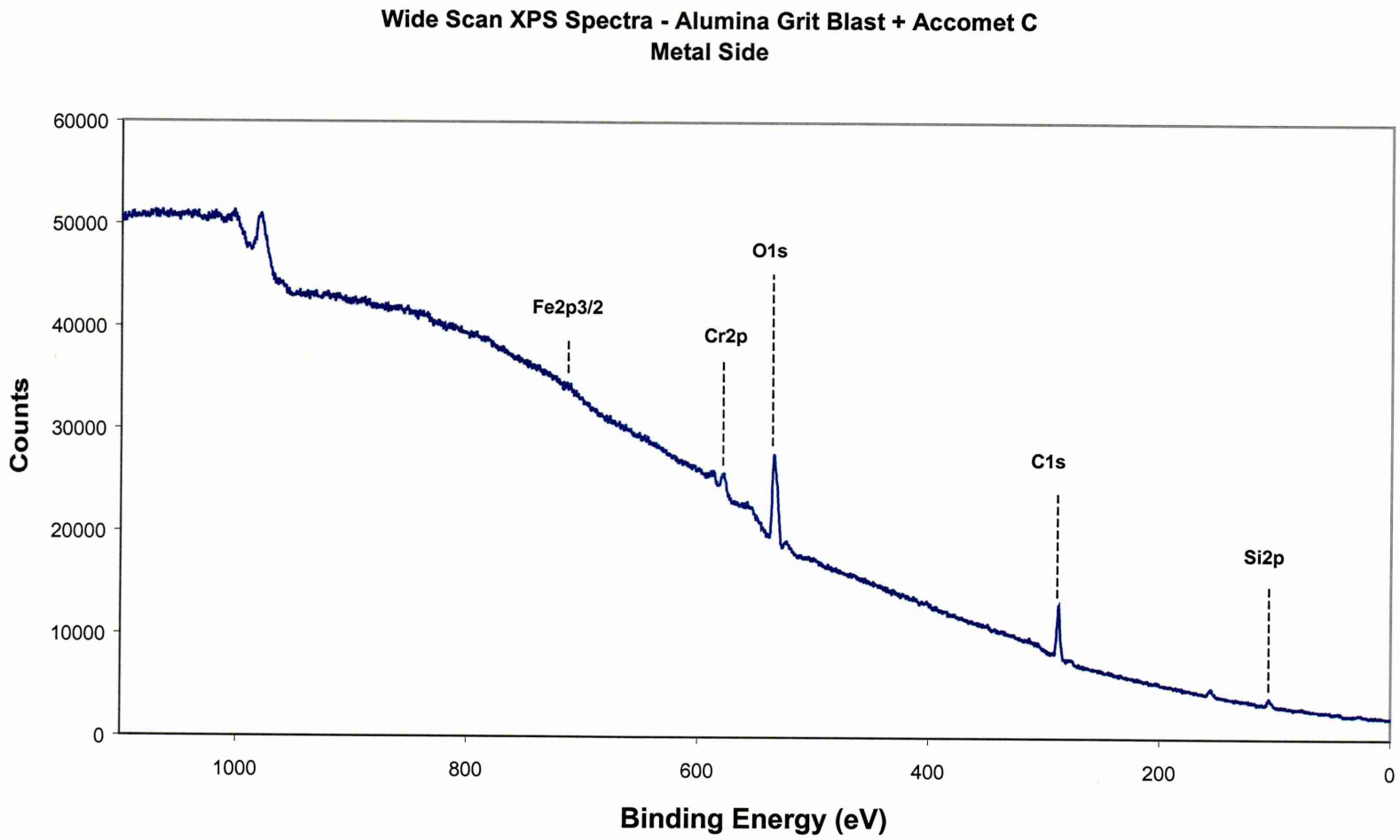

Figure 4.110 – *XPS wide scan spectra of metal side of alumina grit blast + Accomet C specimen*

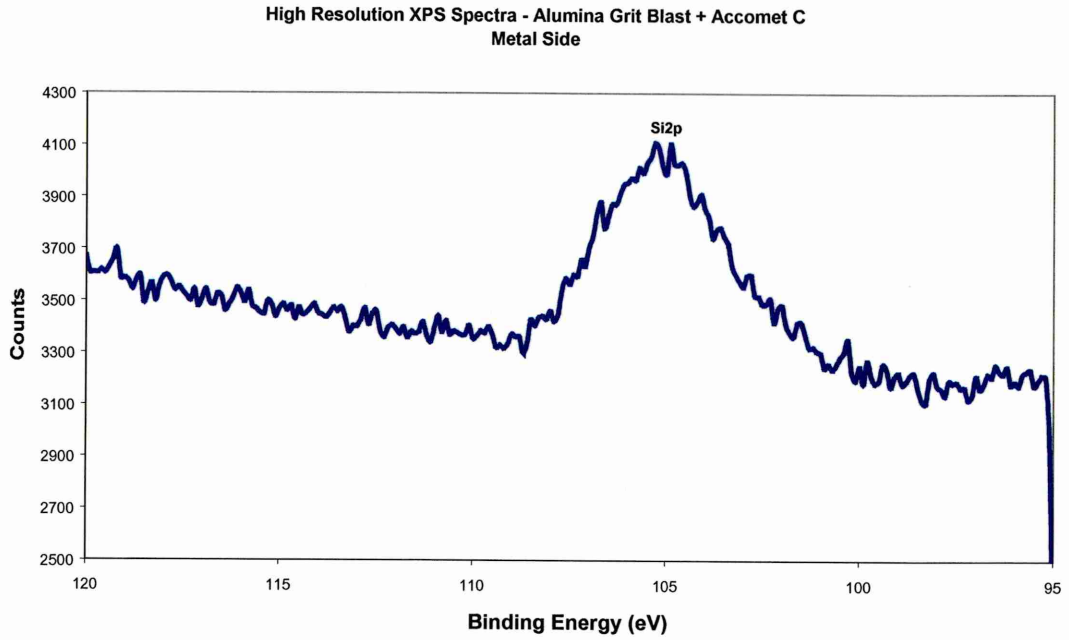

Figure 4.111(a) *– High resolution XPS spectra of silicon peak*

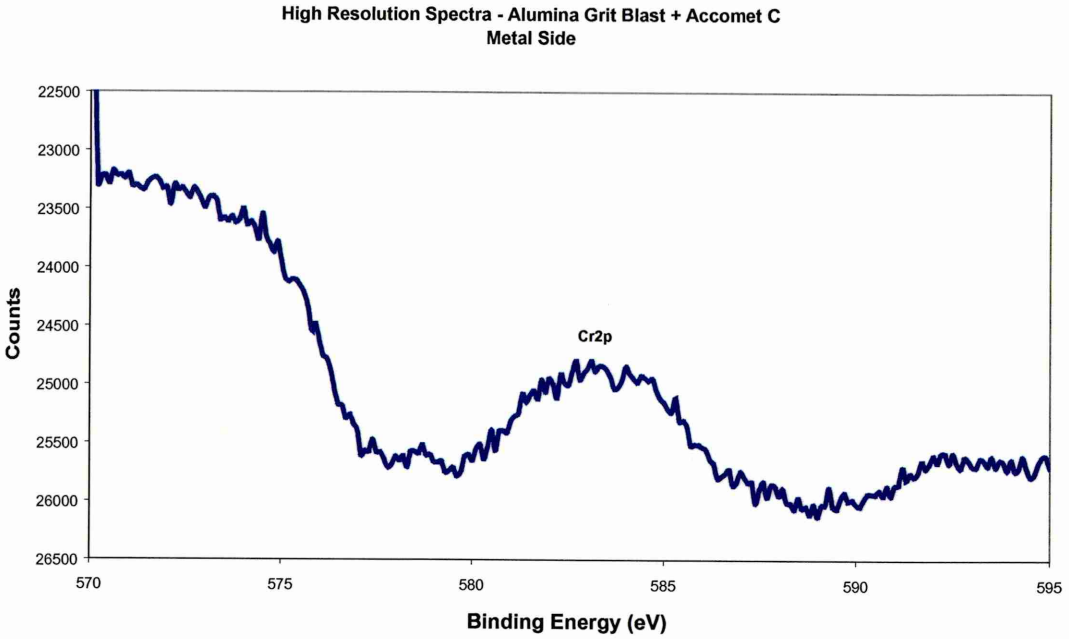

Figure 4.111(b) *– High resolution XPS spectra of chromium peak*

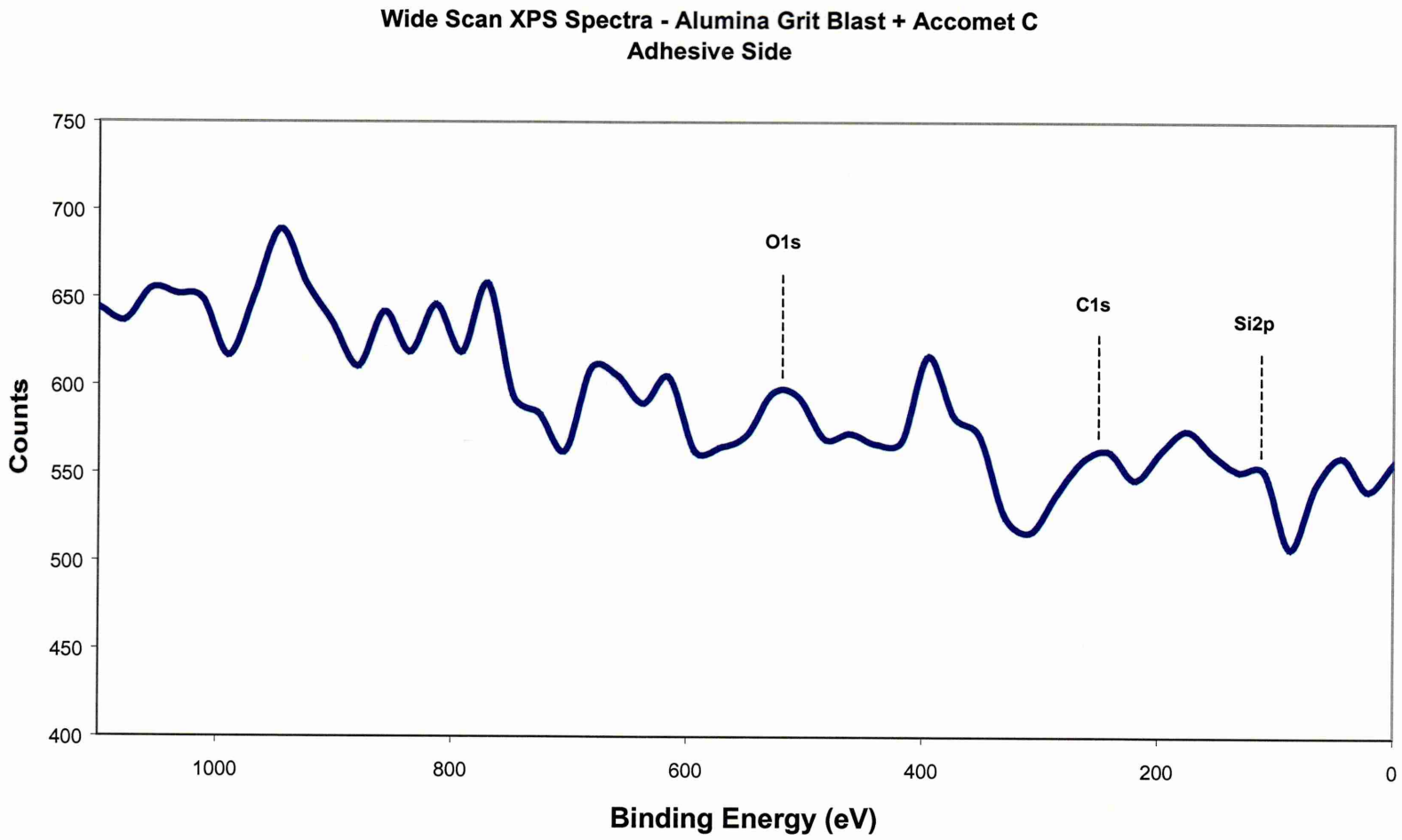

Figure 4.112 – *XPS wide scan spectra of adhesive side of alumina grit blast + Accomet C specimen*

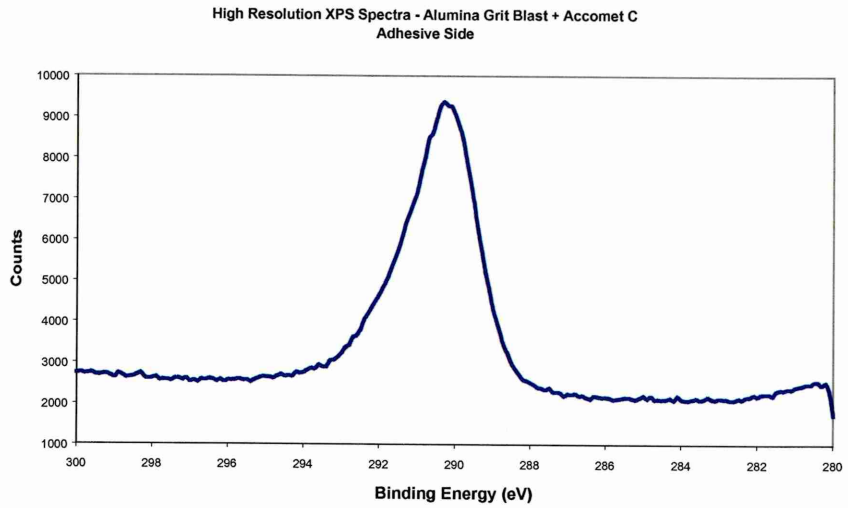

Figure 4.113(a) *– High resolution XPS spectra of carbon peak*

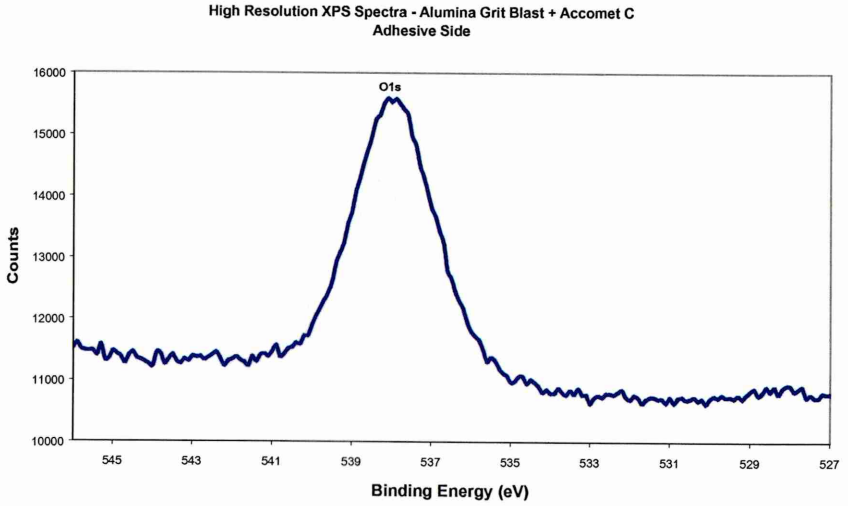

Figure 4.113(b) *– High resolution XPS spectra of oxygen peak*

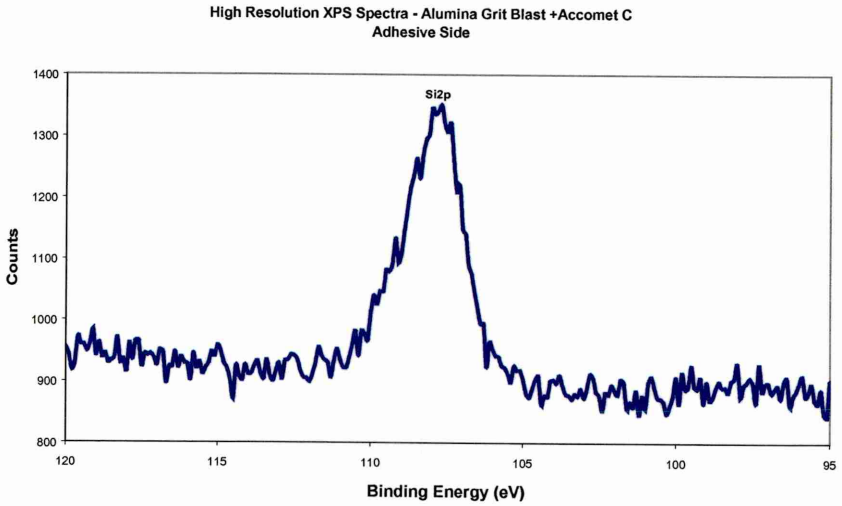

Figure 4.113(c) *– High resolution XPS spectra of silicon peak*

4.5.5 Closing Remarks on Failure Analysis

Different failure modes have occurred within the wedge test specimens as a function of surface pre-treatment, each failure type has been studied using various surface analysis techniques. The general trend is joints that exhibited the poorest durability tended to fail between the adhesive-metallic oxide interface or adhesive-primer/coating interface. For the electro-chemical pre-treatments SEM has shown the adhesive has penetrated into the anodised oxide layer, suggesting some form of mechanical interlocking has taken place. XPS analysis of the sulphuric acid sodium dichromate anodised specimen support the conclusion the adhesive has imbedded into the pores of the substrate, but failure has occurred within the bulk adhesive very close to the adhesive-oxide interface. Analysis of the nitric acid anodised specimen indicates that failure has been a mixture of through the oxide layer and between the bulk adhesive that has penetrated the oxide layer. The alumina grit blast + Accomet C treated specimens have failed predominately between the adhesive-Accomet C interface. The mechanism how Accomet C enhances bond durability is not well understood but it clearly promotes excellent adhesion for stainless steel-epoxy joints.

4.6 Discussion

4.6.1 Effect of Surface Condition

The commercially available surface finishes, i.e. 2B, 2D and BA, of AISI 304L stainless steel influences the durability of stainless-epoxy adhesive joints, when exposed to a high humidity environment. The least durable joints incorporated the bright annealed (BA) finish, the poor performance can be attributed to its relatively smooth surface, R_A = 0.03μm. The smooth featureless surface is typified in Plate 4.3. The durability of single lap joints exposed to a hydro-thermal regime was found to improve in joints incorporating the semi-bright (2B) and dull matt (2D) surface finishes. All three surface finishes evaluated had the same oxide composition and nominal thickness, ~3nm: measured using Static Neutral Mass Spectrometry (SNMS). However, the 2B and 2D surfaces are rougher compared with BA, where R_A = 0.17μm and 0.21μm, respectively. SEM revealed areas of grain boundary attack, which is characteristic of the 2B and 2D finishes from acid pickling stage of production. The improvement in stressed durability afforded by 2B or 2D surfaces is very likely due to the increase in surface roughness and hence the increased area available for bonding. The relationship between surface roughness and the time to failure of lap joints loaded to 1.6kN is shown in Figure 4.114. It was also shown the ability to sustain the application of stress in a high humidity environment can be considerably increased using the relatively simplistic alumina grit blasting surface pre-treatment. Although SEM showed the resultant pre-bonding surface is not indicative of topography suited for mechanical interlocking, whereby the adhesive can lock into surface artefacts, the substantial increase in surface area must be a contributing factor to enhancing load bearing capacity.

Stressed durability tests exposed to a high humidity environment adversely affects the residual strength of adhesive joints. For specimens fabricated from all three surface conditions evaluated, joints that had been stressed produced lower retained strength when compared with un-stressed controls.

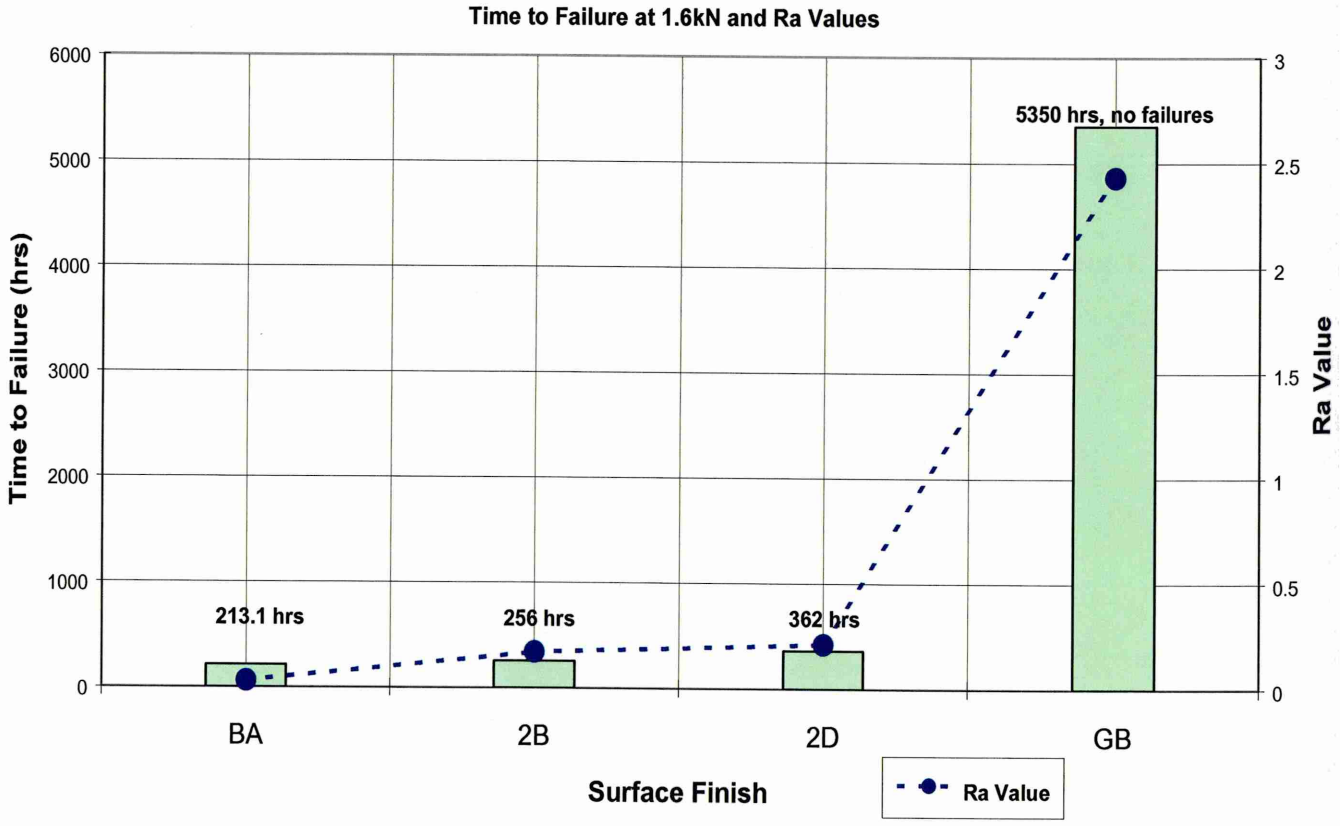

Figure 4.114 *– The relationship between stressed durability and surface roughness*

4.6.2 Effect of Surface Pre-treatment

The use of the standard lap shear configuration, using a 12.5mm overlap and width of 25mm has proven suitable for discriminating between stainless steel surface finishes of the same grade. However, this test specimen does not have the ability to differentiate between surface pre-treatments within a convenient time scale. Therefore the perforated lap shear specimen with reduced surface area was introduced. Of the eleven pre-treatments appraised the most durable joints were fabricated using;

- *Alumina grit blast + Accomet C*
- *Sulphuric acid sodium dichromate anodising*
- *Nitric acid anodising*

The latter two treatments are complex electro-chemical processes. Several limitations would arise if they were to be used on an industrial scale, these include;

- *Cost of heating the electrolyte in large scale tanks*
- *Cost of applying a voltage*
- *Problems disposing of the waste products*
- *Continuous monitoring of bath conditions for optimum treatment*

In addition the electro-chemical techniques treat both sides of the substrate to be joined. This severely diminishes the use of these pre-treatments if the opposing side of the bonded overlap is used for atheistic appeal such as architectural applications.

The alumina grit blast + Accomet C pre-treatment produces the most durable adhesive joints when exposed to a hydro-thermal stress regime. The Accomet C process offers excellent environmental durability, and out performs established chemical treatments such as the oxalic acid etch. Although Accomet C consists of hexavalent chromium as chromate, the formulation is such that its oxidising property is extremely weak, thus Accomet C is a comparatively benign process. Another beneficial aspect of this process is only the side of the adherend to be bonded is treated, which is encouraging for applications where durability and aesthetic appearance are a prerequisite.

It was found from the perforated lap shear tests, that joints exhibiting a high initial joint strength did not necessarily perform well in the durability trials. For example, joints incorporating alumina grit blast + CP30. Secondly the chemical composition and morphology of stainless steel is modified in some form when subjected to a pre-bonding treatment, it is these physical and chemical changes that influences joint durability. Table 4.32 details the surface chromium to iron ratios determined from the XPS analysis for selected pre-treatment. The alumina grit blast + Accomet C, sulphuric acid sodium dichromate anodised and nitric acid anodised treatments clearly have a higher chromium to iron ratio.

***Table 4.32** - Chromium-Iron ratios*

Pre-treatment	Chromium/Iron Ratio
Alkaline Degreased	0.84
Alumina Grit Blast	0.61
Alumina Grit Blast + Silane Primer	0.70
Alumina Grit Blast + Accomet C	7.11
Sulphuric Acid Sodium Dichromate Anodised	2.33
Nitric Acid Anodised	2.17
Ferric Chloride Etch	0.97
Oxalic Acid Etch	0.99

Figure 4.115 is a plot of the average time to failure of perforated lap joints loaded to 0.5kN versus the chromium-iron ratio of the outer surface of the adherend. The trend indicates that as

the chromium-iron ratio at the surface is increased the ability to resist fracture in a warm humid environment also increases. Similarly Figure 4.116 is a plot of the wedge crack extension observed after 24 hours of exposure against the chromium-iron ratio of the outer surface of the substrate. The same pattern emerges, where enhanced durability is greater as the chromium-iron ratio increases.

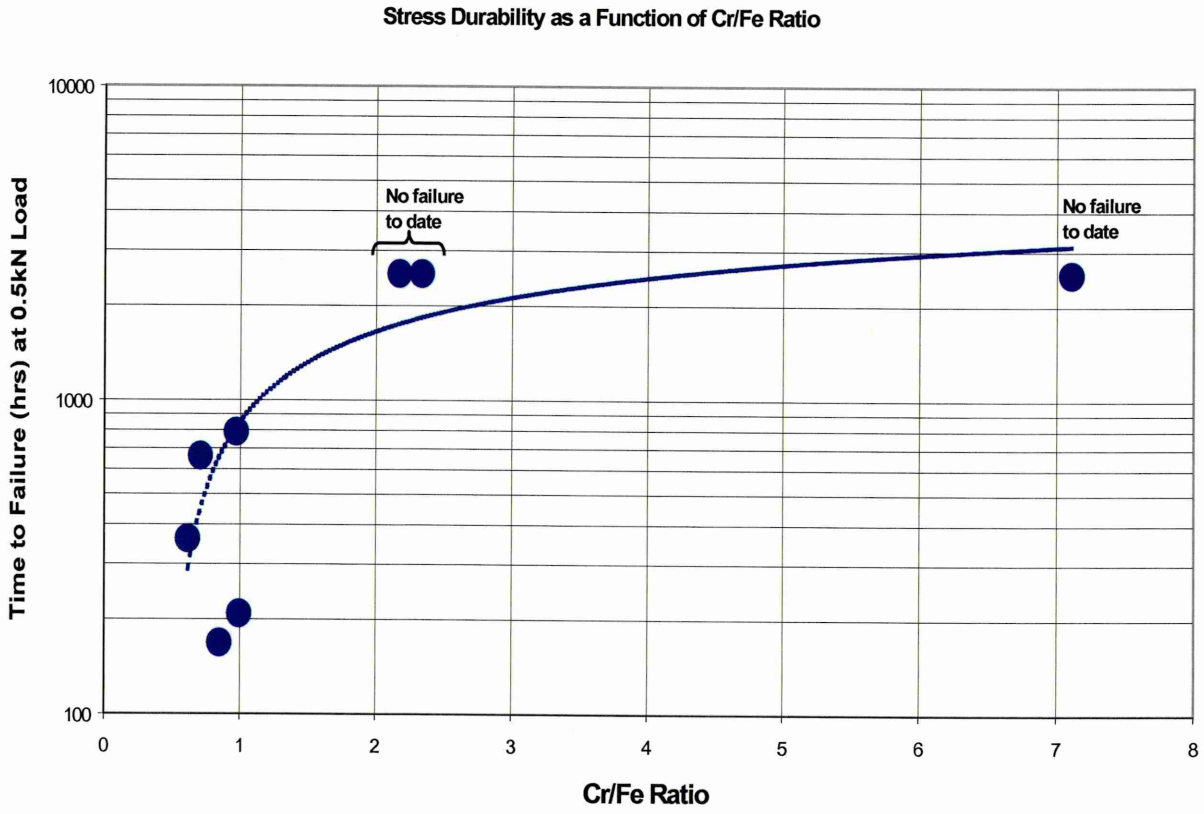

Figure 4.115 *– Stressed durability performance versus chromium-iron ratio of the adherend surface*

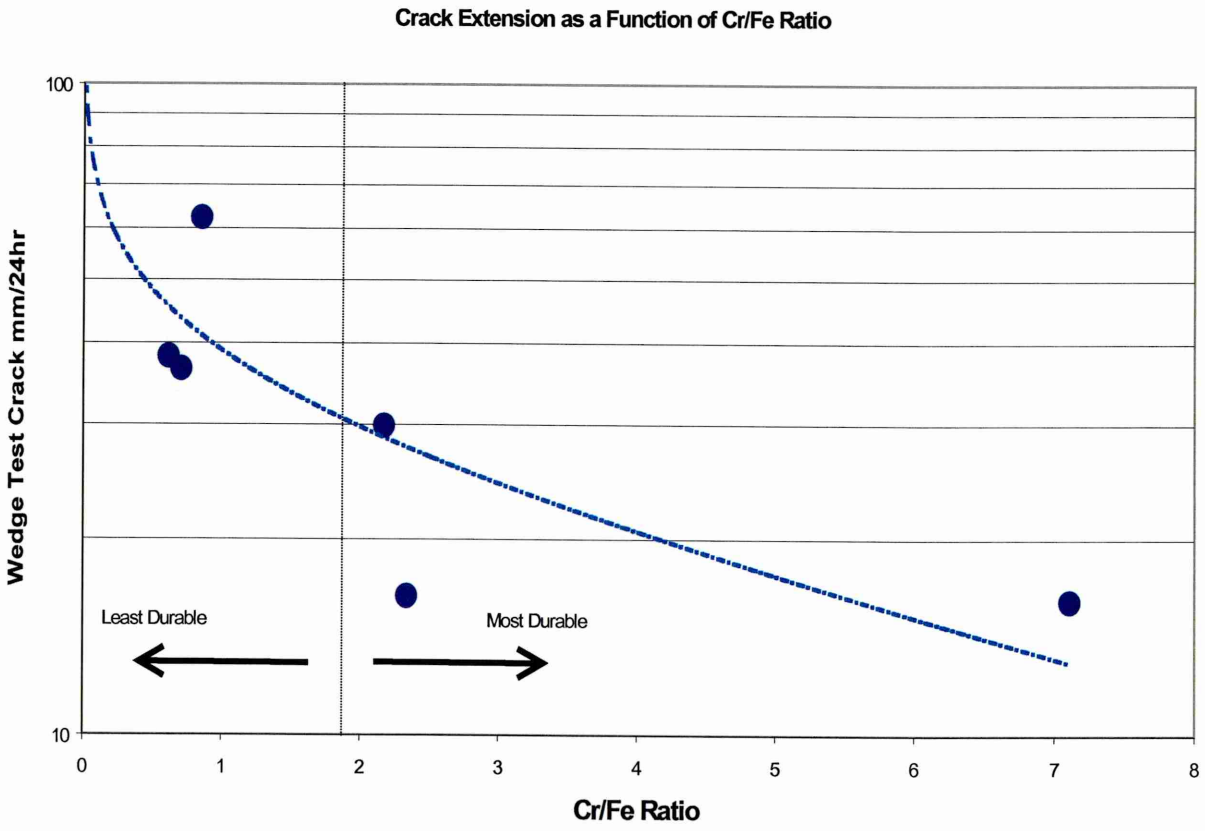

Figure 4.116 *– Wedge crack extension versus chromium-iron ratio of adherend surface*

Thirdly the influence of surface roughness on joint durability has been studied using surface profilometry and electron microscopy. Surface profilometry results give misleading information, if a correlation was made between surface roughness and adhesive joint durability. Figure 4.117 plots the relationship between the time to failure of perforated lap joints loaded to 0.5kN against the R_A values of the adherend surface. It is obvious the R_A measurements do not form a trend that corresponds to the performance of the pre-treatment. For example the nitric acid anodise surface has R_A = 0.15, which implies a smooth surface even though it is a durable pre-treatment. SEM analysis of a pre-treated surface provides much more information on surface roughness. The electro-chemically treated surfaces have been chemically attacked which apart from attacking the grain boundaries has formed a porous structure on the surface, as shown in Plates 4.38 and 4.39. An explanation why these surfaces promote durability would be the pre-treatment increases the chromium content of the surface, which seems to be beneficial when using epoxy resins, and the adhesive penetrates the surface pores.

Failure analysis of failed wedge test specimens was performed using SEM and XPS to fully elucidate the mechanisms of failure that have occurred. It was shown that after environmental

exposure the less durable specimens tend to fail adhesively between the adhesive and either the metal oxide or relevant coating. The Accomet C treated specimens also fail between the coating and adhesive, however this pre-treatment resists moisture ingressing into the bondline by a mechanism that can not be fully explained. The sulphuric acid sodium dichromate and nitric acid anodised specimens have failed through a mixture of oxide and interfacial failure whilst occasionally meandering cohesively in the bulk adhesive very close to the surface.

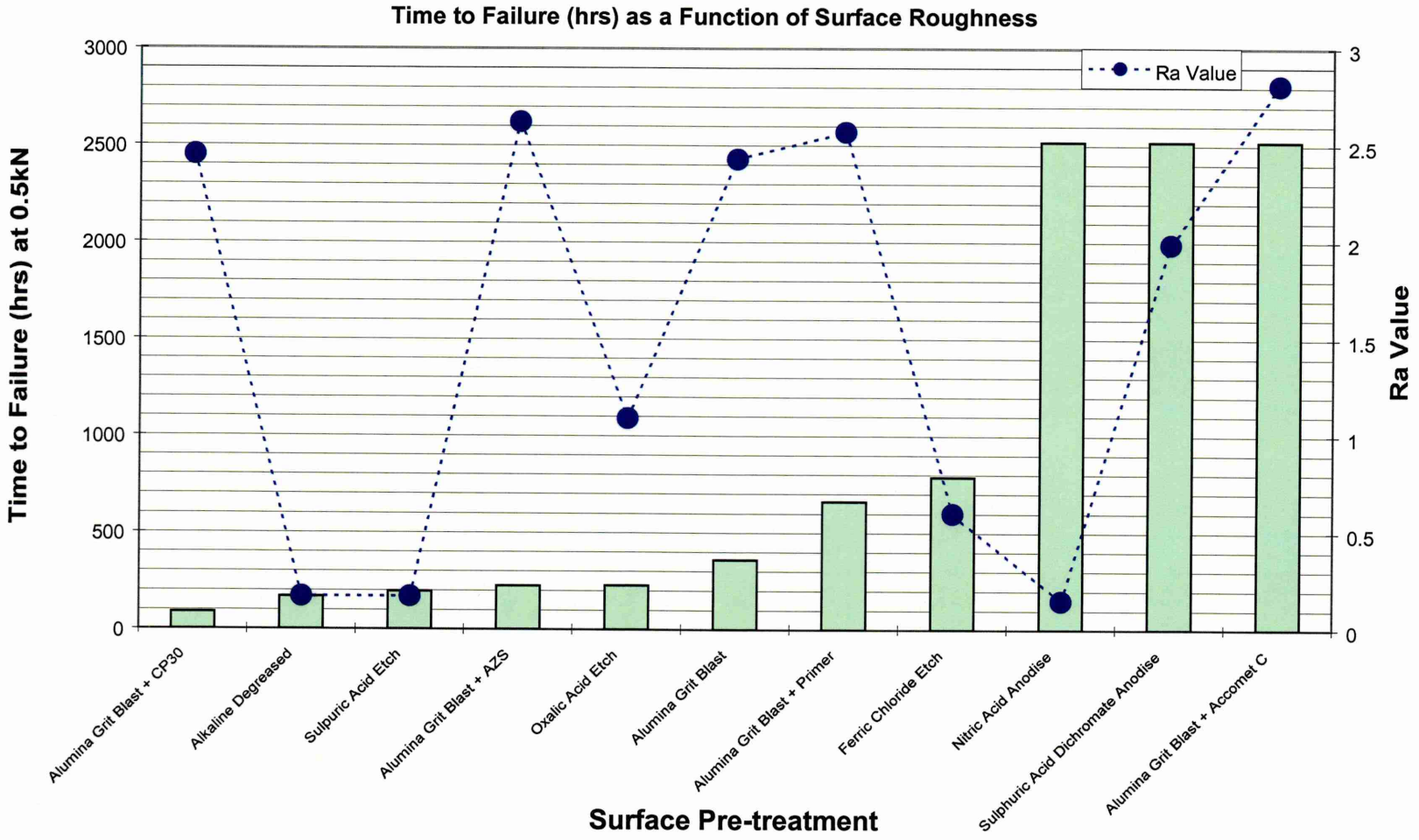

Figure 4.117 – *Relationship between surface roughness and stressed durability performance, using a 2B substrate*

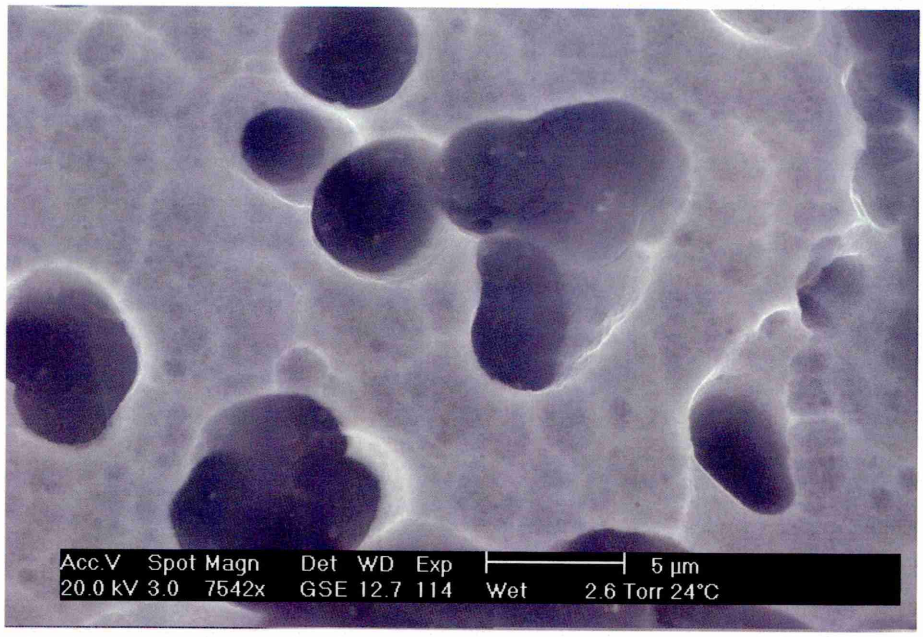

***Plate 4.38** – Porosity of electro-chemically treated surface*

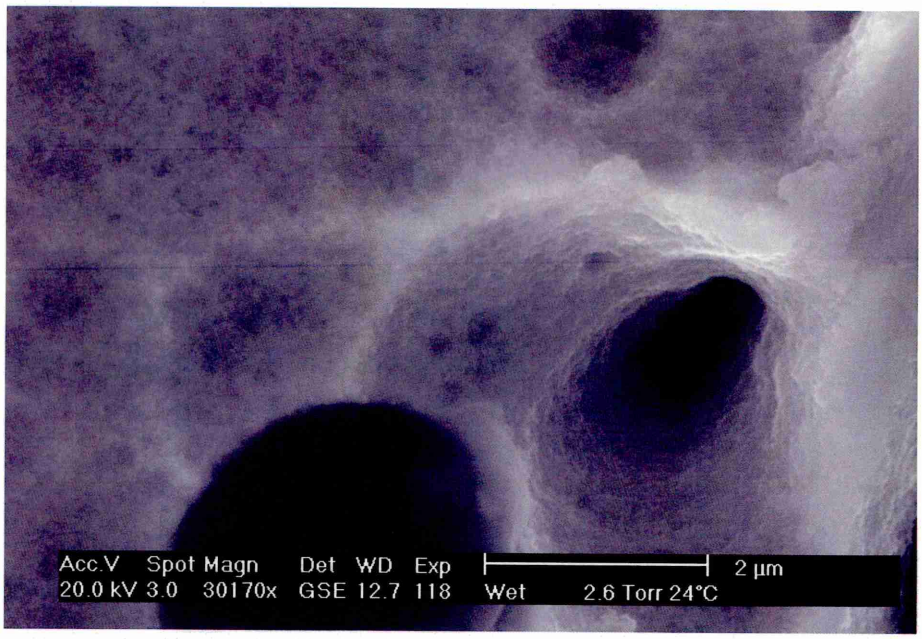

***Plate 4.39** – Surface pore on electro-chemically treated surface*

4.7 Chapter References

[1] Hartshorn S.R., Structural Adhesives – Chemistry and Technology, Ed Hartshorn S.R., Chapter 8, p347-403, Plenum, ISBN 0-306-42121-6, 1986

[2] Boyes R., "Adhesive Bonding of Stainless Steel: Strength and Durability", PhD Thesis, Sheffield Hallam University, 1998

[3] M^{C}Cann S., Final Year Project, Sheffield Hallam University, 1997

[4] Maddison A., Arrowsmith D.J., "The use of perforated lap shear specimens to test the durability of adhesive-bonded aluminium", International Journal of Adhesion and Adhesives, vol. 7, no. 1, January 1987, p15-24

Chapter 5
Dynamic Performance of Stainless Steel Adhesive Joints

5.1 Introduction

Engineering components and structures frequently operate under applied cyclic loads that result in catastrophic failing, known as *fatigue failure*. The severity of failure in this form has now made fatigue resistance a priority design parameter, as a consequence of structures failing at loads below their static capacity. It has been recognised since 1830[1] that a metal subjected to a repetitive or fluctuating stress will fail at a stress much lower than that required to cause fracture from the application of a single load. Three basic factors have been identified to cause fatigue failure[1];

- Maximum tensile stress of sufficiently high value
- Large enough variation or fluctuation in the applied stress
- Sufficiently large number of cycles of applied stress

In addition, other factors may include; stress concentration, corrosion, temperature, overload, and stresses that may alter the conditions for fatigue.

The cyclic form of the applied stresses may be in a variety of forms, these include; (i) reversed stress, where the maximum and minimum stresses are equal, (ii) repeated stress, where the maximum and minimum stresses are not equal and (iii) irregular or fluctuating stress cycle, where the maximum and minimum stress are unpredictable for example aeroplane wings and marine structures subjected to wave damage.

Figure 5.1 shows a schematic of a stress or load cycle and associated parameters, where;

P_{max} = maximum applied load
P_{min} = minimum applied load
P_r = load range
P_m = mean applied load
P_a = load amplitude

Where, the mean load is the algebraic mean of the maximum and minimum loads in the fatigue cycle,

$$P_m = \frac{(P_{max} + P_{min})}{2} \qquad (5.1)$$

load range, P_r, is given by,

$$P_r = P_{max} - P_{min} \qquad (5.2)$$

load amplitude, P_a,

$$Pa = \frac{\Pr}{2} \qquad (5.3)$$

load ratio, R,

$$R = \frac{P\min}{P\max} \qquad (5.4)$$

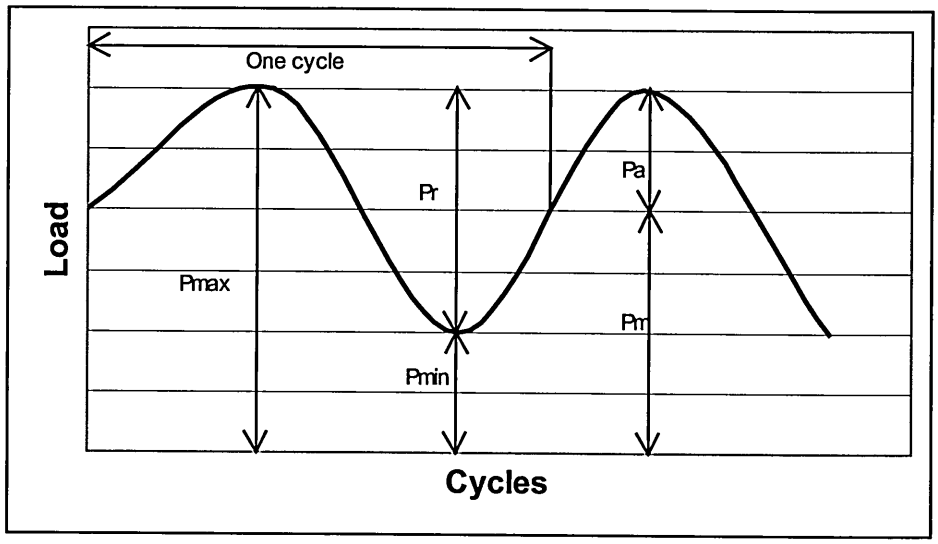

Figure 5.1 *- Cyclic load cycle.*

The basic graphical representation of fatigue data is the stress amplitude versus fatigue life (cycles to failure) plot, which is commonly referred to as the S-N curve. By formulating an S-N plot for matching specimens, an endurance or fatigue limit may be estimated for a comparative stress or load amplitude that does not cause failure of the specimen. The S-N curve is primarily concerned with fatigue failure at high number of cycles, where in general for these conditions the stresses are predominately elastic. As the intensity of applied stress increases the fatigue life of the component is reduced.

When a polymeric material, such as a structural adhesive, is subjected to an applied load a variety of chemical and rheological events occur at a given temperature[2]. Some of the major properties and deformation modes that are important in the fatigue behaviour of polymeric materials are[2];

- Molecular characteristics, such as molecular weight
- Chemical changes, such as bond breakage
- Homogeneous deformation, (elastic, inelastic and viscoelastic)
- Inhomogeneous deformation (crazing and shear banding)

- Morphological changes, such as drawing, orientation and crystallisation.
- Transition phenomena, such as glass-to-rubber and secondary transitions
- Thermal effects, such as hysteretic heating

As with many manufactured materials adhesives contain flaws and defects such as voids and foreign matter, which may act as crack initiation sites. If the applied stress level is sufficiently high the defect or flaw may develop into a macro-crack and propagate. Failure will occur when these cracks have dimensions that permit the crack growth to depend on bulk properties rather than localised properties.

The area of work presented in this chapter concerns the effects of surface pre-treatments, test frequency, load amplitude and the consequence of ageing in an aqueous environment, for adhesive bonded stainless steel single overlap joints, and provides sufficient data to produce characteristic S-N curves.

5.2 Experimental Work

5.2.1 Surface Pre-treatment

In order to evaluate the effects of surface pre-treatment on fatigue performance the parameters of the fatigue test were standardised, as given below;

- Test frequency fixed at 20Hz, this is a typical frequency used to evaluate the fatigue performance of metallic components
- Load ratio set at 0.1
- Tests conducted in standard laboratory conditions, 23±2°C and 50±5% relative humidity
- Specimens bonded with DP490
- Specimens manufactured as described in section 3.5.1
- Fillets left in-tact

Two different surface pre-treatments were considered in the experimental work; alumina grit blasting was chosen because it offers improved bond strength and joint durability, it is also a simple reproducible economically viable process. Alkaline degreasing was chosen as a simple cleaning technique regarded as a recommended minimal treatment used in industry, allowing direct comparisons to be made.

5.2.2 Test Frequency

The fatigue conditions were as described above in surface pre-treatment. However, the tests were carried out at a number of test frequencies. Three test frequencies were selected, namely; 1Hz, 5Hz and 20Hz. Frequencies 1Hz and 5Hz were used to mimic the periodicity of ocean wave damage on marine structures. The following test parameters were used;

- All pre-bonded substrates were alumina grit blasted to standardise the test
- Load ratio set at 0.1
- Tests conducted in standard laboratory conditions, 23±2°C and 50±5% relative humidity
- Specimens bonded with DP490
- Specimens manufactured as described in section 3.5.1
- Fillets left in-tact

5.2.3 Load Ratio

The fatigue test conditions were used as described above, except the test frequency was set at 5Hz. Load ratios of 0.1 and 0.5 were considered. All pre-bonded substrates were alumina grit blasted to standardise the test.

5.2.4 Aqueous Environment

Single overlap joints incorporating the alumina grit blasted surfaces and bonded with DP490, were aged in distilled water at ambient temperature. Fatigue tests were performed as follows;

- Test frequency fixed at 5Hz, this is a typical frequency used to evaluate the fatigue performance of metallic components
- Load ratio set at 0.1
- Tests conducted in distilled water at ambient conditions
- Specimens bonded with DP490
- Specimens manufactured as described in section 3.5.1
- Fillets left in-tact

Fatigue tests were carried out after 4, 24, 48 and 72 weeks. An ambient ageing temperature was selected so no accelerated ageing effects, such as post curing, would be associated with the deterioration of the fatigue specimens.

The fatigue testing schedule is summarised below in Table 5.1.

***Table 5.1** – Summary of fatigue testing schedule*

Experiment	Test Environment	Surface condition	Test frequency (Hz)	Load Ratio (R)	Overlap Area (mm^2)	Bondline thickness (mm)	Ageing Time (weeks)
Surface Pre-treatment	Air	AD	20	0.1	312.5	0.25	N/A
Surface Pre-treatment	Air	GB	20	0.1	312.5	0.25	N/A
Test Frequency	Air	GB	20	0.1	312.5	0.25	N/A
Test Frequency	Air	GB	5	0.1	312.5	0.25	N/A
Test Frequency	Air	GB	1	0.1	312.5	0.25	N/A
Load Ratio	Air	GB	5	0.1	312.5	0.25	N/A
Load Ratio	Air	GB	5	0.5	312.5	0.25	N/A
Aqueous Environment	Water	GB	5	0.1	312.5	0.25	4
Aqueous Environment	Water	GB	5	0.1	312.5	0.25	24
Aqueous Environment	Water	GB	5	0.1	312.5	0.25	48
Aqueous Environment	Water	GB	5	0.1	312.5	0.25	72

5.3 Results

5.3.1 S-N Curves

The S-N curves showing the effects of surface pre-treatment, frequency, variable load ratio and ageing in aqueous environment are given in Figures 5.2 to 5.5 respectively, and given in tabulated form in Tables 5.2 to 5.5 respectively.

5.3.1.1 Surface Pre-treatment, Figure 5.2

Considering Figure 5.2 the following observations can be made with respect to the affects of surface pre-treated condition on the dynamic fatigue performance. At maximum applied loads below 1.8kN the results are inconclusive because tests were terminated and left to run-out. However, at loads greater than 1.8kN the alumina grit blasted specimens showed a much greater fatigue resistance, not only at the same load but even at higher maximum loads per cycle.

5.3.1.2 Test Frequency, Figure 5.3

From Figure 5.3 there was no notable difference observed in the fatigue tests carried out at 5Hz and 20Hz. However, the joints tested at 1Hz exhibited a notable decrease in fatigue life. There was no appreciable improvement in fatigue life at lower loads.

5.3.1.3 Load Ratio, Figure 5.4

It can be seen from Figure 5.4, that the enhanced fatigue life was achieved with a reduced load range. For a given mean load, reducing the stress cycle improves the fatigue life. Also the mean load value compromises fatigue performance despite the reduced load ratio.

5.3.1.4 Aqueous Environment, Figure 5.5

The ageing of single lap joints up to 24 weeks does not appear to significantly alter fatigue performance for all load levels tested. However for the specimens aged for 48 weeks, a marked reduction in fatigue response is observed. Furthermore samples aged for 72 weeks exhibited complete displacement of the adhesive from the bond area.

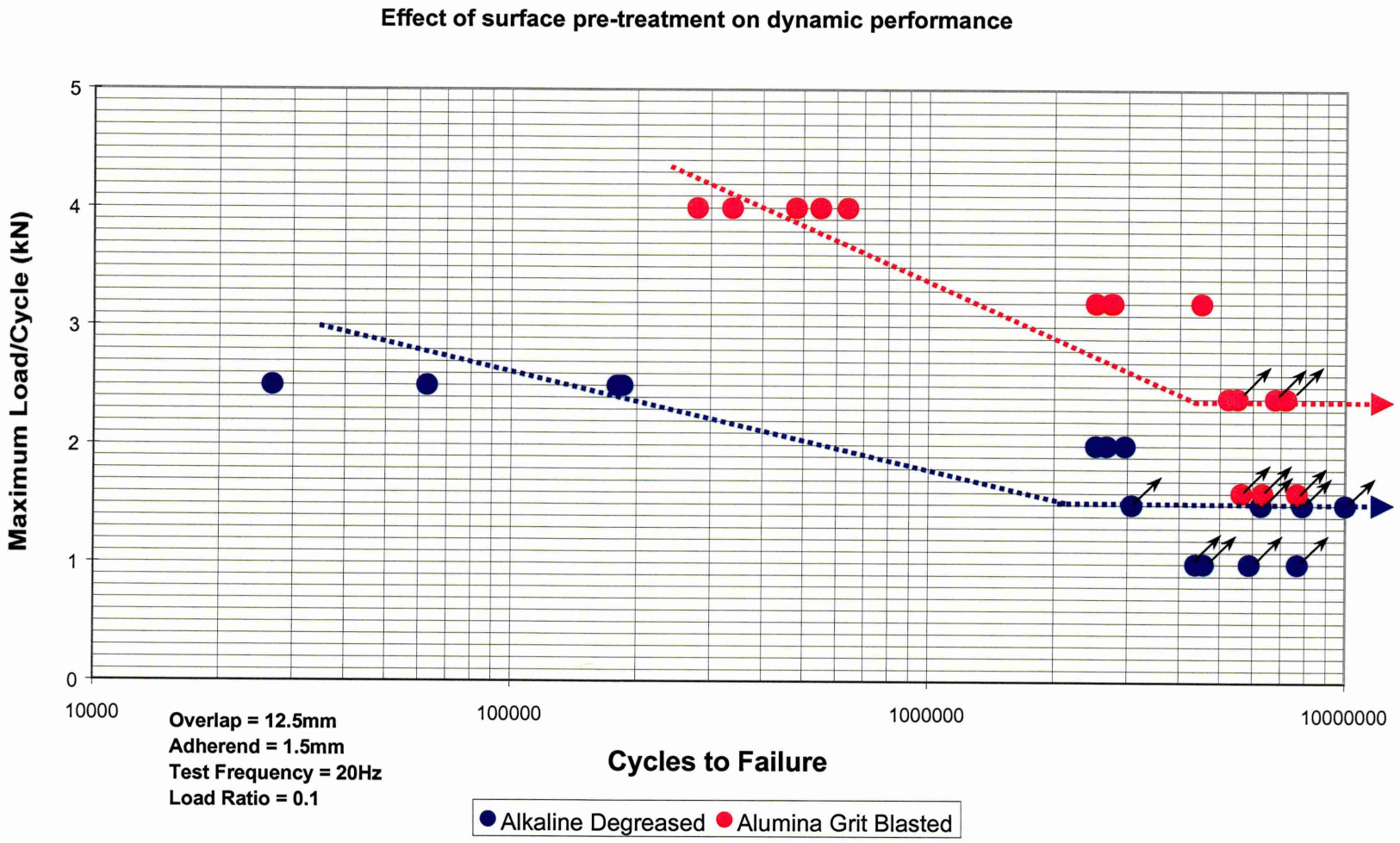

Figure 5.2 – *Effect of surface pre-treatment on dynamic performance*

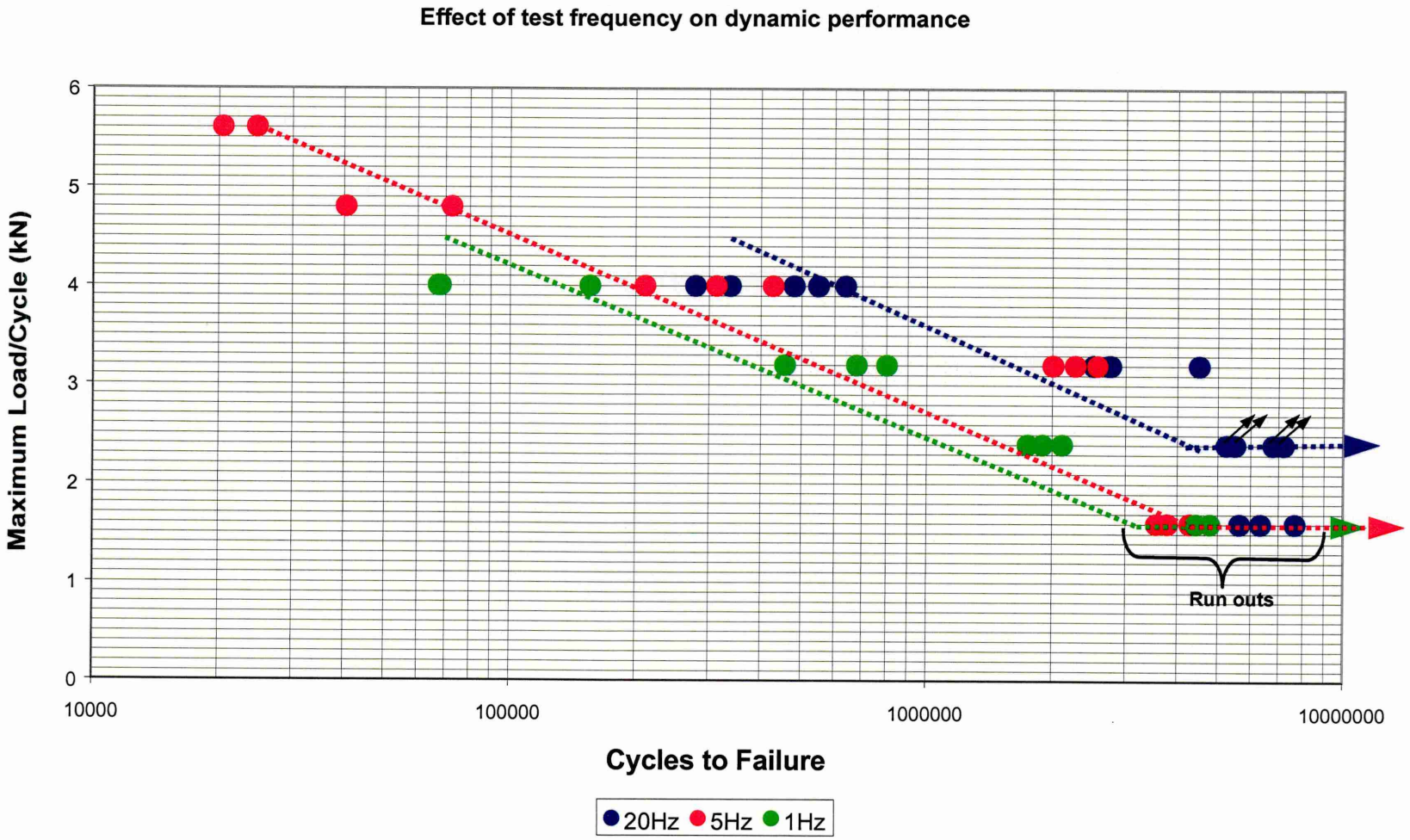

Figure 5.3 – *Effect of test frequency on dynamic performance*

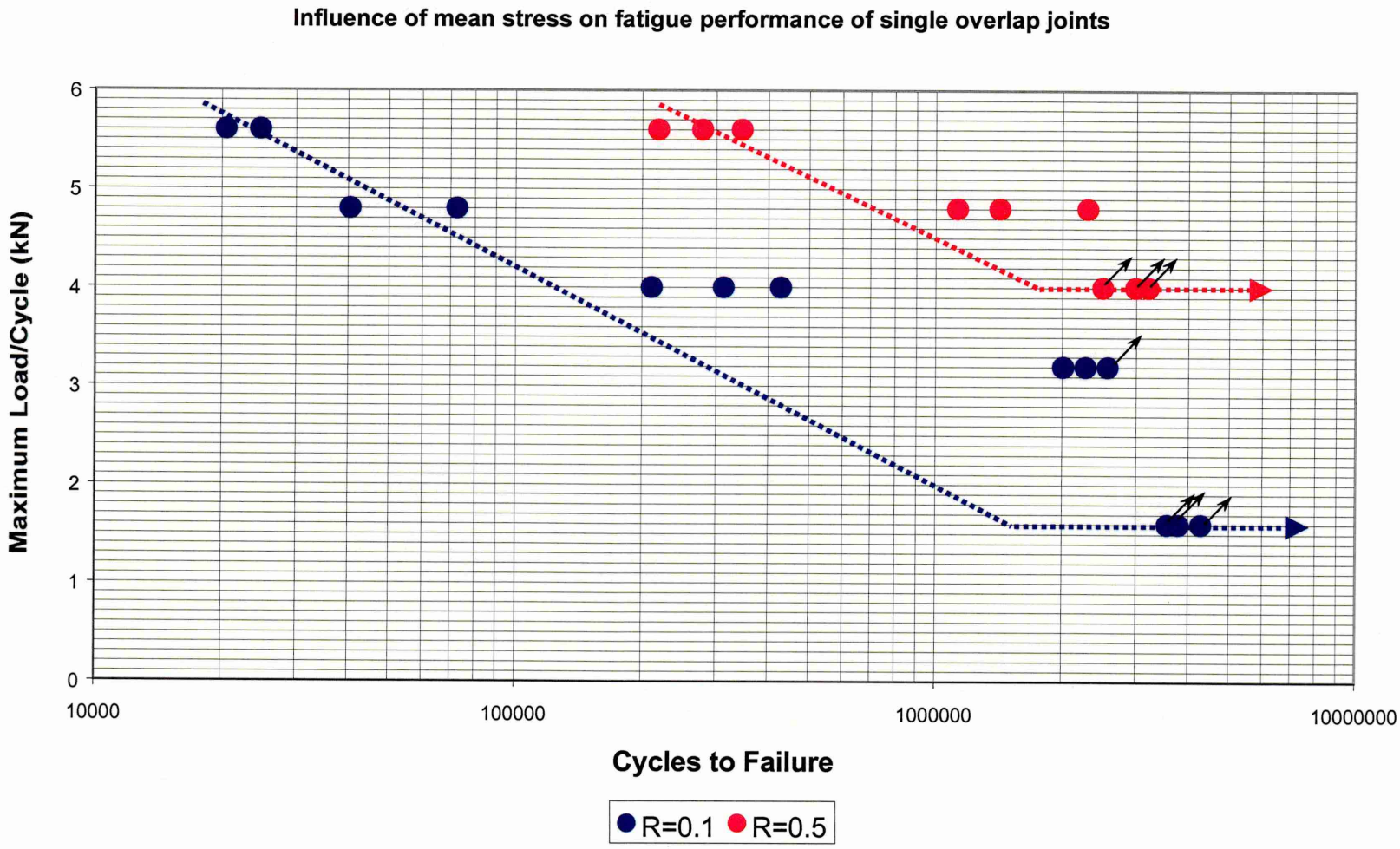

Figure 5.4 – *Effect of R-Ratio on dynamic performance*

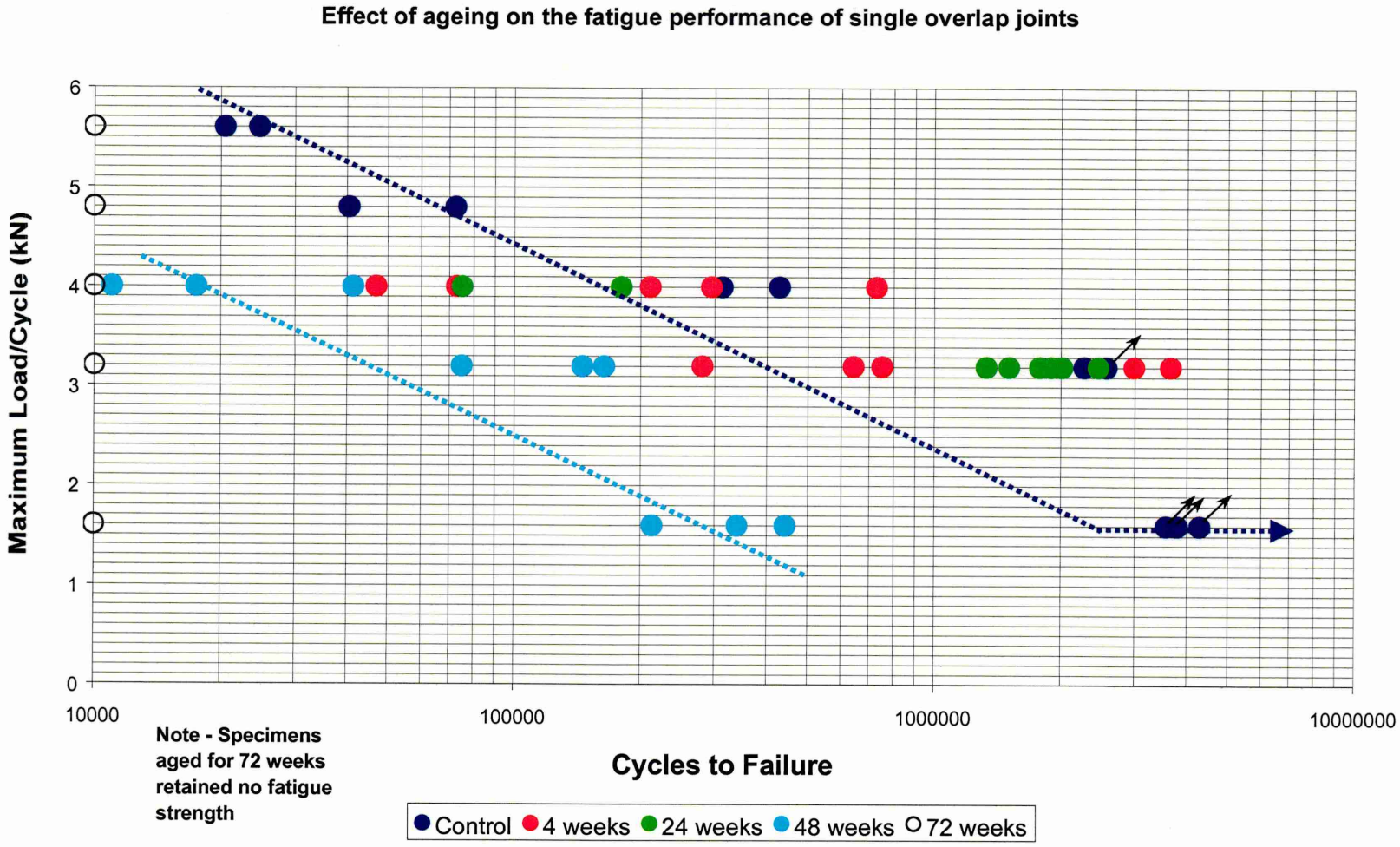

Figure 5.5 – *Effect of aqueous ageing on dynamic performance*

***Table 5.2** - Fatigue performance of alkaline degreased versus alumina grit blasted single lap joints.*

Surface Pre-treatment	Percentage of mean static failure load	Maximum Load (kN)	Minimum Load (kN)	Load Range (kN)	Cycles to Failure (N_f)
AD	20	1	0.1	0.9	4577890 RO
AD	20	1	0.1	0.9	4381240 RO
AD	20	1	0.1	0.9	5893360 RO
AD	20	1	0.1	0.9	7678220 RO
AD	30	1.5	0.15	1.35	7889690 RO
AD	30	1.5	0.15	1.35	9999990 RO
AD	30	1.5	0.15	1.35	3075550 RO
AD	30	1.5	0.15	1.35	6280190 RO
AD	40	2	0.2	1.8	2520830
AD	40	2	0.2	1.8	2671630
AD	40	2	0.2	1.8	2960340
AD	50	2.5	0.25	2.25	26790
AD	50	2.5	0.25	2.25	185000
AD	50	2.5	0.25	2.25	179580
AD	50	2.5	0.25	2.25	62880
GB	20	1.6	0.16	1.44	7671570 RO
GB	20	1.6	0.16	1.44	5646540 RO
GB	20	1.6	0.16	1.44	6336540 RO
GB	30	2.4	0.24	2.16	6788850 RO
GB	30	2.4	0.24	2.16	7205560 RO
GB	30	2.4	0.24	2.16	5504500 RO
GB	30	2.4	0.24	2.16	5244300 RO
GB	40	3.2	0.32	2.88	4510500
GB	40	3.2	0.32	2.88	2739730
GB	40	3.2	0.32	2.88	2516760 RO
GB	40	3.2	0.32	2.88	2766900 RO
GB	50	4	0.4	3.2	278650
GB	50	4	0.4	3.2	337800
GB	50	4	0.4	3.2	480740
GB	50	4	0.4	3.2	550160
GB	50	4	0.4	3.2	639170

Test frequency 20Hz, R = 0.1. AD = Alkaline Degreased, GB = Alumina Grit Blasted.

Table 5.3 - The effect of test frequency on the fatigue performance of single overlap joints.

Percentage of mean static load	Test Frequency (Hz)	Maximum Load (kN)	Load Range (kN)	Cycles to Failure (N_f)
20	20	1.6	1.44	7671570 RO
20	20	1.6	1.44	5646540 RO
20	20	1.6	1.44	6336540 RO
30	20	2.4	2.16	6788850 RO
30	20	2.4	2.16	7205560 RO
30	20	2.4	2.16	5504500 RO
30	20	2.4	2.16	5244300 RO
40	20	3.2	2.88	4510500
40	20	3.2	2.88	2739730
40	20	3.2	2.88	2516760 RO
40	20	3.2	2.88	2766900 RO
50	20	4	3.6	278650
50	20	4	3.6	337800
50	20	4	3.6	480740
50	20	4	3.6	550160
50	20	4	3.6	639170
20	5	1.6	1.44	3789660 RO
20	5	1.6	1.44	3566770 RO
20	5	1.6	1.44	4289920 RO
40	5	3.2	2.88	2567890 RO
40	5	3.2	2.88	2275560
40	5	3.2	2.88	2010000
40	5	3.2	2.88	2011440
50	5	4	3.6	210840
50	5	4	3.6	428240
50	5	4	3.6	312840
60	5	4.8	4.32	40450
60	5	4.8	4.32	72580
70	5	5.6	5.04	24736
70	5	5.6	5.04	20461
20	1	1.6	1.44	4437800 RO
20	1	1.6	1.44	4791400 RO
30	1	2.4	2.16	1894820
30	1	2.4	2.16	2114730
30	1	2.4	2.16	1745320
40	1	3.2	2.88	801040
40	1	3.2	2.88	678150
40	1	3.2	2.88	456760
50	1	4	3.6	67280
50	1	4	3.6	155500
50	1	4	3.6	68150

***Table 5.4** - The effect of the load ratio on the fatigue performance of single overlap joints.*

Percentage of mean static load	R Ratio	Maximum Load (kN)	Load Range (kN)	Cycles to Failure (N_f)
20	0.1	1.6	1.44	3789660 RO
20	0.1	1.6	1.44	3566770 RO
20	0.1	1.6	1.44	4289920 RO
40	0.1	3.2	2.88	2567890 RO
40	0.1	3.2	2.88	2275560
40	0.1	3.2	2.88	2010000
40	0.1	3.2	2.88	2011440
50	0.1	4	3.6	210840
50	0.1	4	3.6	428240
50	0.1	4	3.6	312840
60	0.1	4.8	4.32	40450
60	0.1	4.8	4.32	72580
70	0.1	5.6	5.04	24736
70	0.1	5.6	5.04	20461
50	0.5	4	2.00	2500000 RO
50	0.5	4	2.00	2996730 RO
50	0.5	4	2.00	3211480 RO
60	0.5	4.8	2.40	2300000
60	0.5	4.8	2.40	1127316
60	0.5	4.8	2.40	1421672
70	0.5	5.6	2.80	346144
70	0.5	5.6	2.80	218605
70	0.5	5.6	2.80	278289

Table 5.5 - The influence of ageing duration on the fatigue performance of single overlap joints.

Ageing Duration (weeks)	Percentage of mean static load	Maximum Load (kN)	Load Range (kN)	Cycles to Failure (N_f)
Control	20	1.6	1.44	3789660 RO
Control	20	1.6	1.44	3566770 RO
Control	20	1.6	1.44	4289920 RO
Control	40	3.2	2.88	2567890 RO
Control	40	3.2	2.88	2275560
Control	40	3.2	2.88	2010000
Control	40	3.2	2.88	2011440
Control	50	4	3.6	210840
Control	50	4	3.6	428240
Control	50	4	3.6	312840
Control	60	4.8	4.32	40450
Control	60	4.8	4.32	72580
Control	70	5.6	5.04	24736
Control	70	5.6	5.04	20461
4	40	3.2	2.88	752010 MF
4	40	3.2	2.88	280560 MF
4	40	3.2	2.88	642080 MF
4	40	3.2	2.88	3656300 RO
4	40	3.2	2.88	2991940 RO
4	50	4	3.6	729180
4	50	4	3.6	46980
4	50	4	3.6	73010
4	50	4	3.6	210840
4	50	4	3.6	295180
24	40	3.2	2.88	1330030
24	40	3.2	2.88	1785130
24	40	3.2	2.88	2456970
24	40	3.2	2.88	1505560
24	40	3.2	2.88	1896670
24	40	3.2	2.88	2011440
24	40	3.2	2.88	1779950
24	50	4	3.6	75160
24	50	4	3.6	179760
48	20	1.6	1.44	441450
48	20	1.6	1.44	339460
48	20	1.6	1.44	212910
48	40	3.2	2.88	145120
48	40	3.2	2.88	163710
48	40	3.2	2.88	74860
48	50	4	3.6	41320
48	50	4	3.6	17490
48	50	4	3.6	11010

5.3.2 Fracture Analysis

Electron microscopy and digital macrographs were used to evaluate the fracture surfaces of selected specimens.

5.3.2.1 Surface Pre-treatment

Plates 5.1 and 5.2 show electron micrographs of alkaline degreased and alumina grit blasted surfaces respectively.

***Plate 5.1** – Micrograph of bright annealed surface*

The bright annealed surface which has been degreased only, is characterised only by rolling lines with very little surface artifacts. The smoothness of the surface is a result of the annealing stage, after cold rolling, which takes place in a furnace with a controlled atmosphere that prevents oxidation.

In contrast the alumina blasted adherend exhibits a strongly faceted surface, where a high level of deformation has taken place, this has significantly increased the available interfacial bonding area. Surface coverage is dominated by flake like areas of randomly oriented deformed steel.

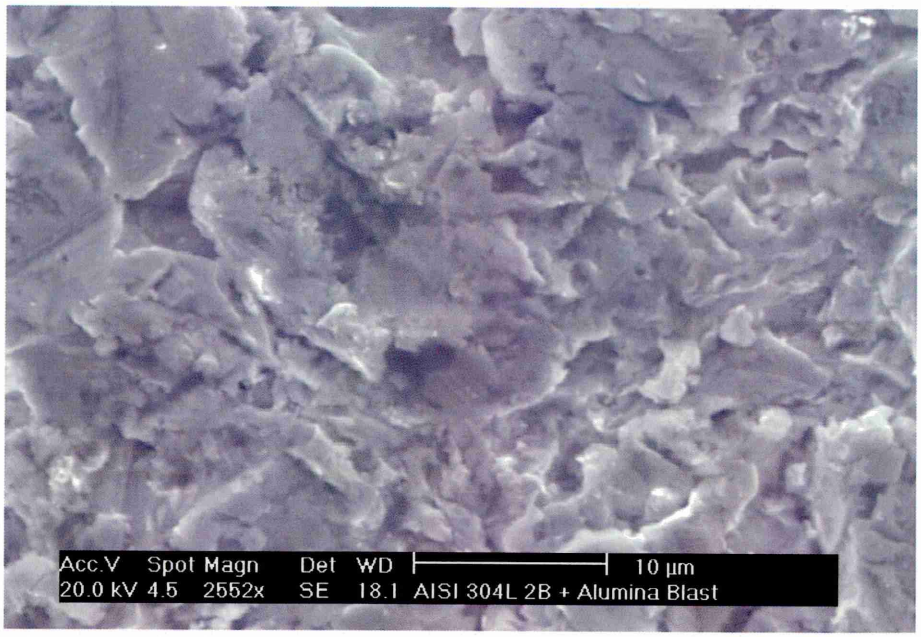

***Plate 5.2** – Micrograph of alumina grit blasted surface*

Visual analysis of the fracture surface revealed two distinct patterns. The bright annealed alkaline degreased joints indicated total adhesive failure, where the adhesive had completely delaminated from one adherend. Figure 5.6 shows a macrograph of a typical fracture for bright annealed specimens.

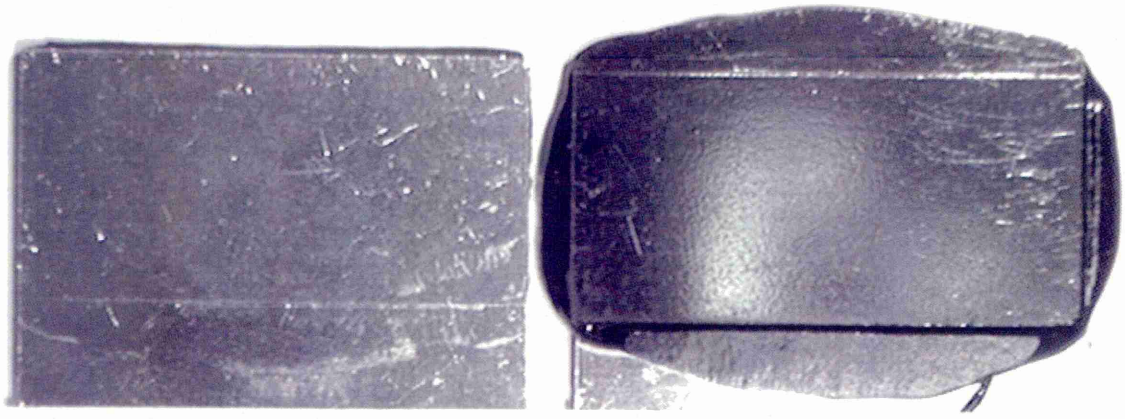

***Figure 5.6** – Typical fracture surface observed on failed joints with bright annealed adherends*

In contrast the alumina blasted samples showed both cohesive failure within the adhesive, and interfacial failure near the interface. Figure 5.7 reveals a typical fracture surface for mechanically roughened specimens.

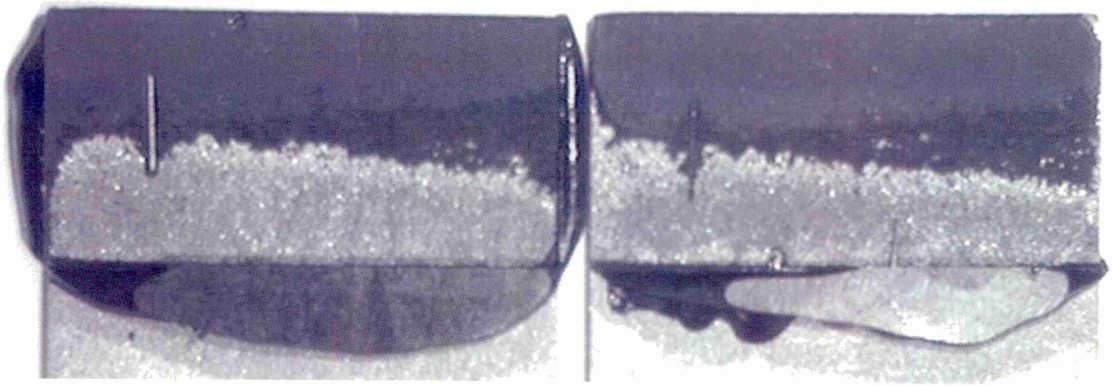

***Figure 5.7** – Typical fracture surface observed on failed joints with mechanically roughened adherends*

5.3.2.2 Test Frequency

Visual inspection of fracture surfaces did not reveal any significant changes as a result of test frequency. Figure 5.8 shows a typical failed specimen. However more detailed micrographs using SEM have highlighted the differences in crack growth behaviour, taken approximately from area 1 in Figure 5.8. Plates 5.3 and 5.4 are specimens tested at 1 and 5Hz respectively.

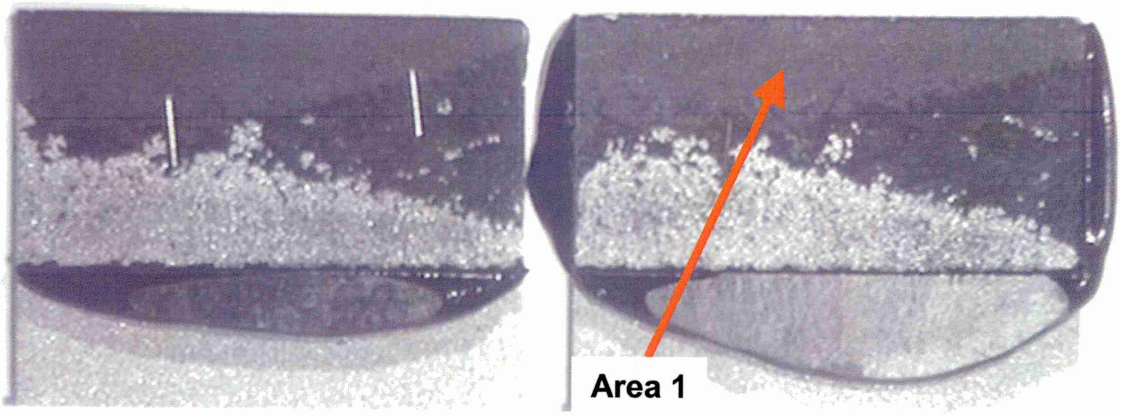

***Figure 5.8** – Typical fatigue fracture surface from a joint incorporated in the effect of frequency trials*

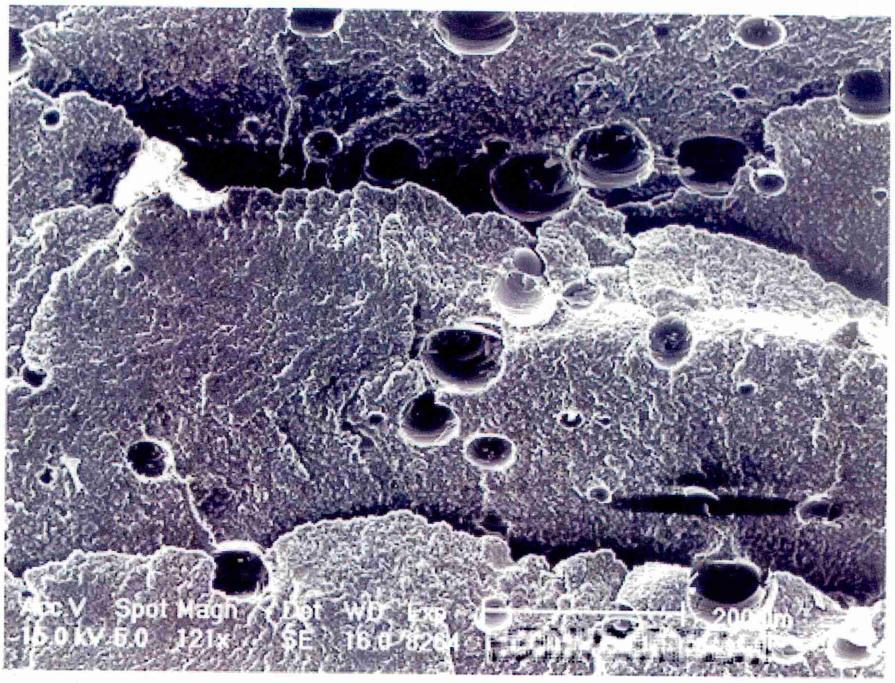

***Plate 5.3** – Micrograph of specimen tested at 1Hz*

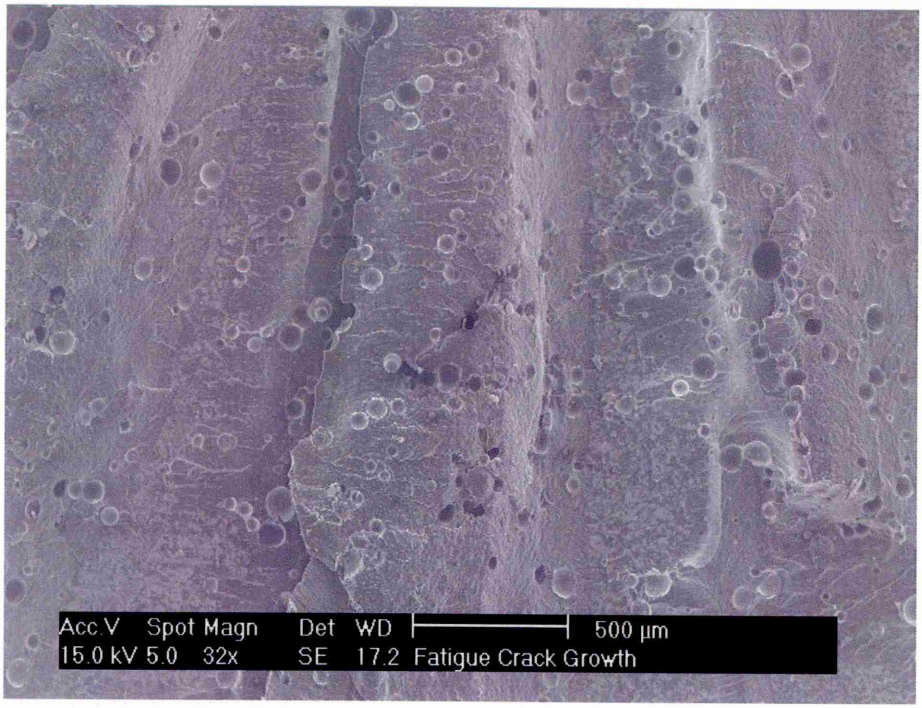

***Plate 5.4** – Micrograph of specimen tested at 5Hz*

Plates 5.3 and 5.4 both reveal characteristic fracture surfaces for relatively brittle adhesives that have been stressed in the mode II direction of in-plane shear. High stresses ahead of initially coplanar cohesive crack causes microcracks to form at 45° to the plane of the bond. The length of the fatigue damage striations differs between frequencies, in Plate 5.3 a typical damage zone

is approximately 200μm in length, compare this to Plate 5.4 where the test frequency has been increased and the damage zone is typically 500μm long. As load or dynamic damage increases the microcracks grow until they reach the interface, where they link and extend. The linking of microcracks is shown Plate 5.5, demonstrating the stepping down of the crack towards the interface, in addition the shearing nature of the crack is observed from the fracture of silica filler material. Interesting to note the lengths of the striations, before the mouth of the microcracks intersect with the near interface region, are larger in specimens tested at higher frequencies.

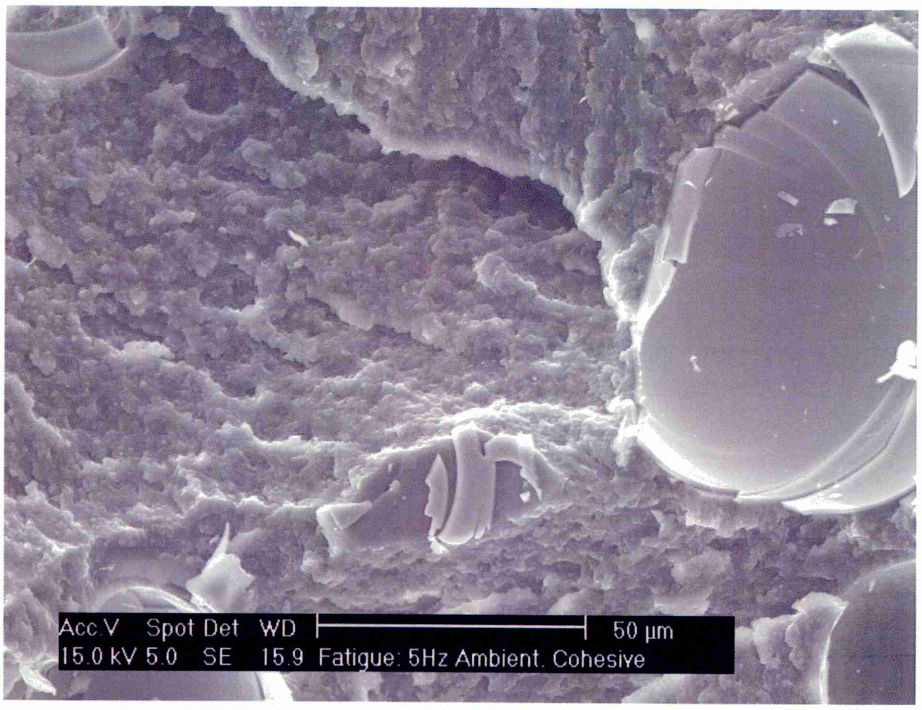

Plate 5.5 *– Microcrack linkage from dynamic damage*

5.3.2.3 Aqueous Environment

Figures 5.9 shows the typical fracture face of specimens that have been fatigue tested to failure after 48 weeks of exposure. It appears the edges of the bond area have undergone degradation from environmental attack. For specimens exposed for 72 weeks, there was total separation of the adhesive layer from the stainless steel substrate, as shown in Figure 5.10. The river markings indicate how water has gradually ingressed into the bonded region. It appears excessive exposure will result in the complete deterioration of the bond integrity.

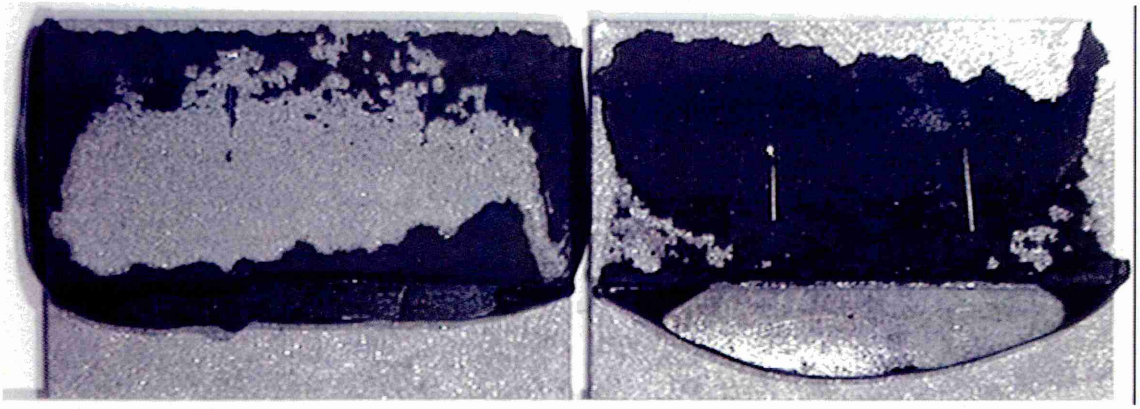

Figure 5.9 – *Fracture faces of specimen fatigue tested to failure after 48 weeks exposure*

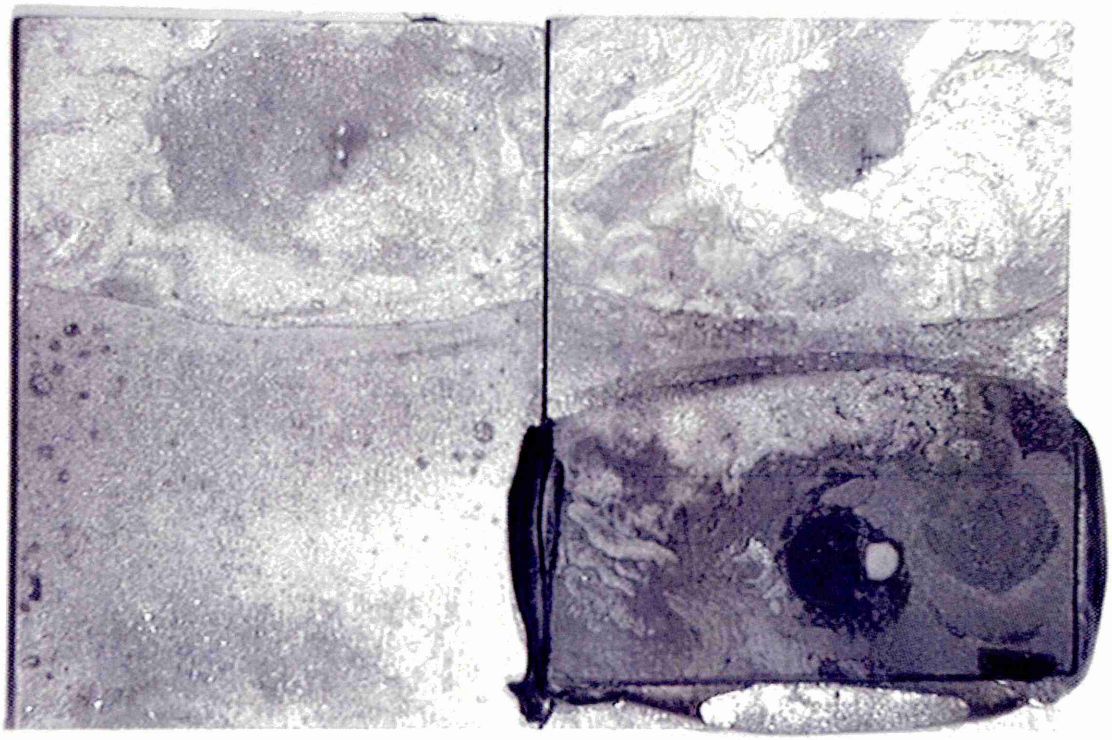

Figure 5.10 – *Complete adhesive delamination after 72 weeks exposure*

5.4 Discussion

5.4.1 Effect of surface pre-treatment

The fatigue performance of adhesive bonded stainless steel single lap joints has been assessed using two surface pre-bonding treatments. It appears the fatigue response of the specimens is enhanced when the adherends were mechanically roughened using alumina particles. It is often viewed[3-5], that some form of mechanical abrasion will increases the measured joint strength of single lap joints bonded with epoxides. The surfaces generated do not necessarily provide cavities or sites that would be able to promote mechanical interlocking or keying of the adhesive with the substrate, this is in agreement with comments by Kinloch[6]. However, abrasive processes will completely remove the original oxide layer on the stainless steel surface, thus displacing any lubricating oils, release agents and scale deposited from the manufacturing process. Hence any weak boundary layers between the adhesive and adherend will be kept to a minimum. The removal of foreign matter will also improve the wettability of the adhesive and aid spreading, which will be of particular importance since the area available for bonding has been considerable increased. The improvement in fatigue life using grit blasting also has aesthetic appeal, because only one side of the adherend is treated the opposing side will not hinder any architectural applications. The grit blasting treatment is a relatively simple process, well suited to industrial applications, however it does appear that the complexity of the degreasing stage after blasting will influence dynamic performance.

5.4.2 Effect of frequency

The response of DP490 is frequency dependent. It has been reported[6] at lower frequencies the adhesive is subjected to creep strains, and that the straining will not only be concentrated at the overlap edges but throughout the adhesive layer (which is easily envisaged with the present work where relatively short overlaps are used). Once the creep strains have accumulated to a critical level the adhesive joint will fail prematurely. As the cyclic frequency is increased these strains do not have enough time to form or build up, and the load will be removed before the adhesive has time to suffer any creep deformation.

5.4.3 Effect of R-Ratio

The effect of R-Ratio, or mean load, has been found to have a significant effect on the fatigue response of single lap joints. If the test data is plotted, maximum load versus cycles to failure, then it appears that the increase in load range has detrimental effects on fatigue life, rather than the maximum load imposed per cycle. However, if the fatigue data is plotted load amplitude versus cycles to failure as shown in Figure 5.11, than a different view is obtained. As the load ratio was increased the load amplitude of the fatigue cycle was reduced, which had a deleterious effect on fatigue performance. It is suggested therefore that the fatigue response of stainless steel joint bonded with DP490 can not be determined from the knowledge of a single load ratio.

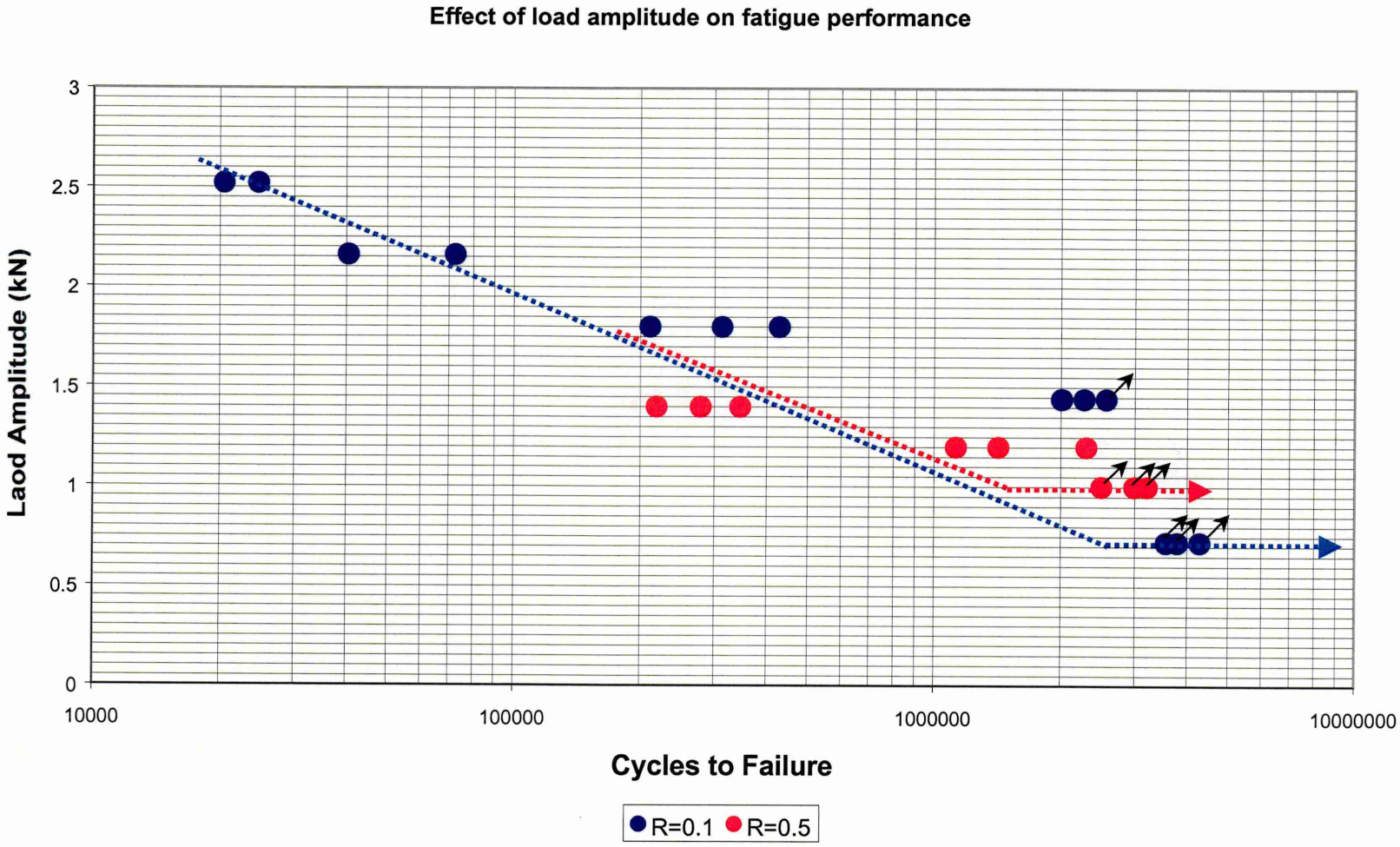

Figure 5.11 – *Effect of R-Ratio when plotted against load amplitude*

5.4.4 Effect of Ageing

Mechanically treating the adherends, when exposing to room temperature water immersion reduces long term fatigue performance. Specimens aged for duration of 24 weeks show no evidence of deterioration in fatigue life. However, above 24 weeks the adhesive/adherend interface began to suffer from environmental degradation, where moisture may have started to depress the degree of intrinsic adhesion. The continual seepage of moisture into the interface region may have ruptured chemical bonds and created an unstable oxide layer. There is evidence from Figure 5.9 that after 48 weeks exposure the edges of the bond have already suffered some form of environmental attack, and after 72 weeks exposure complete adhesive delamination has occurred.

The alumina grit blasting technique forms large voids on the surface. It is suggested these voids, which will be situated between the metal oxide and adhesive, are possible locations for air entrapment. Other research[7] on alumina grit blasted surfaces has suggested that these large interfacial voids will act as points of stress concentration and result in intrinsically weak adhesive-metal interface. Therefore, when moisture does attack and penetrate the adhesive layer these interfacial macro-voids will readily fill the interfacial region with water. As the rate of water penetration intensifies the degree of environmental attack will become more detrimental. As the ageing of the single lap joints increases the amount of water entering the adhesive-metal oxide region will increase. This mechanism of attack may explain why the fatigue performance of stainless steel adhesive joints treated with alumina blast media, deteriorates markedly once ageing has exceeded 48 weeks.

5.5 Comparison with other joining techniques

To further encourage the use of structural adhesives in primary and secondary loading applications, the dynamic performance must be compared with the more traditional joining techniques such as spot welding. Figure 5.12 shows the fatigue performance of AISI 304L stainless steel lap joints. The fatigue data for spot welded lap joints[8] is presented, where an adherend thickness, t, of 1.5mm and 4mm was used. The adhesive joint data was taken from the results in shown in Figure 5.3.

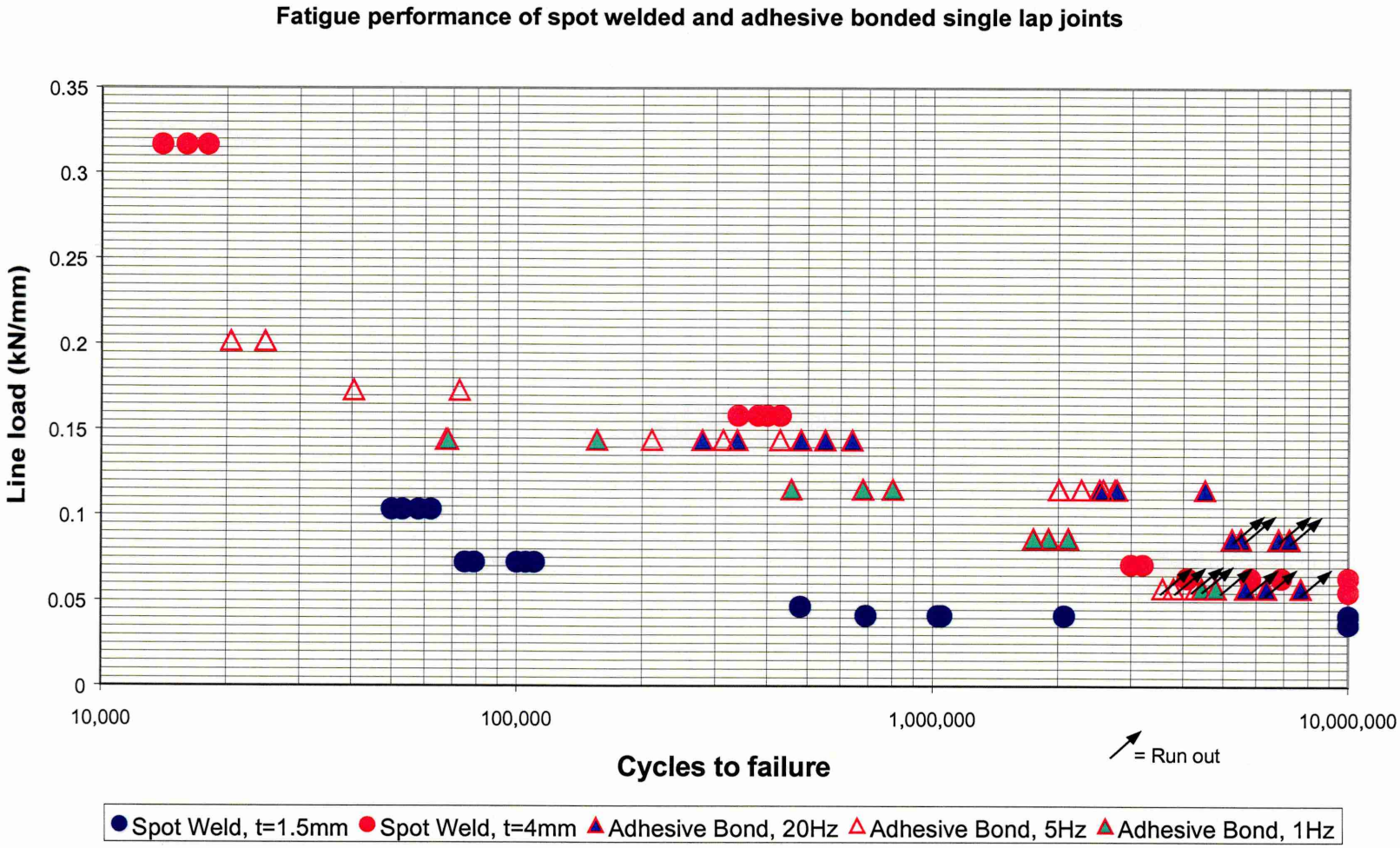

Figure 5.12 – *Comparison of fatigue performance of spot welded and adhesive bonded single lap joints*

5.6 Chapter References

[1] Dieter G.E., Mechanical Metallurgy, McGraw Hill Materials Science and Metallurgy, ISBN 0-07-100406-8, 1988.

[2] Hertzberg R.W. and Manson J.A., Fatigue of Engineering Plastics, Academic Press, ISBN 0-12-343550-1, 1980.

[3] Critchlow G.W., Brewis D.M., "Influence of surface macroroughness on durability of epoxide-aluminium joints", International Journal of Adhesion and Adhesives, vol. 15, 1995, p173-176.

[4] Brockmann W., Durability of Structural Adhesives, Ed Kinloch A.J., Chapter 8, Applied Science Publications, ISBN 0-85334-214-8, 1983.

[5] Ring-Groth M., "The adhesive bonding of stainless steel", Licentiate Thesis, Luleå University of Technology, 1998.

[6] Kinloch A.J., Adhesion and Adhesives - Science and Technology, Chapman Hall, London, ISBN 0-412-27440-X, 1987.

[7] Kinloch A.J., Little M.S.G., Watts J.F., "The role of the interface in the environmental failure of adhesive joints", Acta Materialia, vol. 48, 2000, p4543-4553.

Chapter 6 Single Lap Joint Properties

6.1 Introduction

The single overlap is one of the most commonly occurring joints and is the configuration most often used for testing adhesives. However, when loaded in tension the stress state becomes complex. The loads in a single lap joint are not collinear, therefore a bending moment must exist and the joint will rotate to find a common axis as shown in Figure 6.1. Supplementary to the shear stresses acting in the adhesive layer there will be tearing stresses at the joint ends, commonly referred to as peel stresses.

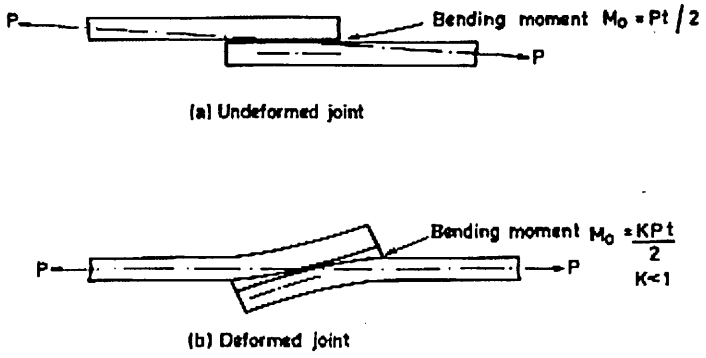

***Figure 6.1** – Joint rotation of a single lap joint as a function of the bending moment*[1]

Stress analyses of adhesive joints is a complex problem. The joint is not made up of separate elastic materials with defined mathematical geometry. The adhesive 'system' consists of adherends that are usually rough and have an oxide layer, the thickness and properties of which may be difficult to determine. A primer is often applied prior to bonding where the thickness and properties are not easily resolved. In addition adhesive properties may differ between the adhesive within a joint or those from bulk specimens.

This chapter will focus on two topics. Firstly, the calculation of elastic rotation within a single lap joint as a function of adherend thickness and overlap length, using analytical and experimental methods. Secondly, the effect of overlap length, spew fillets and adherend thickness on joint strength will be addressed.

6.2 Single Lap Joint Analysis

The simplest shear strength analysis of single lap joints is given by;

$$\tau = \frac{P}{bl} \qquad (6.1)$$

Where; P = applied load

b = overlap width

l = overlap length

τ = shear stress

Equation 6.1 assumes the adherends are rigid and the adhesive will only deform in shear, as shown in Figure 6.2, where the adherend tensile stress will decrease linearly to zero over the overlap length. However, if the adherends are elastic and able to deform as depicted in Figure 6.3, the maximum tensile stress for the upper adherend is at point A and falls to zero at B. Therefore the tensile strain at A is larger than at B, and the strain must progressively reduce over the overlap length. The distorted segments of the adhesive layer in Figure 6.3 represents the phenomenon called differential shear.

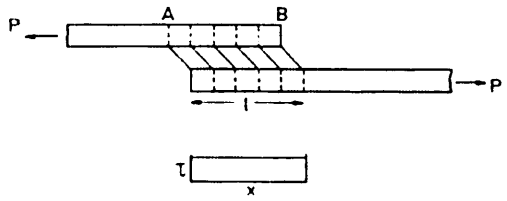

***Figure 6.2** – Deformations in a loaded single lap joint with rigid adherends*[1]

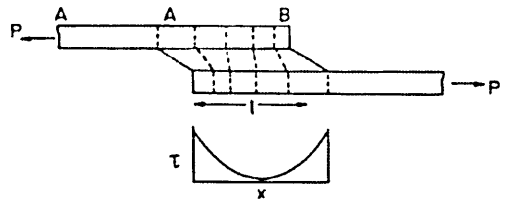

***Figure 6.3** – Deformations in a loaded single lap joint with elastic adherends*[1]

The pioneering work of Volkersen[2] in 1938 and, Goland and Reissner[3] in 1944 was limited because it assumed the shear and peel stresses were constant across the adhesive thickness. The shear was assumed to be a maximum at the overlap end, and not zero as it must be at a free surface, and the shear of the adherend was neglected. Volkersen's analysis did not take into account, firstly the bending moment and secondly the bending and rotation of the adherends. Goland and Reissner did take rotation into account by introducing the bending moment factor, k, which related to the bending moment on the adherend at the end of the overlap, M_O, by;

$$M_o = kP\frac{t}{2} \qquad (6.2)$$

Where; P = applied load

t = adherend thickness (adhesive layer omitted)

As the applied load was increased, the overlap will rotated bringing the line of action of the load closer to the centre line of the adherends as shown in Figure 6.3. The bending moment factor was further developed by Hart-Smith[4].

6.3 Elastic Rotation of Single Overlap Joints

6.3.1 Analytical Solution

The following analytical derivation, developed by Nordberg and the author[5], is based upon beam theory pertinent to small deflections with small angles of rotation. Considering a single overlap joint loaded in tension; due to the non-symmetry of the loading path, a bending moment is introduced and the joint rotates to bring the load to a common axis that reduces the bending moment. If it is assumed all sections of the joint act elastically, the rotation is comparable with the rotation of a cantilever beam as shown in Figure 6.4, where the angle of rotation (θ_{max}) and the length of the beam (L) are analogous with the angle of rotation due to the bending moment (θ_m) and the half grip to grip distance (a), as illustrated in Figure 6.5. However, in an adhesively bonded single overlap joint there is some resistance to rotation from the adhesive bond strength, more specifically the peel stresses. This analogy is represented in Figure 6.6.

From Figure 6.7, the load, P, is divided into a shear force by:

$$P \times \cos\theta \qquad (6.3)$$

and a peel force by:

$$T \times P \qquad (6.4)$$

Where θ is the angle of rotation. For small θ:

$$P \times \cos\theta = P \qquad (6.5)$$

The stress distribution in the sheet due to the shear load moment is found from :

$$\int \sigma(\chi) d\chi = P \qquad \text{and} \qquad \int \sigma(\chi) \cdot \chi \cdot d\chi = 0 \qquad \text{to be:}$$

$$\sigma = \frac{2P}{t}\left(2 - 3\frac{\chi}{t}\right) \tag{6.6}$$

Where χ = distance from the sheet interface, resulting in a maximum stress at the inner surface of:

$$\sigma = -\frac{4P}{t} \tag{6.7}$$

and the neutral line at:

$$\chi = \frac{2t}{3} \tag{6.8}$$

The shear loading creates a bending moment:

$$M = \frac{2t}{3} \cdot P \tag{6.9}$$

Due to the symmetry, the calculated deflection by the moment and by the transverse load must cancel each other out, thus:

$$\frac{2}{3} t \cdot P \cdot \frac{a^2}{2EI} = T \cdot P \frac{a^3}{3EI} \tag{6.10}$$

Resulting in a value for the factor:

$$T = \frac{t}{a} \tag{6.11}$$

Under line load conditions, (where $P = \frac{P}{b}$, where b = adherend width) and beam theory, the rotation due to the moment and the transverse force can be calculated (assuming no movement occurs in the grips) from

$$\theta_m = \frac{M.a}{E.I} = \frac{2 \cdot t \cdot P}{3} \cdot \frac{a}{EI} \qquad (6.12)$$

where; M = bending moment

a = half grip to grip distance, mm

E = Young's modulus of elasticity, MPa

I = second moment of area (Figure 6.8), given by;

or, $$I = \frac{b.t^3}{12} \qquad (6.14)$$

where; b = joint width, mm

t = adherend thickness, mm

The deflection due to the transverse load, TP, is given by (from Figure 6.6):

$$\theta_T = \frac{TP \cdot a^2}{2 \cdot EI} = \frac{P \cdot t}{a} \cdot \frac{a^2}{2 \cdot EI} \qquad (6.15)$$

Since:

$$\theta_{Total} = \theta_{Moment} - \theta_T = \theta \qquad (6.16)$$

The total net rotation is given by:

$$\theta = \frac{2 \cdot t \cdot P}{3} \cdot \frac{a}{EI} - \frac{P \cdot t}{2} \frac{a}{EI} = \frac{P \cdot t \cdot a}{6.EI} = \frac{2 \cdot a}{E \cdot t^2} \cdot P \qquad (6.17)$$

If there is a gap between the two sheets (or adhesive bondline), the angle of rotation, θ, can be calculated from

$$\theta = \frac{2 \cdot z \cdot a}{E \cdot t^2} \cdot P \qquad (6.18)$$

The 'z' factor is given by:

$$z = \frac{3 \cdot c}{2 \cdot t} + \frac{6 \cdot t + 9 \cdot c}{6 \cdot t + 4 \cdot c} \qquad (6.19)$$

where a = "free" half-length of the specimen or sheets.
t = sheet thickness.
2c = distance between sheets or bondline thickness.
θ = rotation in Radians

The 2 dimensional model of an adhesive joint is shown in Figure 6.9. The stresses and rotations are calculated in a similar manner by superimposing solutions for the two loads, and for reasons of symmetry, setting the displacement at the length (a+e) to nil. The solution is similar to equation 6.17 but incorporates an effective half length, a^*:

$$\theta = \frac{2 \cdot a^*}{E \cdot t^2} \cdot P \qquad (6.20)$$

Where:

$$a^* = a \cdot \left(1 - 2 \cdot \frac{e}{a} + 1.5 \cdot \left(\frac{e}{a} \right)^2 \right) \qquad (6.21)$$

Where e = half the overlap length.

Single overlap adhesive joints will invariably have an overlap length and adhesive thickness. To determine the rotation in adhesive joints the equation must combine both the a* and z factors, thus:

$$\theta = \frac{2 \cdot a^* \cdot z}{E \cdot t^2} \cdot P \qquad (6.22)$$

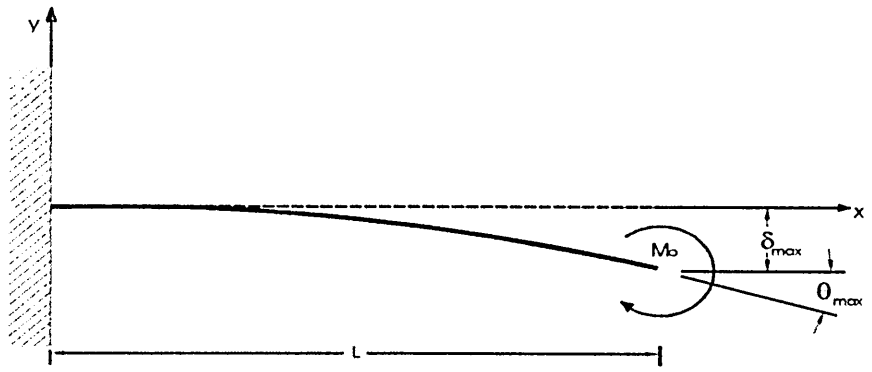

$$\delta = \frac{M_o.x^2}{2E.I} \qquad \delta_{max} = \frac{M_o.L^2}{2E.I} \qquad \theta_{max} = \frac{M_o.L}{E.I}$$

***Figure 6.4** – Deflection of a cantilever beam, rotation due to moment*[6]

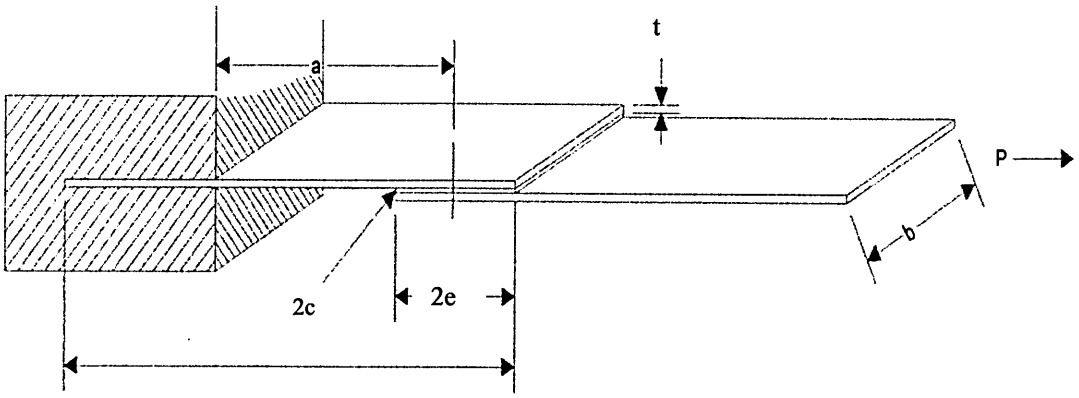

***Figure 6.5** – Adhesive joint configuration*

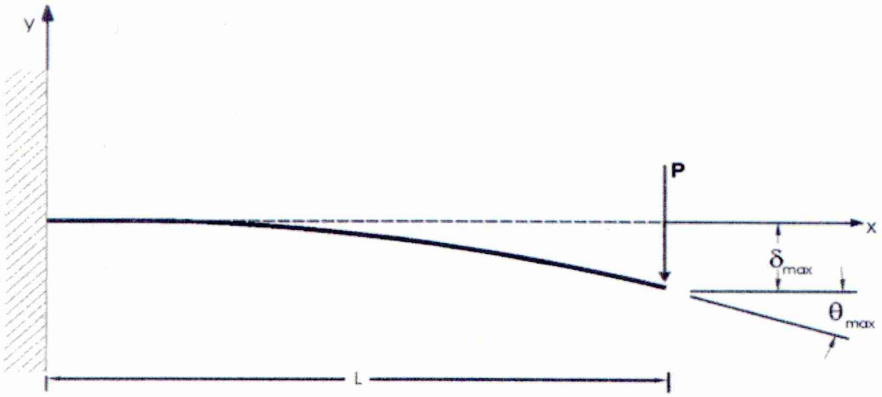

$$\delta = \frac{P.x^2}{6E.I}.(3L - x) \qquad \delta_{max} = \frac{P.L^3}{3E.I} \qquad \theta_{max} = \frac{P.L^2}{2E.I}$$

Figure 6.6 *– Deflection of a cantilever beam, rotation due to load*[6]

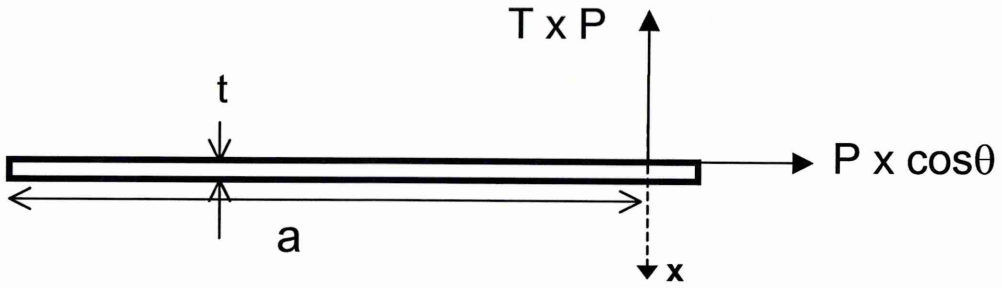

Figure 6.7 *– Schematic load distribution in a lap joint*

AREA	MOMENT OF INERTIA
$A = b.h$	$I_x = \frac{b.h^3}{3}$
$x_c = \frac{b}{2}$	$I_y = \frac{h.b^3}{3}$
$y_c = \frac{h}{2}$	$I_{xc} = \frac{b.h^3}{12}$
	$I_{yc} = \frac{h.b^3}{12}$

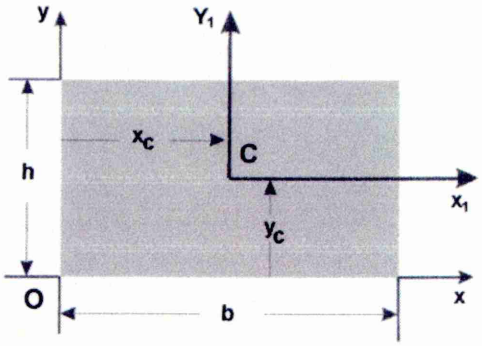

Figure 6.8 *– Second moment of area for a rectangular plane*[6]

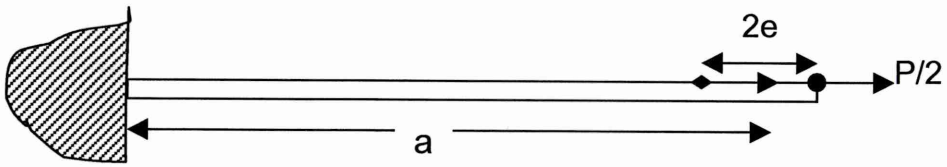

Where: 2e = overlap length

P = applied load

a = half grip to grip distance

Figure 6.9 *– Schematic load distribution in a double line load lap joint*

6.4 Calculation of Joint Rotation

6.4.1 Experimental Procedure

Single overlap adhesive joints were manufactured as described in section 3.5.1. All the specimens consisted of AISI 304L stainless steel substrates with a 2B finish. The bondable region of the overlap was alumina grit blasted, section 3.4.2, to attain suitable bond strength. Table 6.1 below details the specimen dimensions used in this study.

***Table 6.1** – Specimen dimension and geometry's*

Overlap Length (mm)	Adherend Thickness (mm)	Bondline Thickness (mm)	Fillets Intact
12.5	1.5	0.25	No
20	1.5	0.25	No
30	1.5	0.25	No
40	1.5	0.25	No
12.5	3.0	0.25	No
20	3.0	0.25	No
30	3.0	0.25	No
40	3.0	0.25	No

Once all adhesive joints were fully cured, a piece of mirrored glass measuring 15mm x 10mm was attached using double sided sticky tape to one side of the overlap as shown in Plate 6.1. To determine the rotation of the overlap with respect to an applied load, a sample was placed into the grips of the tensile testing machine with the side with the mirrored glass facing out. A laser was mounted 3m away from the tensile test machine and aimed at the mirrored glass. Above the laser a board was erected such that graph paper could be attached to it, this set-up is shown schematically in Figure 6.10. As the load was applied to the adhesive joint the overlap rotated to find a common axis, as rotation commences the reflected laser beam travel upwards. Once the value of the applied load was established a corresponding mark was made on the graph paper where the reflected laser beam landed. Using simple trigonometry the total rotation of the joint was determined. For each dimension detailed in Table 6.1 a maximum of 4 specimens were constructed, 3 were used to measure joint rotation and the remaining joint was loaded and then unloaded and subsequently inspected to find the load required to produce plastic deformation in the adherends.

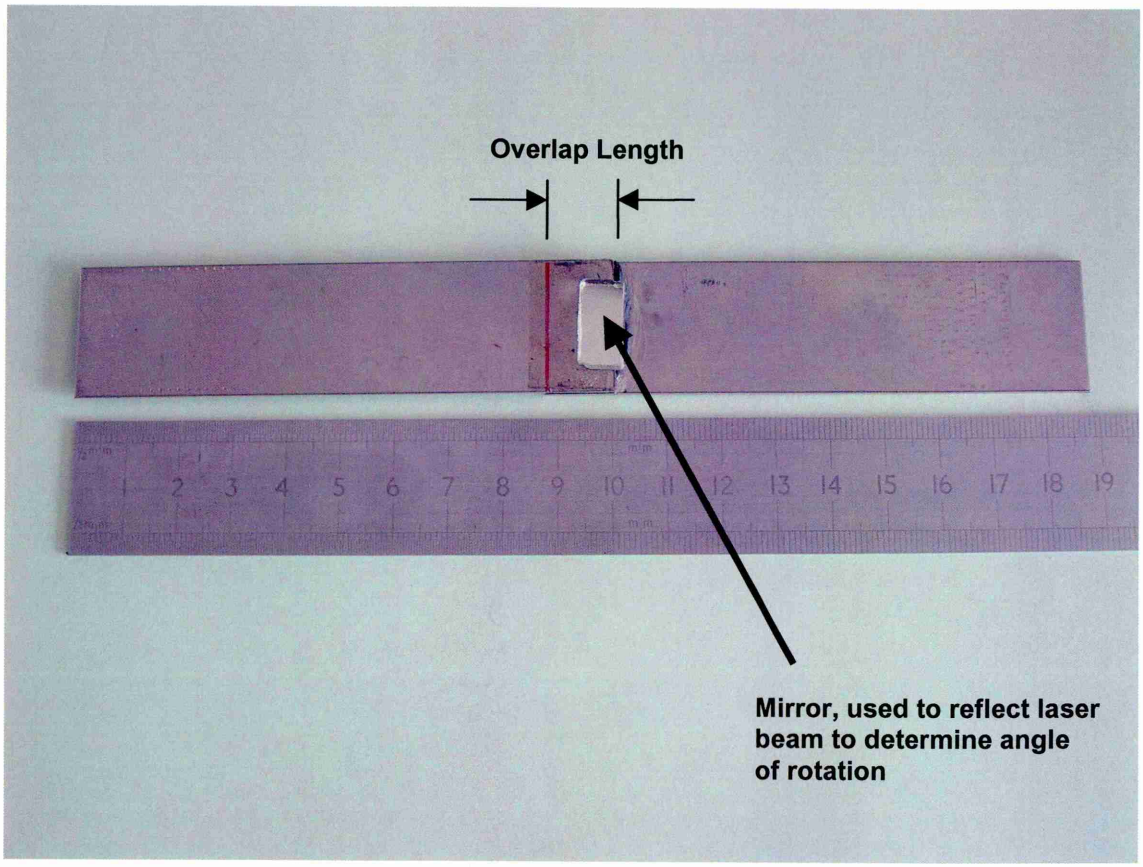

Plate 6.1 *– Adhesive joint preparation used for overlap rotation measurements*

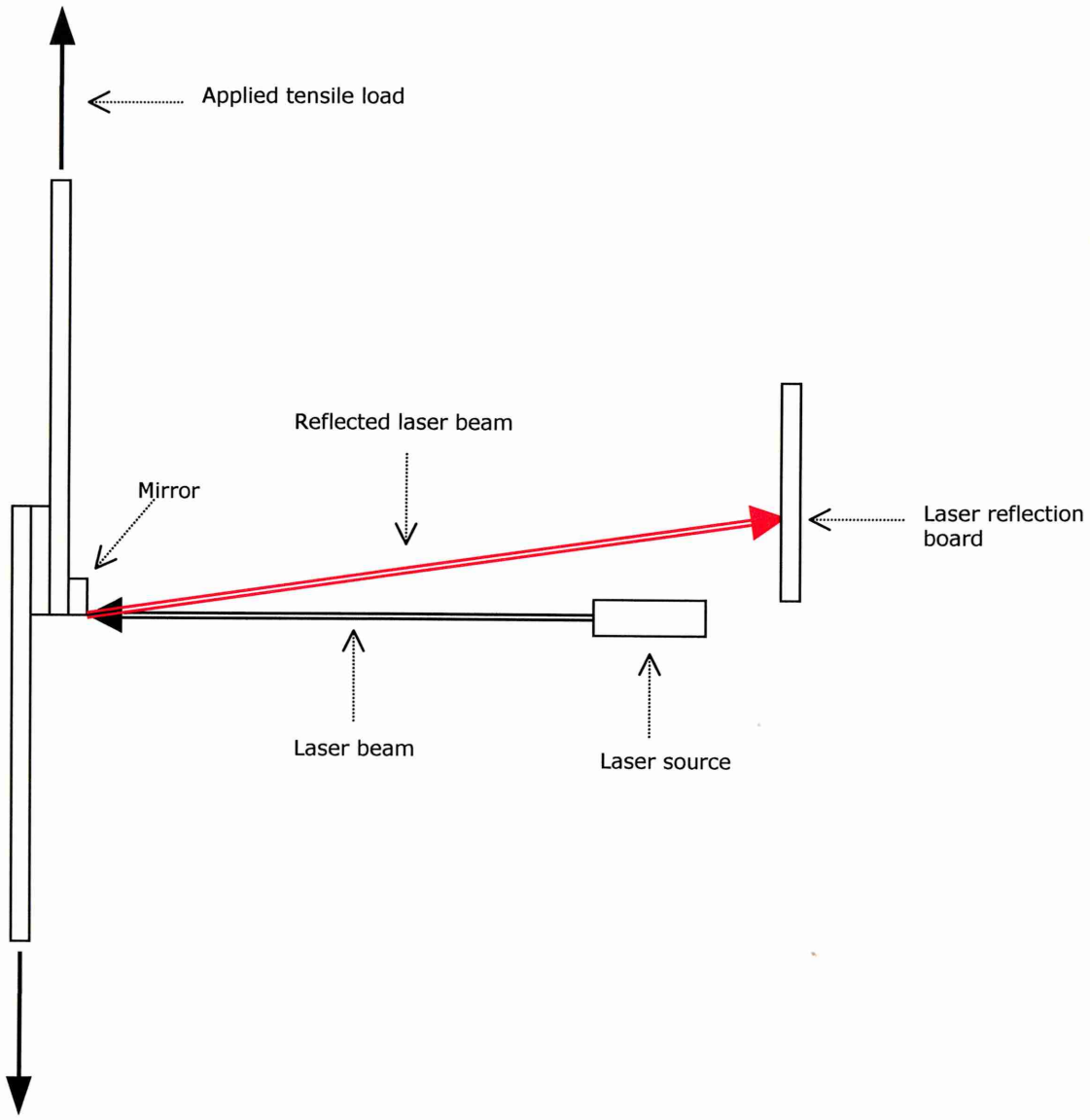

Figure 6.10 *- Schematic of set-up used to calculate the rotation of single overlap joints*

6.4.2 Results of Overlap Rotation

Below the results of the elastic rotation of single overlap joints is presented. The results are sectioned into: (1) adherend thickness, and, (2) overlap length.

1.5mm adherend, 0.25mm bondline thickness, 12.5mm overlap without fillets

Figure 6.11 shows very good correlation between the actual and predicted rotation at low levels of applied load. When the applied line load exceeds 50N/mm the analytical model predicts a higher angle of rotation.

1.5mm adherend, 0.25mm bondline thickness, 20.0mm overlap without fillets

Figure 6.12 reveals a comparable relationship between the model and actual measurements, up to and including the assumed load required to produce plastic deformation.

1.5mm adherend, 0.25mm bondline thickness, 30.0mm overlap without fillets

Figure 6.13 shows good correlation, whereby both sets of results are of the same magnitude. However, the values from the analytical model where lower than the experimental values up to the yield point of the adherends.

1.5mm adherend, 0.25mm bondline thickness, 40.0mm overlap without fillets

Figure 6.14. Results for the 40mm overlap specimens shows excellent correlation between the analytical and experimental values up to the point of where adherend plastic deformation takes place.

1.5mm adherend, 0.25mm bondline thickness, comparison of analytical model with overlaps of 12.5-50.0mm and no fillets

Figure 6.15. The analytical model shows that as the overlap length is increased for a given applied line load (N/mm) the amount of rotation imparted on the bonded region is reduced. Each of the overlap lengths evaluated all behaved in a linear manner.

1.5mm adherend, 0.25mm bondline thickness, comparison of experimental results with overlaps of 12.5-40.0mm and no fillets

Figure 6.16. For overlap length 12.5mm, 20mm and 30mm there is very little deviation in the measured angle of rotation up to the applied line load of 80N/mm. However, for all load levels the 40mm overlap specimens produced the smallest angle of rotation.

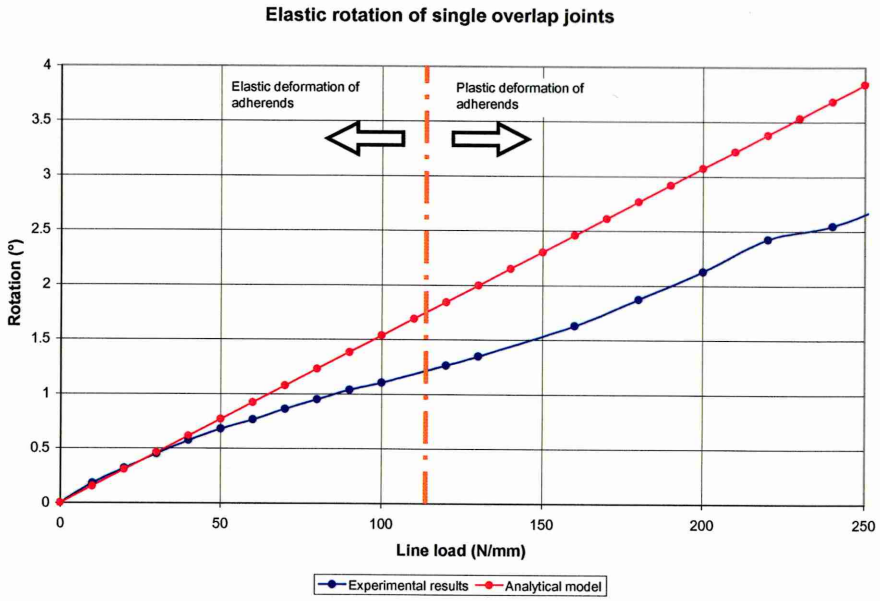

Figure 6.11 *– Comparison of analytical and experimental results on the joint rotation of single overlap joints, where: adherend = 1.5mm, adhesive layer = 0.25mm, overlap length = 12.5mm*

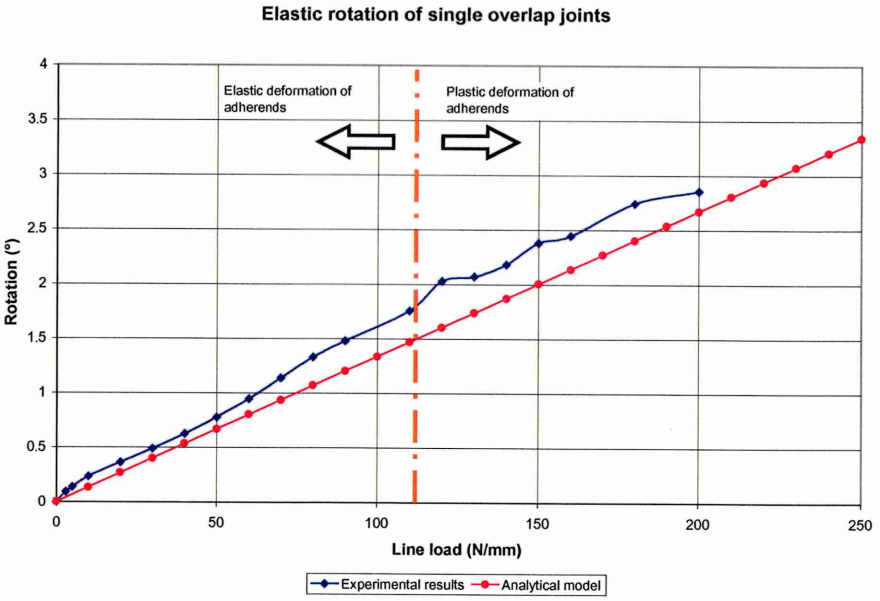

Figure 6.12 *– Comparison of analytical and experimental results on the joint rotation of single overlap joints, where: adherend = 1.5mm, adhesive layer = 0.25mm, overlap length = 20.0mm*

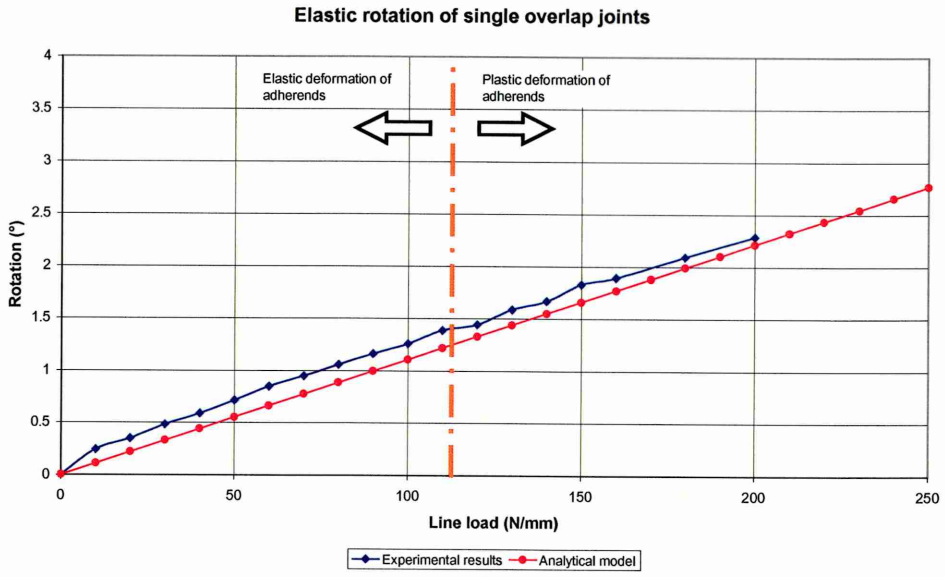

Figure 6.13 *– Comparison of analytical and experimental results on the joint rotation of single overlap joints, where: adherend = 1.5mm, adhesive layer = 0.25mm, overlap length = 30.0mm*

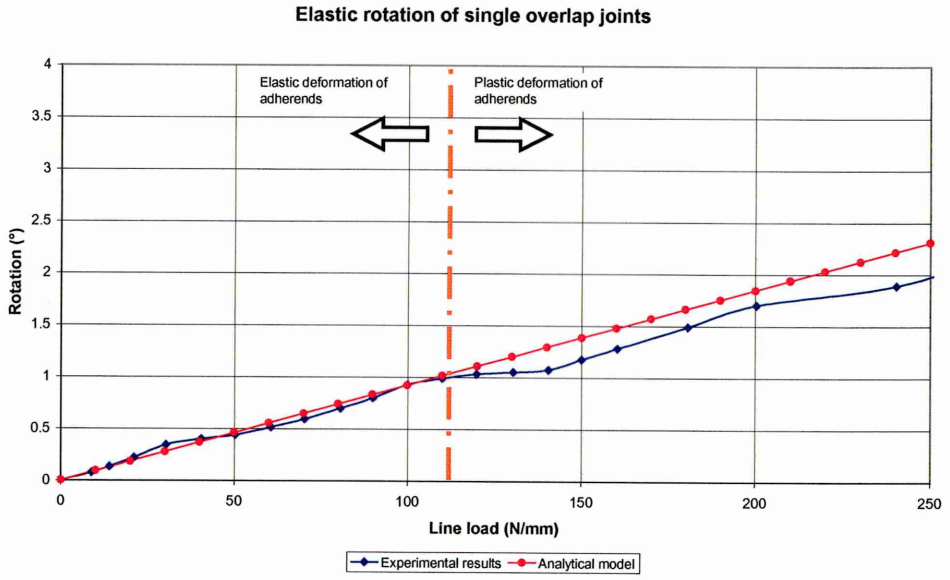

Figure 6.14 *– Comparison of analytical and experimental results on the joint rotation of single overlap joints, where: adherend = 1.5mm, adhesive layer = 0.25mm, overlap length = 40.0mm*

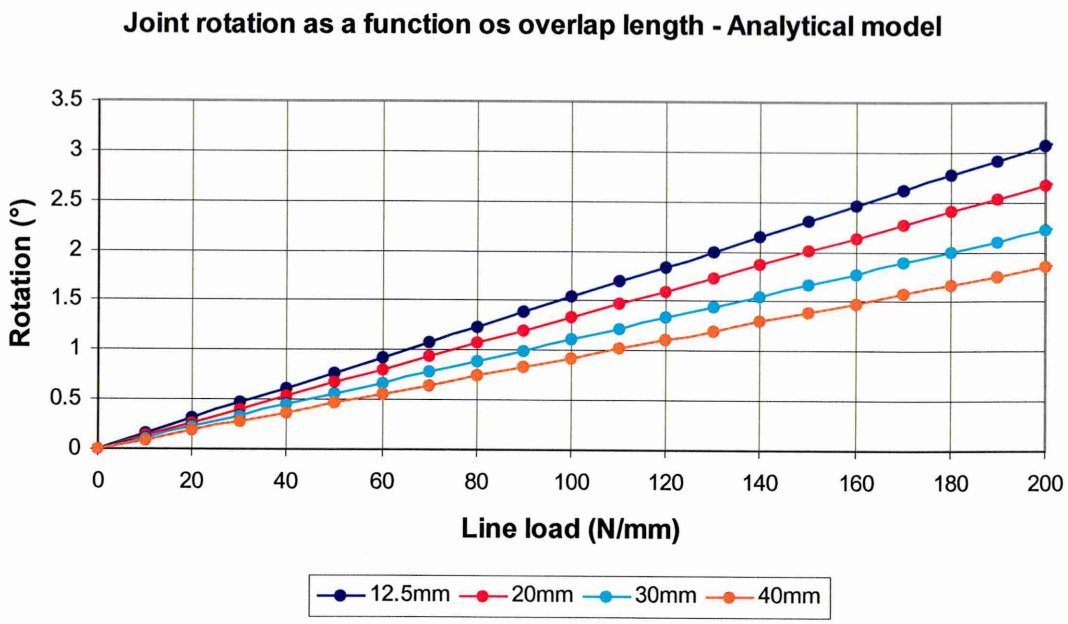

Figure 6.15 *– The effect of overlap length on the joint rotation of single overlap joints using the analytical model, where: adherend = 1.5mm, adhesive layer = 0.25mm and no fillets*

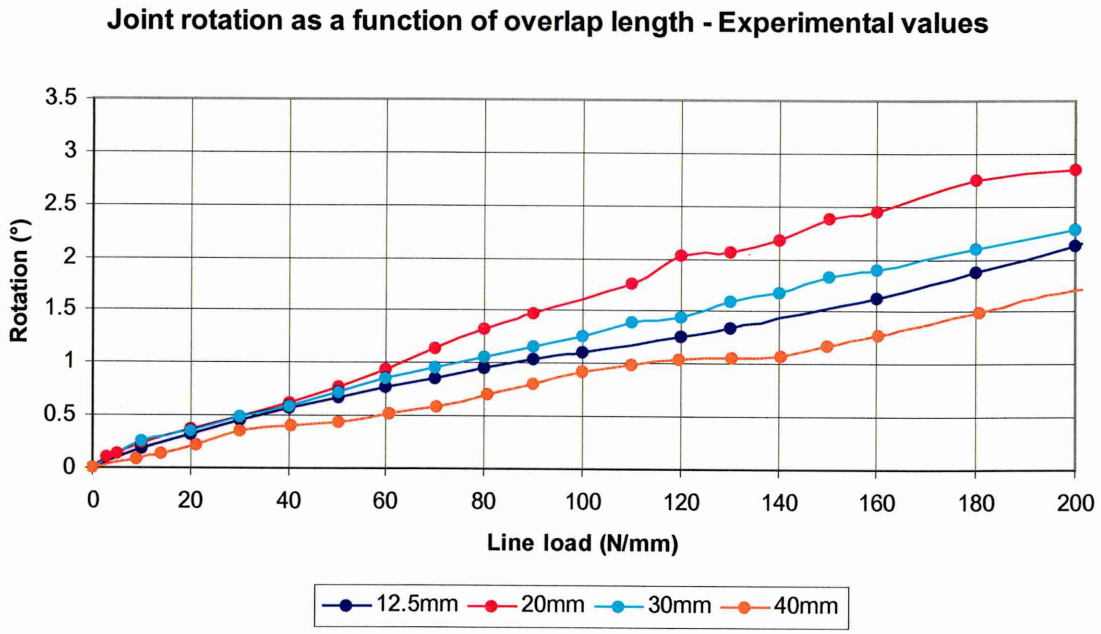

Figure 6.16 *– The effect of overlap length on the joint rotation of single overlap joints using experimental results, where: adherend = 1.5mm, adhesive layer = 0.25mm and no fillets*

3.0mm adherend, 0.25mm bondline thickness, 12.5mm overlap without fillets

Figure 6.17. The model and experimental results are very similar for loads up to and including ~150N/mm. As the load increases the model predicts a slightly higher angle of rotation.

3.0mm adherend, 0.25mm bondline thickness, 20.0mm overlap without fillets

From Figure 6.18, a good degree of similarity was found between the two sets of results. However, after an applied load of ~110N/mm is applied the model starts to predict higher values of rotation.

3.0mm adherend, 0.25mm bondline thickness, 30.0mm overlap without fillets

Figure 6.19, for both sets of results there is good correlation. When the applied load was above ~125N/mm the model tends to predict slightly larger angles of rotation.

3.0mm adherend, 0.25mm bondline thickness, 40.0mm overlap without fillets

Figure 6.20, both groups of results exhibit adequate correlation. The measured angle of rotation is very slightly higher, ~0.05°, for all applied loads up to the calculated point of plastic deformation.

3.0mm adherend, 0.25mm bondline thickness, comparison of analytical model with overlaps of 12.5-50.0mm and no fillets

Figure 6.21. The pattern is the same to that for specimens with 1.5mm adherends. Whereby as the overlap is increased the amount of rotation decreases. For all overlap lengths there is linear behaviour.

3.0mm adherend, 0.25mm bondline thickness, comparison of experimental results with overlaps of 12.5-40.0mm and no fillets

Figure 6.22. The specimens with the 12.5mm overlap rotate the most for all levels of applied load (N/mm). At low load levels the 20mm, 30mm and 40mm overlap specimens exhibit very similar angles of rotation. However, generally the longer the overlap the less the rotation.

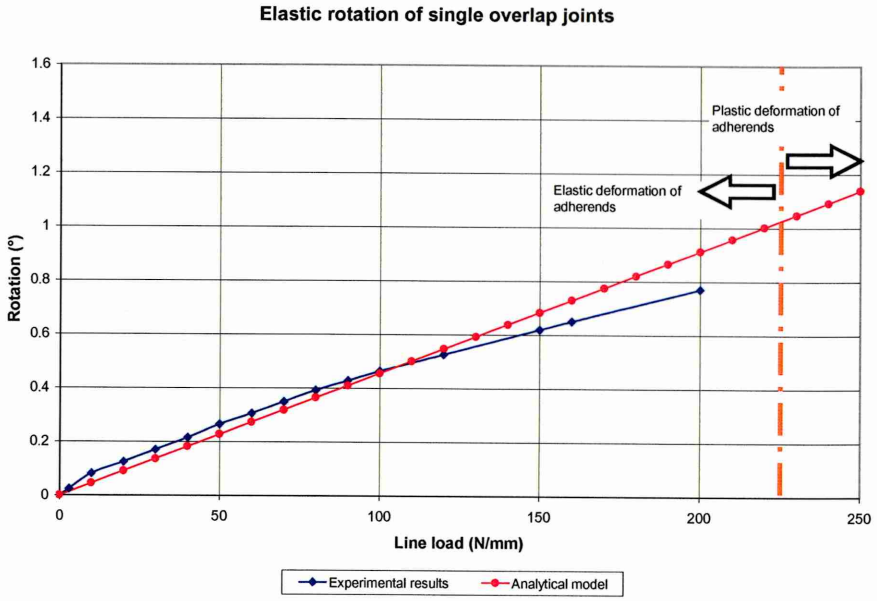

Figure 6.17 *– Comparison of analytical and experimental results on the joint rotation of single overlap joints, where: adherend = 3.0mm, adhesive layer = 0.25mm, overlap length = 12.5mm*

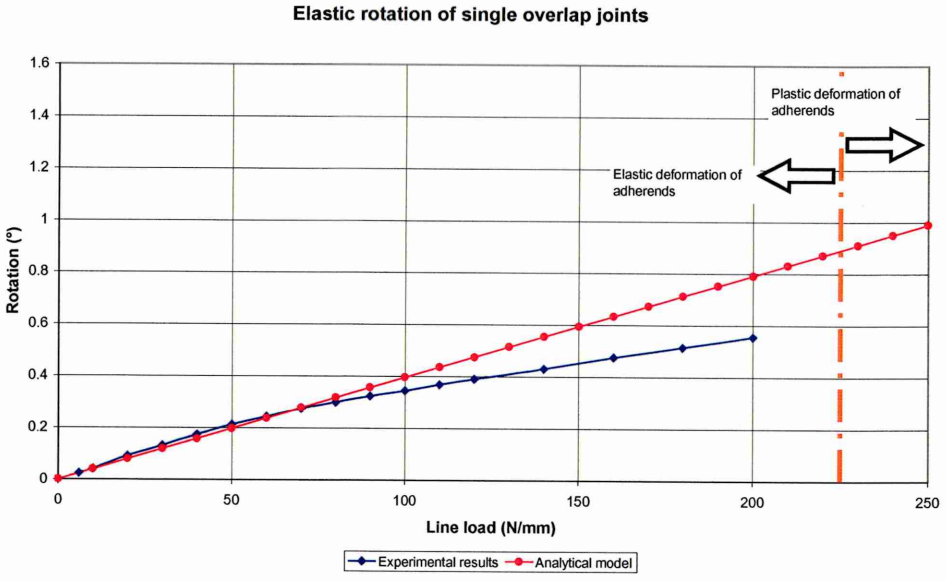

Figure 6.18 *– Comparison of analytical and experimental results on the joint rotation of single overlap joints, where: adherend = 3.0mm, adhesive layer = 0.25mm, overlap length = 20.0mm*

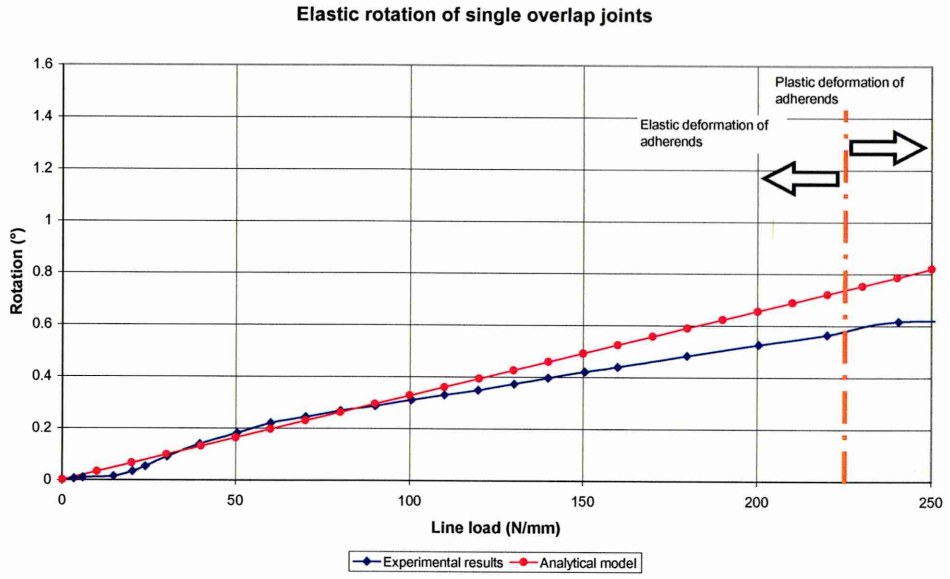

Figure 6.19 *– Comparison of analytical and experimental results on the joint rotation of single overlap joints, where: adherend = 3.0mm, adhesive layer = 0.25mm, overlap length = 30.0mm*

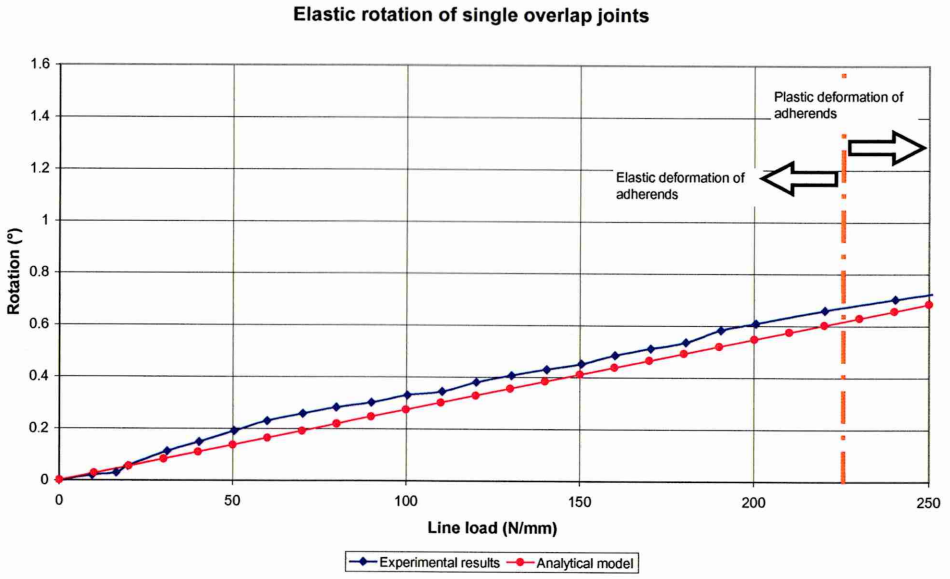

Figure 6.20 *– Comparison of analytical and experimental results on the joint rotation of single overlap joints, where: adherend = 3.0mm, adhesive layer = 0.25mm, overlap length = 40.0mm*

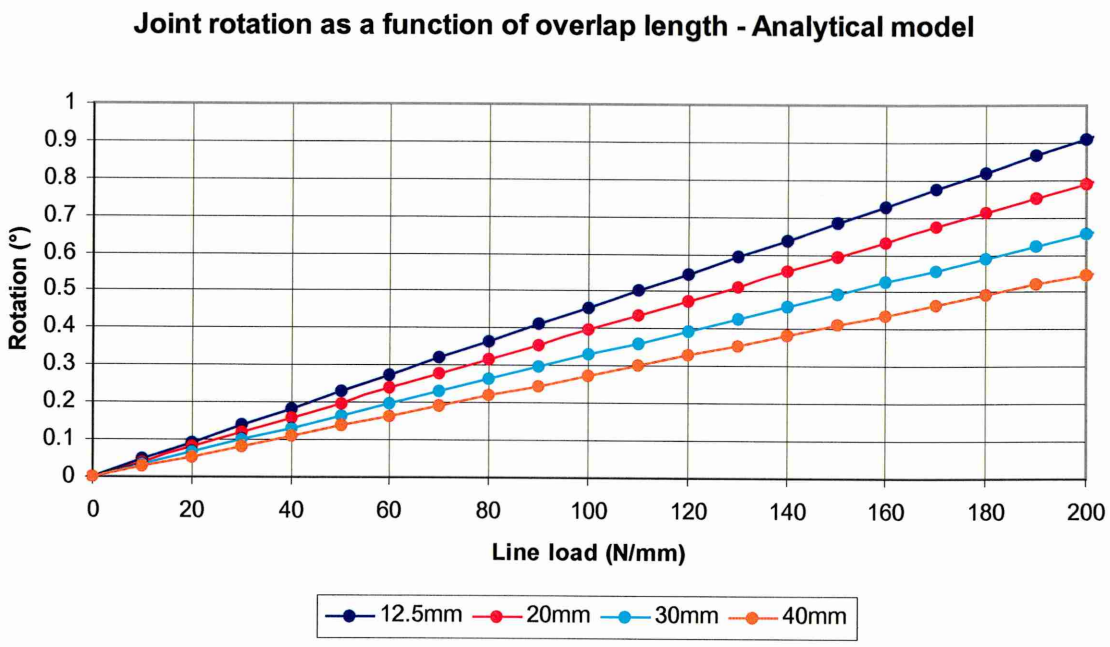

Figure 6.21 *– The effect of overlap length on the joint rotation of single overlap joints using the analytical model, where: adherend = 3.0mm, adhesive layer = 0.25mm and no fillets*

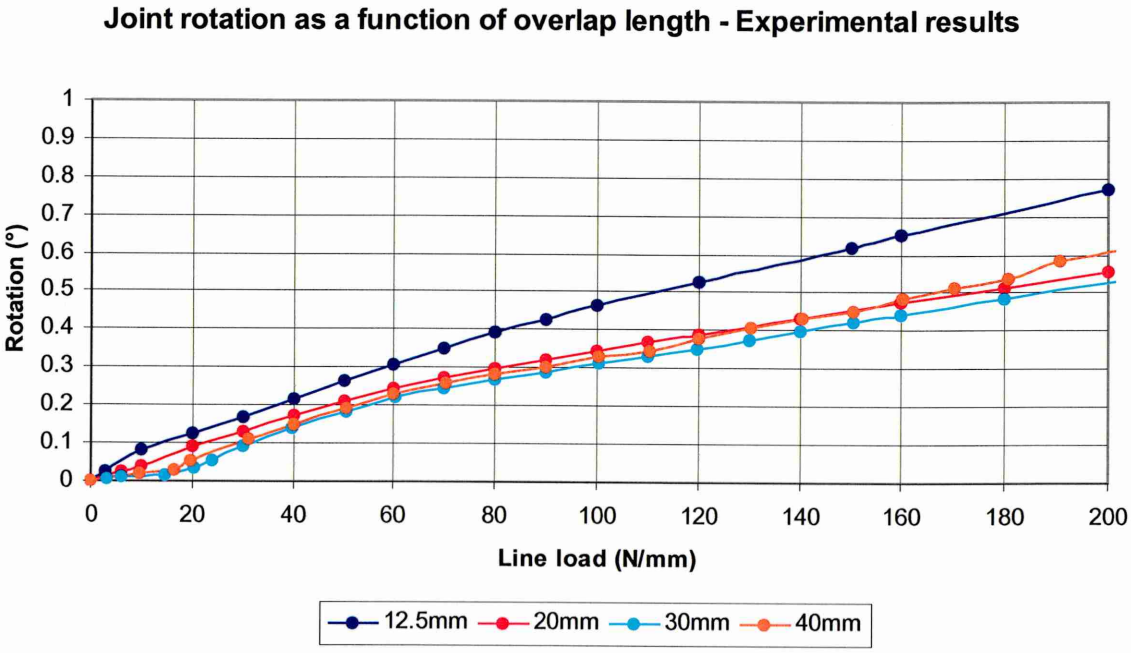

Figure 6.22 *– The effect of overlap length on the joint rotation of single overlap joints using experimental results, where: adherend = 3.0mm, adhesive layer = 0.25mm and no fillets*

6.5 Mechanical Testing

6.5.1 Experiment Programme

Mechanical testing of a single lap joint was performed to assess the effect of the following parameters on joint strength:

- Effect of overlap length
- Effect of adherend thickness
- Effect of fillets

All tensile testing was carried out as described in section 3.6.1. Table 6.3 below details the specimen geometry's, a batch size of 6 was used for each parameter.

***Table 6.2** - Specimen geometry's*

Overlap (mm)	Adherend thickness (mm)	Bondline thickness (mm)	Bond area (mm^2)	Fillets Intact	Grip to grip distance (mm)
12.5	1.5	0.25	312.5	Y	112.5
20.0	1.5	0.25	500	Y	112.5
30.0	1.5	0.25	750	Y	112.5
40.0	1.5	0.25	1000	Y	112.5
50.0	1.5	0.25	1250	Y	112.5
12.5	3.0	0.25	312.5	Y	112.5
20.0	3.0	0.25	500	Y	112.5
30.0	3.0	0.25	750	Y	112.5
40.0	3.0	0.25	1000	Y	112.5
50.0	3.0	0.25	1250	Y	112.5
12.5	1.5	0.25	312.5	N	112.5
20.0	1.5	0.25	500	N	112.5
30.0	1.5	0.25	750	N	112.5
40.0	1.5	0.25	1000	N	112.5
50.0	1.5	0.25	1250	N	112.5
12.5	3.0	0.25	312.5	N	112.5
20.0	3.0	0.25	500	N	112.5
30.0	3.0	0.25	750	N	112.5
40.0	3.0	0.25	1000	N	112.5
50.0	3.0	0.25	1250	N	112.5

6.5.2 Results

6.5.2.1 Effect of overlap

1.5mm Adherends

From Figure 6.23 it is shown that an increase in overlap length plays a significant role in the strength of the adhesive joints. As the overlap distance is lengthened the load required to break the joint increases. The inclusion of fillets at the overlap ends also influences the strength of the joint. For all overlap lengths evaluated, joints that incorporated fillets performed best. At small overlap lengths the difference is negligible, but as the overlap distance increases so too does the difference in strength between filleted and non-filleted specimens. The influence of fillets is shown, where the average strength of a joint with a 30mm overlap and fillets (14.40kN) is almost the same as that of a specimen with no fillets and 40mm overlap length (14.99kN).

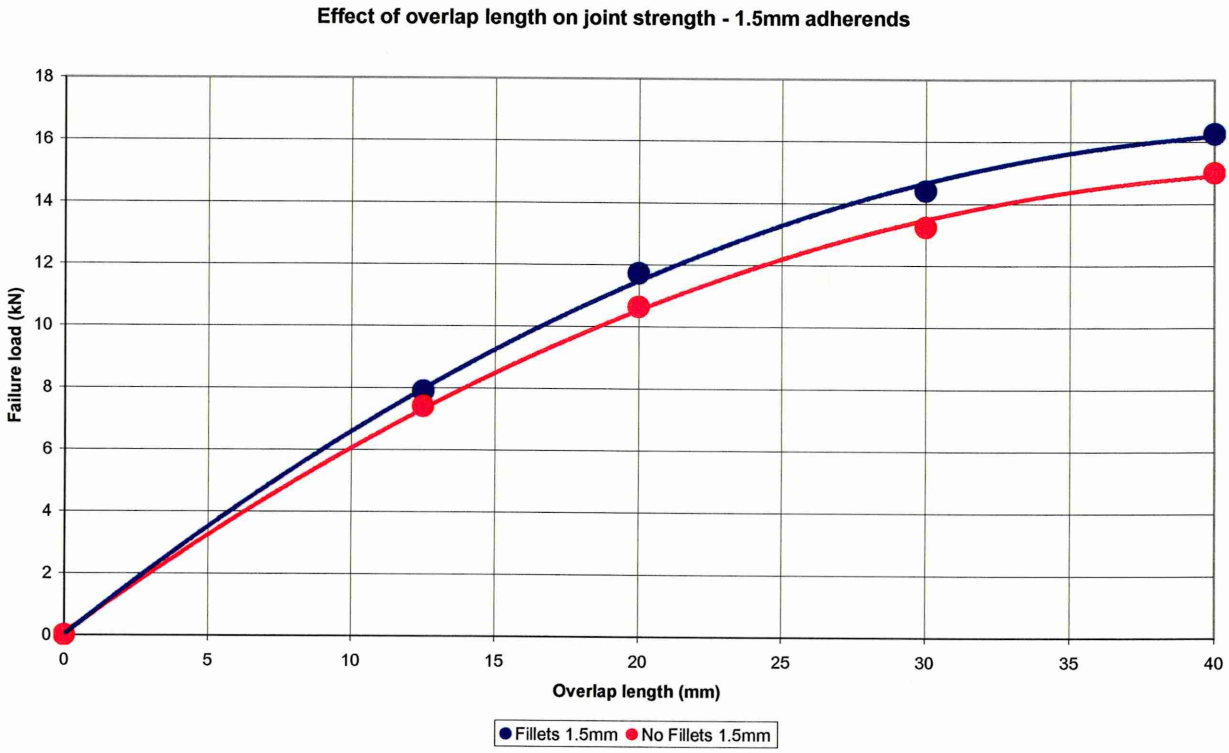

Figure 6.23 *– Effect of overlap on joint strength, 1.5mm adherends*

3.0mm Adherends

Figure 6.24 reveals a similar pattern to the 1.5mm specimens. As the overlap length is increased so too is the strength of the joint. The influence of fillets on joint strength is less dramatic as the substrate thickness is increased. Between overlap lengths of 12.5mm and 50mm there is little difference in the joint strengths of filleted and non-filleted joints. The curves are linear in nature indicating that joint strength would presumably increase with a larger overlap before a plateau is reached.

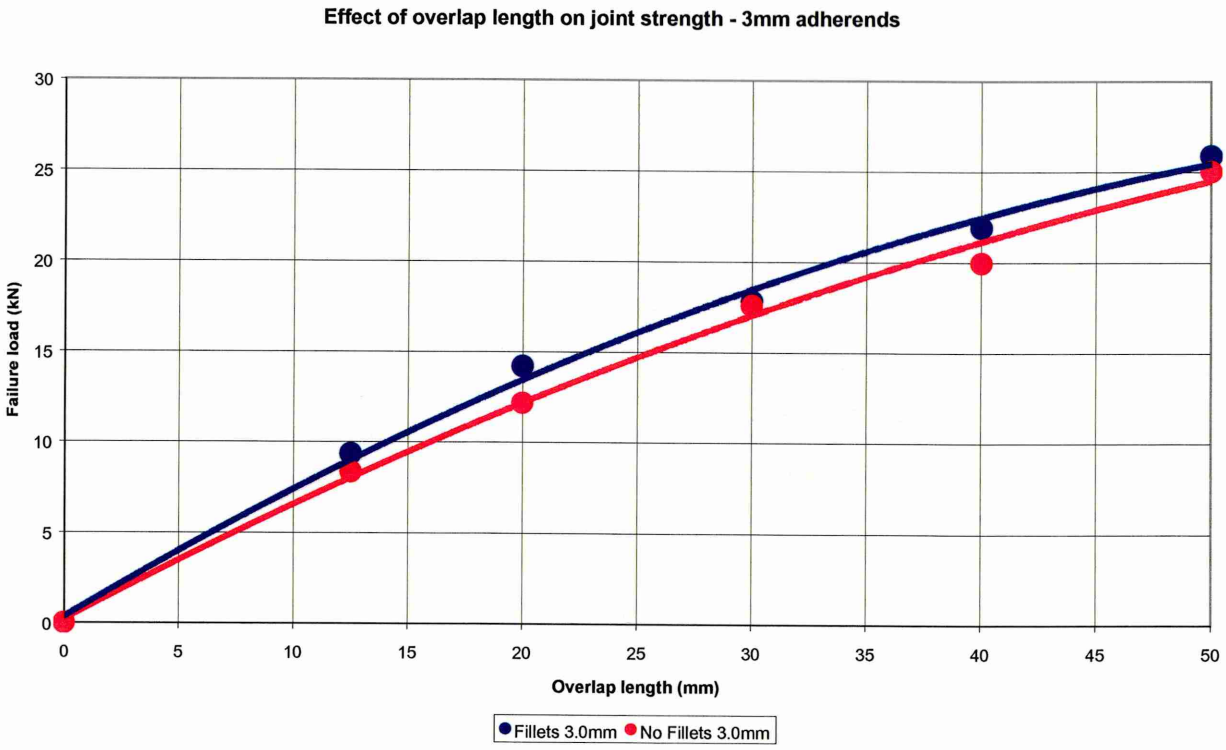

Figure 6.24 *– Effect of overlap on joint strength, 3.0mm adherends*

6.5.2.2 Effect of adherend thickness

Figure 6.25 compares the effect of adherend thickness on failure stress for specimens incorporating both 1.5mm and 3mm adherends with and without fillets. It can be seen that the increase in substrate thickness offers enhanced joint strength. The joints with 3mm adherends did not plastically deform as much as the joints with 1.5mm substrates. This suggests that joints with thinner adherends are controlled by the plastic deformation of the adherend, and joints with thicker adherends are controlled by the strength of the adhesive.

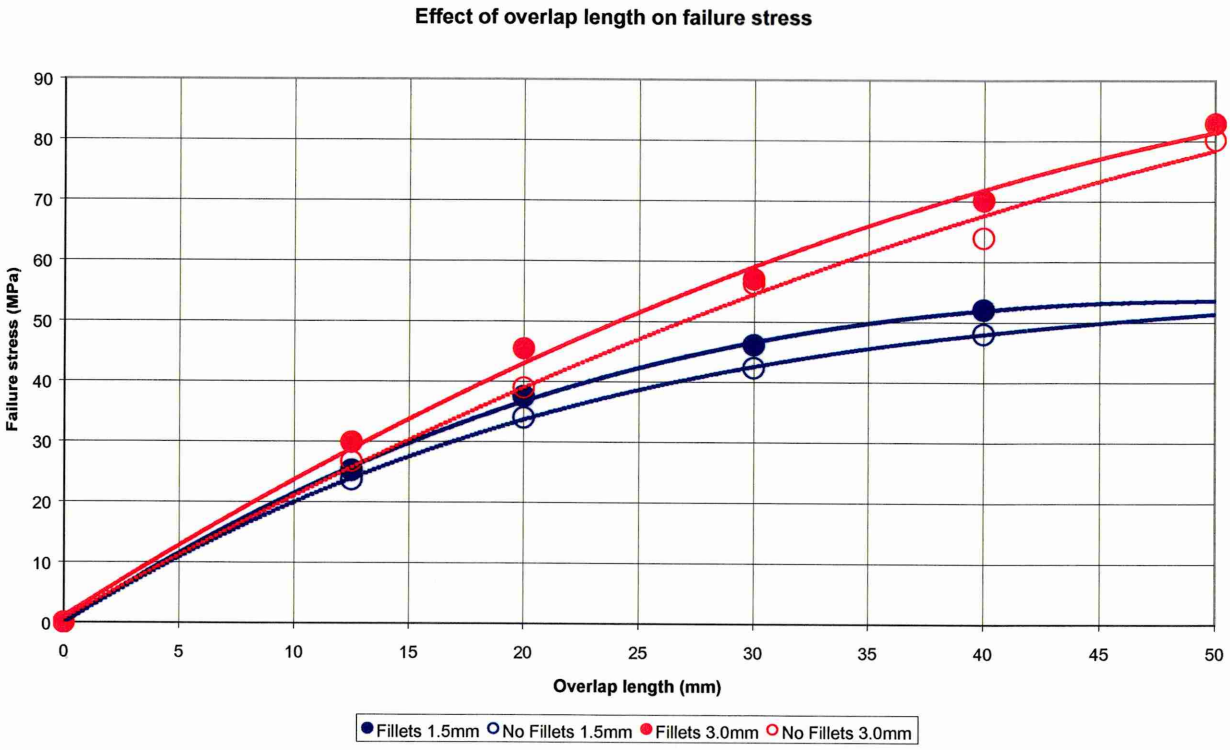

Figure 6.25 *– Effect of adherend thickness on joint strength*

6.5.2.3 Effect of adherend plasticity

The stiffness imparted on the structure by the adherends influences the strength of the joint. Figure 6.26 compares the failure load of joints manufactured with 304L stainless steel and DP490 structural epoxy with that of specimens constructed from hard and mild steel substrates with a structural epoxy. The graph clearly reveals that the adherend plasticity effects the strength of the joint. Specimens incorporating the mild steel, yield strength = 172MPa, reach a plateau after an overlap length of 20mm had been used. No additional strength was afforded by increasing the overlap. As the yield strength of the substrates increased there was a substantial enhancement in joint strength. This is highlighted where a failure load of 14.8kN was achieved for hard steel specimens with only a 12.5mm overlap, for stainless steel joints to achieve this an overlap of 30mm would have to be employed.

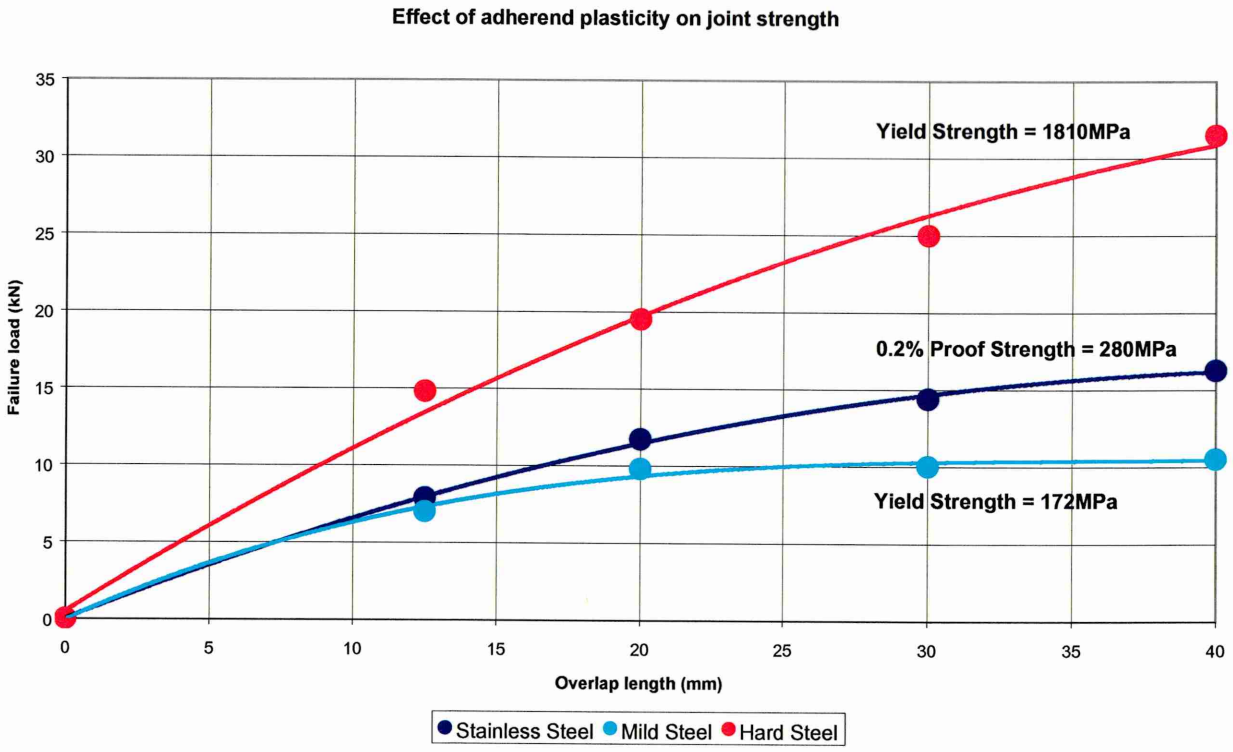

Figure 6.26 *– Effect of adherend plasticity on joint strength*

6.6 Summary

6.6.1 Analytical Model

An analytical model based on beam theory has been developed to determine the elastic rotation incurred on the overlap region of single lap joints. There was good correlation between the model and the experimental results, where the variables evaluated were overlap length and adherend thickness. The limiting factor of the elastic model is the nominal stress required to produce localised plastic deformation of the substrates. For single overlap joints this will occur at the inner fibre, i.e. the stress at the surface where the sheets join, first to reach the yield point. The fibre stress is determined by:

$$\sigma_{MAX} = 4 \times \frac{P}{t} \qquad (6.23)$$

Where: σ_{MAX} = 300MPa - typical 0.2% proof stress of austenitic stainless steel

t = adherend thickness (mm)

P = line load (N/mm)

Hence for substrate thicknesses of 1.5mm and 3mm, the adherends will yield at approximately 112.5N/mm and 225N/mm respectively. Above these values the elastic theory will not be valid and the calculated values will become increasingly inaccurate.

6.6.2 Mechanical Testing

Experimental work has been carried out to evaluate the effects of overlap length, adherend thickness and the influence of fillets on the apparent strength of single overlap joints. For both 1.5mm and 3mm substrates, increasing the overlap lap has a beneficial effect on the strength of the joint. For joints incorporating the 1.5mm adherends it appears a plateau is reached when an overlap of in excess of 30mm is used. As the overlap length is increased on specimens with the 3mm substrates, the strength of the joint increases in a linear fashion. A plateau was not reached even when an overlap of 50mm was used. From Figure 6.25, a clear comparison can be made on the effect of adherend thickness. For all overlap lengths considered, joint manufactured from the thicker substrate obtain the highest failure load. The additional strength given by using thicker adherends will be a consequence of increased stiffness in the joint and an improved resistance against the substrates deforming, or the overlap region rotating. The experimental work has highlighted that to fabricate adhesive joints using an epoxy adhesive that will produce high initial strengths, then thick adherends with a high yield strength must be used. One area of interest is the influence of fillets. The mechanical testing revealed that the removal of fillets does not have a huge impact on initial joint strength. However, it must be noted that the inclusion of fillets may be beneficial in increasing the time it takes moisture to ingress into the bond interface if the specimens were subjected to a hydro-thermal stress regime.

6.7 Chapter References

[1] Adams R.D., Comyn J. and Wake W.C., Structural Adhesive Joints in Engineering, 2nd Edition, 1997, ISBN 0-412-70920-1

[2] Volkersen O., Luftfahrtforchung 15, 41, 1938

[3] Goland M. and Reissner E., 'Stresses in Cemented Joints', J. Applied Mech., Trans ASME, 66, A17, 1944

[4] Hart-Smith L.J., 'Adhesive bonded single lap joints', CR-112236, NASA, Langley Research Centre, 1973

[5] Nordberg H. and M^{C}Cann S., 'Rotation of overlap joints under load', AvestaPolarit Research Centre, Report SE20020403, 2003

[6] Lardner T.J., Archer R.R., Mechanics of Solids: An Introduction, M^{C}Graw Hill, 1994

7.1 Discussion

The review of literature in Chapter 2 summarised how adhesively bonded structures are complex systems, where several interfaces interact with one another. It is also clear that there is only a limited amount of data available on the structural adhesive bonding of stainless steel, especially with adhesive formulations other than structural epoxies. The objectives set out in Chapter 1 can be summarised as follows:

- To assess the environmental durability of surface pre-treatments applicable to austenitic stainless steel, and to use analytical techniques to physically and chemically characterise the stainless steel surfaces, reported in Chapter 4.
- To appraise the fatigue performance of austenitic stainless steel joints bonded with a structural epoxy adhesive reported in Chapter 5.
- To develop an analytical model to determine the elastic rotation of single overlap joints under the application of a tensile load, reported in Chapter 6.

The single most important factor to attaining durable adhesive joints is the surface condition of the adherends before the bonding operation. Not only do surface pre-treatments alter the way in which the adhesive will interact with the substrate, it also alters the stability of the interfacial region where it is considered that it controls the durability of the bonded structure. The durability studies in Chapter 4 concluded that a simple grit blast operation offers enhanced durability performance when compared with alkaline degreased treatments, when specimens were exposed to a high temperature/humidity environment. It is the author's view that when bonding austenitic stainless steel substrates, grit blasting followed by a thorough alkaline degreasing process must be the minimum pre-treatment employed. Further work is needed to investigate the effects of grit blasting parameters such as; blast angle, blast pressure and the type of blast media used. However, the results in Chapter 4 reveal that if any medium to long term resistance to moisture ingression is required, then much more sophisticated surface pre-treatments are required that will reduce the tendency for moisture to migrate to the interface region and start the delamination process and the premature failure of the bonded component.

The testing programme in Chapter 4 utilised three configurations, namely; standard overlap joints, perforated single overlap joint and the wedge test. Using the latter two specimen types greatly reduced the overall testing time and more importantly generated the same order of ranking for the surface pre-treatments appraised. The reduction in testing time compared with the standard overlap joint environmental exposure allows a large amount of valuable data to be generated relatively quickly. However, further work should be carried out to evaluate the performance of all the surface pre-treatments used over a wider range of temperatures and humidities. Unfortunately the limited time available for the current research did not permit this. One important conclusion to be drawn from this work is that to successfully appraise the

performance of surface pre-treatments then specimens must be subjected to a moisture rich environment coupled with the application of an applied load.

The most durable surface pre-treatment assessed was the alumina grit blasting + Accomet C process. This is a very encouraging result, not only did the treatment offer excellent resistance to hydro-thermal conditioning, but compared to the more elaborate electro-chemical pre-treatments it is very cost effective. The only real cost is the energy required whilst curing the Accomet C coating. In addition to this, the Accomet C process is very flexible because only the area to be bonded requires treatment. This may be its best selling point, because of the vast increase in architectural and construction applications for stainless steel where one of the material properties is aesthetic appearance. The main limitation of the Accomet C operation is the compound contains chromate, albeit that its oxidising property is very weak, this could in the future limit its use if the present day environmental legislation's are tightened. However it is considered within the industry that the future state of pre-treatments will eventually be 'chromate free'. Encouraging information here however, is that the manufacturers of Accomet C are in the developmental stages of 'chromate free' pre-treatment solutions for the adhesive bonding of metallic assemblies.

The relevant chemical and physical attributes of all the surface pre-treatments used were ascertained. The results indicated that topographical information alone is not enough to indicate how well a surface will perform in hot/humid conditions. It appears that the chemical state of a pre-treated surface is of paramount importance. XPS studies showed that the chromium to iron ratio (Cr:Fe) of treated austenitic stainless steel substrates greatly influences adhesive joint durability. As shown in Figure 4.115 and 4.116, the higher the Cr:Fe ratio the more resistant the bonded assemblies were to environmental degradation. The evaluation of fractured wedge test specimens using XPS and SEM as complimentary techniques showed that joints incorporating the higher Cr:Fe ratio treatments tended to fail initially cohesively within the adhesive and after environmental exposure a tendency for the failure mode to change to interfacial between the adhesive and associated oxide layer was observed. The less durable specimens tendered to exhibit an adhesive failure, whereas the least durable specimens showed evidence of total delamination of the adhesive after only relatively short exposure times. It is quite clear that further work is needed to fully elucidate why an increase in the Cr:Fe ratio at the surface provides durable chemical bonds between the stainless steel oxide layer and the DP490 epoxy adhesive, or with epoxy adhesives in general. However, it is possible to speculate that the epoxy adhesive will readily wet a chromium oxide better than iron oxide. The experimental work in Chapter 4 has shown that to manufacture reliable adhesive joints then the adherend surfaces must be free from contamination. To further confirm this, the more durable treatments tended to have the least amount of carbon on the surface, as shown using XPS. Two explanations can be offered: (i) durable pre-treatments remove weak boundary layers much more effectively, or (ii)

substrates pre-treated with durable treatments do not allow carbon to readily deposit on the surface as readily as less durable treatments.

It is not only resistance to environmental conditioning that is beneficial to the longevity of adhesive joints. Industrial applications using adhesive systems suffer greatly from fatigue failure, usually resulting in premature unexpected failure. For this reason it is of interest to study the fatigue performance of adhesive joints consisting of the standard overlap specimens as used in Chapter 4. Chapter 5 details a comprehensive study on the following parameters that affect the fatigue performance of stainless steel adhesive joints:

- Effect of surface pre-treatment
- Effect of fatigue test frequency
- Effect of the R-Ratio
- Effect of aqueous ageing

For the first part the results revealed that even relatively modest surface conditioning increases the fatigue resistance of single overlap joints. Therefore grit blasting the area to be bonded with high purity alumina particles followed by a comprehensive alkaline degreasing process has successfully improved dynamic performance. As mentioned in 5.4.1 the complexity of the degreasing stage will influence the fatigue performance, particularly the ability to readily remove as much particulate residue as possible, thus allowing intimate contact between the adhesive and the stainless steel.

It is well known that during the lifetime of structural components, they will be subjected to a variety of loads and load cycle frequencies. Under normal in-service conditions, most structural adhesive joints will probably be exposed to frequencies that are not constant but rather erratic and sporadic. For this reason it has been extremely useful to assess the effect of test frequency on the dynamic response of adhesive joints. The work in section 5.2.2 shows that the fatigue performances of joints manufactured with DP490 were frequency dependent, this behaviour being more prominent at lower test frequencies. The experimental work showed that lowering the test frequency from 20Hz to 5Hz and below had detrimental effects on performance. The effect of mean load was also evaluated. It was shown that an increase in the mean load amplitude seriously diminished the fatigue lifetime of specimens. The effects of aqueous ageing were also assessed, the results showed that the fatigue performance of specimens conditioned with alumina grit blasted surfaces was reduced after immersion in distilled water for a duration of up to 72 weeks. After subsequent examination of the fracture surfaces it was realised that the surface topography is well suited to entrap air during the bonding process. It is suggested that as water ingressed into the interfacial region the moisture will fill the voids and displace the adhesive from the substrate, thus causing delamination. Due to the time constraints of the fatigue-testing programme it was not possible to evaluate other surface pre-treatments resistance to aqueous ageing and subsequent fatigue testing. However, it is proposed that

future work should concentrate on appraising the surface pre-treatments used in section 4.3, e.g. alumina grit blast + Accomet C or sulphuric acid sodium dichromate anodisation, so a comparative assessment can be made against hydrothermal and fatigue performance. The next stage in the experimental programme was to understand what happens to the overlap region of a single lap joint under the action of an applied tensile load. This is of importance for industrial applications using structural adhesive joints so structures can be assembled without fear of large deflections in the bonded structure occurring. Chapter 6 appraised two areas, firstly, an analytical model that was developed to predict the elastic rotation of single overlap joints, and secondly, an experimental programme to assess the following overlap variables on joint strength:

- Effect of overlap length
- Effect of adherend thickness
- Effect of fillets
- Effect of adherend plasticity

An analytical model based on beam theory has been developed, which has been used to predict the elastic rotation of single overlap joints. The elastic rotation is derived from, (a full derivation is given in Chapter 6):

$$\theta = \frac{2 \cdot a^* \cdot z}{E \cdot t^2} \cdot P \qquad (7.1)$$

Where: θ = elastic rotation (radians)

a^* = 'free' half length of the specimen or sheet (mm)

z = geometrical factor

E = Young's Modulus of Elasticity (MPa)

t = Sheet thickness (mm)

P = Applied line load (N/mm)

It has been shown that the elastic model shows good correlation compared with the experimental results when evaluating the elastic rotation of stainless steel overlap joints, incorporating 1.5mm and 3mm adherends with overlap lengths in the range 12.5mm to 40mm. The main drawback of the elastic model is that rotation after plastic deformation has occurred cannot be determined due to the model's constraints. The elastic rotation prediction deviates from the actual experimental rotation when the adherends begin to plastically deform. The volume between the sheets in the model is assumed to be stiff, which is not reality for many structural adhesives. One important use for the model will be as a design aid to provide

designers using bonded assemblies a clear indication of movement that will occur when the structure is under an applied load.

The mechanical testing program in Chapter 6 showed that by increasing the adherend thickness from 1.5mm to 3mm produced an increase in joint strength. It was also revealed that by leaving the adhesive fillets intact also had a beneficial effect on joint strength. However, the increase in strength was minimal, and many stainless steel structural adhesive applications require a high degree of aesthetic appeal for example architectural cladding, where spew fillets would be unsightly. The mechanical testing also showed that by increasing the overlap length a gain in joint strength was achieved. The thinner the adherend substrate the quicker a plateau is reached where no additional strength is gained, but for thicker adherends there was an increase in joint strength as the overlap was extended. This observable fact can be explained in terms of plastic rotation of the overlap, as the increase in strength occurs from the increase in substrate thickness and inherent yield strength which reduces the tendency for rotations to occur. In contrast, the fracture of joints at lower loads incorporating thin gauge substrates will have the tendency to rotate more and thus fail from the action of peel stresses at the end of the overlap. The results are comparable with the work of Boyes[1] and Ring-Groth[2]. The final part of the experimental work showed that the yield strength of the substrate to be bonded plays a significant role in the apparent strength of the joint. Hence to produce bonded assemblies with high initial strengths, then adherends with high yield strength and sufficient thickness must be used.

In summary, the work presented in this thesis has revealed that using a structural epoxy adhesive (DP490) is a viable way of joining austenitic stainless steel intended for use in structural applications. In addition, if the correct surface pre-treatments are implemented then the bonded assembly will be able to resist the ingression of moisture also coupled with the effects of temperature and applied load. In all, eleven pre-treatments have been evaluated, ranging from the relatively simple through to the complex and costly. The evaluations have shown that a variety of surface analytical techniques, namely SEM and XPS, are required to complement one another to fully characterise the physical and chemical attributes of treated surfaces. To fully assess the response of an adhesive joint after environmental exposure, surface analytical techniques must be used at both the pre-bonding stage and on the examination of fracture surfaces to attain what type of failure has occurred. The fatigue work revealed how exposing adhesively bonded structures to cyclic loads has deleterious affects on the performance of adhesive joints. Importantly it was shown that aqueous ageing prior to fatigue testing is particularly damaging to fatigue life. Also the fatigue response was shown to be heavily dependent on the test frequency the dynamic testing was carried out at. So if an adhesively bonded structure are somehow exposed to low frequency cyclic loads some form of strengthening or re-designing of the structure will be required, for example stiffeners or rigidising

of the sheet, which effectively reduces the free length of the structure and reduces the rotation of an overlap region. Encouragingly it was shown in Section 5.5 that adhesive bonding offers better fatigue performance when compared to spot welded and weldbonded joints under similar fatigue conditions. The next stage in promoting the increased use of adhesives will no doubt lie in educating designers and specifiers of their merits. Finally a model has been developed to predict the amount of elastic rotation occurring on the overlap region of a single lap joint under the application of a tensile load. This model has the potential aid designers to specify the correct length and gauge for sheet to be bonded, for example off-shore structures that are exposed to wave damage or food/beverage tanker linings that are used under pressure.

7.2 Conclusions

- The commercially available surface finish of AISI 304L stainless steel had an effect on the environmental durability of standard lap shear specimens. The semi bright (2B) and dull matt (2D) finishes both offer enhanced durability compared with the bright annealed (BA) surface when exposed to a high humidity environment.

- Alumina grit blasting extends the lifetime of stressed standard lap shear joints when exposed to a high humidity environment, probably from an increase in the area available for bonding if the adhesively bonded structure is not exposed to demanding conditions, this form of pre-treatment is a cost-effective process.

- The application of stress to standard lap shear joints coupled with exposure to a high humidity reduces the residual strength of the bonded assembly.

- The retained strength of stressed and un-stressed standard lap shear joints incorporating alkaline degreased 2B and 2D finish, is only marginally affected after 1-year exposure to natural outdoor conditions.

- The perforated lap shear specimen has proved a useful tool for discriminating between the influence of surface pre-treatments on adhesive joint durability, within a convenient time scale.

- Alumina grit blast + Accomet C, sulphuric acid sodium dichromate anodising and nitric acid anodising were the most durable pre-treatments for stainless steel-epoxy adhesive joints exposed to a high humidity environment.

- Improvements on adhesive joint durability are a combination of physical and chemical contributions.

- The chromium to iron ratio of treated stainless steel surfaces influences joint durability. The higher the chromium to iron ratio the more resistant the bonded joint to environmental degradation.

- The initial strength of perforated lap joints is not representative of durability performance.

- The room temperature fatigue performance of adhesive bonded stainless steel single overlap joints was enhanced when adherends were subjected to an alumina grit blasting pre-treatment. This relatively simple surface conditioning may increase fatigue life by; (a) increasing the wetting characteristics of the adhesive by removing weakly adhered layers, and (b) increasing the surface roughness and area available for bonding, thus producing a higher level of intrinsic adhesion between the adhesive and substrate.

- Fatigue life is compromised at test frequencies of 1Hz. Single overlap adhesive joints incorporating the DP490 adhesive are frequency dependent when subjected to cyclic sinusoidal loads. Between frequencies of 5 Hz and 20Hz, the difference in fatigue life is not so prevalent, however, as the test frequency is further reduced to 1Hz there is a notable reduction in dynamic capacity. It appears that at lower frequencies the adhesive layer has more time to accumulate creep strains, which hinder fatigue response. If very low frequencies were used, for example 0.1Hz and below, there may be fatigue time constraints. It may take the expected lifetime of the structure to reach 1 million cycles.

- The fatigue performance of single overlap joints is dependent upon the R-ratio. Care must be taken on how test data is interpreted. For instance when experimental data is represented by plotting maximum load applied per cycle versus cycles to failure, a reduction in the R-ratio from 0.5 to 0.1 is severely damaging. If however, the same data is plotted load amplitude per cycle versus cycles to failure the converse effect is shown.

- Joints exposed to aqueous environments will exhibit reduced fatigue performance. It is postulated that the migration of water molecules to the adhesive-metal oxide interface is responsible for the reduction in fatigue strength and inevitably the complete separation of the adhesive from the adherend.

- An analytical model based on beam theory has been developed that successfully predicts the elastic rotation of single lap joints subjected to a tensile load.

- Increasing the overlap length reduces the amount of rotation in the overlap region.

- Increasing the adherend thickness reduces the amount of rotation in the overlap region.

- Increasing the overlap length has a beneficial effect on joint strength.

- The removal of spew fillets marginally reduces single overlap adhesive joint strength.

- The higher the yield strength of the adherend, the better the improvement on the initial strength of the joint.

7.3 Further Work

The results chapters have highlighted area of future work that needs carrying out to further explain more specifically the conclusions that have been reached. The following section will describe the proposals for further work by results chapter.

Environmental Durability

The experimental work evaluated a number of surface pre-treatments that are applicable to austenitic stainless steel for structural bonding applications. The pre-treatments that merit further attention are Accomet C, sulphuric acid-sodium dichromate anodisation and primers. The first two should be further appraised due to the excellent durability performance and resistance to moisture ingression into the bond area and resistance to specimen fracture. It is the author's view that primers should be given more consideration. Working with adhesive manufacturers to refine primer recipes for applications involving austenitic stainless steels will not only increase the amount of reliable data available, but will look at a pre-treatment that is relatively simple to implement, and does not have additional costs from energy consumption, waste disposal problems and complex manufacturing processes. Similarly future work should include the development of chromate free and environmentally friendly pre-treatments. This area of pre-treatment development will become ever more paramount as tighter environmental legislation is introduced and tougher policing by the Environment Agency.

To study the pre-treatments named above, it is proposed that perforated single lap Joints are used, because they have proved an excellent method of evaluating adhesive systems where the load levels and environmental conditioning can be changed quickly. However, more benign testing environments should be used, i.e. ambient hydro-thermal exposure. More realistic conditions will yield more representative data. Therefore the proposed testing regime should be longer term where low load levels are applied to specimens. This will enable the performance of the entire adhesive system to be assessed, instead of high load levels, which may have the tendency to monitor the mechanical response of the adhesive only.

Failure analysis work revealed some very interesting facts on the subsequent environmental durability of the surface pre-treatments that where evaluated. It was reported that by increasing

the chromium levels on the surface of the substrate to be bonded greatly improved the resistance to ingressing moisture and increased the longevity of the perforated single lap joints and wedge test specimens. This is shown in Figures 4.115 and 4.116. Further work should look closer at the interaction between the epoxy adhesive and the surface and sub-surface regions of the adherends. It is known that the tenacity of chromium oxide increases as the chromium level is increased. However, there is only limited data available on this subject.

Dynamic Performance of Stainless Steel Adhesive Joints

The proposed experimental program should be extended to include the more durable pre-treatments. One novel idea would be to incorporate perforated single lap shear joints, tested at room temperature whilst submersed in water. This will compliment the environmental durability work, to monitor the resistance to water ingression versus static and dynamic loading conditions. Chapter 5 showed that the fatigue performance of single lap joints was affected by the test frequency, especially at lower frequencies such as 1Hz. It is these frequencies that are encountered by wave and wind damage. Therefore further work must include reduced testing frequencies, i.e. 0.1-1Hz.

Single Lap Joint Properties

The analytical model proposed in Chapter 6 proved very useful for predicting the elastic rotation incurred on standard single overlap joints under the application of a tensile load. The analytical and experimental information generated is useful for design engineers who are utilising adhesively bonded structures in industry, especially when proposing safety factors to avoid plastic deformation. The main downside of the model is that it does not take plastic deformation into account. Proposed areas of future work should include adherend plasticity, the author envisages that Finite Element Analysis must be used to fully elucidate this area. In addition, the experimental and analytical work should be extended to include thinner gauge cold rolled stainless steel adherends, i.e. less than 1mm. The reason for this is that ever more stainless steel applications using structural adhesive bonding are demanding thinner gauges and panels with large surface areas. Hence the use of the elastic rotation model will be more critical due to the increased chance of permanent deformation.

7.4 Chapter References

[1] Boyes R., PhD Thesis 'Adhesive Bonding of Stainless Steel: Strength and Durability', Sheffield Hallam University, 1998.

[2] Ring-Groth M., Licentiate Thesis 'The Influence of Joint Stiffness on the Strength of Adhesive Bonds in Stainless Steel', Luleå University of Technology, 1998.